# MECHANICAL PERFORMANCE OF V-RIBBED BELT DRIVES

**Seyed Mohammad Tabatabaei Lotfy**

A thesis submitted in accordance with the requirements

for the degree of Doctor of Philosophy

**The University of Leeds**

**Department of Mechanical Engineering**

**April 1996**

(The candidate confirms that the work submitted is his own and that appropriate)

(credit has been given where reference has been made to the work of others)

# ABSTRACT

The design and shape of a v-ribbed belt affects its radial movement in the pulley grooves. When rib bottom / groove tip contact occurs the wedge action decreases. The beginning of the contact depends on belt tension, fit between rib and groove, wear and material properties.

For the first time a non-contact laser displacement meter has been used for dynamic measurements of the radial movement of a v-ribbed belt (type 3PK) around the arc of wrap running on a belt testing rig. Accurate and repeatable results are possible. By the help of this device, the radial movement and the beginning of the rib bottom / groove tip contact around the arc of wrap have been determined experimentally for tested v-ribbed belts. This point plays an important role in the mechanical performance of v-ribbed belt drives.

Two sizes of standard pulleys were used for mechanical testing. These were paired with nominal effective diameters, $d_e$=*45 mm* and $d_e$=*80 mm*. Tests were carried out at the speed of $\omega$=*2000 RPM* and two different values of total belt tensions ($F_t + F_r$) for three different types of rib bottom / groove tip contact.

**(i)** Without contact

**(ii)** With contact

**(iii)** Mixed contact

Slip, torque loss and maximum torque capacity have been measured experimentally during the tests.

A v-ribbed belt is assumed to be a combination of a flat belt and a v-belt with the same radial movement of the two parts. Based on these assumptions a new theory is developed for the mechanical performance of v-ribbed belt drives, which gives a new modification to Euler's equation (capstan formula). By the help of Maple V (mathematical standard library software) numerical solutions for theoretical modelling give the variation of non-dimensional values of v-ribbed belt tension, flat belt part of v-ribbed belt tension, v-belt part of v-ribbed belt tension, radial movement and sliding angle with the length of active arc. This theory has been developed to obtain expressions for speed loss (slip) in linear and non-linear zones.

The experimental and theoretical results show that the radial movement and slip of the v-ribbed belt with rib bottom / groove tip contact is slightly less than the values without contact. However, in spite of more or less apparent similar performance of v-ribbed belt with and without rib bottom contact, it is found experimentally and theoretically that the compressed rubber of the belt (between cord and pulley) is subjected to a variable internal shear force around the pulley after contact.

## Acknowledgement

The author wishes to express his sincere gratitude to his supervisor Prof. T. H. C. Childs for his assistance, guidance and encouragement throughout this work.

Thanks are also due to superb technical assistance provided by the staff of the Department of Mechanical Engineering and all the friends in the department for their support and assistance.

The financial support by the Islamic Republic of Iran, specially Ministry of Culture and Higher Education and Ministry of Education and Training, is gratefully acknowledged.

Finally, the author wishes to express his utmost appreciation to his wife and children for their support and patience during this work.

**In the name of God**

*To my parents*

*and*

*my family*

# Table of Contents


**Table of Contents** i

**List of Tables** v

**List of Figures** vii

**List of Symbols** xii

**Chapter One: Introduction** 1

**Chapter Two: Belt Drives (Literature Review)** 4

2.1 Introduction 4

2.2 Flat Belt Drives 6

2.2.1 Classical Theory 6

2.2.2 Different Mechanisms of Speed Loss 8

2.2.2.1 Belt extension 8

2.2.2.2 Rubber compliance 8

2.2.2.3 Shear deflection 9

2.2.2.4 Seating and unseating 10

2.2.3 Torque Loss 11

2.3 V-belt Drives 12

2.3.1 Classical Theory 12

2.3.2 Radial Movement 12

2.3.3 Gerbert's V-belt Theory 15

2.3.3.1 Gerbert's Contribution to Radial Movement 18

2.3.3.2 V-belt Equations Solution 22

2.3.3.3 Non-Linear Slip 28

2.3.4 Torque Loss 30

2.4 V-ribbed Belt Drives 31

2.4.1 Torque Capacity 33

2.4.2 V-ribbed Belt Slip 34

2.4.3 Gerbert's V-ribbed Theory 37

2.4.4 V-ribbed Belt Torque Loss 43

2.4.5 Development of V-ribbed Belt in This Thesis 43

**Chapter Three: V-ribbed Belt Theory 44**

3.1 Introduction 44

3.2 Equilibrium Equations 46

3.3 Radial Movement 47

3.3.1 Radial Movement of V-belt Part 48

3.3.2 Radial Movement of Flat Belt Part 52

3.4 Basic Equations 53

3.4.1 V-ribbed Belt Equations Solution 56

3.4.2 Non-Linear Slip 68

**Chapter Four: Belt Testing Rig and Instrumentation 72**

4.1 Introduction 72

4.2 Dynamometer 73

4.3 Instrumentation of Dynamometer 75

4.3.1 Non-Contact Laser Displacement Meter 75

4.3.2 Speed Measurements 76

4.3.3 Torque Measurements 76

4.4 Rig Calibration 78

4.4.1 Radial Movement 79

4.4.2 Slip Calibration 80

4.4.3 Torque Calibration 81

4.4.4 Total Tension Calibration 85

**Chapter Five: V-ribbed Belt Material Properties 86**

5.1 Introduction 86

5.2 Radial Spring Constants 91

5.2.1 Preliminary Test 91

5.2.2 Tests For Determination of Radial Spring Constant $k_V$ 92

5.2.3 Tests For Determination of Radial Spring Constant $k_F$ 96

5.3 Coefficient of Friction 98

5.3.1 Introduction 98

5.3.2 Coefficient of Friction for V-ribbed Belts 99

5.3.3 Measurements Methods 100

5.4 Extension Modulus, c 102

**Chapter Six: Experimental Investigation of V-ribbed Belt Performance** **104**

6.1 Introduction 104

6.2 Experimental Method 105

6.3 Fundamental Experiments 109

6.3.1 Radial Movement 109

6.3.2 Slip and Torque Loss 121

6.3.3 Subsidiary Tests for Slip and Torque Loss 125

**Chapter Seven: Discussion of the Experimental and Theoretical Results** **140**

7.1 Introduction 140

7.2 Radial Movement 141

7.2.1 Experimental Results 141

7.2.2 Theoretical Non-Skidding Condition Results 144

7.2.3 Theoretical Skidding Condition Results 144

7.2.4 Mixed Contact 146

7.2.5 Discussion of Results 156

7.3 Slip 159

7.4 Maximum Traction 164

| | | |
|---|---|---|
| | 7.5 Torque Loss and Efficiency | 167 |
| | 7.6 Is the V-ribbed Belt a V-belt or Flat Belt? | 169 |
| **Chapter Eight:** | **Conclusions and Recommendations for Future Work** | **174** |
| | 8.1 Conclusions | 174 |
| | 8.2 Recommendations for Future Work | 176 |
| **References** | | **178** |
| **Appendix (A)** | | **186** |
| **Appendix (B)** | | **191** |
| **Appendix (C)** | | **192** |
| **Appendix (D)** | | **196** |

## List of Tables


Table 2.1 Numerical results for Gerbert's equations (driven pulley) 26

Table 2.2 Numerical results for Gerbert's equations (driving pulley) 27

Table 3.1 Numerical results for v-ribbed belt equation (driven pulley) 70

Table 3.2 Numerical results for v-ribbed belt equation (driving pulley) 71

Table 4.1 Pulley diameter measurements 81

Table 4.2 Experimental results for linearity between digital units and applied torque 83

Table 4.3 Experimental results for windage calibration 84

Table 5.1 Sheave or pulley groove dimensions for v-ribbed belts 88

Table 5.2 Tests for the variation of $H_T$ across the belt width at angular position *90* degrees 92

Table 5.3 Tests for determination of $k_V$ 95

Table 5.4 Tests for determination of $k_F$ 97

Table 6.1 Range of variables in mechanical tests 107

Table 6.2 The amount of wear during each set of tests 109

Table 6.3 Experimental readings of $H_T$ (mm), for ($F_t + F_r = 200\ N$, $d_e = 45mm$) 129

Table 6.4 Experimental readings of $H_T$ (mm), for ($F_t + F_r = 300\ N$, $d_e = 45mm$) 130

Table 6.5 Experimental readings of $H_T$ (mm), for ($F_t + F_r = 200\ N$, $d_e = 80mm$) 131

Table 6.6 Experimental readings of $H_T$ (mm), for ($F_t + F_r = 600\ N$, $d_e = 80mm$) 132, 133

Table 6.7 Experimental readings of $H_T$ (mm), for ($F_t + F_r = 600\ N$, $d_e = 45mm$) 134

Table 6.8 Experimental data for slip and torque loss, $d_e = 45mm$ 135

Table 6.9 Experimental data for slip and torque loss, $d_e = 80mm$ 136

Table 6.10 Experimental data for slip and torque loss, subsidiary tests, $d_e$=80mm 137, 138, 139

Table 7.1 Determination of $H_{T\max}$ $(mm)$ 143

Table 7.2 Experimental values of $\lambda_{max}$ for new belt (without rib bottom contact) and used belt (with rib bottom contact) and extreme condition test (mixed contact) 165

Table 7.3 Experimental values of lack of contact angle 166

## List of Figures


Fig. 2.1 Typical view of a belt drive 5

Fig. 2.2 Flat belt power transmission (driving pulley) 7

Fig. 2.3 Tension variation for driving pulley 11

Fig. 2.4 An exaggerated view of a v-belt drive 14

Fig. 2.5 Defining the sliding angle $\gamma$ 14

Fig. 2.6 Forces acting on a v-belt element 17

Fig. 2.7 Belt wedge angle at the sliding angle 17

Fig. 2.8 Three sources of belt deformation allowing radial movement 19

Fig. 2.9 Perpendicular forces acting on a belt cross-section 19

Fig. 2.10 Solution to Gerbert's equations for driven pulley 24

Fig. 2.11 Solution to Gerbert's equations for driving pulley 25

Fig. 2.12 Theoretical relation between $F / F_s$ and $\varphi$ for matching real and fictitious system 29

Fig. 2.13 Theoretical slip $sc / (F_t + F_r)$ as a function of traction coefficient 29

Fig. 2.14 Cross-section of a K-section v-ribbed belt (dimensions mm) 32

Fig. 2.15 The slip as a function of transmitted torque in a v-ribbed belt 34

Fig. 2.16 Experimental slip quantity $(\frac{c}{F_t + F_r} \cdot \frac{\Delta\omega}{\omega})$ vs coefficient of traction $\lambda$ for different total tension $(F_t + F_r)$, (v-ribbed belt). Comparison with "classical" flat belt theory 36

Fig. 2.17 Theoretical slip quantity $(\frac{c}{F_t + F_r} \cdot \frac{\Delta\omega}{\omega})$ vs coefficient of traction $\lambda$ for different total tension $(F_t + F_r)$, (v-ribbed belt) 36

Fig. 2.18 Wedge load $p_V$ and bottom load $p_F$ of the rib 38

Fig. 2.19 Defining the mechanism of rib bottom / groove tip contact 42

Fig. 3.1 Flat belt part and v-belt part of a v-ribbed belt load 45

Fig. 3.2 Forces acting on a v-ribbed element 46

Fig. 3.3 Perpendicular forces acting on a v-ribbed belt cross-section 47

Fig. 3.4 Geometry of radial movement and axial strain 49

Fig. 3.5 Solution to v-ribbed belt theory for driven pulley ($d_e$=45mm) 62

Fig. 3.6 Solution to v-ribbed belt theory for driven pulley ($d_e$=80mm) 63
Fig. 3.7 Solution to v-ribbed belt theory for driving pulley ($d_e$=45mm) 64
Fig. 3.8 Solution to v-ribbed belt theory for driven pulley ($d_e$=80mm) 65
Fig. 3.9 Variation of belt tractions of flat and v- belt parts of a v-ribbed belt against active arc for driven pulley 66
Fig. 3.10 Variation of belt tractions of flat and v- belt parts of a v-ribbed belt against active arc for driving pulley 66
Fig. 3.11 Variation of belt normal load of flat and v- belt parts of a v-ribbed belt against active arc for driven pulley 67
Fig. 3.12 Variation of belt tractions of flat and v- belt parts of a v-ribbed belt against active arc for driven pulley 67
Fig. 3.13 Theoretical slip $sc/(F_t+F_r)$ as a function of traction coefficient 68
Fig. 4.1 Schematic of the belt testing rig 74
Fig. 4.2 Schematic of the non-contact laser displacement meter 76
Fig 4.3 Configuration of laser sensor head stand and speed measurement arrangements 77
Fig. 4.4 Determination of pitch diameter 79
Fig. 4.5 Response between transducer and digital output 82
Fig. 4.6 Windage resistance against speed 84
Fig. 5.1 Fully molded v-ribbed belt construction 87
Fig. 5.2 V-ribbed belt with ribs formed by grinding 87
Fig. 5.3 Standard groove dimensions 89
Fig. 5.4 The variation of radius $R_T$ against belt tension $F$, for a new v-ribbed belt 95
Fig. 5.5 The variation of radius $R_T$ against belt tension $F$, for a used v-ribbed belt 97
Fig. 5.6 Test rig for coefficient of friction measurements 102
Fig. 6.1 Variation of drive radius and radial movement against angular position for a new v-ribbed belt (without rib bottom contact) ($F_t+F_r$=200 N, $d_e$=45 mm) 112
Fig. 6.2 Variation of drive radius and radial movement against angular position for a used v-ribbed belt (with rib bottom contact) ($F_t+F_r$=200 N, $d_e$=45 mm) 113

Fig. 6.3 Variation of drive radius and radial movement against angular position for a new v-ribbed belt (without rib bottom contact) ($F_t + F_r = 300\ N$, $d_e = 45\ mm$) 114

Fig. 6.4 Variation of drive radius and radial movement against angular position for a used v-ribbed belt (with rib bottom contact) ($F_t + F_r = 300\ N$, $d_e = 45\ mm$) 115

Fig. 6.5 Variation of drive radius and radial movement against angular position for a new v-ribbed belt (without rib bottom contact) ($F_t + F_r = 200\ N$, $d_e = 80\ mm$) 116

Fig. 6.6 Variation of drive radius and radial movement against angular position for a used v-ribbed belt (with rib bottom contact) ($F_t + F_r = 200\ N$, $d_e = 80\ mm$) 117

Fig. 6.7 Variation of drive radius and radial movement against angular position for a new v-ribbed belt (without rib bottom contact) ($F_t + F_r = 600\ N$, $d_e = 80\ mm$) 118

Fig. 6.8 Variation of drive radius and radial movement against angular position for a used v-ribbed belt (with rib bottom contact) ($F_t + F_r = 600\ N$, $d_e = 80\ mm$) 119

Fig. 6.9 Variation of drive radius and radial movement against angular position for a new v-ribbed belt (extreme conditions test with mixed contact) ($F_t + F_r = 600\ N$, $d_e = 45\ mm$) 120

Fig. 6.10 Slip (s) verses ($F_t - F_r$) for new (without rib bottom contact) and used (with rib bottom contact) v-ribbed belts and extreme conditions test (mixed contact) ($d_e = 45mm$) 128

Fig. 6.11 Slip (s) verses ($F_t - F_r$) for new (without rib bottom contact) and used (with rib bottom contact) v-ribbed belts ($d_e = 80mm$) 128

Fig. 6.12 Torque loss ($T_L$) verses ($F_t - F_r$) for new (without rib bottom contact) and used (with rib bottom contact) v-ribbed belts ($d_e = 45mm$), (a) $F_t + F_r = 200\ N$, (b) $F_t + F_r = 300\ N$, (c) extreme conditions test, $F_t + F_r = 600\ N$ 130

Fig. 6.13 Torque loss ($T_L$) verses ($F_t - F_r$) for new (without rib bottom contact) and used (with rib bottom contact) v-ribbed belts ($d_e = 80mm$), 131

(a) $F_t + F_r = 200\ N$, (b) $F_t + F_r = 600\ N$

Fig. 6.14 Slip (s) verses $(F_t - F_r)$ for (a) new, half-used and used cut belts (b) new cut, new molded and new anti-wear belts (c) new cut, $\omega = 1000\ RPM$ and $\omega = 2000\ RPM$ ($d_e = 80mm$, $F_t + F_r = 470\ N$) 133

Fig. 6.15 Torque loss verses $(F_t - F_r)$ for (a) new, half-used and used belts (b) cut, molded and anti-wear belts (c) $\omega = 1000\ RPM$, $\omega = 2000\ RPM$ ($d_e = 80mm$, $F_t + F_r = 470\ N$) 134

Fig. 7.1 Experimental and theoretical results of radial movement against angular position for v-ribbed belt with rib bottom / groove tip contact (used belt) and without contact (new belt), ($d_e = 45mm$, $F_t + F_r = 200N.m$, *non-skidding condition, Torque* $= 2.5N.m$) 147

Fig. 7.2 Experimental and theoretical results of radial movement against angular position for v-ribbed belt with rib bottom / groove tip contact (used belt) and without contact (new belt), ($d_e = 45mm$, $F_t + F_r = 200N.m$, *skidding condition, Torque* $= 4N.m$) 148

Fig. 7.3 Experimental and theoretical results of radial movement against angular position for v-ribbed belt with rib bottom / groove tip contact (used belt) and without contact (new belt), ($d_e = 45mm$, $F_t + F_r = 300N.m$, *non-skidding condition, Torque* $= 2.5N.m$) 149

Fig. 7.4 Experimental and theoretical results of radial movement against angular position for v-ribbed belt with rib bottom / groove tip contact (used belt) and without contact (new belt), ($d_e = 45mm$, $F_t + F_r = 300N.m$, *skidding condition, Torque* $= 6N.m$) 150

Fig. 7.5 Experimental and theoretical results of radial movement against angular position for v-ribbed belt with rib bottom / groove tip contact (used belt) and without contact (new belt), ($d_e = 80mm$, $F_t + F_r = 200N.m$, *non-skidding condition, Torque* $= 5N.m$) 151

Fig. 7.6 Experimental and theoretical results of radial movement against angular position for v-ribbed belt with rib bottom / groove tip contact (used belt) and without contact (new belt), ($d_e = 80mm$, $F_t + F_r = 200N.m$, *skidding condition, Torque* $= 8N.m$) 152

Fig. 7.7 Experimental and theoretical results of radial movement against angular position for v-ribbed belt with rib bottom / groove tip contact (used belt) and without contact (new belt), ($d_e$=*800mm*, $F_t + F_r$=*600N.m, non-skidding condition, Torque =10N.m*) 153

Fig. 7.8 Experimental and theoretical results of radial movement against angular position for v-ribbed belt with rib bottom / groove tip contact (used belt) and without contact (new belt), ($d_e$=*80mm*, $F_t + F_r$=*600N.m, skidding condition, Torque =23N.m*) 154

Fig. 7.9 Experimental and theoretical results of radial movement against angular position for v-ribbed belt (extreme conditions test) with mixed rib bottom / groove tip contact ($d_e$=*45mm*, $F_t + F_r$=*600N.m, skidding condition, Torque =13N.m*) 155

Fig. 7.10 Variation of *F/R* against $H_T$, for a new v-ribbed belt or without rib bottom / groove tip contact (data from table 5.3)

Fig. 7.11 Variation of *F/R* against $H_T$, for a used v-ribbed belt or with rib bottom / groove tip contact (data from table 5.4) 158

Fig. 7.12 Experimental, theoretical and semi-theoretical slip $(s \cdot c)/(F_t + F_r)$ as a function of traction coefficient ($d_e$=*45mm*) 162

Fig. 7.13 Experimental, theoretical and semi-theoretical slip $(s \cdot c)/(F_t + F_r)$ as a function of traction coefficient ($d_e$=*80mm*) 163

Fig. 7.14 Efficiency versus transmitted torque for new, half-used, used, molded, anti-wear v-ribbed belt ($\omega$=*1000 RPM* and $\omega$=*2000 RPM*) 168

## List of Symbols

| | |
|---|---|
| $B$ | Belt pitch |
| $E$ | Young's modulus |
| $F$ | Belt tension |
| $H$ | Total belt depth |
| $H_T$ | Radial belt depth (Fig. 4.4) |
| $P$ | Input power |
| $P_L$ | Power loss |
| $R$ | Pitch radius of belt |
| $R_e$ | Pulley effective radius (outside Radius) |
| $R_{ea}$ | Pulley actual effective radius |
| $R_T$ | Pulley radius over top of belt ($R_T=H_T+R_{ea}$) |
| $T$ | Input torque |
| $T_L$ | Torque loss |
| $T$ | Traction force per unit length |
| $V$ | Belt tension member speed |
| $c$ | Belt extension modulus ($F=c\varepsilon$) |
| $d_e$ | Pulley nominal effective diameter |
| $d_{ea}$ | Pulley actual effective diameter |
| $k$ | Spring constant |

| | |
|---|---|
| $k_1$ | Axial spring constant |
| $k_2$ | Radial spring constant |
| $k_3$ | Longitudinal spring constant |
| $k_F$ | Radial spring constant of flat belt part of a v-ribbed belt |
| $k_V$ | Radial spring constant of v-belt part of a v-ribbed belt |
| $k_{VR}$ | Total spring constant of v-ribbed belt ($k_{VR}=k_V+k_F$) |
| $p$ | Groove pressure (force per unit length) |
| $p_N$ | Normal force per unit length |
| $s$ | Slip factor |
| $x$ | Radial movement |
| $\alpha$ | Arc of wrap |
| $\alpha_p$ | Angular position |
| $\beta$ | Half angle of pulley groove |
| $\beta_s$ | Belt half wedge angle at sliding angle (Fig. 2.7) |
| $\varepsilon$ | Longitudinal strain |
| $\varphi$ | Angular co-ordinate (active arc) |
| $\varphi_F$ | Length of arc of wrap with rib bottom / groove tip contact (Fig. 2.19) |
| $\varphi_V$ | Length of arc of wrap without rib bottom / groove tip contact (Fig. 2.19) |
| $\gamma$ | Sliding angle |
| $\lambda$ | Coefficient of traction ($\lambda = F_t - F_r / F_t + F_r$) |
| $\theta$ | Inclination of belt in groove |
| $\mu$ | Coefficient of friction |

| | |
|---|---|
| $\nu$ | Poisson's ratio |
| $\omega$ | Angular speed |

**Indices**

| | |
|---|---|
| *F* | Flat belt of a v-ribbed belt |
| *V* | V-belt part of a v-ribbed belt |
| *dg* | Driving pulley |
| *dn* | Driven pulley |
| *g* | Generator |
| *m* | Motor |
| *r* | Relax (slack) side |
| *t* | Tight side |
| *w* | Windage |
| *x, y, z* | Radial, circumferential (longitudinal) and axial directions |

# CHAPTER ONE

# INTRODUCTION

Belt drives have played an important role in the industrial development of the world for more than 200 years. They are used as a means of transmitting power by frictional forces developed between the belt and the pulley. Belt drives are used in a wide range of power transmissions due to their advantages such as low maintenance cost, quiet operation, low initial cost and fairly efficient operation (usually 95% for v- and v-ribbed belt drives).

In 1917 John Gates developed the first rubber v-belt to replace the round hemp rope used to drive the fan on a 1917 Cole coupe'. V-belts through wedge action, increased the frictional force between the belt and the pulley for the same coefficient of friction. This gave the v-belt a very fast rise in popularity within a few years.

The v-ribbed belt was introduced in the 1950s. It is a cross between a flat and a v-belt. This belt is essentially a flat belt with v-shaped ribs projecting from the bottom of the belt which guides the belt and make it more stable than a flat belt. In the original concept, the v-ribs of the belt completely filled the grooves of the pulley. For this reason, the v-ribbed belt did not have the wedging action of the v-belt and

consequently had to operate at higher belt tensions. Later versions of v-ribbed belts have truncated ribs to more closely emulate the wedging effect of a v-belt [1,29].

The design and shape of a v-ribbed belt affects its radial movement in the pulley grooves. When rib bottom / groove tip contact occurs the wedge action decreases. The beginning of the contact depends on belt tension, fit between rib and groove, wear and material properties. Therefore it is not obvious if a v-ribbed belt functions as a v-belt or a flat belt. The purpose of this work was to investigate theoretically and experimentally the factors that influence the mechanical performance of v-ribbed belt drives. Investigating the mechanical performance of v-ribbed belt drives requires a clear idea to be developed on radial movement of the v-ribbed belt and its effect on the other parameters of the mechanism.

Chapter two gives a literature review on v-ribbed belt drives and elements of theory from flat and v-belt drives related to v-ribbed belt mechanical performance.

In chapter three on belt theory, a v-ribbed belt is assumed to be a combination of a flat belt and a v-belt with the same radial movement of the two parts. Based on these assumptions a new theory is developed for the mechanical performance of v-ribbed belt drives, which gives a new modification to Euler's equation (capstan formula). By the help of Maple V (mathematical standard library software) numerical solutions for theoretical modelling give the variation of non-dimensional values of v-ribbed belt tension, flat belt part of v-ribbed belt tension, v-belt part of v-ribbed belt tension, radial movement and sliding angle with the length of active arc. This theory has been developed to obtain expressions for speed loss (slip) in linear and non-linear zones.

Chapter four describes a test rig and its instrumentation to measure the values of radial movement, speed and torque losses.

For the first time a non-contact laser displacement meter has been used for dynamic measurements of the radial movement of a v-ribbed belt (type 3PK) around the arc of wrap running on a belt testing rig. Accurate and repeatable results are

possible. By the help of this device, the radial movement and the beginning of the rib bottom / groove tip contact around the arc of wrap have been determined experimentally for tested v-ribbed belts. This point plays an important role in the mechanical performance of v-ribbed belt drives.

Material properties of v-ribbed belts required in the theoretical modelling have been measured experimentally in chapter five.

Experimental results of the tests carried out are given in chapter six. Two sizes of standard pulleys were used for mechanical testing. These were paired with nominal effective diameters, $d_e$=*45 mm* and $d_e$=*80 mm*. Tests were carried out at the speed of $\omega$=*2000 RPM* and two different values of total belt tensions ($F_t + F_r$) for three different types of rib bottom / groove tip contact.

(i) Without contact

(ii) With contact

(iii) Mixed contact

Slip, torque loss and maximum torque capacity have been measured experimentally during the tests.

The experimental and theoretical results are compared and discussed in chapter seven. The results show that the radial movement and slip of the v-ribbed belt with rib bottom / groove tip contact is slightly less than the values without contact. However, in spite of more or less apparent similar performance of v-ribbed belt with and without contact, it is found experimentally and theoretically that he compressed rubber of the belt (between cord and pulley) is subjected to a variable internal shear force around the pulley after contact.

Chapter eight summarises the major findings of the work and makes recommendations for future programmes of research in this and related areas.

# CHAPTER TWO

# BELT DRIVES

## (Literature Review)

## 2.1 Introduction

This chapter will review v-ribbed belt drive literature and elements of theory from flat and v-belt drives related to v-ribbed belt mechanical performance. In this work special attention will be made to radial movement and its contribution to the slip and speed loss. There will also be a brief review of torque loss contribution to power loss.

When a belt drive is transmitting power, the strand tensions are not equal. There is a tight side tension $F_t$ and a slack side tension $F_r$ and difference between these tensions is often called the effective tension or net pull. This is the force that produces work, and the rate at which work is performed is called power.

In Fig. 2.1 a typical view of a belt drive with two pulleys is shown. The pulleys are taken to be rotating clockwise. The belt is represented as a band by its cord line. The driving pulley is denoted *dg* and the driven pulley *dn*. The drive consists of two pulleys with pitch radius *R*.

When torque is applied to the system, the input power to the driving pulley is given by $(\omega T)_{dg}$ where $\omega$ is the angular speed and $T$ is the torque on the pulley. The output power from the driven pulley is $(\omega T)_{dn}$. Their difference is the power loss $P_L$ in the drive.

$$P_L = (\omega T)_{dg} - (\omega T)_{dn}$$

For pulleys of equal size the power loss may be written

$$P_L = (\omega_{dg} - \omega_{dn})T_{dg} + (T_{dg} - T_{dn})\omega_{dn}$$

Dividing by the input power $P$ we have the fractional power loss

$$\frac{P_L}{P} = s + \frac{T_L}{T} \tag{2.1}$$

where

$$s = 1 - \frac{\omega_{dn}}{\omega_{dg}} \tag{2.2}$$

$$T_L = T_{dg} - T_{dn} \tag{2.3}$$

In a belt drive the slip $s$ and the fractional torque loss $T_L / T$ result from several effects [1].

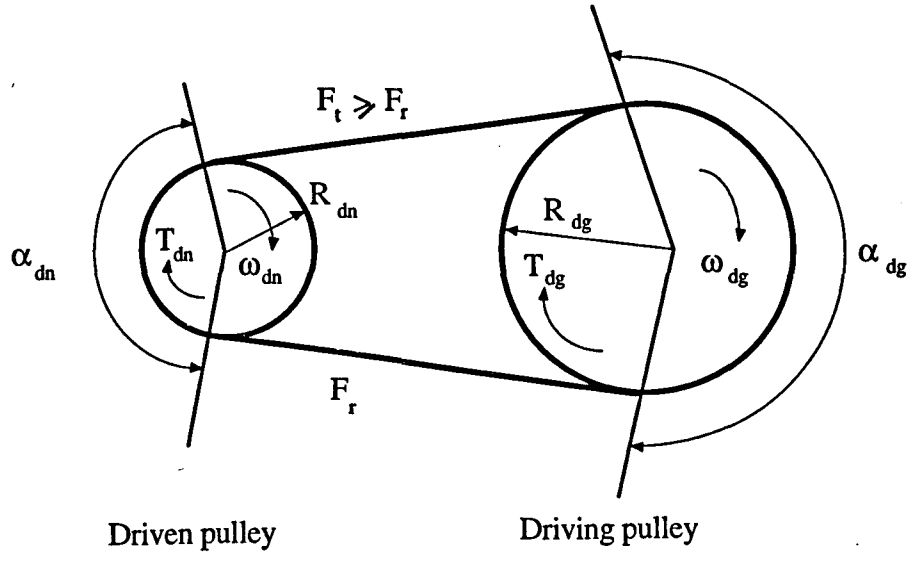


**Fig. 2.1 Typical view of a belt drive**

## 2.2 Flat Belt Drives

It is appropriate to review flat belt theory as some aspects are related to v-ribbed belt drives.

### 2.2.1 Classical Theory

The role of friction in the equilibrium of ropes wrapped around shafts was analysed by Euler [2]. He presented the well-known capstan formula, which relates the slack and tight tensions of a rope to the friction coefficient $\mu$ and angle of wrap of the rope on the pulley $\alpha$.

$$\frac{F_t}{F_r} = \exp(\mu\alpha) \tag{2.4}$$

According to Gerbert [3], this theory was applied to flat and v-belt drives by Eytelwein [4]. The angle $\alpha$ was taken as the geometrical angle of wrap. Norman [5] recognised that stiffness in the belt causes arching in the strands between the pulleys and reduces the arc of contact between belt and pulley. More comprehensive theory was given by Hornung [6]. The lack of contact angle reduces the maximum traction of the drive [1].

When equation (2.4) is satisfied and skidding occurs, the fractional speed loss $s$ tends to 1.0. A smaller tension ratio than in equation (2.4) requires a sliding arc $\varphi_s$ (active or sliding arc ) obtained from

$$\frac{F_t}{F_r} = \exp(\mu\varphi_s)$$

$\varphi_s$ is located towards the exit region (Fig. 2.2). In this region belt tension $F$ is given by (for a driving pulley)

$$\frac{F}{F_r} = \exp(\mu\varphi)$$

$\varphi$ is the angular co-ordinate and $F_r$ is the tension at $\varphi = 0$. If the geometric contact arc is $\alpha$ there is no sliding and no friction within the arc $\varphi_a = \alpha - \varphi_s$ (adhesion or

idle arc). At this region the belt force remains constant [7]. The size of the active arc is dependent on $(F_t - F_r)$.

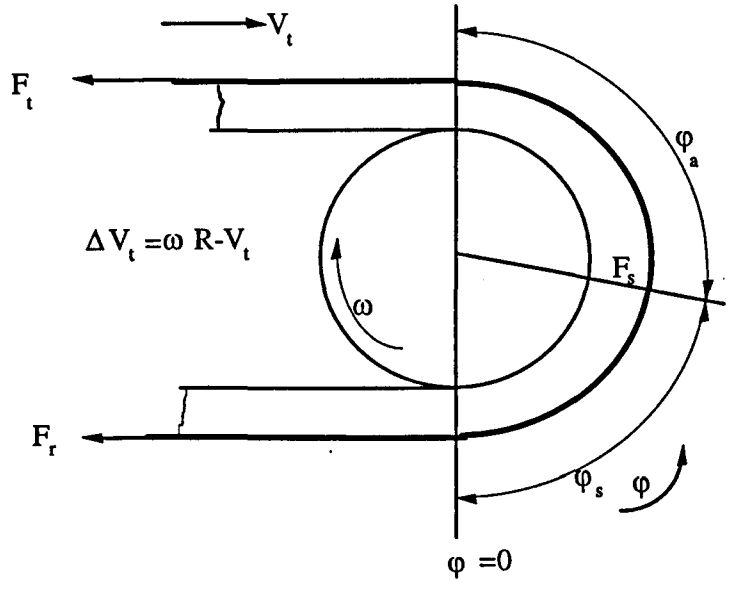


**Fig. 2.2 Flat belt power transmission (driving pulley)**

When torque is applied to the system the resulting difference in tension $(F_t - F_r)$ round the pulleys causes the elastic belt to change length. On the driving pulley there is a reduction in tension from $F_t$ to $F_r$ and the belt will contract. The speed of the belt is therefore slightly less than the pulley and belt is said to lag the pulley. On the driven side the tension increases from $F_r$ to $F_t$ the belt stretches and leads the pulley. Extension of the belt, caused by the variable tension, makes the belt slide against the pulley and different velocities $V_r$ and $V_t$ arise at the slack side and tight side. Conservation of mass leads to the relationship

$$s = \frac{V_t - V_r}{V_r} = \frac{F_t - F_r}{c} \tag{2.5}$$

where $c$ is longitudinal extension stiffness and having units of force defined by

$$F = c\varepsilon$$

Here $\varepsilon$ is longitudinal strain. $(\frac{F_t - F_r}{c})$ the speed loss due to extensional elasticity of the belt, is termed the extensional creep [8,9].

### 2.2.2 Different Mechanisms of Speed Loss

Childs et al. [10,11] in extensive measurements found that both belt speed and torque losses increased more rapidly with decreasing pulley radius than expected by current theories. Based on experimental results of Childs's work Gerbert [12] considered the following list to highlight the different mechanisms that may contribute to speed loss on belt drives.

- Belt extension (along the belt)
- Rubber compliance(radial direction)
- Shear deflection
- Seating and unseating

**2.2.2.1 Belt extension** already discussed in the last section (2.1.1), is the most familiar mechanism and known since long ago (see Ref. 13). The major property to consider is the extension stiffness along the belt.

**2.2.2.2 Rubber compliance** is not mentioned in the literature on flat belts before Gerbert [12], but it is well known for v-belts. He mentioned that it should be considered on thick flat belts, depending on combination of cross sectional data and material properties.

The rubber layer is subjected to a radial load per unit length $F/R$ when it is pressed against a pulley with pitch radius $R$. The compression is

$$x = \frac{1}{k_F} \cdot \frac{F}{R} \tag{2.6}$$

where $k_F$ is a radial spring stiffness.

When the belt seats on the driven pulley, the slack side velocity $V_r$ follows the pulley giving

$$V_r = (R - x_r)\omega_{dn}$$
$$x_r = \frac{1}{k_F} \cdot \frac{F_r}{R}$$

In the same way the tight side velocity follows the driving pulley giving

$$V_t = (R - x_t)\omega_{dg}$$
$$x_t = \frac{1}{k_F} \cdot \frac{F_t}{R}$$

Conservation of mass leads to the relation ship,

$$V_t = V_r[1 + (F_t - F_r)/c] \tag{2.7}$$

From equation (2.6) we have

$$(1 - \frac{F_t}{k_F R^2})\omega_{dg} = (1 + \frac{F_t - F_r}{c})(1 - \frac{F_r}{k_F R^2})\omega_{dn} \tag{2.8}$$

Neglecting small quantities results in a decrease in the output speed by

$$s = \frac{F_t - F_r}{c} + \frac{F_t - F_r}{k_F R^2} \tag{2.9}$$

The first term is the extensional creep (equation 2.5). The second term is the decrease in output speed due to the radial compression of the rubber.

**2.2.2.3 Shear deflection** of the rubber occurs when the frictional forces between belt and pulley are transferred to the cord. According to Gerbert [12] the mechanism

was first analysed by Firbank [14], but others too have dealt with the same problem [15,16,17]. Gerbert considered its effect on additional speed loss.

Circumferential shear of the rubber layer between the tension layer and the pulley allows the belt and the pulley to run with different velocities when the belt seats on the pulley. The differences in speed for a driving and driven pulleys are respectively $\Delta V_t$ and $\Delta V_r$ . The effect of shear deflection is added to the other contributions to the decrease of output speed in equation (2.9).

$$s = \frac{F_t - F_r}{c} + \frac{F_t - F_r}{k_F R^2} + \left(\frac{\Delta V_t}{V} + \frac{\Delta V_r}{V}\right) \tag{2.10}$$

For a thick belt the contribution to the slip is considerable.

**2.2.2.4 Seating and unseating** take place under considerable rotational motion of the cross section of the belt due to the rapid change of curvature in these regions. Lack of contact angle due to the bending stiffness of the belt at the seating and unseating regions and its effect on the traction of the drive was introduced earlier (2.1.1). Gerbert calculated the length of the lack of contact angle at seating and unseating regions for both driving and driven pulleys. He noted that the rapid change of curvature in the seating and unseating regions releases the friction in these zones. At the driving pulley, the frictional forces in the seating and unseating regions are counter-directed to the ones assumed in the creep and shear theories (see Ref. 12). Schematically, he showed that the belt tension at the driving pulley varies according to Fig. 2.3. Here $F_b$ is belt tension at the beginning of the adhesion zone and $F_c$ is belt tension at the beginning of the outlet zone.

Finally by taking into consideration these features Gerbert explained that the experimental observations noticed by Childs et al.. [10,11] fits the theory.

Later Gerbert [18] developed a unified belt slip theory for flat, v- and v-ribbed belt which will be discussed in section 2.4.2.

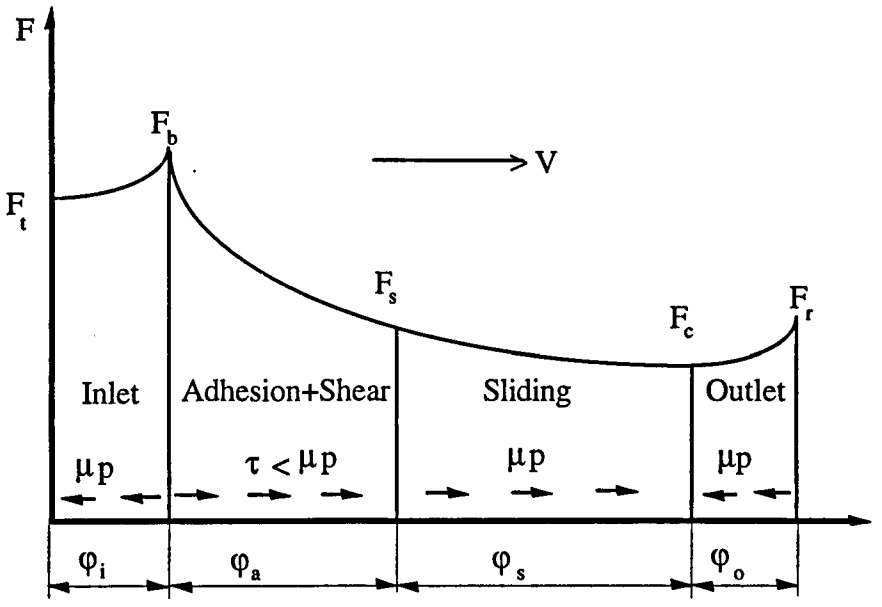


**Fig. 2.3 Tension variation for driving pulley [12]**

## 2.2.3 Torque Loss

Torque loss contribution to the power loss can be divided into two main parts [19].

- losses due to external friction (sliding between belt and pulley)
- losses due to internal friction (sliding between molecules and hysteresis)

Bending and unbending round a pulley, stretch and relaxation and carcass compression are the main components of the hysteresis losses .

A complete review of the literature for torque loss is out side of the aim of this work. However, some detailed analysis about torque loss of flat belt drives is presented by Childs et al.. [10,11,20] and Gerbert [19,21].

## 2.3 V-belt Drives

V-belt literature related to v-ribbed belt theory will be reviewed in this section and radial movement will be discussed in detail

### 2.3.1 Classical Theory

For the case of v-belt drives in the capstan formula (equation 2.4) $\mu$ may be modified to $\mu / \sin\beta$, $\beta$ being the half angle of the pulley groove.

$$\frac{F_t}{F_r} = \exp\left(\frac{\mu\alpha}{\sin\beta}\right) \tag{2.11}$$

Extensional creep (equation 2.5) or classical theory for speed loss is also valid for v-belt drives.

$$s = \frac{F_t - F_r}{c} \tag{2.12}$$

### 2.3.2 Radial Movement

The fundamental difference in action between a flat belt and a v-belt is the possibility of the belt to move in a radial direction and develop a wedge action [3].

Morgan [22], Dittrich [8], and Worley [23] during largely experimental work on pulleys with movable flanges, noted that the axial force on the driving pulley was larger than that on the driven. This was deduced correctly as relating to the different motion of the belt in the driving pulley as compared with the driven [1].

When the belt enters the pulley (Fig. 2.4) at *A*, it is bent rapidly from a virtually straight strand of infinite radius to that of the pulley at *B* (because of stiffness of the

belt, some arching may occur between the pulleys). Because of wedging, the belt is compressed and moves radially in the groove. The amount of radial movement $x_s$ is measured from the pitch circle radius $R$ of the pulley. $R$ is defined as the radius that the cord line would take, if the belt had no strand tension (unloaded). When torque is applied to the system the resulting difference in tension $(F_t - F_r)$ round the pulleys causes the elastic belt to change length. On the driving pulley there is a reduction in tension from $F_t$ to $F_r$ and the belt will contract. The speed of the belt is therefore slightly less than the pulley. On the driven side the tension increases from $F_r$ to $F_t$, the belt stretches and leads the pulley.

Relative motion (slip) can only occur between the belt and pulley if the shear forces on the belt sheaves interface are overcome. Generally this does not occur over the whole contact arc and there exists an active arc *(C-S)* in which the belt slips, and an arc of adhesion *(B-S)* where the shear forces are not overcome. The size of the active arc is dependent on $(F_t - F_r)$ and because of a difference in behaviour between the driving and driven pulleys the active arc sizes differ on the two pulleys. If the force difference is large enough sliding may occur on the whole of the contact arc and the belt will skid.

In the active arc the force changes. This causes the belt to move radially from its value $x_s$ at point *S*. Simultaneously the belt slides circumferentially. The resultant sliding velocity, $V_s$ is directed at an angle $\gamma$ to the pulley radius. This is shown in Fig. 2.5, where $V_b$ is the velocity of the belt and $(R-x)\omega$ that of the pulley.

In the exit region *(C-D)* as the belt leaves the pulley, its radius changes from *(R-x)* to virtually straight [1].

Radial movement gives rise to a second form of speed loss due to radial settle, similar to that already considered for a thick flat belt in section 2.2.2.2. In the idle arcs of the driving and driven pulleys *(B-S)* of Fig. 2.4, there is no relative motion between the belt and pulley. On the driving pulley

$$\omega_{dg}(R - x_{s_{dg}}) = V_t \tag{2.13}$$

while on the driven pulley

$$\omega_{dn}(R - x_{s_{dn}}) = V_r \tag{2.14}$$

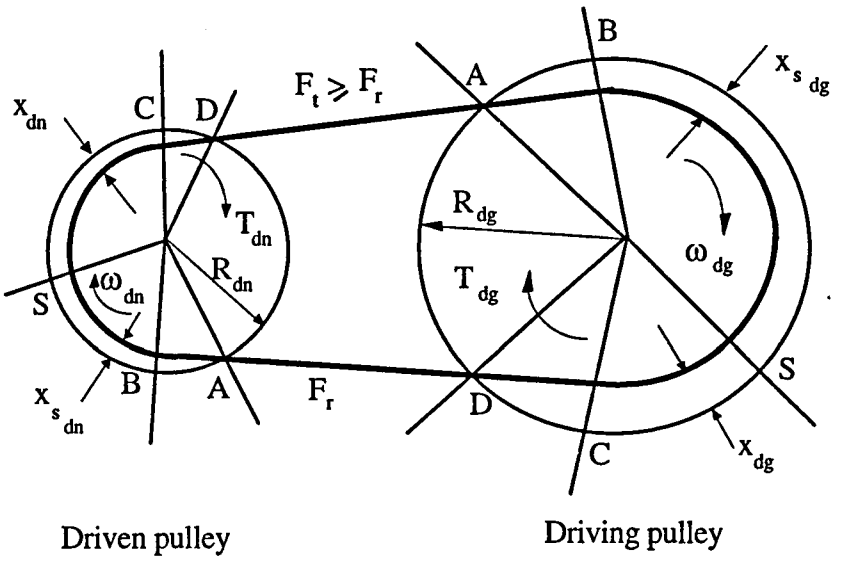


**Fig. 2.4 An exaggerated view of a v-belt drive [1]**

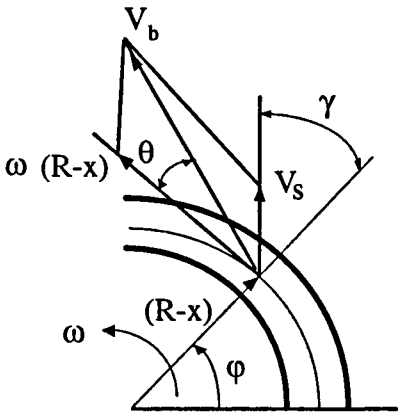


**Fig. 2.5 Defining the sliding angle$\gamma$ [1]**

For pulleys of equal radius

$$1-\frac{\omega_{dn}}{\omega_{dg}} \approx \frac{V_t - V_r}{V_t} + \frac{x_{s_{dg}} - x_{s_{dn}}}{R} \tag{2.15}$$

The first term is the extensional creep of the equation (2.5). The second arises if $x_{s_{dg}} \neq x_{s_{dn}}$ .

If it is supposed that the radial settle $x_s$ is proportional to the belt tension force *F*, by

$$x_s = \frac{F_s}{k_V R} \tag{2.16}$$

where $k_V$ is a radial spring stiffness, then by assuming that there is a portion of idle arc on each pulley (section 2.3.3.3), and considering equations (2.5) and (2.15)

$$s = \frac{F_t - F_r}{c} + \frac{F_t - F_r}{k_V R^2} \tag{2.17}$$

This equation is similar to the equation (2.9), for flat belt.

### 2.3.3 Gerbert's V-belt Theory

The most comprehensive analysis of v-belt radial movement is due to Gerbert [3]. He made the following assumptions to put forward the theory. This section will deal with some relevant aspects of Gerbert's work which are related to this work.

1. The belt can be considered as a band with a certain width but without thickness.
2. The coefficient of friction is constant.
3. The frictional forces are directed counter to the sliding velocity.
4. The belt has no bending stiffness, i.e. there are no bending moments.
5. The belt has no mass or the velocity is very slow, i.e. inertia forces are neglected.

Fig 2.6 shows the forces acting on a part of v-belt groove of a pulley. $O$ is the centre of the pulley and $Q$ is the centre of curvature of the belt. Furthermore:

$F$ belt force (tension)

$p$ compressive force divided by length between belt and pulley

$r,\varphi$ polar co-ordinates

$\beta$ wedge angle of the pulley

$\beta_s$ wedge angle in a plain inclined the sliding angle $\gamma$ to the radius (see Fig. 2.7)

$\gamma$ angle between radius and sliding velocity in the rotational plane (see Fig. 2.5)

$\mu$ coefficient of friction between belt and pulley

$\rho$ radius of curvature of the belt

$\theta$ angle between the belt and the circumferential direction

The frictional force $\mu p$ is perpendicular to the compressive force $p$ and counter directed to the sliding velocity between belt and pulley.

The equilibrium of the belt element $ds$ along the belt gives

$$dF + 2p\,ds \sin\beta\, \sin\theta - 2\mu\, p\,ds\, \cos\beta_s \sin(\theta+\gamma) = 0$$

and perpendicular to the belt

$$-F\,d\psi + 2p\,ds \sin\beta\, \cos\theta - 2\mu\, p\,ds \cos\beta_s \cos(\theta+\gamma) = 0$$

Introduce the radius of curvature

$$\rho = \frac{ds}{d\psi}$$

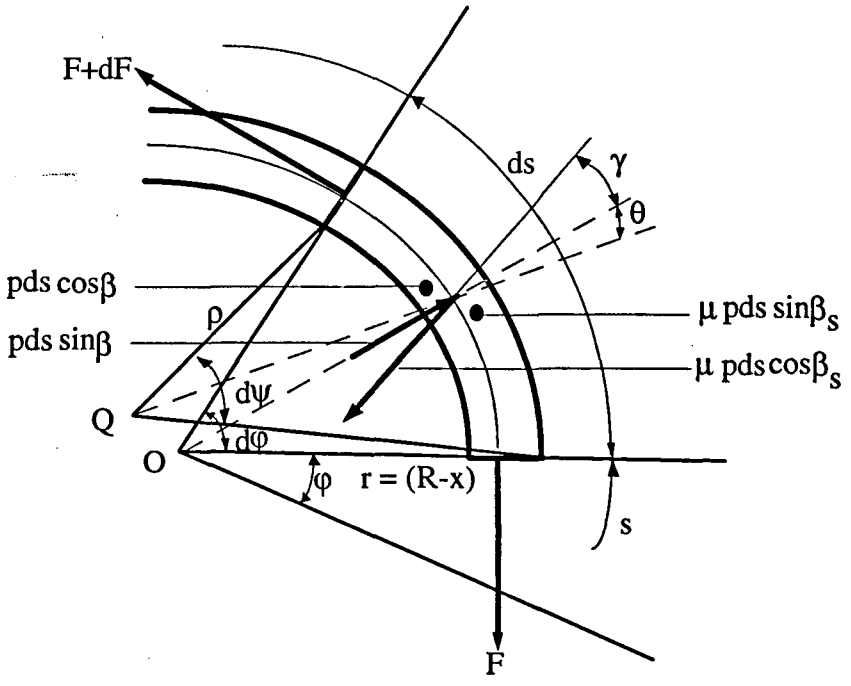


**Fig. 2.6 Forces acting on a v-belt element [3]**

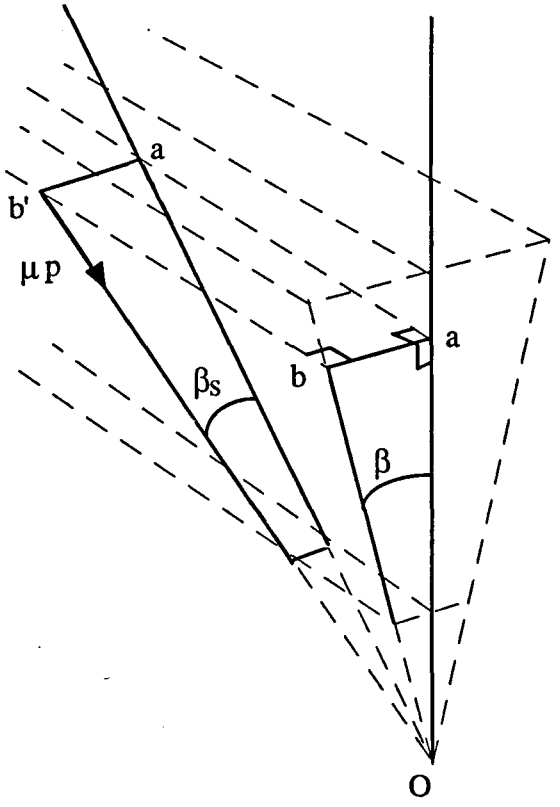


**Fig. 2.7 Belt wedge angle at the sliding angle [1]**

Then

$$\frac{dF}{ds} = 2p[-\sin\beta\ \sin\theta + \mu\cos\beta_s\ \sin(\theta+\gamma)] \tag{2.18}$$

$$\frac{F}{\rho} = 2p[\sin\beta\ \cos\theta - \mu\ \cos\beta_s\ \cos(\theta+\gamma)] \tag{2.19}$$

Fig. 2.7 shows an axial element $a'\,b'$ of a belt where $a'$ lies in the belt mid-plane and $b'$ on the pulley groove. An angle $\beta_s$, the effective wedge angle of the belt is introduced which by trigonometry depends on $\beta$ and $\gamma$ by

$$\tan\beta_s = \tan\beta\ \cos\gamma \tag{2.20}$$

It can be seen that when the belt slides radially inwards, $\gamma = 180°$, $\beta_s = -\beta$, and when sliding radially outwards, $\gamma = 0°$ and $\beta_s = \beta$.

Later Gerbert in his analyses to simplify the equations assumed $\theta = 0$, therefore, these solutions are invalid in the entry and exit regions and

$$\rho\ d\psi = Rd\varphi$$

Then equations (2.18,2.19) become

$$\frac{1}{R}\cdot\frac{dF}{d\varphi} = 2p\,(\mu\cos\beta_s\sin\gamma) \tag{2.21}$$

$$\frac{F}{R} = 2\,p(\sin\beta - \mu\cos\beta_s\cos\gamma) \tag{2.22}$$

Dividing the first by the second of these equations we have a further modification to Euler's equation.

$$\frac{1}{F}\cdot\frac{dF}{d\varphi} = \frac{\mu\cos\beta_s\sin\gamma}{\sin\beta - \mu\cos\beta_s\cos\gamma} \tag{2.23}$$

### 2.3.3.1 Gerbert's Contribution to Radial Movement

Gerbert considered the radial movement $x$ has contributions, $x_1, x_2$ and $x_3$ arising from the three stress related quantities $p_z, F/R$ and $F$ as shown schematically in Fig.2.8.

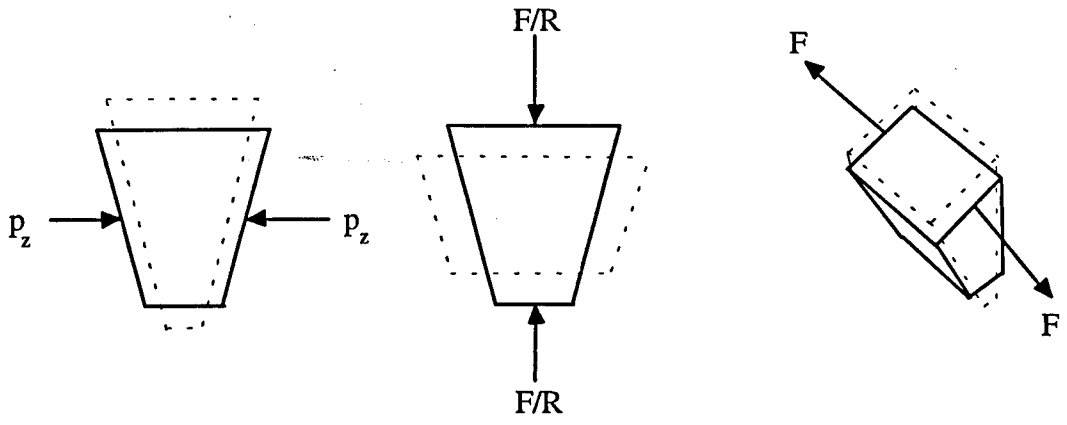


**Fig. 2.8 Three sources of belt deformation allowing radial movement [1]**

**(i) Axial component, $x_1$**

The axial pressure $p_z$ is distributed over the groove face. From Fig. 2.9, the axial pressure

$$p_z = p(\cos\beta + \mu \sin\beta_s) \tag{2.24}$$

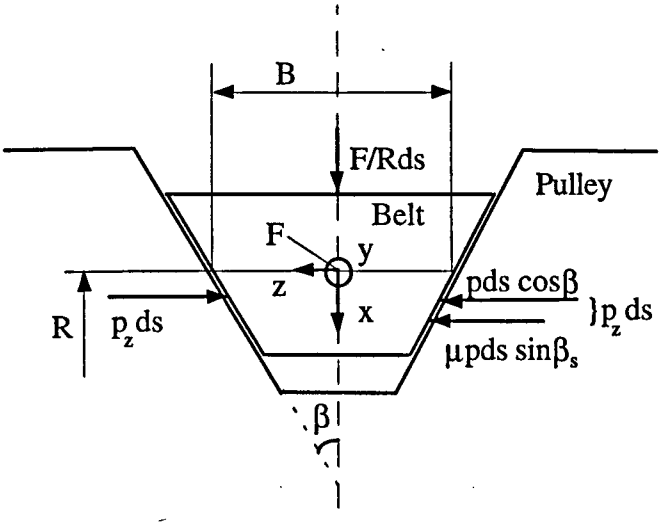


**Fig. 2.9 Perpendicular forces acting on a belt cross-section [3]**

This force $p_z$ contributes with $2p_z / k_1$, which is the dominating part of the displacement. Here $k_1$ is a kind of spring constant.

$$x_1 = \frac{2p_z}{k_1} \tag{2.25}$$

**(ii) Radial component, $x_2$**

The distributed force *F/R* compresses the belt in the radial direction. The Poisson effect causes the belt to expand axially and resist radial motion. A displacement $x_2$ and the compression modulus $k_2$ is recognised.

$$x_2 = \frac{-F}{Rk_2} \tag{2.26}$$

**(iii) Longitudinal component, $x_3$**

The force *F* causes strain of the belt of the amount *F/c*. If this is matched by a strain resulting from the radial displacement $x_3$,

$$\frac{x_3 \tan\beta}{(B/2)} = \frac{\nu_z}{c} \tag{2.27}$$

By superposition, the total radial displacement will be

$$x = \frac{F f(\gamma)}{Rk_1} - \frac{F}{Rk_2} + \frac{F}{k_3} \tag{2.28}$$

where

$$f(\gamma) = \frac{\cos\beta + \mu \sin\beta_s}{\sin\beta - \mu \cos\beta_s \cos\gamma} \tag{2.29}$$

Introducing

$$k_o = \frac{k_1}{k_2} - R\frac{k_1}{k_3} \tag{2.30}$$

$$k_{V(\gamma)} = \frac{1}{\frac{1}{k_1}[f(\gamma) - k_o]} \tag{2.31}$$

we have

$$x = \frac{F}{Rk_{V(\gamma)}} \tag{2.32}$$

Gerbert further related $k_1, k_3$ to belt geometry and elastic properties and estimated $k_1 / k_2 = 0.5$ for normal standard v-belts.

$$\begin{aligned} k_1 &= 4E_z \tan\beta (H/B) \\ k_3 &= 2c \tan\beta / \nu_z B \end{aligned} \tag{2.33}$$

where $E_z$ is the axial elastic modulus of the carcass, $c$ is the belt extension modulus as before and $\nu_z$ is the Poisson's ratio for contraction in the $z$-direction due to belt longitudinal extension.

The boundary between the idle and active arcs was chosen the origin by Gerbert, and the values of the parameters at this point ($S$), denoted $F_s, x_s$ and $\gamma_s$. In the idle arc regions there is no circumferential slip, therefore the direction of friction force remains unchanged from entry and is therefore directed radially outward ($\gamma_s = 180^\circ$). The value of $x_s$, the radial movement at this point is

$$x_s = \frac{F_s}{Rk_V} \tag{2.34}$$

where

$$k_V = \frac{1}{\frac{1}{k_1}[f(\gamma_s) - k_o]} \tag{2.35}$$

We now have a model for the radial spring stiffness ($k_V$), at equation (2.17).

A further equation is required to be able to calculate the path of the belt in the pulley and the rate of change of belt tension round the active arc. The sliding and geometric relationships between the belt and pulley leads to the following equation (see Ref. 1,3).

$$\frac{d(\frac{x}{x_s})}{d\varphi}\tan\gamma = 1-(\frac{x}{x_s})+\frac{1-(\frac{F}{F_s})}{c_o} \tag{2.36}$$

Where

$$c_o = \frac{c}{k_V R^2}$$

The equations (2.19) and (2.32) in non-dimensional form are

$$\frac{d(\frac{F}{F_s})}{d\varphi}\cdot\frac{1}{(\frac{F}{F_s})} = \frac{\mu\cos\beta_s\sin\gamma}{\sin\beta-\mu\cos\beta_s\cos\gamma} \tag{2.37}$$

$$(\frac{x}{x_s}) = (\frac{F}{F_s})\cdot\frac{k_V}{k_{V(\gamma)}} \tag{2.38}$$

Equations (2.36), (2.37) and (2.38) together with equation (2.20), form 4 equations for the variation of $(F/F_s),(x/x_s),\gamma_s$ and $\beta_s$ with $\varphi$.

### 2.3.3.2 V-belt Equations Solution

Numerical solutions of these equations was carried out by Gerbert [3] on a computer, using Runge-Kutta's method. Cowburn [1] to solve the equations wrote a computer program in Fortran 77 which used a NAG library routine.

In the present thesis the equations have been solved numerically by the help of Maple V (mathematical standard library software) using Runge-Kutta's method (Appendix A). It requires input of the physical and geometrical properties $c_o$ , $k_V$ , $\mu$

and $\beta$. These equations form the starting point for v-ribbed belt theory developments in this thesis (chapter 3).

Solutions for the driven pulley are shown in Fig. 2.10 and for driver in Fig. 2.11. Numerical results are presented in tables 2.1(a, b) and 2.2(a, b). The solutions are for a two pulley drive with $R_{dg} = R_{dn} = 45\,mm$ and $80\,mm$ ($\alpha = 180°$). The belt properties are those determined in chapter five for a new v-ribbed belt [$k_V = 117\,N/mm^2$ ($R = 45mm$) and $76\,N/mm^2$ ($R = 80mm$), $\beta = 20°$ and $\mu = 0.32$]. By taking these values it will be possible to compare the results of two different theories for v- and v-ribbed belts.

Figures 2.10a and 2.11a show the force variation $F/F_s$ against the active arc length $\varphi$. Values of $\varphi$ above 180 degrees are in the region which causes extensive slip of the belt, (*S*, located at an imaginary point outside the arc of contact). It can be seen from these figures that for any particular force ratio $F/F_s$ the driving pulley has a smaller value of $\varphi$ and therefore a higher torque capacity.

The sliding angle $\gamma$ in figures 2.10b and 2.11b starts from 180 degrees in both cases: this is the idle arc value. On the driven pulley $\gamma$ increases (the belt leads the pulley) until skidding occurs. On the driving pulley $\gamma$ increase (the belt lags the pulley).

The radial movement for driven and driving are shown in figures 2.10c and 2.11c. On the driven pulley radial movement increases from its idle arc value $x/x_s$ and the belt moves into the groove. On the driving pulley the radial movement again is slightly inwards, at the beginning. The amount of radial movement as compared with the driven pulley is small.

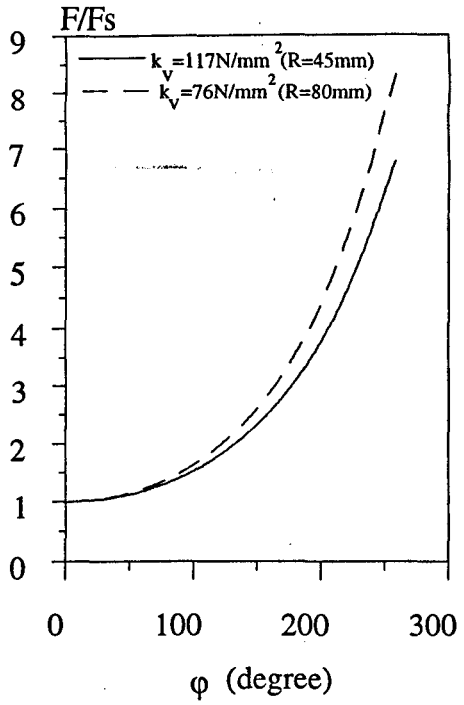


(a) Relative force

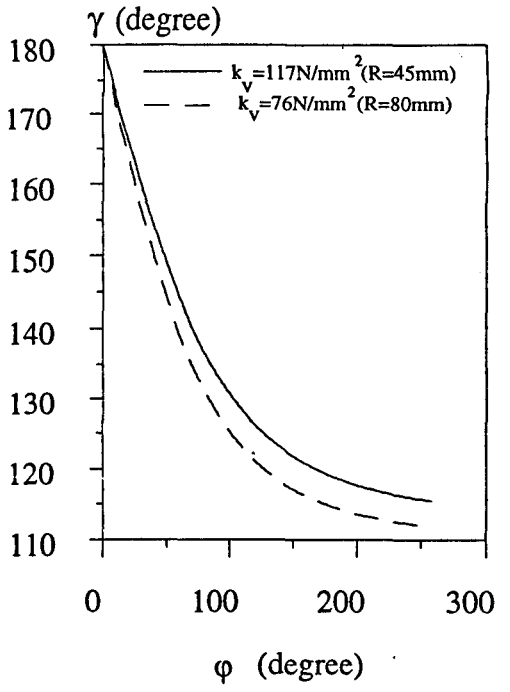


(b) Sliding angle (degree)

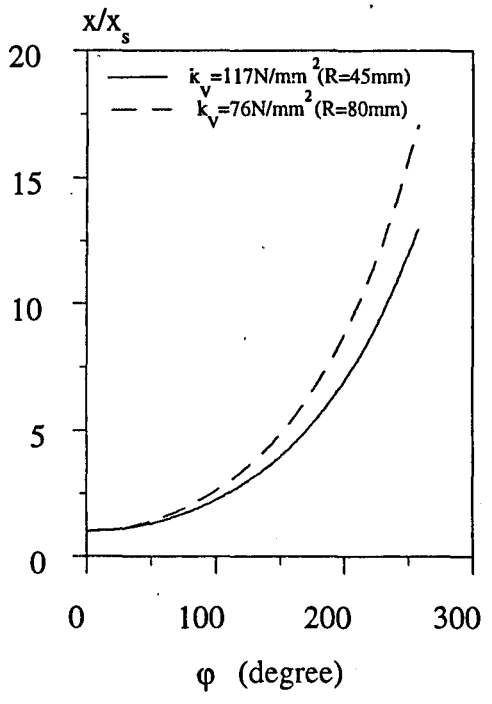


(c) Relative radial movemnt

**Fig. 2.10 Solution to Gerbert's equations for driven pulley**

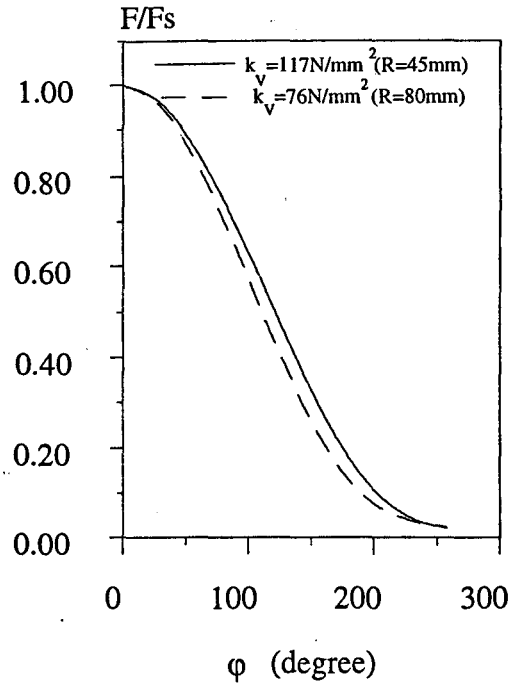


(a) Relative force

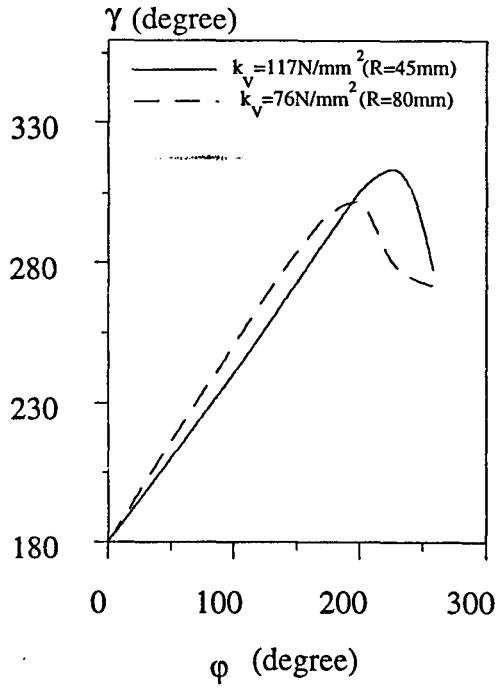


(b) Sliding angle (degree)

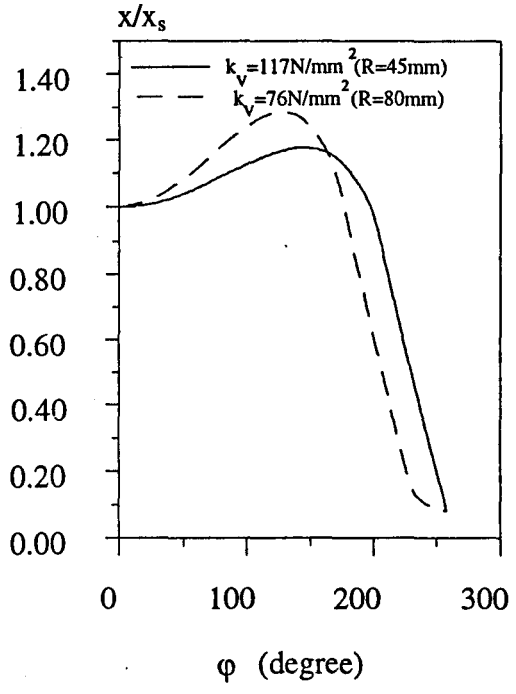


(c) Relative radial movement

**Fig. 2.11 Solution to Gerbert's equations for driving pulley**

Table 2.1 Numerical results for Gerbert's equations (driven pulley)

(a) driven pulley, $k_v = 117\,N/mm^2$ ($R$=45mm)

| active arc length (degree) | relative belt tension (force) | sliding angle (degree) | relative radial movement |
|---|---|---|---|
| 0.000 | 1 | 180 | 1.000 |
| 28.648 | 1.045 | 160.827 | 1.110 |
| 57.295 | 1.167 | 145.701 | 1.414 |
| 85.943 | 1.386 | 134.758 | 1.928 |
| 114.590 | 1.720 | 127.424 | 2.671 |
| 143.238 | 2.200 | 122.726 | 3.696 |
| 171.885 | 2.873 | 119.689 | 5.091 |
| 200.533 | 3.803 | 117.741 | 6.986 |
| 229.180 | 5.080 | 116.423 | 9.555 |
| 257.828 | 6.826 | 115.564 | 13.051 |

(b) driven pulley, $k_v = 76\,N/mm^2$ ($R$=80mm)

| active arc length (degree) | relative belt tension (force) | sliding angle (degree) | relative radial movement |
|---|---|---|---|
| 0.000 | 1 | 180 | 1.000 |
| 28.648 | 1.050 | 157.561 | 1.140 |
| 57.295 | 1.198 | 140.659 | 1.539 |
| 85.943 | 1.459 | 129.258 | 2.202 |
| 114.590 | 1.862 | 122.210 | 3.158 |
| 143.238 | 2.448 | 117.856 | 4.485 |
| 171.885 | 3.281 | 115.278 | 6.313 |
| 200.533 | 4.450 | 113.616 | 8.833 |
| 229.180 | 6.082 | 112.585 | 12.322 |
| 257.828 | 8.355 | 111.897 | 17.161 |

Table 2.2 Numerical results for Gerbert's equations (driving pulley)

(a) driving pulley, $k_V = 117\,N/mm^2$ ($R$=45mm)

| active arc length (degree) | relative belt tension (force) | sliding angle (degree) | relative radial movement |
|---|---|---|---|
| 0.000 | 1 | 180 | 1.000 |
| 28.648 | .962 | 197.668 | 1.013 |
| 57.295 | .862 | 214.684 | 1.050 |
| 85.943 | .715 | 231.987 | 1.102 |
| 114.590 | .541 | 249.806 | 1.152 |
| 143.238 | .366 | 268.427 | 1.178 |
| 171.885 | .214 | 287.850 | 1.142 |
| 200.533 | .105 | 306.299 | 0.973 |
| 229.180 | .044 | 313.346 | 0.512 |
| 257.828 | .021 | 277.537 | 0.085 |

(b) driving pulley, $k_V = 76\,N/mm^2$ ($R$=80mm)

| active arc length (degree) | relative belt tension (force) | sliding angle (degree) | relative radial movement |
|---|---|---|---|
| 0.000 | 1 | 180 | 1.000 |
| 28.648 | .955 | 201.163 | 1.029 |
| 57.295 | .837 | 221.331 | 1.104 |
| 85.943 | .667 | 241.097 | 1.201 |
| 114.590 | .475 | 260.692 | 1.275 |
| 143.238 | .296 | 279.714 | 1.267 |
| 171.885 | .158 | 296.387 | 1.080 |
| 200.533 | .075 | 301.945 | 0.606 |
| 229.180 | .038 | 278.683 | 0.158 |
| 257.828 | .023 | 271.922 | 0.081 |

### 2.3.3.3 Non-Linear Slip

The fractional speed loss when an idle arc exists can be determined by equation (2.17), for equal radius pulleys. Non-linear speed loss when the whole angle of wrap becomes active was also developed by Gerbert. He imagined the actual belt paths to be replaced by fictitious paths, with angles of wrap sufficiently greater than $\alpha$ (the actual wrap angle ) to contain an idle point, to obtain expressions for speed loss in the non-linear range (see Ref. 1 and 3 ). In terms of fictitious forces $F_{sdg}$ and $F_{sdn}$, acting at $S$ on the driving and driven pulleys, fractional speed loss is

$$s=(F_{sdg}-F_{sdn})(\frac{1}{c}+\frac{1}{k_V R^2}) \tag{2.39}$$

The variation of $F/F_s$ with $\varphi$ in the fictitious system may be obtained from the theory of the last section, resulting in Figs. 2.10 and 2.11 for the driven and driving pulleys respectively and sketched again in Fig. 2.12. In order that the fictitious and actual systems match over the actual angle of wrap.

$$[\frac{F}{F_s}]_{\varphi=\varphi_o}=\frac{F_t}{F_{sdg}}$$
$$[\frac{F}{F_s}]_{\varphi=\varphi_o+\alpha}=\frac{F_r}{F_{sdg}} \qquad \text{on the driving pulley} \tag{2.40}$$

$$[\frac{F}{F_s}]_{\varphi=\varphi_o}=\frac{F_r}{F_{sdn}}$$
$$[\frac{F}{F_s}]_{\varphi=\varphi_o+\alpha}=\frac{F_t}{F_{sdn}} \qquad \text{on the driven pulley} \tag{2.41}$$

These pairs of simultaneous equations determine unique values for $\varphi_o$ and $F_s$ in the fictitious system. $F_{sdg}$ and $F_{sdn}$ can be expressed in terms of $F_t$ and $F_r$ respectively to convert equation (2.39) to

$$s=[\frac{F_t}{(F/F_s)_{\varphi_{odg}}}-\frac{F_r}{(F/F_s)_{\varphi_{odn}}}][\frac{1}{c}+\frac{1}{k_V R^2}] \tag{2.42}$$

Slip ($s$) can be seen to become non-linear in $(F_t - F_r)$ as the values of $(\frac{F}{F_s})_{\varphi_o}$ depart from 1.0. In practice in a drive consisting of two equal pulleys, the driving pulley always has an idle arc, because torque is limited by slip on the driven pulley. $(\frac{F}{F_s})_{\varphi_{odg}} = 1.0$, but $(\frac{F}{F_s})_{\varphi_{odn}}$ can become>1.0. The equation for $s$ (equation 2.42) can be normalised and non-dimensionalised [1] to give

$$\frac{sc}{(F_t + F_r)} = \frac{F_t / F_r}{(F_t / F_r + 1)} [\frac{1}{(F/F_s)_{\varphi_{odg}}} - \frac{1}{(F/F_s)_{\varphi_{o+\alpha,dn}}}][1 + \frac{c}{k_V R^2}] \quad (2.43)$$

$F_t / F_r$ can further be related to the traction coefficient $\lambda$

$$\lambda = \frac{F_t - F_r}{F_t + F_r} = \frac{F_t / F_r - 1}{F_t / F_r + 1} \quad (2.44)$$

In Fig. 2.13, $sc/(F_t + F_r)$ is plotted against $\lambda$ for the data in tables 2.1 and 2.2. The ends of the linear slip ranges are shown by the arrows.

Gerbert [18] later developed a unified approach for flat, v- and v-ribbed belts slip, which we will discuss at section 2.4.2

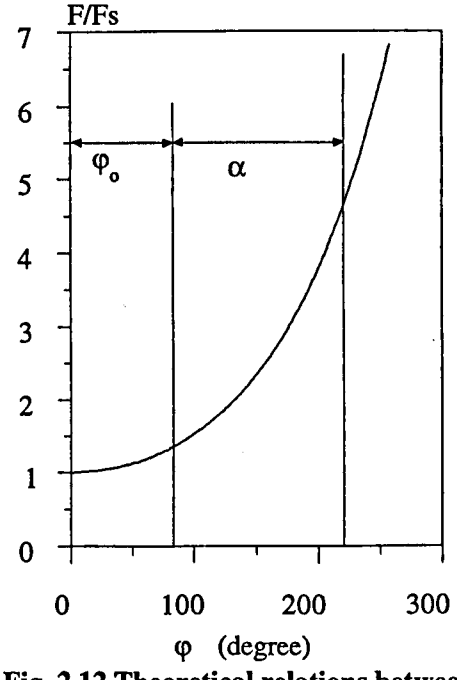


**Fig. 2.12 Theoretical relations between F/Fs and φ for matching real and fictitious system**

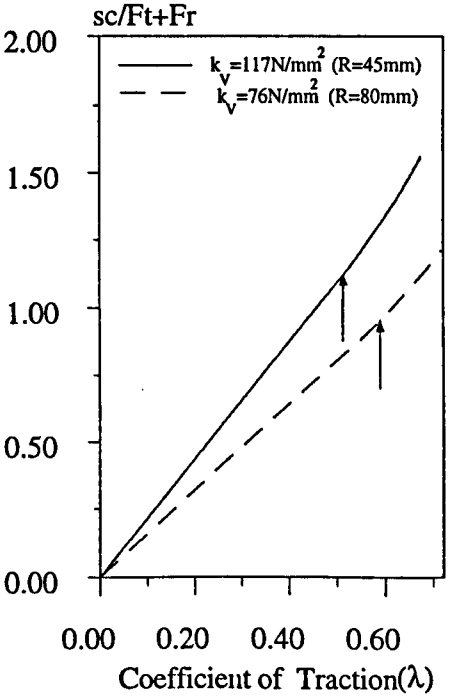


**Fig. 2.13 Theoretical slip sc/(Ft+Fr) as a function of traction coefficient**

### 2.3.4 Torque Loss

Torque losses in a v-belt drive basically are the same as for a flat belt, and arise from two main sources. For the case of a v-belt a major part of external losses is due to sliding in the pulley groove at entry and exit regions.

Torque and power losses were studied earlier by Norman [5] and Gervas and Pronin [24,25]. Gerbert in his v-belt theory [3], calculated the fractional power loss due to sliding in the active arc excluding entry and exit regions. The much larger portion of the torque loss is the no-load loss due to hysteresis and wedging at entry and exit.

Gerbert in later papers [26,27] considered the shear deflection and a non- uniform pressure distribution across a thick belt. He also allows the belt to have stiffness, and recognised other sources of power loss. The results given by Gerbert [26] are in graphical form. Cowburn [1] reduced these to the approximate form

$$\begin{aligned} \mu \le 0.4 \quad & T_{L_{ex}} = 7.10^{-3} \mu R(F_t + F_r)\left[1 + 0.35\, Ln 10^5 (s / R^4 k_1)\right] \\ \mu \le 0.4 \quad & T_{L_{en}} = 3.10^{-3} \mu R(F_t + F_r)\left[1 + 0.28\, Ln 10^5 (s / R^4 k_1)\right] \end{aligned} \tag{2.45}$$

where $T_{L_{ex}}$ is contribution to torque loss at exit from the pulley and $T_{L_{en}}$ is contribution at entry. s, is the belt bending stiffness. For $\mu > 0.4$, torque loss remains constant with friction and equation (2.45) is valid with $\mu = 0.4$.

Losses due to hysteresis during bending and carcass compression are reported experimentally [25]. The bending hysteresis is given by the empirical formula

$$T_{L_b} = 4.7 / R^{0.6} \quad (Nm) \tag{2.46}$$

and for the compression loss

$$T_{L_c} = 1.6 \cdot 10^{-5} (F_t + F_r)^2 / R \quad (Nm) \tag{2.47}$$

According to Cowburn [1], their contribution to the total no-load losses when $R=177.5\ mm$ and $(F_t + F_r) = 800\ N$ is $T_{L_b} / T_L = 40\%$ and $T_{L_c} / T_L = 11\%$. When $R=62.5\ mm$ for the same tension, $T_{L_b} / T_L = 46\%$ and $T_{L_c} / T_L = 19\%$.

## 2.4 V-ribbed Belt Drives

The v-ribbed belt was introduced in the 1950s. It is a cross between a flat and a v-belt. This belt is essentially a flat belt with v-shaped ribs projecting from the bottom of the belt which guides the belt and make it more stable than a flat belt. In the original concept, the v-ribs of the belt completely filled the grooves of the pulley. For this reason, the v-ribbed belt did not have the wedging action of the v-belt and consequently had to operate at higher belt tensions. Later versions of v-ribbed belts have truncated ribs to more closely emulate the wedging effect of a v-belt .

V-ribbed belts have recently been applied in accessory drives by the automotive industry and they have become the dominating belt, and have thereby attracted some research attention.

Due to the shape of the v-ribbed belt (Fig. 2.14), it is not obvious if a v-ribbed drive functions as a v-belt or a flat belt. The design and shape of a v-ribbed belt affects its radial movement in the pulley grooves. When rib bottom / groove tip contact occurs the wedge action decreases. The beginning of the contact depends on belt tension, fit between rib and groove, wear and material properties [28,29].

Compared with the normal v-belt, there are very few fundamental studies on the v-ribbed belt drives. The purpose of this work is to investigate theoretically and experimentally the factors that influence the mechanical performance of v-ribbed belt drives. Investigating the mechanical performance of v-ribbed belt drives requires a clear idea to be developed on radial movement of the v-ribbed belt and its effect on the other parameters of the mechanism. In the following v-ribbed belt literature related to this thesis will be reviewed.

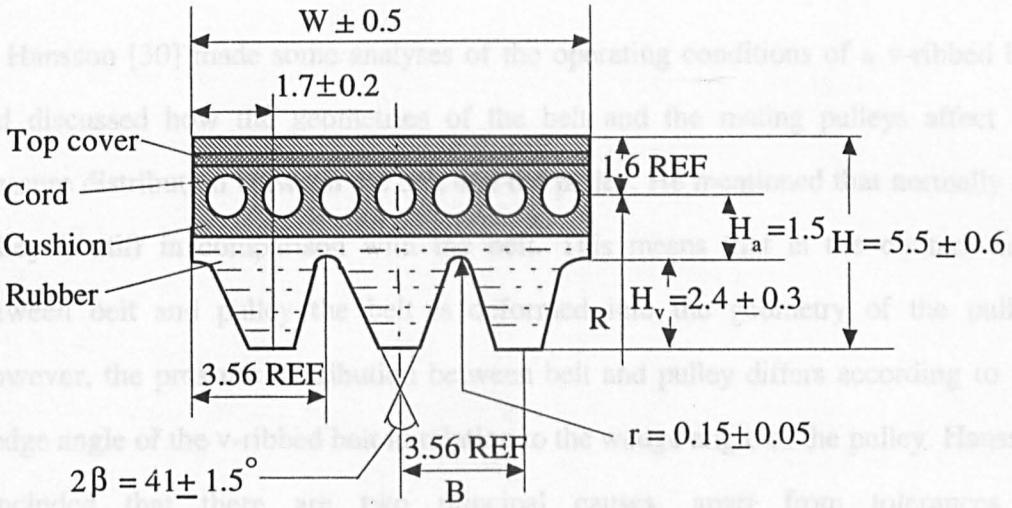


**(a) Belt**

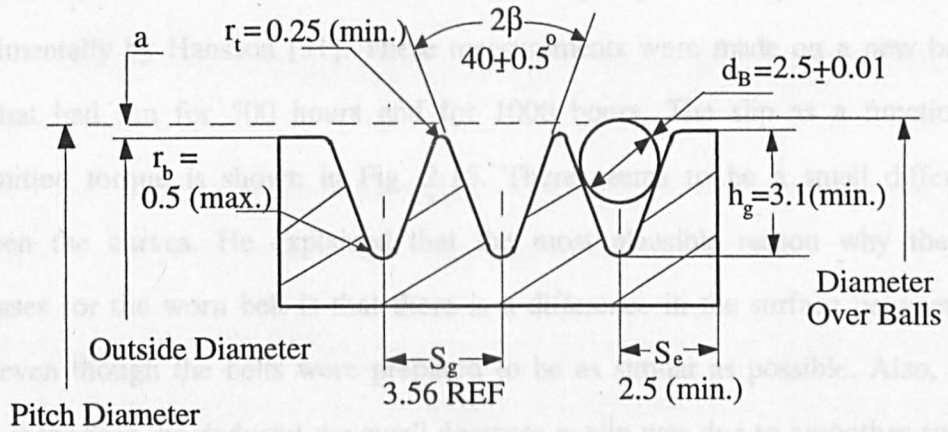


**(b) Pulley**

**Fig. 2.14 Cross-section of a K-section v-ribbed belt and pulley (dimensions mm)**

### 2.4.1 Torque Capacity

Hansson [30] made some analyses of the operating conditions of a v-ribbed belt and discussed how the geometries of the belt and the mating pulleys affect the pressure distribution between the belt and the pulley. He mentioned that normally the pulley is stiff in comparison with the belt. This means that in the contact zone between belt and pulley the belt is deformed into the geometry of the pulley. However, the pressure distribution between belt and pulley differs according to the wedge angle of the v-ribbed belt in relation to the wedge angle of the pulley. Hansson concluded that there are two principal causes, apart from tolerances in manufacturing, explaining why the wedge angles of the belt and pulley are unequal. First, the wedge angle of the belt changes with the curvature of the belt and, second, wear may change the wedge angle of the belt. Torque capacity of a v-ribbed belt is highly dependent on the pressure distribution. A poor fit between rib and groove implies large local compression of the rib and a decrease in torque capacity.

Later, influence of wear on torque capacity and slip was measured experimentally by Hansson [31]. These measurements were made on a new belt, a belt that had run for 500 hours and for 1000 hours. The slip as a function of transmitted torque is shown in Fig. 2.15. There seems to be a small difference between the curves. He explained that the most plausible reason why the slip decreases for the worn belt is that there is a difference in the surface between the belts even though the belts were prepared to be as similar as possible. Also, from visual inspection, he deduced the small decrease in slip was due to smoother surface of used belt (see Ref. 31,32 for belt surface roughness). However, his results showed that the worn v-ribbed belts, even if there is contact between the outer diameter of the pulley and the bottom of the belt (rib bottom / groove tip), will keep their torque capacity during the run. Thus a v-ribbed belt continues to function as a v-belt and not as a flat belt [31].

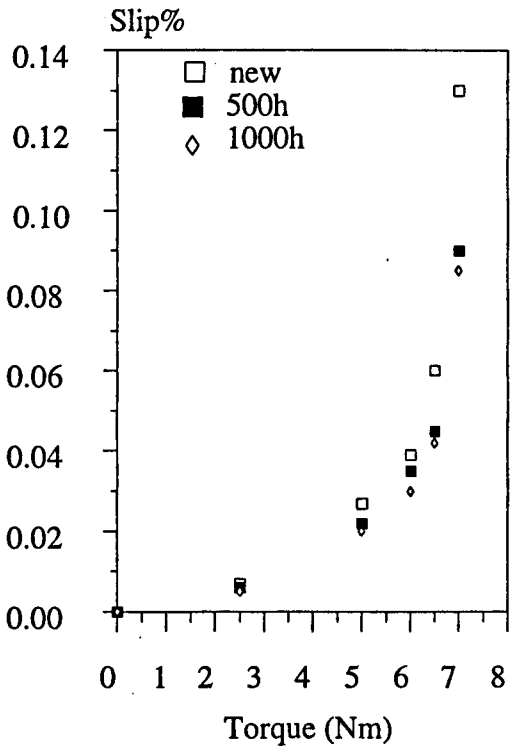


**Fig. 2.15 The slip as a function of transmitted torque in a v-ribbed belt [31]**

## 2.4.2 V-ribbed Belt Slip

Extensive measurements of slip and torque loss with a thick flat belt running on small pulleys by Childs et al. [10,11] exhibited higher slip and torque loss than expected from simple theory. Amijima [33] measured the traction capacity and shear deflection of a piece of v-ribbed belt pressed against a groove plate.

The experiments showed reduction in traction capacity for high loads. Influence of shear was mainly considered and developed theoretically for explanation of these phenomena by Gerbert using Amijima's results, not only for flat belt but also for v- and v-ribbed belts slip. He developed a unified slip theory considering the following four contributions [18].

- Creep (along the belt)
- Compliance (radially)

- Shear deflection (radial and axial variation )
- Flexural rigidity (seating and unseating)

He mentioned that shear deflection of the belt is a major factor to consider when dealing with belt slip. Within the idle arc (adhesion arc) the frictional forces are partly released. They are transferred from the belt-pulley contact through the rubber to the cord layer, thereby causing shear deflection along the belt. The shear deflection varies both radially (flat, v- and v-ribbed belts) and axially (v- and v-ribbed belts). Flat, v- and v-ribbed belts have different cross sectional shape and different contact pattern between pulley and belt, which requires separate treatments of the shear deflection analysis of the different belt types. The radial movement also contributes to the shear [18]. Gerbert applied Finite Element Analysis [FEA] to get the variation of shear deflection by transmission force.

The radial movement (rubber compliance) contribution to the speed loss for all types of belts is given by

$$x = \frac{1}{k} \cdot \frac{F}{R} \tag{2.48}$$

where $k$ is spring stiffness constant. This theory for radial movement does not consider the effect of sliding angle $\gamma$ and non-linear part of slip due to skidding (see section 2.3.3.3).

Finally Gerbert mentioned that on v- and v-ribbed belts running on small pulleys the belt is relatively thick compared to the pulley radius. Therefore classical creep theory predicts slip which is substantially lower than the measured ones. He concluded by taking into account all of the four contributions and good experimental data (especially the material data) that the fit between theory and experiments is very good for three practical tension levels (Figs. 2.16,2.17). For lower tension the measured slip level was higher than the calculated one. The reason is probable poor fit between the belt and pulley.

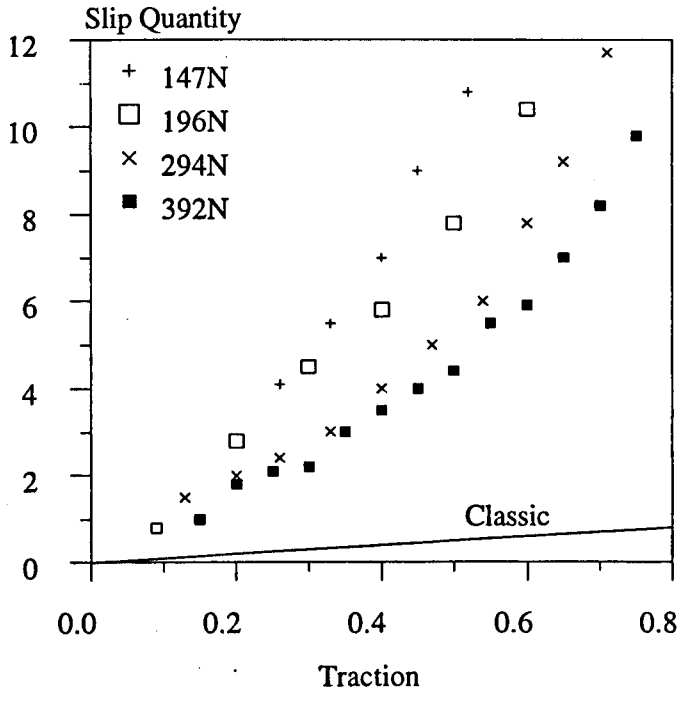


**Fig. 2.16 Experimental slip quantity ($\frac{c}{F_t+F_r}\cdot\frac{\Delta\omega}{\omega}$) vs coefficient of traction $\lambda$ for different total tension ($F_t+F_r$), (v-ribbed belt). Comparison with "classical" flat belt theory [23]**

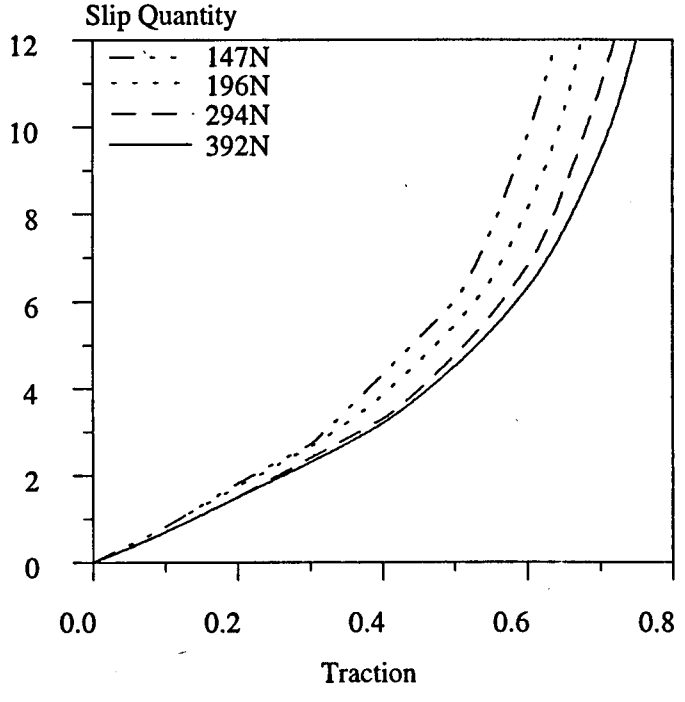


**Fig. 2.17 Theoretical slip quantity ($\frac{c}{F_t+F_r}\cdot\frac{\Delta\omega}{\omega}$) vs coefficient of traction $\lambda$ for different total tension ($F_t+F_r$), (v-ribbed belt) [23]**

### 2.4.3 Gerbert's V-ribbed belt Theory

In a later paper [34] Gerbert recognised the different radial movement of a v-ribbed belt from flat belt and v-belt. He explained that flat and v-belts are to some extent free to move on the pulley or in the groove respectively. The design and constraint of a v-ribbed belt limits its motion in the pulley grooves. Due to the shape of the belt (Fig. 2.14) ribs can not penetrate the pulley grooves individually. Maximal penetration (due to the high load or rib wear) is limited by the outer radius of the pulley. When rib bottom / groove tip interaction occurs the wedge action decreases. The extent of the reduction in the wedge action depends on belt tension, fit between rib and groove, wear and material properties.

Three different cases can be identified for mechanical performance of v-ribbed belt.

**(i)** Without rib bottom / groove tip interaction (due to low load or less wear)

**(ii)** With rib bottom / groove tip interaction

**(iii)** Mixed contact

A simple theoretical model was developed by Gerbert [34] to calculate variation of gross slip torque (maximum torque capacity) versus total tension ($F_t + F_r$).

**(i) Without rib bottom contact** - For this case, Gerbert assumed that a v-ribbed belt without rib bottom / groove tip contact acts as a v-belt and applied the classical v-belt formula (equation 2.11). In this formula the effect of sliding angle is neglected.

**(ii) With rib bottom contact -** Gerbert in this paper [34] attempted to model the reduction in traction capacity for high loads that was reported by Amijima [33]. Two alternatives (Fig. 2.18) were traced

- Case 1- All normal load per unit length $p_N$ is taken at the bottom of the rib.
- Case 2- Normal load per unit length $p_N$ is shared between the side and bottom of the rib.

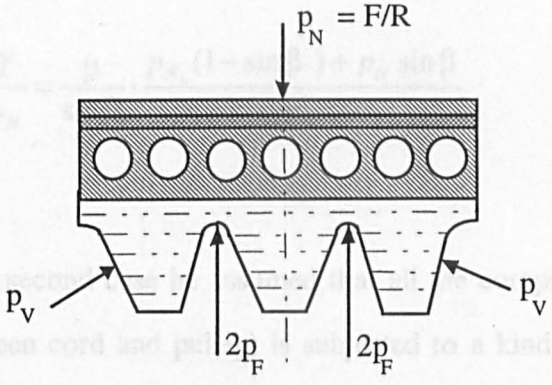


**Fig. 2.18 Wedge load $p_V$ and bottom load $p_F$ of the rib**

**Case 1-** For the first case he assumed that the ribs are not able to penetrate further when the pulley hits the bottom of the rib. Thus the side load is constant and all additional load is taken up at the bottom of the rib.

Fig. (2.18) shows a v-ribbed belt with both sides loaded (wedge load per unit length $p_V$ and bottom load per unit length $p_F$). Vertical equilibrium yields (for one rib)

$$p_N = 2p_V \sin\beta + 2p_F$$

The traction force per unit length along the belt is

$$T = 2\mu\,(p_V + p_F)$$

Thus we get the relative traction

$$\frac{T}{p_N} = \frac{2\mu\,(p_V + p_F)}{p_N} \tag{2.49}$$

Suppose at the instant that rib bottom contact is made ( $p_F = 0$) $p_N$ has the value $p_{N_L}$ and then $p_V$ = *constant*= $p_{V_L}$. Then

$$p_{N_L} = 2p_{V_L}\sin\beta \tag{2.50}$$

If further loading causes no change to $p_V$,

$$p_N - p_{N_L} = 2p_F \tag{2.51}$$

Therefore

$$\frac{T}{p_N} = \frac{\mu}{\sin\beta}\cdot\frac{p_{N_L}(1-\sin\beta) + p_N\sin\beta}{p_N} \tag{2.51}$$

**Case 2-** For the second case he assumed that all the compressed rubber of the belt (all rubber between cord and pulley) is subjected to a kind of hydrostatic pressure. This implies that all vertical loads increases to the **same extent** (we will discuss in chapter 3 about this assumption). Suppose that for $p_N > p_{N_L}$, additional loads develop in both the side and bottom of the rib in proportion to the additional overlap between belt and pulley. Then

$$2(p_V - p_{V_L}) = \frac{2p_F}{\sin\beta} \tag{2.52}$$

giving

$$P_N = 2p_V\sin\beta + 2p_F = 2(p_F + p_{V_L}\sin\beta) + 2p_F$$

$$p_N = (p_{N_L} + 2p_F) + 2p_F \tag{2.53}$$

$$T = \mu\,(\frac{p_{N_L} + 2p_F}{\sin\beta} + 2p_F) \tag{2.54}$$

Eliminating $p_F$ gives the relative traction

$$\frac{T}{p_N} = \frac{\mu}{\sin\beta} \cdot \frac{p_{N_L}(1-\sin\beta) + p_N(1+\sin\beta)}{2p_N} \tag{2.55}$$

Gerbert then compared these two cases with *FEA* results and mentioned that the second case is fairly close to the *FEA* results.

Thus he applied this concept in the following. $T$ and $p_N$ are loads per unit length on a piece of belt pressed against a grooved plate. In a drive application, belt tension $F$ presses the belt against the pulley (radius $R$) by the radial load per unit length $F/R = p_N$, (see Fig. 2.18). Thus equation (2.53) is replaced by

$$\frac{F}{R} = p_{N_L} + 4p_F \tag{2.56}$$

Traction $T$ is equivalent of increasing belt tension by

$$dF = T\,R d\varphi \tag{2.56a}$$

$\varphi$ is angular co-ordinate. Thus equation (2.54) gives

$$dF = \frac{\mu}{\sin\beta}[p_{N_L} + (1+\sin\beta)2p_F]R\,d\varphi \tag{2.57}$$

Eliminating $p_F$ yields

$$dF = \mu_F(F + A)d\varphi \tag{2.58}$$

where

$$\mu_F = \frac{\mu(1+\sin\beta)}{2\sin\beta}$$
$$A = \frac{1-\sin\beta}{1+\sin\beta}(p_{N_L}R) \tag{2.58a}$$

**(iii) Mixed contact -** Suppose that rib bottom / groove tip contact occurs only over an angle $\varphi_F$ (Fig. 2.19). At the beginning of that angle belt tension is

$$F_L = p_{N_L}R \tag{2.59}$$

and at the end $F_t$ = tight side tension. Thus integration of equation (2.58) gives the solution

$$\frac{F_t + A}{F_L + A} = \exp(\mu_F \varphi_F) \tag{2.60}$$

over the angle where contact occurs. This is a slight modification of Euler's equation. Pure wedge action when rib bottom / groove tip contact does not occur is

$$\frac{T_{max}}{p_N} = \frac{\mu}{\sin\beta} = \mu_V \tag{2.61}$$

Pure wedge action takes place over an angle $\varphi_V$. Slack side tension $F_r$ prevails at the beginning of that angle and $F_L$ at the end. Then Euler's equation gives the tension ratio

$$\frac{F_L}{F_r} = \exp(\mu_V \varphi_V) \tag{2.62}$$

as long as pure wedge action occurs.

Maximal tension ratio becomes $F_t / F_r$. Instead of tension ratio we can deal with the coefficient of traction

$$\lambda_{max} = \frac{F_t - F_r}{F_t + F_r} \tag{2.63}$$

The total wrap angle is

$$\alpha = \varphi_V + \varphi_F \tag{2.64}$$

Gerbert [34] then performed some experiments to measure variation of the maximum coefficient of traction ($\lambda_{max}$) versus total tension ($F_t + F_r$) and calculated the variation of ($\lambda_{max}$) versus ($F_t + F_r$) by putting a constant value for $p_{N_L}$ (equations 2.59 to 2.64) and varying $\varphi_V$ from 180° (minimum $F_t + F_r$ and without rib bottom contact) to 0° (maximum $F_t + F_r$ and with rib bottom contact at all arc of wrap). He adjusted the coefficient of friction so the experimental results fits the calculations. The results showed that $\lambda_{max}$ decreased by increasing ($F_t + F_r$).

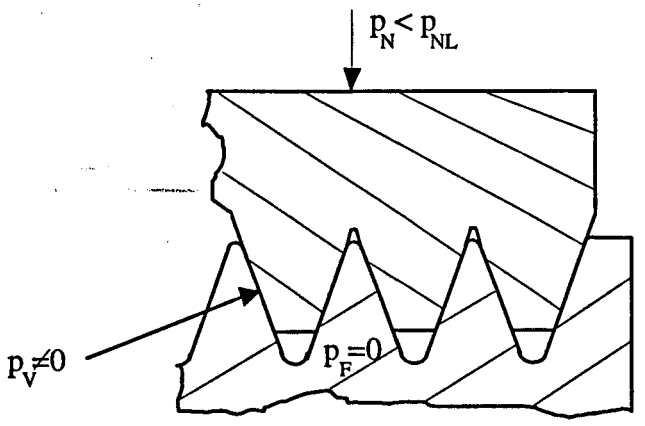


**(a) Without rib bottom / groove tip contact**

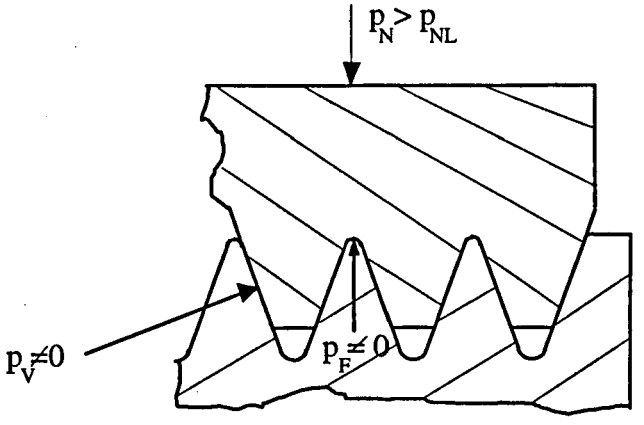


**(b) With rib bottom / groove tip contact**

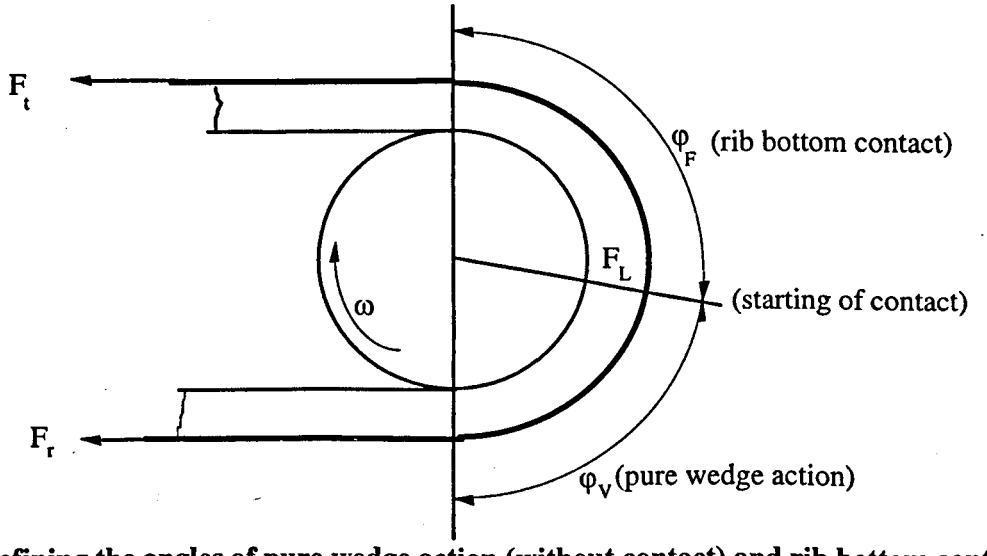


**(c) Defining the angles of pure wedge action (without contact) and rib bottom contact**

**Fig. 2.19 Defining the mechanism of rib bottom / groove tip contact**

### 2.4.4 V-ribbed Belt Torque Loss

V-ribbed belt literature review showed nothing related to this subject, neither experimentally nor theoretically. Torque loss contribution to power loss will be measured experimentally for v-ribbed belt drives in this work.

### 2.4.5 Development of V-ribbed Belt in This Thesis

Literature review revealed that v-ribbed belt drive mechanics have been studied by some authors. Study on mechanical performance of v-ribbed belt requires to have a clear idea on radial movement and its effect on the other parameters. Because of the belief that radial movement is important, it was measured in this thesis. Later chapters deal with the Non-Contact Laser Displacement Meter (NCLDM) used in this work (to measure radial movement) and with the results. In the next chapter a new theory for v-ribbed belt mechanics is developed. Special attention is made to radial movement.

# CHAPTER THREE

# V-RIBBED BELT THEORY

## 3.1 Introduction

Wedge action and radial movement of v-ribbed belt are the fundamental differences in action between an ordinary v-belt and v-ribbed belt. Due to the shape of a v-ribbed belt, wedge action and radial movement depend on pressure variation along the belt and wear.

Three different cases can be identified for mechanical performance of v-ribbed belt.

**(i)** Without rib bottom / groove tip interaction (due to low load or less wear)

**(ii)** With rib bottom / groove tip interaction

**(iii)** Mixed contact

Gerbert [34] in his v-ribbed belt theory assumed that v-ribbed belt acts as a v-belt in the first case. For the second case he assumed that some portion of belt tension

will be taken by the groove tip. Then he considered two possibilities, which we discussed earlier (2.4.2).

- All additional normal load is taken up at the bottom of the rib
- Additional normal load is shared between the side and the bottom of the rib

Gerbert assumed the additional load after starting rib bottom / groove tip interaction is shared to the **same extent** between rib side and rib bottom without any explanation. At a private communication [35] he said this was because the results of this assumption were fairly close to the *FEA* results. However we will show later (section 3.4) that this is not always the case. Here we develop a new theory.

For a theory development some assumptions must be made. The initial assumptions for v-belt theory (2.3.3) are still valid. Furthermore we assume that v-ribbed belt is a combination of a flat belt with width of $B_F$ and belt force per unit length $p_F$, and a v-belt with mean width of $B_V$ and belt force per unit length $p_V$ (Fig. 3.1). Let us further assume that the radial movement of the flat belt part $x_F$, and the radial movement of the v-belt part $x_V$ are equal. This has the effect that the top of the cord surface deflects radially in a uniform way across the belt width. It is shown later experimentally (section 5.2.1) that this is the case.

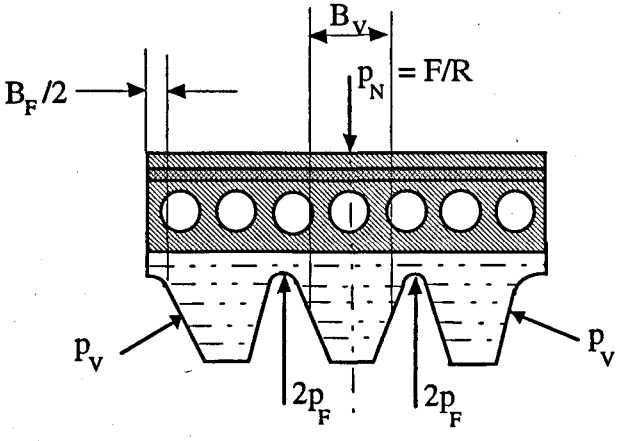


**Fig. 3.1 Flat belt part and v-belt part of of v-ribbed belt load**

This gives

$$x_V = x_F = x \tag{3.1}$$

and

$$F = F_F + F_V \tag{3.2}$$

where, $F_F$ = flat belt part tension and $F_V$ =v-belt part tension.

## 3.2 Equilibrium Equations

We consider the equilibrium for v-ribbed belt as a combination of flat and v-belt theory from sections (2.2,2.3). Fig. 3.2 and 3.3 show the forces acting on a part of a v-ribbed belt in the groove of a pulley. $p_F$ and $p_V$ are distributed forces which are taken by the rib bottom and rib side.

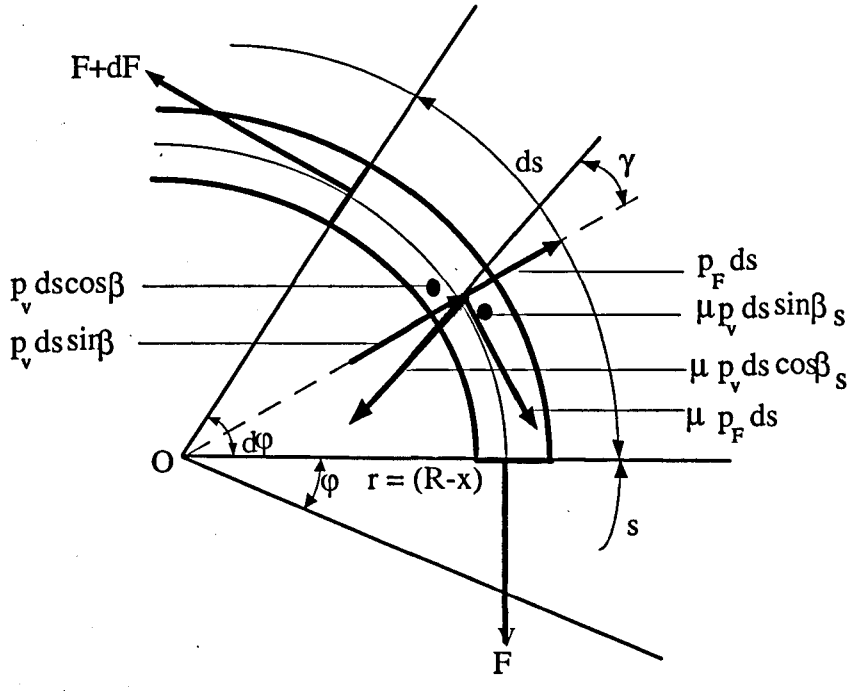


**Fig. 3.2 Forces acting on a v-ribbed belt element**

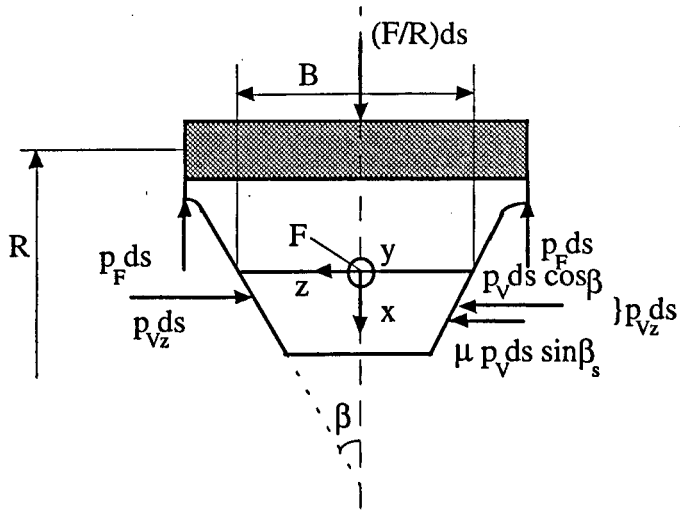


**Fig. 3.3 Perpendicular forces acting on a v-ribbed belt cross-section**

The equilibrium of the belt element *ds* along the belt gives

$$dF - 2\mu\ p_V\, ds \cos\beta_s \sin\gamma - 2\mu\ p_F\, ds = 0 \tag{3.3}$$

and perpendicular to the belt

$$-F\, d\varphi + 2 p_V\, ds \sin\beta - 2\mu\ p_V\, ds \cos\beta_s \cos\gamma - 2 p_F\, ds = 0 \tag{3.4}$$

put

$$ds = R d\varphi \tag{3.5}$$

then

$$\frac{dF}{R d\varphi} = 2 p_V [\mu \cos\beta_s \sin\gamma\ ] + 2\mu\ p_F \tag{3.6}$$

$$\frac{F}{R} = 2 p_V [\sin\beta - \mu \cos\beta_s \cos\gamma\ ] + 2\ p_F \tag{3.7}$$

## 3.3 Radial Movement

This section deals with theoretical analysis for the flat belt and v-belt parts of a v-ribbed belt radial movement.

### 3.3.1 Radial Movement of V-belt Part, $x_V$

The contributions, $x_{V1}, x_{V2}$ and $x_{V3}$ for v-belt part radial movement will be discussed here one by one by analogy with the discussion of section 2.3.3.1 for v-belts.

#### (i) Axial Component, $x_{V1}$

The axial pressure $P_{Vz}$ is distributed over the groove face. This force causes the belt to reduce its thickness ($B_V$) and to sink into the groove. From the geometry (Fig. 3.4) we have

$$x_{V1} = \frac{\Delta B_V}{2} \cdot \frac{1}{\tan\beta} \tag{3.8}$$

The axial strain ($\Delta B_V / B_V$) resulting from $P_{Vz}$ (Fig. 3.3) is

$$\frac{\Delta B_V}{B_V} = \frac{p_{Vz}}{H_V E_z} \tag{3.9}$$

From equations (3.8,3.9)

$$x_{V1} = \frac{p_{Vz} B_V}{2 H_V E_Z \tan\beta} \tag{3.10}$$

Where $H_V$ is the v-ribbed part thickness. If we write

$$x_{V1} = \frac{2 p_{Vz}}{k_1} \tag{3.11}$$

where $k_1$ is a type of spring constant, then

$$k_1 = \frac{4 \tan\beta \; E_z H_V}{B_V}$$

This equation is the same as $x_1$ for v-belt theory. In the case of a v-ribbed belt, rubber is not combined with fibre, therefore it can be considered as a homogeneous material. Then, $E_x = E_z = E$ and

$$k_1 = \frac{4 \tan\beta \, E \cdot H_V}{B_V} \tag{3.12}$$

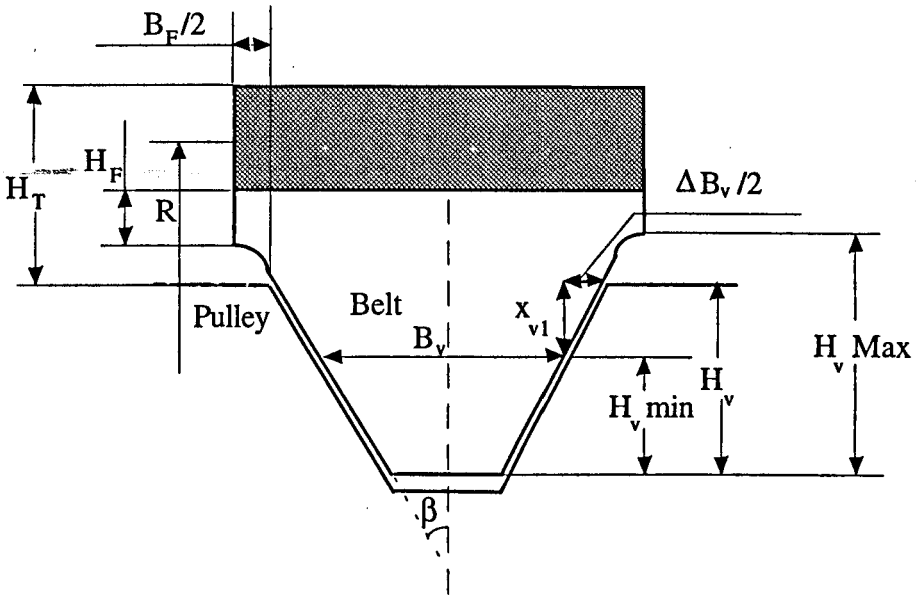


**Fig. 3.4 Geometry of radial movement and axial strain**

Furthermore there is a small difference concerning belt depth ( $H_V$ ) when dealing with a v-ribbed belt. A v-belt has a constant depth. But depth of a v-ribbed belt ( $H_V$ ) increases with radial movement (Fig. 3.4), or

$$H_V = \text{constant} \quad \text{for v-belt}$$

$$H_V = H_{Vm} + x \quad \text{for v-ribbed belt}$$

where $H_{Vm}$ is the minimum or no load depth. It will be shown (section 5.2.2) that for a k-section standard v-ribbed belt we can neglect the effect of variable depth, if we use mean depth value for $H_V$. Then

$$H_V = \frac{H_{VM} + H_{Vm}}{2} \tag{3.13}$$

Here $H_{VM}$ is the maximum depth (Fig. 3.4). Consider equations (2.22,2.24) from v-belt theory

$$p_{Vz} = p_V(\cos\beta + \mu \sin\beta_s)$$

$$\frac{F_V}{R} = 2p_V(\sin\beta - \mu \cos\beta_s \cos\gamma)$$

then we can write

$$x_{V1} = \frac{F_V f(\gamma)}{Rk_1} \tag{3.14}$$

where,

$$f(\gamma) = \frac{\cos\beta + \mu \sin\beta_s}{\sin\beta - \mu \cos\beta_s \cos\gamma}$$

**(ii) Radial Component, $x_{V2}$**

The distributed force *F/R* on the top compresses the belt. This makes the rubber a little wider and thus prevents inward motion caused by the force *F*. The contribution (similar to $x_{V1}$), can be written

$$x_{V2} = \frac{\Delta B_V}{2} \cdot \frac{1}{\tan\beta} \tag{3.15}$$

The axial strain ($\Delta B_V / B_V$) from the Poisson effect is

$$\frac{\Delta B}{B} = \frac{F_V}{2RBE} \cdot \nu \tag{3.16}$$

where $\nu$ is Poisson's ratio. If we write

$$x_{V2} = -\frac{F_V}{Rk_2} \tag{3.17}$$

then

$$k_2 = -\frac{4E\tan\beta}{\nu} \tag{3.18}$$

where $k_2$ is a kind of spring constant. Gerbert [3] in the case of v-belt, made a rough estimation for $k_2$, when thickness and width are about the same and the cord is placed on the top of the belt. He estimated $k_1 / k_2 = 0.5$ for this case. In the later papers [27,36] for a similar belt this figure is near 1.0. For v-ribbed belt from equations (3.12 and 3.18)

$$\frac{k_1}{k_2} = -\frac{H_V \cdot \nu}{B_V}$$

Considering Fig. 2.14 and putting $H_V = 2.4mm$, $B_V = 1.78mm$ and $\nu = 0.5$ it can be estimated $k_1 / k_2 = 0.67$.

### (iii) Longitudinal Component, $x_{V3}$

The cord and rubber are stretched by the force *F*. The belt becomes narrower and sinks into the groove. Its contribution to the radial movement is

$$x_{V3} = \frac{F}{k_3} \tag{3.19}$$

where $k_3$ is a spring constant depending on Poison's ratio $\nu$. If this is matched by strain resulting from the radial movement $x_{V3}$ [3]

$$k_3 = \frac{2c \tan \beta}{\nu \ B_V} \tag{3.20}$$

and

$$x_{V3} = \frac{F}{k_3} \tag{3.21}$$

Cowburn [1] showed that the contribution of $k_3$ on total radial movement is very small. Therefore it can be neglected. Then

$$x_{V3} \approx 0$$

From these observations and putting $x_{V3} = 0$, the total radial movement for v-belt part of v-ribbed belt is

$$x_V = \frac{F_V}{R} \cdot \frac{1}{k_{V(\gamma)}} \tag{3.22}$$

where,

$$k_{V(\gamma)} = \frac{1}{[\frac{f(\gamma)}{k_1} - \frac{1}{k_2}]} \tag{3.23}$$

### 3.3.2 Radial Movement of Flat Belt Part, $x_F$

Flat belt part of the v-ribbed belt is subjected to a radial load $F_F / R$, when it is pressed against the rib of the pulley with pitch radius $R$. The compression is

$$x_F = \frac{1}{k_F} \cdot \frac{F_F}{R} \tag{3.24}$$

where $F_F / R = 2p_F$ and $k_F$ is radial spring stiffness.

The radial strain (Fig. 3.4) resulting from $p_F$ is

$$\frac{x_F}{H_F} = \frac{2p_F}{B_F E} \tag{3.25}$$

then

$$x_F = \frac{2p_F}{E} \cdot \frac{H_F}{B_F} \tag{3.26}$$

From equations (3.25 and 3.26)

$$k_F = \frac{B_F E}{H_F} \tag{3.27}$$

From equations (3.12 and 3.27)

$$\frac{k_1}{k_F} = 4 \tan\beta \cdot \frac{H_V \cdot H_F}{B_V \cdot B_F}$$

Considering the geometry of v-ribbed belt and putting $H_F \cong B_F$, roughly it can be estimated $k_1 / k_F = 2$. Substituting $x_V$ and $x_F$ (from equations 3.22,3.24) into equation 3.1 gives

$$\frac{F_F}{k_F} = \frac{F_V}{k_{V(\gamma)}} \tag{3.28}$$

Consider equation (3.2), then

$$x = \frac{F}{R} \cdot \frac{1}{k_{V(\gamma)} + k_F} \tag{3.29}$$

At origin point $S$ (see next section)

$$x_s = \frac{F}{R} \cdot \frac{1}{k_V + k_F} \tag{3.30}$$

For the v-ribbed belt we can write

$$x_s = \frac{F}{R} \cdot \frac{1}{k_{VR}} \tag{3.31}$$

where $k_{VR}$ is total radial spring stiffness for v-ribbed belt.

$$k_{VR} = k_V + k_F \tag{3.31a}$$

Now the speed loss (slip) can be determined by

$$s = \frac{F_t - F_r}{c} + \frac{F_t - F_r}{k_{VR} R^2} \tag{3.32}$$

Here the effect of shear deflection and seating /unseating arcs have not been considered.

## 3.4 Basic Equations

In our model, which can be justified by experiment (section 5.2.1), we assume a v-ribbed belt is a flat belt and a v-belt with same amount of radial movement, i.e.

$$x_V = x_F = x \tag{3.33}$$

If we recall equation (2.22) for v-belt

$$\frac{F_V}{R} = 2p_V(\sin\beta - \mu\cos\beta_s\cos\gamma)$$

Then from equations (3.22, 3.25,3.26, 3.28)

$$\frac{2p_V(\sin\beta - \mu\cos\beta_s\cos\gamma)}{k_{V(\gamma)}} = \frac{2p_F}{k_F} \tag{3.34}$$

or

$$p_F = p_V(\sin\beta - \mu\cos\beta_s\cos\gamma)\cdot\frac{k_F}{k_{V(\gamma)}} \tag{3.35}$$

Put $p_F$ in equations (3.6, 3.7)

$$\frac{dF}{Rd\varphi} = 2p_V(\mu\cos\beta_s\sin\gamma) + 2\mu\ p_V(\sin\beta - \mu\cos\beta_s\cos\gamma)\cdot\frac{k_F}{k_{V(\gamma)}} \tag{3.36}$$

$$\frac{F}{R} = 2p_V(\sin\beta - \mu\cos\beta_s\cos\gamma) + 2\,p_V(\sin\beta - \mu\cos\beta_s\cos\gamma)\cdot\frac{k_F}{k_{V(\gamma)}} \quad (3.37)$$

Dividing the equation (3.36) by (3.37) we have a new modification to Euler's equation for v-ribbed belt.

$$\frac{1}{F}\cdot\frac{dF}{d\varphi} = \frac{\dfrac{\mu\cos\beta_s\sin\gamma}{\sin\beta - \mu\cos\beta_s\cos\gamma} + \mu\cdot\dfrac{k_F}{k_{V(\gamma)}}}{1+\dfrac{k_F}{k_{V(\gamma)}}} \quad (3.38)$$

This equation is for the driving pulley. In the case of the driven pulley the equation (3.6) becomes

$$\frac{dF}{Rd\varphi} = 2p_V[\mu\cos\beta_s\sin\gamma] - 2\mu p_F$$

Therefore we have

$$\frac{1}{F}\cdot\frac{dF}{d\varphi} = \frac{\dfrac{\mu\cos\beta_s\sin\gamma}{\sin\beta - \mu\cos\beta_s\cos\gamma} - \mu\cdot\dfrac{k_F}{k_{V(\gamma)}}}{1+\dfrac{k_F}{k_{V(\gamma)}}} \quad (3.39)$$

Equations (3.38 and 3.39) are for a v-ribbed belt with rib bottom / groove tip contact over whole arc of wrap. In these equations if we put $k_F = 0$, it will reduce to equation (2.23) for v-belt and it is applicable to a v-ribbed belt without rib bottom contact.

At the boundary between the idle and active arcs (point *S*) the sliding angle $\gamma = 180°$. If we assume this point as an origin the variables referred to this point will be $F_s, F_{Vs}, F_{Fs}, x_s, x_{Vs}, x_{Fs}, \varphi_s$ and $\gamma = 180°$.

Introduce non-dimensional values:

$$\frac{F}{F_s} = F_o \qquad \textit{belt tension}$$

$$\frac{F_V}{F_s} = F_{Vo} \qquad \textit{v-belt part of v-ribbed belt tension}$$

$$\frac{F_F}{F_s} = F_{Fo} \qquad \textit{flat belt part of v-ribbed belt tension}$$

$$\frac{x}{x_s} = x_o \qquad \textit{radial movement}$$

$$\frac{x_V}{x_s} = x_{Vo} = x_o \qquad \textit{v-belt part of v-ribbed belt radial movement}$$

$$\frac{x_F}{x_s} = x_{Fo} = x_o \qquad \textit{flat belt part of v-ribbed belt radial movement}$$

Equations (3.29,3.38) in non-dimensional form will be

$$x_o = F_o\left(\frac{k_V + k_F}{k_{V(\gamma)} + k_F}\right) \tag{3.41}$$

$$\frac{dF_o}{d\varphi} = F_o h(\gamma) \tag{3.42}$$

where

$$h(\gamma) = \frac{g(\gamma) \pm \mu \dfrac{k_F}{k_{V(\gamma)}}}{1 + \dfrac{k_F}{k_{V(\gamma)}}}$$

$$g(\gamma) = \frac{\mu \cos\beta_s \sin\gamma}{\sin\beta - \mu \cos\beta_s \cos\gamma} \tag{3.43}$$

Apply $F = F_F + F_V$ and put $x_V = x_F = x$, then we have the following equations for belt tensions of flat belt part and v-belt part of a v-ribbed belt.

$$F_F = F \cdot \frac{k_F}{k_{V(\gamma)} + k_F} \tag{3.44}$$

$$F_V = F \cdot \frac{k_{V(\gamma)}}{k_{V(\gamma)} + k_F} \tag{3.45}$$

Dividing the equations (3.44,3.45) by $F_S$ these equations in non-dimensional form are

$$F_{Fo} = F_o \cdot \frac{k_F}{k_{V(\gamma)} + k_F} \tag{3.46}$$

$$F_{Vo} = F_o \cdot \frac{k_{V(\gamma)}}{k_{V(\gamma)} + k_F} \tag{3.47}$$

Sliding condition equation for v-belt (2.36) is also valid for v-ribbed belt.

$$\frac{d(\frac{x}{x_s})}{d\varphi}\tan\gamma = 1-(\frac{x}{x_s})+\frac{1-(\frac{F}{F_s})}{c_o}$$

In the case of v-ribbed belt $F/F_s$, must be replaced by $F_V/F_{Vs}$. Then

$$\frac{d(x_o)}{d\varphi}\tan\gamma = 1-(x_o)+\frac{1-(\frac{F_V}{F_{Vs}})}{c_o} \tag{3.48}$$

From equation (3.45) and considering origin

$$\frac{F_V}{F_{Vs}} = F_o \cdot \frac{k_{V(\gamma)}}{k_F + k_{V(\gamma)}} \cdot \frac{k_F + k_V}{k_V} \tag{3.49}$$

### 3.4.1 V-ribbed Belt Equations Solution

Equations (3.41, 3.42, 3.46, 3.47 and 3.48) and $\tan\beta_s = \tan\beta\cos\gamma$, form 6 equations for the variation of $F_o, F_{Vo}, F_{Fo}, x_o, \gamma$, and $\beta_s$ with $\varphi$. These equations also were solved numerically by the help of Maple V (mathematical standard library software), [Appendix A]. It requires input of the physical and geometrical properties $c_o, k_V, k_F, \mu$ and $\beta$.

Solutions for the driven pulley are shown in Figs. 3.5 and 3.6 and for driving in Figs. 3.7 and 3.8. These are for two different sizes of pulleys, $d_e$=*45mm* ($k_V = 117N/mm^2$) and $d_e$=*80mm* ($k_V = 76N/mm^2$). V-belt results are also represented for comparing with v-ribbed belt solutions. Numerical results are presented in tables 3.1 and 3.2. The belt properties are taken from chapter five ($k_V = 117N/mm^2$ and $76N/mm^2$, $k_F = 20N/mm^2$ $\beta = 20°$ and $\mu = 0.32$).

Figs. 3.5a and 3.6a show the force variation $F / F_s$ against the active arc length $\varphi$ for driven pulley and Figs 3.7a and 3.8a for driving pulley. Values of $\varphi$ above 180 degrees are in the region which causes extensive slip of the belt. It can be seen from these figures that for any particular force ratio $F / F_s$ the driving pulley has a smaller value of $\varphi$ and therefore a higher capacity, same as v-belt theory.

The sliding angle $\gamma$ in Figs. 3.5b and 3.6b for driven pulley and 3.7b and 3.8b for driving pulley starts from 180 degrees in both cases, this is the idle arc value. On the driven pulley $\gamma$ decreases (the belt leads the pulley) until skidding occurs. On the driving pulley $\gamma$ increases (the belt lags the pulley).

The radial movement for driven and driving are shown in Figs. 3.5c to 3.8c. On the driven pulley radial movement increases from its idle arc value $x / x_s$ and the belt moves into the groove. On the driving pulley the radial movement again is slightly inwards, at the beginning. The amount of radial movement as compared with the driven pulley is small.

It can be seen that for three variables $F_o$, $x_o$ and $\gamma$ the trends are almost same, but v-ribbed belt has smaller value for radial movement as compared with v-belt, specially for driving pulley.

In practice rib bottom / groove tip contact in a v-ribbed belt occurs over some part of the wrap angle. Due to wear and running time of the belt and its fitting on the pulley groove every particular belt has a unique value of radial movement $x$, related to the start of contact. In this case for that part of wrap angle without contact, the v-belt theory can be applied. For the remaining part of wrap angle the v-ribbed belt theory is applicable. However, this point is a turning point for v-ribbed belt drives. Gerbert [34] attempted to develop a theoretical model for a mixed contact, and dealt only with the maximum coefficient of traction (see section 2.4.3). But, theoretical modelling for the belt tension ratio in the case of mixed contact, is still missing. In this case the wrap angle is divided into two parts.

$$\alpha = \varphi_F + \varphi_V$$

where $\varphi_V$ is the length of that part of wrap angle without rib bottom / groove tip contact and $\varphi_F$ is with contact. Before the beginning of contact, we can write (from equation 2.23 and 3.43)

$$\frac{1}{F)_{F_r - F_L}} \cdot \frac{dF}{d\varphi)_{0-\varphi_L}} = g(\gamma) \qquad \text{for driven pulley}$$

$$\frac{1}{F)_{F_i - F_L}} \cdot \frac{dF}{d\varphi)_{0-\varphi_L}} = g(\gamma) \qquad \text{for driving pulley} \qquad (3.50a)$$

where $F_L$ is the belt tension and $\varphi_L$ is angular position at the beginning of the contact. For driven pulley the variation of sliding angle $\gamma$, decreases from 180 degrees and for driving pulley increases from 180 degrees. Therefor the right hand side of the above equations are negative (driven pulley) or positive (driving pulley). After contact the belt tension varies according to the equation (3.38, 3.39 and 3.43).

$$\frac{1}{F)_{F_L - F_i}} \cdot \frac{dF}{d\varphi)_{\varphi_L - 180°}} = \frac{g(\gamma) - \mu \cdot \frac{k_F}{k_{V(\gamma)}}}{1 + \frac{k_F}{k_{V(\gamma)}}} \qquad \text{for driven pulley}$$

$$\frac{1}{F)_{F_L - F_r}} \cdot \frac{dF}{d\varphi)_{\varphi_L - 180°}} = \frac{g(\gamma) + \mu \cdot \frac{k_F}{k_{V(\gamma)}}}{1 + \frac{k_F}{k_{V(\gamma)}}} \qquad \text{for driving pulley} \qquad (3.50b)$$

By the help of NCLDM the beginning of the rib bottom / groove tip contact around the arc of wrap $\varphi_L$, can be determined (see section 6.2). Then the tension ratio for a v-ribbed with mixed contact can be decided from figures 2.10 and 2.11 (solutions to v-belt equations for driven and driving pulleys respectively) and figures 3.5 to 3.8 (solutions to v-ribbed belt equations).

The total traction force per unit length along the belt acting on rubber between cord and pulley is $T = dF / Rd\varphi$ (equation 2.56a). From equation (3.36) we can write

$$T = 2\mu p_V[(\cos\beta_s \sin\gamma) + (\sin\beta - \mu\cos\beta_s \cos\gamma)\cdot\frac{k_F}{k_{V(\gamma)}}] \tag{3.51}$$

The traction force per unit length at v-rib part of rubber is (from equation 2.21)

$$T_V = 2\mu p_V(\cos\beta_s \sin\gamma) \tag{3.52}$$

The traction force per unit length at flat part of rubber (see Fig. 3.1) is (from equation 3.35)

$$T_F = 2\mu p_F = 2\mu p_V(\sin\beta - \mu\cos\beta_s \cos\gamma)\cdot\frac{k_F}{k_{V(\gamma)}} \tag{3.53}$$

From equation (3.37) the total normal load per unit length $p_N$, (vertical equilibrium) is

$$p_N = 2p_V(\sin\beta - \mu\cos\beta_s \cos\gamma)(1+\frac{k_F}{k_{V(\gamma)}}) \tag{3.54}$$

Normal load per unit length of v-belt part is

$$p_{VN} = 2p_V(\sin\beta - \mu\cos\beta_s \cos\gamma) \tag{3.55}$$

Normal load per unit length of flat belt part is

$$p_{FN} = p_F = 2p_V(\sin\beta - \mu\cos\beta_s \cos\gamma)(\frac{k_F}{k_{V(\gamma)}}) \tag{3.56}$$

The main difference between v-belt and v-ribbed belt theory is appearing $k_F$ in the equations after rib bottom / groove tip interaction take place. This causes the belt total traction $T$ to be divided into two components $T_F$ and $T_V$, tractions of flat and v-belt parts of a v-ribbed belt (Figs. 3.9 and 3.10), and total normal load to be divided into two companents of flat and v-belt parts (Figs. 3.11 and 3.12). The variation of $T_F / T$ and $T_V / T$ and $p_{NF} / p_N$ and $p_{NV} / p_N$ across the active arc of contact $\varphi$ depends on the value of $k_F / k_V$ and sliding angle $\gamma$. From equation (3.43, 3.51, 3.52 and 3.53) we can write

$$\frac{T_V}{T} = \frac{g(\gamma)}{\mu\cdot\frac{k_F}{k_{V(\gamma)}} + g(\gamma)} \tag{3.57}$$

$$\frac{T_F}{T}=\frac{\mu\cdot\frac{k_F}{k_{V(\gamma)}}}{\mu\cdot\frac{k_F}{k_{V(\gamma)}}+g(\gamma)} \tag{3.58}$$

and from equations (3.54, 3.55 and 3.56)

$$\frac{p_{VN}}{p_N}=\frac{k_{V(\gamma)}}{k_{V(\gamma)}+k_F} \tag{3.59}$$

$$\frac{p_{FN}}{p_N}=\frac{k_F}{k_{V(\gamma)}+k_F} \tag{3.60}$$

$(T_V-T_F)$ causes an internal shear force between flat belt part and v-belt part of v-ribbed belt at rubber between cord and pulley.

When the belt approaches the whole skidding condition (maximum traction), the sliding angle $\gamma\cong 90°$ and $g(\gamma)=\mu/\sin\beta$. Then we can write

$$\frac{T_V}{T})_{\gamma=90}=\frac{1}{\frac{k_F}{k_{V(\gamma=90)}}\cdot\sin\beta+1} \tag{3.61}$$

$$\frac{T_F}{T})_{\gamma=90}=\frac{\frac{k_F}{k_{V(\gamma=90)}}\cdot\sin\beta}{\frac{k_F}{k_{V(\gamma=90)}}\cdot\sin\beta+1} \tag{3.62}$$

Put $\gamma=90°$ into equations (2.23 for v-belt or v-ribbed belt without rib bottom contact and 3.38 for v-ribbed belt with rib bottom contact)

$$\frac{1}{F}\cdot\frac{dF}{d\varphi}=\mu_V \tag{3.63}$$

$$\frac{1}{F}\cdot\frac{dF}{d\varphi}=\mu_F \tag{3.64}$$

where

$$\mu_V=\mu\cdot\frac{1}{\sin\beta} \tag{3.65}$$

$$\mu_F=\mu\cdot\frac{\frac{1}{\sin\beta}+\frac{k_F}{k_{V(\gamma=90)}}}{1+\frac{k_F}{k_{V(\gamma=90)}}} \tag{3.66}$$

Then from equations (3.61 and 3.62) we have

$$\frac{T_V}{T})_{\gamma=90} = \frac{\mu_V}{\mu \cdot \frac{k_F}{k_{V(\gamma=90)}} + \mu_V} \tag{3.67}$$

$$\frac{T_F}{T})_{\gamma=90} = \frac{\mu \cdot \frac{k_F}{k_{V(\gamma=90)}}}{\mu \cdot \frac{k_F}{k_{V(\gamma=90)}} + \mu_V} \tag{3.68}$$

Equations (3.56 to 3.68) are related to maximum traction (skidding condition) at a v-ribbed belt with rib bottom / groove tip contact at whole of arc of wrap angle. This means that rib bottom contact will occur at $p_{N_L} = F_L / R = 0$ (see section 2.4.3 about Gerbert's theoretical model for v-ribbed belt). Put $P_{N_L} = 0$ in equations (2.54, 2.58a and 2.61)

$$\frac{T_V}{T} = \frac{\mu_V}{\mu_V + \mu} \tag{3.69}$$

$$\frac{T_F}{T} = \frac{1}{\mu_V + \mu} \tag{3.70}$$

$$\mu_V = \mu \cdot \frac{1}{\sin\beta} \tag{3.71}$$

$$\mu_F = \mu \cdot \frac{\frac{1}{\sin\beta} + 1}{2} \tag{3.72}$$

Equations (3.69 to 3.72) can be compared with equations (3.65 to 3.68). It can be seen that Gerbert's assumption about the increasing vertical load to the **same extent** $[2(p_V - p_{V_L}) = \frac{2p_F}{\sin\beta}]$ leads to $k_{V(\gamma=90)} = k_F$. But $k_{V(\gamma=90)}$ and $k_F$ depend on fit between rib and groove, wear and material properties, therefore it not obvious if these are equal. We will discuss more about the experimental results at chapters 5, 6 and 7.

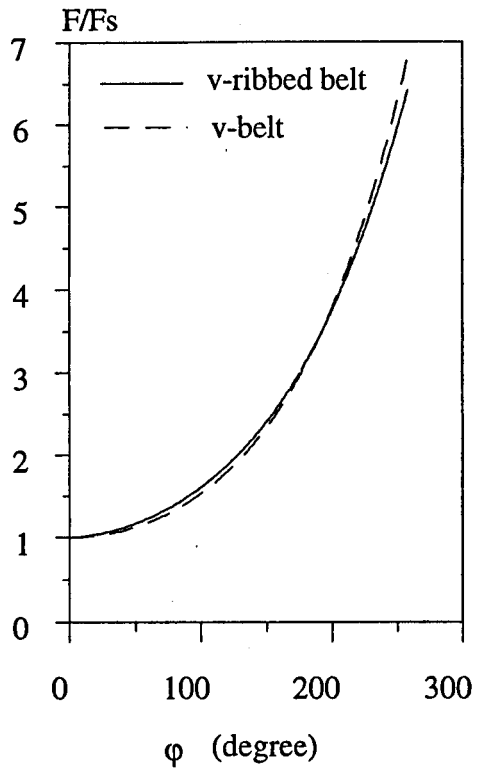


(a) Relative force

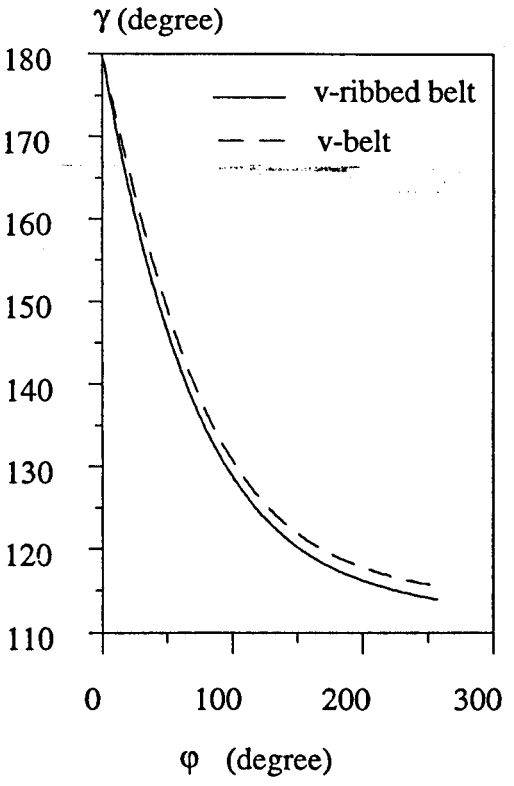


(b) Sliding angle (degree)

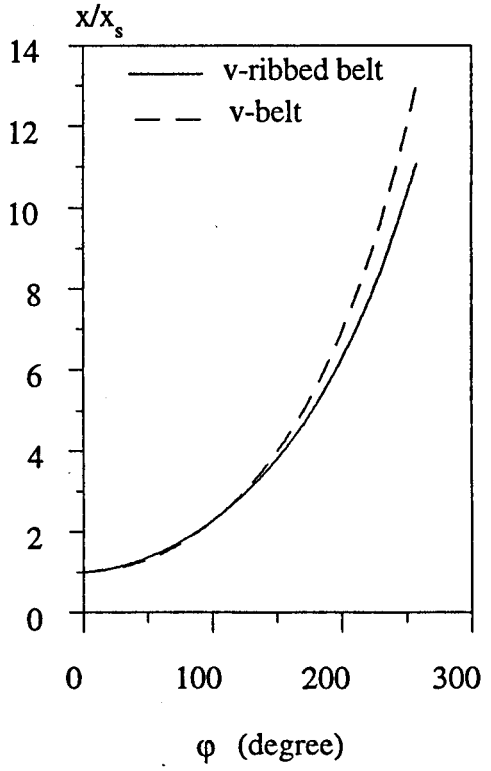


(c) Relative radial movement

**Fig. 3.5 Solution to v-ribbed belt theory for driven pulley (de=45mm)**

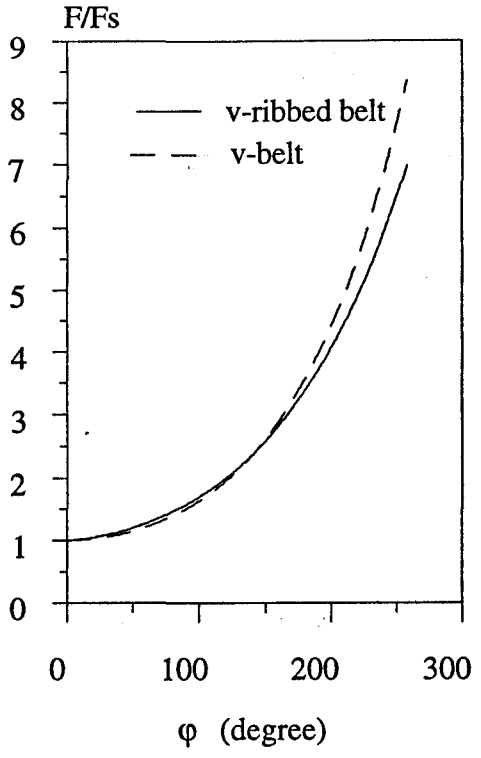


(a) Relative force

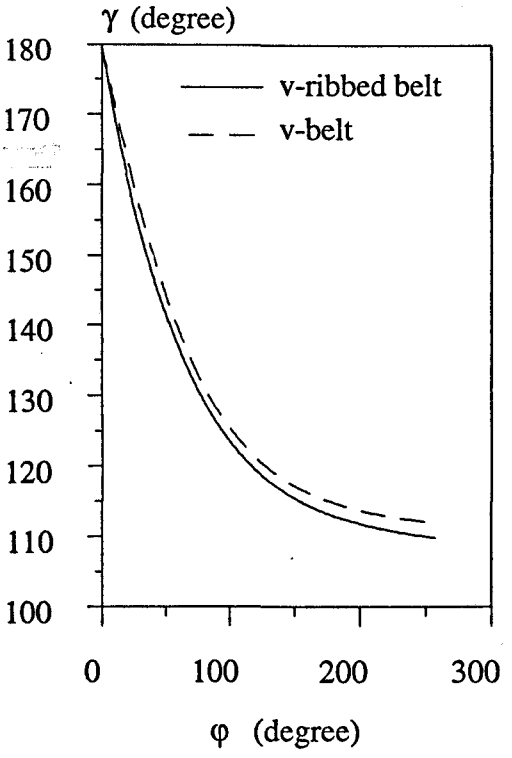


(b) Sliding angle (degree)

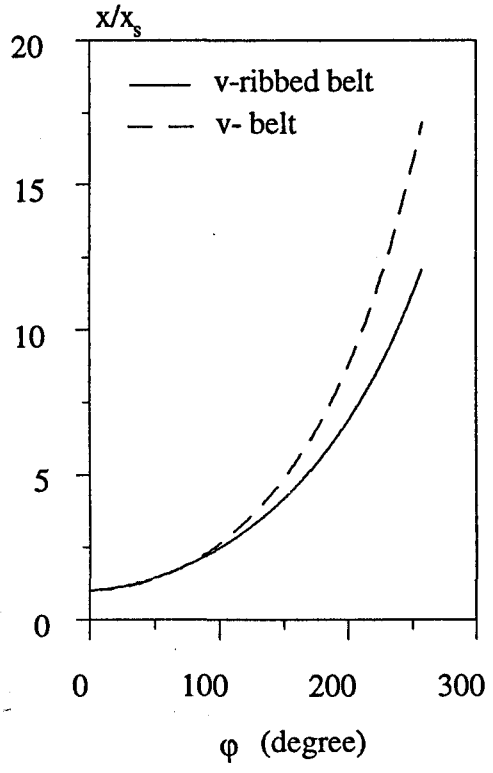


(c) Relative radial movement

**Fig. 3.6 Solution to v-ribbed belt theory for driven pulley (de=80mm)**

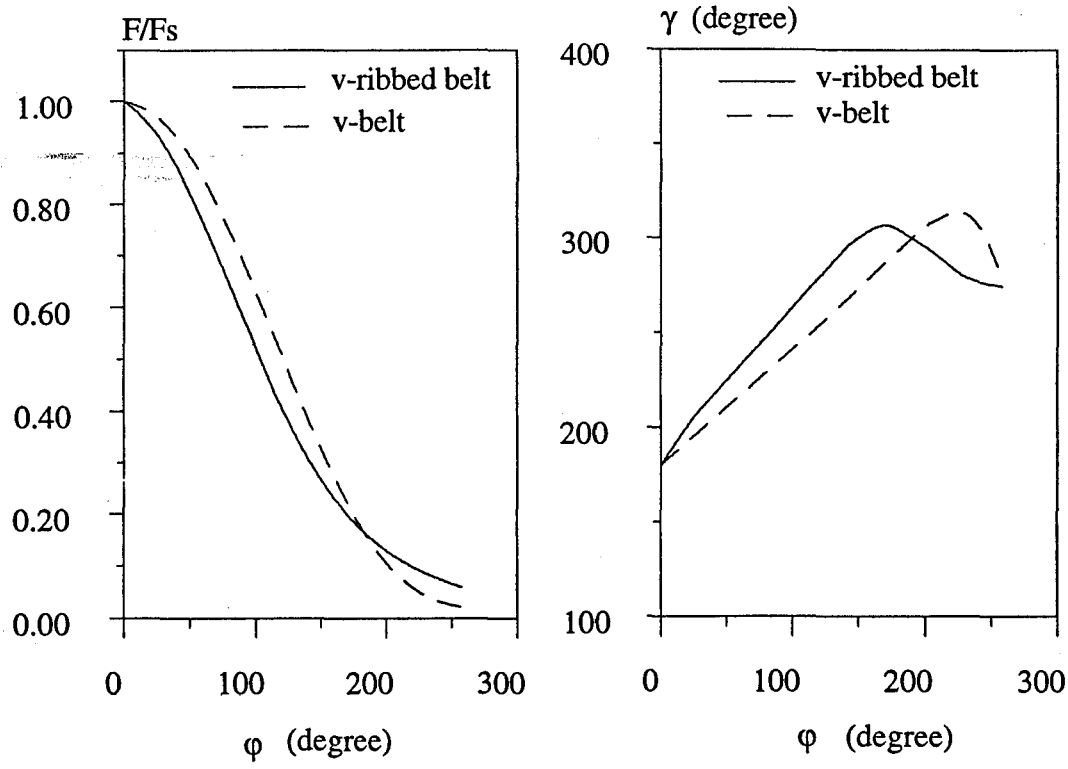


**(a) Relative force** **(b) Sliding angle (degree)**

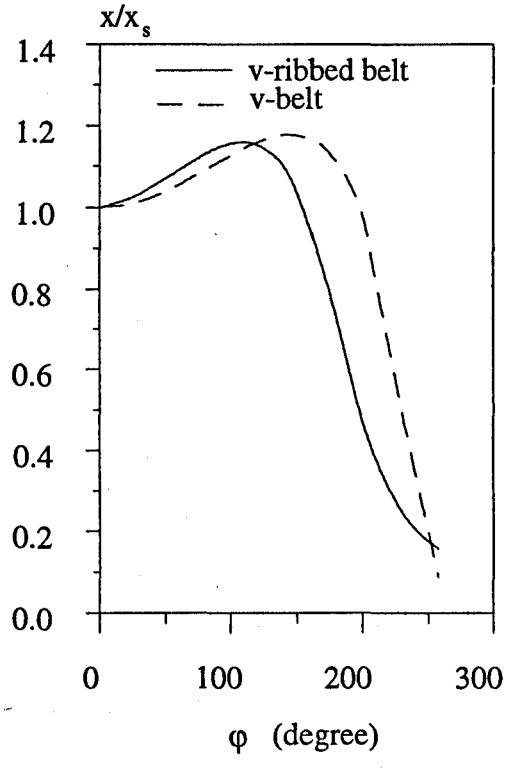


**(c) Relative radial movement**

**Fig. 3.7 Solution to v-ribbed theory for driving pulley ($d_e$=45mm)**

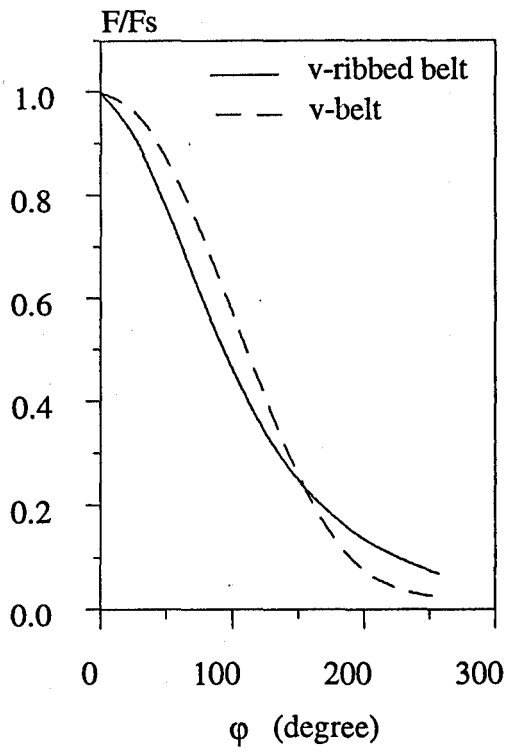


(a) Relative force

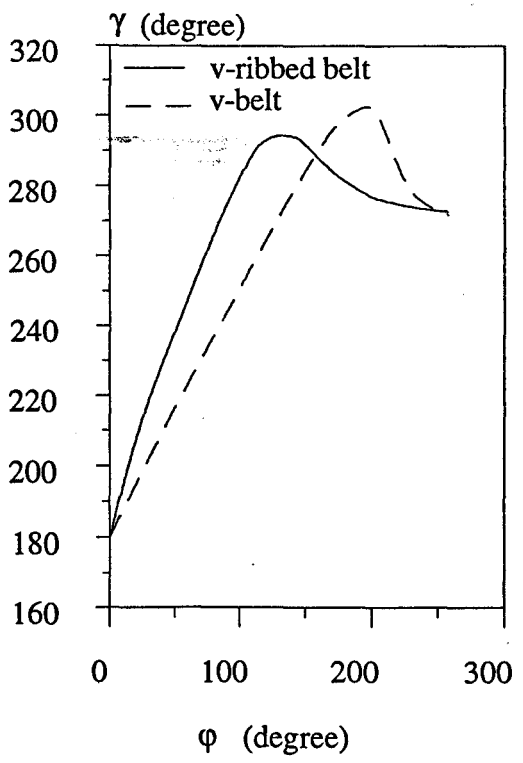


(b) Sliding angle (degree)

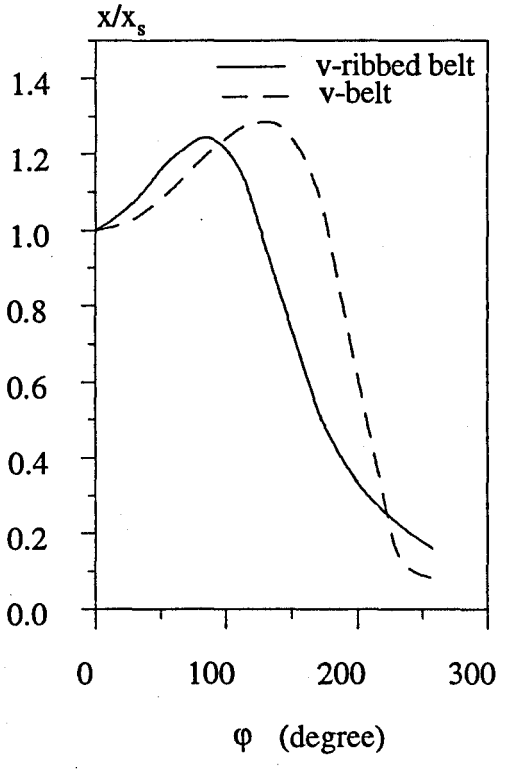


(c) Relative radial movement

**Fig. 3.8 Solution to v-ribbed theory for driving pulley ($d_e$=80mm)**

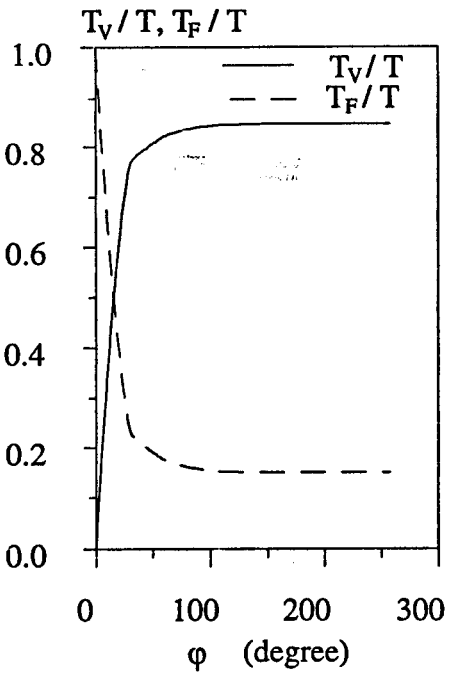


(a) $k_v = 117\,N/mm^2$

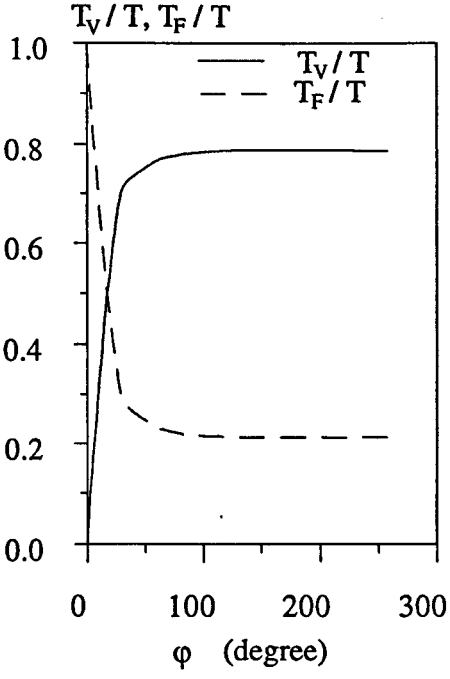


(b) $k_v = 76\,N/mm^2$

**Fig. 3.9 Variation of belt tractions of flat and v- belt parts of a v-ribbed belt against active arc for driven pulley**

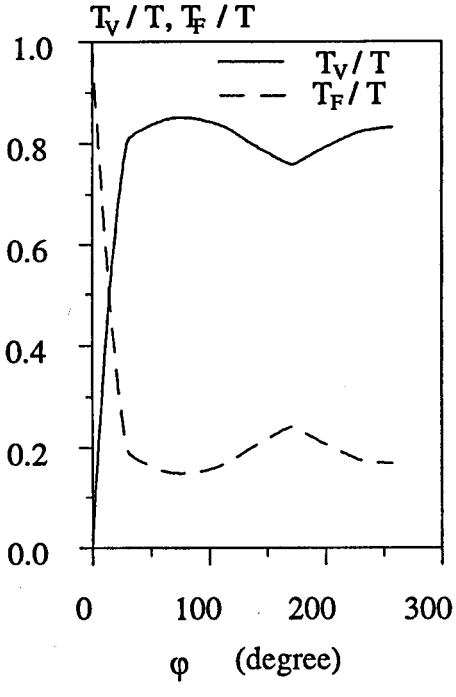


(a) $k_v = 117\,N/mm^2$

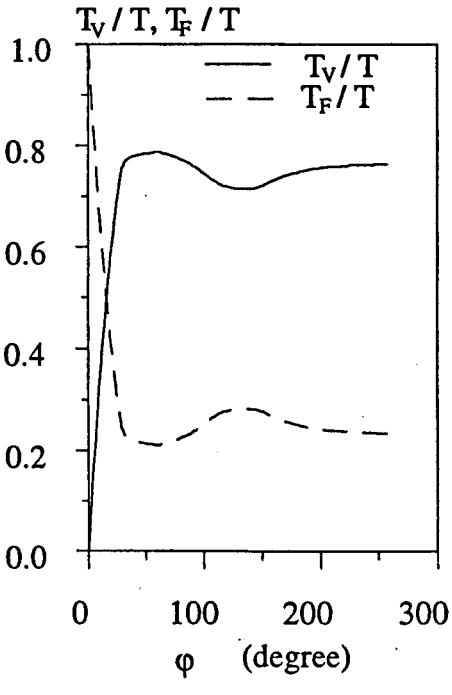


(b) $k_v = 76\,N/mm^2$

**Fig. 3.10 Variation of belt tractions of flat and v- belt parts of a v-ribbed belt against active arc for driving pulley**

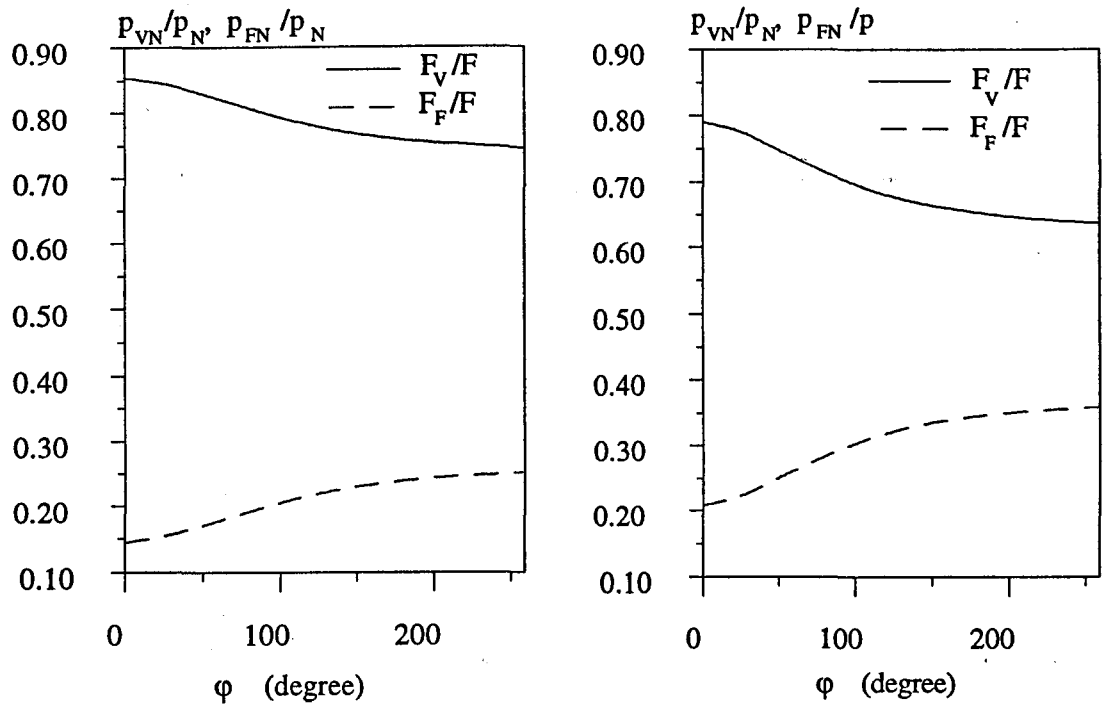


(a) $k_V$=117N/mm$^2$ (b) $k_V$=76N/mm$^2$

**Fig. 3.11 Variation of belt normal load of flat and v- belt parts of a v-ribbed belt against active arc for driven pulley**

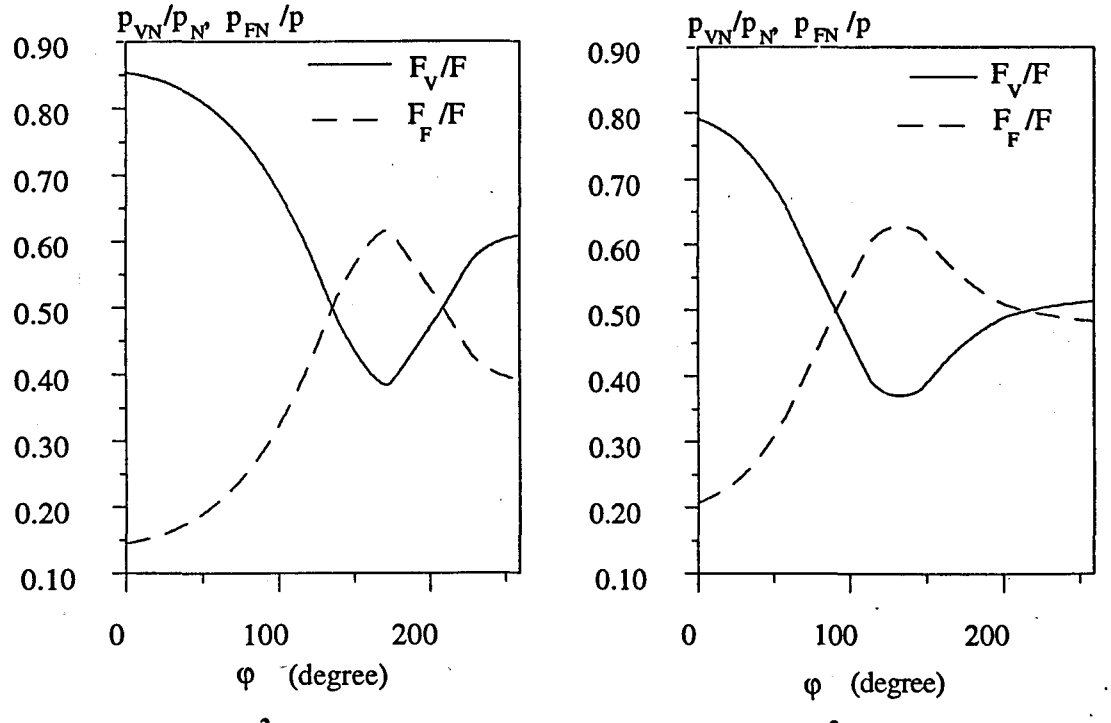


(a) $k_V$=117N/mm$^2$ (b) $k_V$=76N/mm$^2$

**Fig. 3.12 Variation of belt normal load of flat and v- belt parts of a v-ribbed belt against active arc for driving pulley**

### 3.4.2 Non-Linear slip

In the case of the v-ribbed belt the fractional speed loss when an idle arc exists can be determined by equation (3.32), for equal radius pulleys. Similar to v-belt theory, non-linear speed loss when the whole angle of wrap becomes active can be determined by assuming fictitious paths with angles of wrap sufficient greater than $\alpha$ (actual wrap angle) to contain an idle point. Non-linear speed loss can be determined by the equation (2.43) from v-belt theory by replacing $k_V$ by $k_{VR}$.

$$\frac{sc}{(F_t+F_r)}=\frac{F_t/F_r}{(F_t/F_r+1)}\left[\frac{1}{(F/F_s)_{\varphi_o dg}}-\frac{1}{(F/F_s)_{\varphi_o+\alpha,dn}}\right]\left[1+\frac{c}{k_{VR}R^2}\right] \quad (3.73)$$

In Fig. 3.13, $sc/(F_t+F_r)$ is plotted against $\lambda$ for the data in tables 3.1 and 3.2. The ends of the linear slip ranges are shown by the arrows. The v-belt results are also presented in these figures.

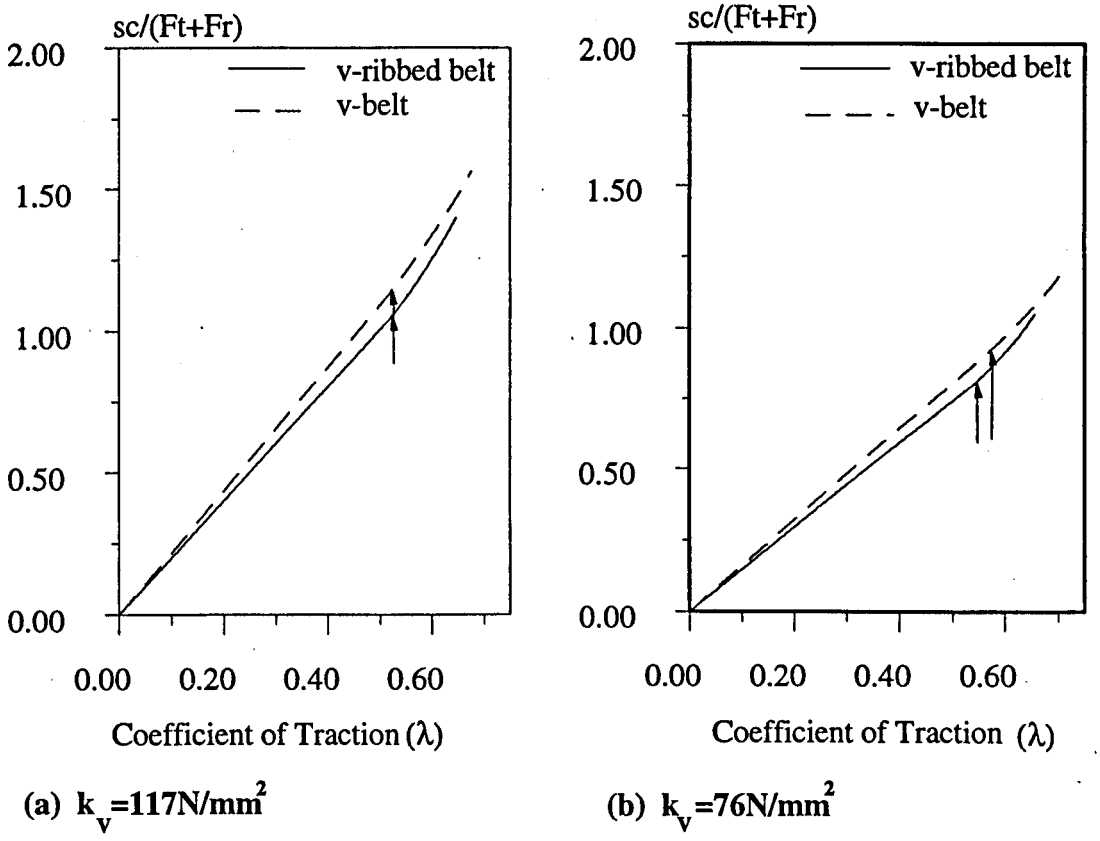


(a) $k_V$=117N/mm$^2$ (b) $k_V$=76N/mm$^2$

**Fig. 3.13 Theoretical slip $sc/(F_t+F_r)$ as a function of traction coefficient**

It can be seen that the slip value of v-ribbed belt is slightly lower than the v-belt, but the difference is not significant. This is same as Hansson's experimental results for v-ribbed belt wedge action (radial movement) and slip [31]. As discussed earlier (2.3.1), his experimental results showed almost no difference between v-belt and v-ribbed belt torque capacity and slip, even for worn v-ribbed belt.

Experimental works and their results will be discussed later (chapter 6 and 7) and it will be shown that it is not possible to predict the start of rib bottom / groove tip contact theoretically due to miss-fitting and wear of any particular v-ribbed belt. This point can be determined experimentally and then it is possible to apply v- or v-ribbed belt theory to the drive for each part.

Table 3.1 Numerical results for v-ribbed belt equations (driven pulley)

(a) driven pulley, $k_v = 117\,N/mm^2$

| active arc length (degree) | relative belt tension (force) | sliding angle (degree) | relative radial move-ment | relative v-belt part normal load | relative flat belt part normal load | relative v-beit part traction | relative flat belt part traction |
|---|---|---|---|---|---|---|---|
| 0.000 | 1 | 180 | 1 | 0 | 1 | .854 | .145 |
| 28.648 | 1.068 | 158.191 | 1.141 | .753 | .247 | .843 | .156 |
| 57.295 | 1.217 | 143.180 | 1.465 | .821 | .179 | .824 | .175 |
| 85.943 | 1.454 | 132.638 | 1.959 | 841 | .159 | .803 | .196 |
| 114.590 | 1.798 | 125.648 | 2.644 | .847 | .153 | .785 | .214 |
| 143.238 | 2.273 | 121.064 | 3.552 | .849 | .150 | .771 | .228 |
| 171.885 | 2.915 | 118.085 | 4.746 | .850 | .149 | .762 | .237 |
| 200.533 | 3.773 | 116.194 | 6.312 | .850 | .149 | .755 | .244 |
| 229.180 | 4.914 | 114.876 | 8.378 | .850 | .149 | .751 | .248 |
| 257.828 | 6.427 | 113.960 | 11.099 | .850 | .149 | .747 | .252 |

(b) driven pulley, $k_v = 76\,N/mm^2$

| active arc length (degree) | relative belt tension (force) | sliding angle (degree) | relative radial move-ment | relative v-belt part normal load | relative flat belt part normal load | relative v-belt part tension | relative flat belt part tension |
|---|---|---|---|---|---|---|---|
| 0.000 | 1 | 180 | 1.000 | 0 | 1 | .791 | 0.208 |
| 28.648 | 1.084 | 154.295 | 1.179 | .694 | .305 | .773 | 0.226 |
| 57.295 | 1.258 | 138.081 | 1.565 | .763 | .237 | .740 | 0.259 |
| 85.943 | 1.529 | 127.252 | 2.133 | .781 | .219 | .709 | 0.290 |
| 114.590 | 1.915 | 120.377 | 2.897 | ..786 | .214 | .684 | 0.315 |
| 143.238 | 2.442 | 116.137 | 3.897 | .787 | .213 | .667 | 0.332 |
| 171.885 | 3.151 | 113.444 | 5.202 | .787 | .213 | .656 | 0.343 |
| 200.533 | 4.092 | 111.725 | 6.903 | .786 | .214 | .648 | 0.351 |
| 229.180 | 5.339 | 110.579 | 9.146 | .786 | .214 | .643 | 0.356 |
| 257.828 | 6.987 | 109.777 | 12.088 | .786 | .214 | .639 | 0.360 |

Table 3.2 Numerical results for v-ribbed belt equations (driving pulley)

(a) driving pulley, $k_v = 117\,N/mm^2$

| active arc length (degree) | relative belt tension (force) | sliding angle (degree) | relative radial move-ment | relative v-belt part normal load | relative flat belt part normal load | relative v-belt part tension | relative flat belt part tension |
|---|---|---|---|---|---|---|---|
| 0.000 | 1 | 180 | 1.000 | 0 | 1 | .854 | .145 |
| 28.648 | .921 | 208.267 | 1.030 | .791 | .209 | .836 | .163 |
| 57.295 | .780 | 229.925 | 1.085 | .843 | .156 | .796 | .203 |
| 85.943 | .608 | 251.582 | 1.141 | .849 | .150 | .726 | .273 |
| 114.590 | .436 | 274.157 | 1.158 | .831 | .168 | .612 | .387 |
| 143.238 | .294 | 296.215 | 1.082 | .790 | .209 | .462 | .537 |
| 171.885 | .195 | 306.815 | 0.824 | .758 | .241 | .383 | .616 |
| 200.533 | .129 | 295.069 | 0.467 | .793 | .206 | .471 | .528 |
| 229.180 | .087 | 279.943 | 0.253 | .823 | .176 | .575 | .424 |
| 257.828 | .059 | 274.500 | 0.158 | .831 | .169 | .609 | .390 |

(b) driving pulley, $k_v = 76\,N/mm^2$

| active arc length (degree) | relative belt tension (force) | sliding angle (degree) | relative radial move-ment | relative v-belt part normal load | relative flat belt part normal load | relative v-belt part tension | relative flat belt part tension |
|---|---|---|---|---|---|---|---|
| 0.000 | 1 | 180 | 1.000 | 0 | 1 | .791 | .208 |
| 28.648 | .900 | 217.263 | 1.072 | .750 | ..249 | .751 | .248 |
| 57.295 | .731 | 245.051 | 1.185 | .787 | .212 | .662 | .337 |
| 85.943 | .545 | 271.177 | 1.243 | .767 | .232 | .524 | .475 |
| 114.590 | .387 | 291.345 | 1.130 | .724 | .275 | .391 | .608 |
| 143.238 | .271 | 293.580 | 0.811 | .717 | .282 | .376 | .623 |
| 171.885 | .191 | 283.610 | 0.509 | .743 | .256 | .444 | .555 |
| 200.533 | .135 | 276.792 | 0.331 | .757 | .242 | .489 | .510 |
| 229.180 | .097 | 274.042 | 0.230 | .762 | .237 | .506 | .493 |
| 257.828 | .069 | 272.610 | 0.160 | .764 | .235 | .514 | .484 |

# CHAPTER FOUR

# BELT TESTING RIG AND INSTRUMENTATION

## 4.1 Introduction

In the following chapter the test rig and attached devices will be described. Experiments were carried out on a dynamometer which was built to test belts. It was used by Cowburn [1] for v-belt experimental investigations. New devices are attached and used to make it more capable for v-ribbed belt tests.

It consisted of two trunnion mounted DC motors regeneratively coupled (Fig.4.1). One was permanently fixed to a bed while the other was free to slide on rails. This enabled a constant tension to be applied to the belt under test. The sliding motor could also be clamped to provide a fixed centre drive arrangement.

The dynamometer was instrumented to measure the speed of both pulleys separately. Torque exerted by the belt on each pulley could also be measured separately.

Radial movement was measured by the help of a Non-Contact Laser Displacement Meter (NCLDM) attached to the fixed motor. An intelligent multi-meter was used for averaging the readings of torques.

## 4.2 Dynamometer

Fig. 4.1 shows the fixed motor *A*, and sliding motor *B*. Two identical 10 kW rated D.C. motors (Mawdsley's Ltd. type 200N) were used, with their shafts facing. The full range of belt length available on the rig was $625 < L < 1375$ mm long, which covers the general automotive range[37,38]. The motors were regeneratively coupled and their roles as generator or motor could be reversed.

They were thyristor controlled (Mawdsley's type DSUA 1717a) and capable of operating at speeds from 600 to 6000 RPM in their rotational direction. The motors were fan cooled but could be driven for short periods without the fans.

The movable motor was mounted on linear bearings (RHP Roundway units Rw-8-s and Rw-8-v) and set to run perpendicular to the fixed motor shaft. Tension forces were applied to the belt by a dead weight and hanger system attached to the sliding motor. The line of action of the force was in line with the pulleys to avoid rotational forces on the sliding motor. A rigid frame supported the motors. This was set on 7 rubber machine mounts (Sunnex Ltd. Model 2) which were height adjustable by 53 mm, allowing the rig to be levelled.

A viscous dash pot (Kinetrol Ltd. Model KD-A300) was connected between the motors, to damp linear vibration.

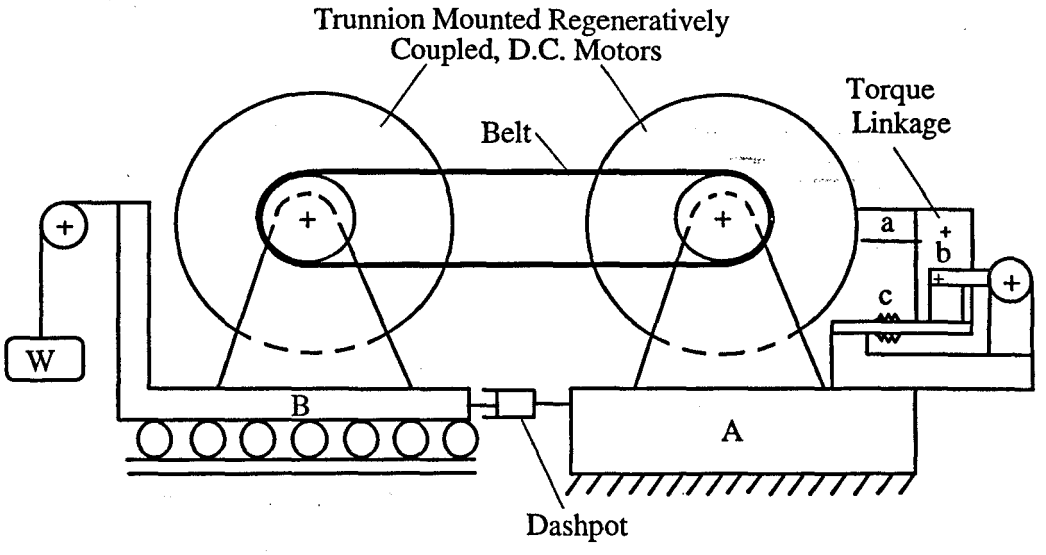


(a)

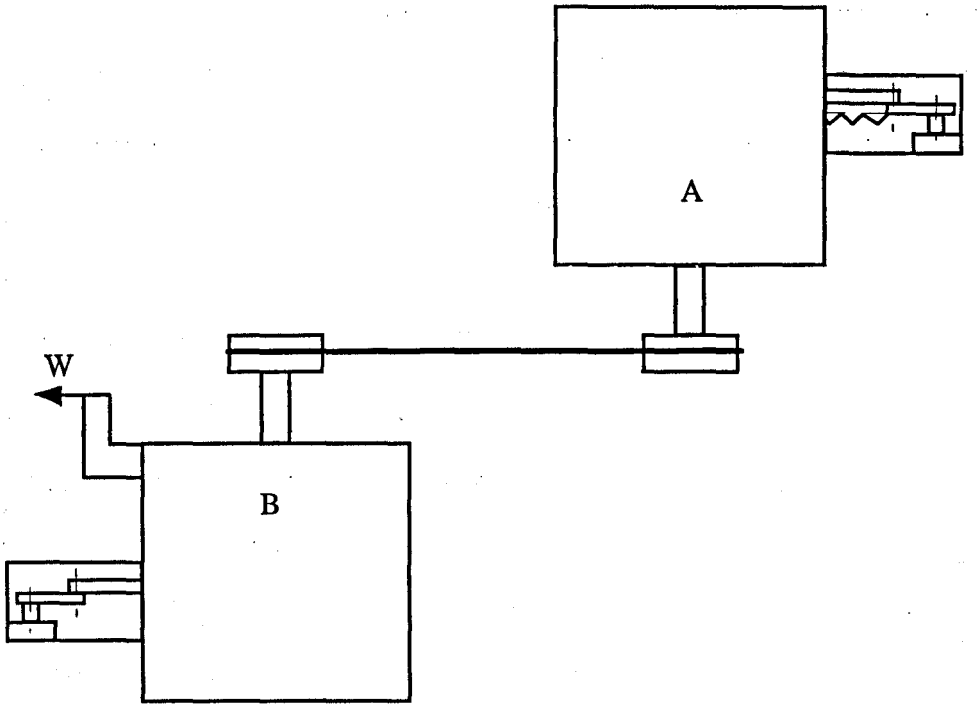


(b)

(Not to Scale)

**Fig 4.1 Schematic of the belt testing rig [1]**

## 4.3 Instrumentation of Dynamometer

The dynamometer was instrumented to measure the values of radial movement, speed and torque. The following section is about the technical specifications of these devices.

### 4.3.1 Non-Contact Laser Displacement Meter

Radial movement is recognised from larger axial force on the driving pulley than that on driven (see 2.2.2). The fundamental difference in action between a flat belt, v-belt and v-ribbed belt drives is their different radial movement performance. Thus it is important to analyse this phenomenon theoretically (see chapter 3) as well as to measure it experimentally. Gerbert [3] measured radial movement of v-belt for two sliding angles $\gamma = 180°$ and $\gamma = 90°$ by a dial gauge for static case. Cowburn [1] carried out the measurement on v-belt by a dial gauge rotating with pulleys at low rotation speed and with no torque transmission case. Hyunsoo Kim et al [39,40] measured the radial movement of a metal v-belt CVT and a rubber v-belt CVT by specially designed displacement sensors and strain gauges. This device was a contact displacement meter.

Non-contact displacement devices were used by some authors [41,42,43,44] for vibration and noise measurements. For the first time a Non-Contact Laser Displacement Meter (NCLDM) has been used in this work for measurement of radial movement of v-ribbed belt.

This equipment (Anritsu Corporation, type KL133B) which uses visible red laser light as the light source, measures the displacement of objects at high precision without contact. It can measures the dimensions of an object, including the height, step difference, width and thickness. The dynamic response of mechanical elements, also can be measured by this equipment.

The equipment consisted of a sensor head containing the optical system, a sensor processing unit for processing the signal from the sensor head, and a display unit for displaying the measured values (Fig. 4.2).

The sensor processing unit was mounted in the rear of the display unit. A three meter signal cable was used to connect the sensor head and sensor processing unit [45].

The repeatability of equipment was $\pm 0.03\%$ of the measuring range, and it had 16 steps of number of averaging. More detailed specifications are shown at [Appendix B and C].

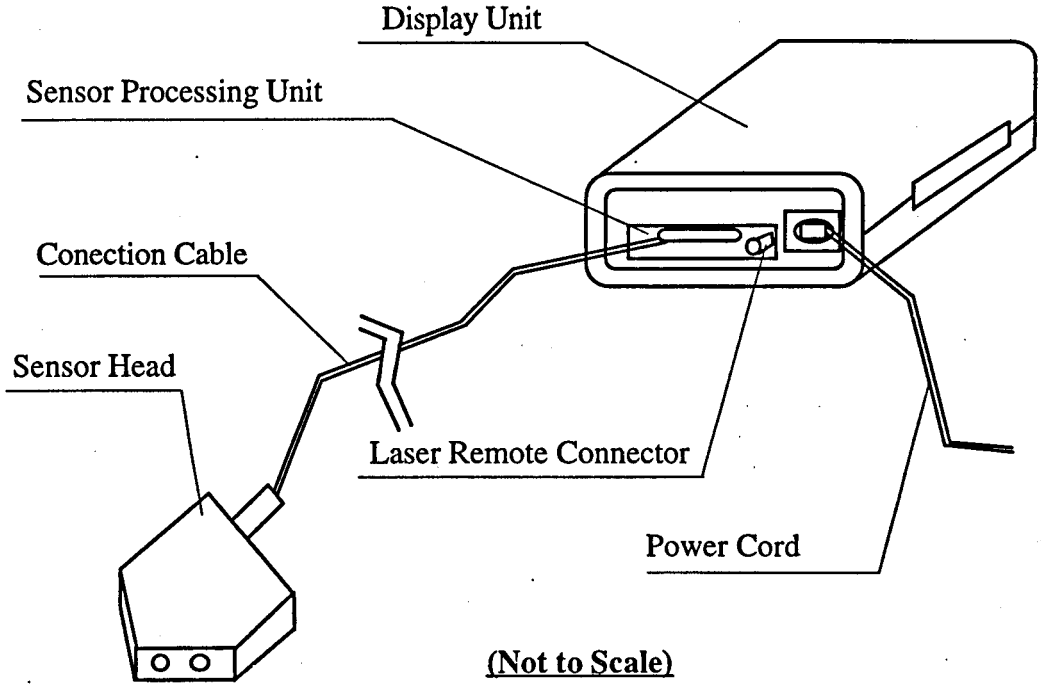


**Fig. 4.2 Schematic of the non-contact laser displacement meter**

Fixing the device to the dynamometer by the ordinary stands was not possible. Therefore a special stand was designed and fitted to the dynamometer. The configuration of this arrangement is shown in Fig.4.3. By the help of this stand the radius of drive could be measured precisely at different angular positions.

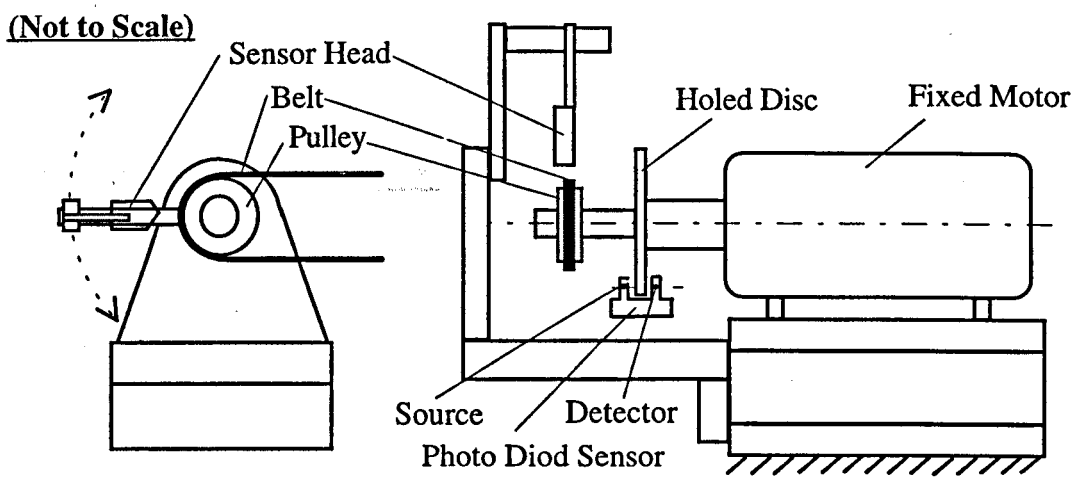


**Fig. 4.3 Configuration of laser sensor head stand and speed measurement arrangements**

## 4.3.2 Speed Measurement

Rotational speed of each pulley was measured by recording the frequency of interruption of a light beam by a 60-holed disc rotating with each pulley (Fig. 4.3). Line of sight from a source to a photo-diode through a hole in the disc is broken and remade as the disc rotates. Each hole as it passes the line of sight causes an electric pulse from the photo diode. A counter-timer (Racal-Dana Instruments Ltd. type 99000) counted these pulses which were converted into rotational speed. This universal counter-timer had modes of operation enabling the driving and driven pulley speeds to be read and displayed either individually or through their ratio. Pulse counts from 1 to $10^5$ could be averaged depending on the time base range selected. $10^4$ range gave a good resolution for the speeds required for belt testing. The accuracy on this setting is $\pm$ 1 count.

## 4.3.3 Torque Measurement

Torque in the drive was measured on the motor and generator trunnion cases by a strain gauged load cell (Fig. 4.1). Links *a, b, c* prevent the trunnion case rotating

under torque. Link *c* is the load cell. It is protected from shock loading and damped by a rotational viscous dash pot. These transducers were capable of recording the maximum torque *25 Nm* available from the motors. A transducer meter (Sangmo-Schlumberger type C56) was used to display the readings. This was fitted with a digital L.E.D. indicator module, two transducer amplifiers and a summation module. The digital display had a full scale reading of $\pm 1000$. Either of amplifier's six range settings from *0.25* to *100* could be set to read $\pm 1000$ at full scale deflection of the load cell. This gave the required accuracy. The summation module was able to read the difference between the two channels, being useful for torque loss measurements.

Torsional vibrations in the motor trunnions were damped. Small roller bearings in the connection rods were found to be necessary to avoid frictional interference affecting the readings.

Digital display was given every third of a second and because of vibration in the drive, accurate manual readings were difficult in all but the smoothest drives. To alleviate this problem Cowburn [1] used a microprocessor, but in this work an intelligent multi meter (Thuby-Thander Ltd. type 1905) was connected to the transducer meter. This multi meter had an averaging mode, to average the readings. This enabled the average of torque and torque loss, lowest reading and highest reading that occurred while the program was being run to be stored in memory for recall later.

## 4.4 Rig Calibration

There are some sources of apparent measurements in the rig. which must be identified and separated from the actual values. In the following these sources will be discussed.

### 4.4.1 Radial Movement

An unload belt fits the pulley at a reference radius $R$, e.g. the pitch radius. When the belt is loaded by the force $F$ we get a radial movement $x$ and the belt fits the pulley at a radius $R$-$x$. The fit of a v-ribbed belt in the corresponding pulley is shown in Fig. 4.4. The true pitch radius $R$ of a v-ribbed belt drive is slightly larger than effective radius (outside radius) $R_e$. The surface of pulley shoulder (the actual outside diameter) was used as a reference surface for radial movement measurements.

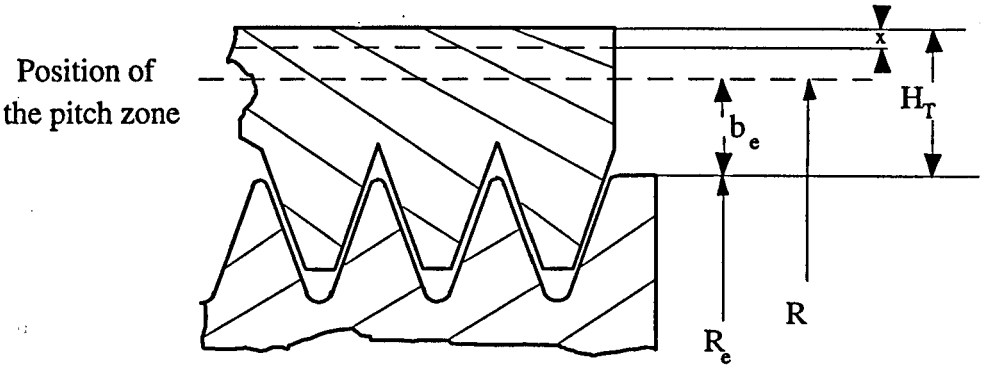


**Fig. 4.4 Determination of pitch diameter**

By the help of NCLDM (see section 6.2) the difference between the top of the belt cord and pulley shoulder $H_T$ was measured at different running conditions around the pulley. These readings show very accurate values for the variation of the radial movement around the pulley. The stand was attached to the fixed motor, and the radial movement for driven and driving pulleys was measured by changing the role of motors as a generator or motor. Two different points must be considered regarding radial movement of the belt.

**(i)** The radial movement $x$, shows a linear and stable relationship with belt tension $F$ at high tensions, but at low tensions ($F<150N$) it is distinctly non-linear and unstable (see sections 5.2.2 and 6.2). Therefore determination of an exact value for pitch radius $R$ at no-load ($F=0$) is difficult. In this work, the main interest is to measure change of radial movement. Instead of selecting the datum as the no-load ($F=0$) pitch radius, at every total tension ($F_t + F_r$), the datum was chosen as the radial height $H_T$ at angular position $90$ degrees when there was zero torque transmission ($T=0$) and no slip ($s=0$). This choice showed a very good stability and repeatability. Thus this point was chosen as a reference point for the experimental measurements of the variation of radial movement $x_e$ and

$$\Delta x_e = \Delta x = -\Delta H_T$$

**(ii)** A small amount of wear occurred during each set of data collection, due to experimental method and long running time of each set of the tests (see section 6.2) giving rise to an apparent radial movement $x_a$. The apparent radial movement was corrected by measuring the value of $H_T$ at the beginning and end of each set at applied torque $T=0$. Then $\Delta x_e$ can be calculated from

$$\Delta x_e = \Delta x_a - \Delta H_T)_{T=0} \qquad (4.1)$$

### 4.4.2 Slip Calibration

In this work both pulleys were of nominally equal size. Because of manufacturing errors a small difference in their diameters was noted. This resulted in the pulleys running at different speeds and giving rise to an apparent speed loss. The apparent speed loss must be corrected for calculating the actual speed loss caused by slip of the belt. This is achieved by multiplying the speed ratio of the driven to driving pulleys, $\omega_{dn} / \omega_{dg}$ by the pulley radius ratio $R_{dn} / R_{dg}$. Slip in the drive is then calculated from

$$s = 1 - \frac{(\omega R)_{dn}}{(\omega R)_{dg}} = 1 - \frac{\omega_{dn}}{\omega_{dg}} \cdot \frac{R_{dn}}{R_{dg}} \tag{4.2}$$

Pulley effective diameters (Fig. 4.4) were measured with a micrometer and the results are shown in table 4.1.

Table 4.1 Pulley diameter measurements

| Nominal Pulley Effective Diameter | Measured Pulley Effective Diameter |
|---|---|
| $d_e = 45$ (on fixed motor) | $d_{ea} = 45.16$ (on fixed motor) |
| $d_e = 45$ (on sliding motor) | $d_{ea} = 45.08$ (on sliding motor) |
| $d_e = 80$ (on fixed motor) | $d_{ea} = 80.15$ (on fixed motor) |
| $d_e = 80$ (on sliding motor) | $d_{ea} = 80.12$ (on sliding motor) |

To determine the values of pitch radius $R$, the difference between the top of the belt cord and pulley shoulder $H_T$ was measured at no load ($T=0$) and no slip ($s=0$) condition for every total tension ($F_t + F_r$). As shown in figures 2.14 and 4.4, the value of $R$ for slip measurements for a standard K-section v-ribbed belt is determined by

$$R = R_{ea} + (H_T - 1.6)\,mm \tag{4.3}$$

This method was only used for the ratio $R_{dn} / R_{dg}$. For other cases the pulley pitch radius was taken $R = R_e + 1.5mm$.

### 4.4.3 Torque Calibration

In the rig the rotor and trunnion were locked together. Dead weights were hung at a radius of *120 mm* on the motor shaft. The weights were calculated to give a torque on the casing in steps of *2.67 Nm* up to maximum *21.35 Nm*. A transducer meter (section 4.3.3) was used to record the torque. After a preliminary calibration to establish linearity of response between torque and digital output (Fig. 4.5 and table

4.2), the amplifier gauge factors were adjusted to give a response of *427* digital units for an applied torque of *21.35 Nm*, with the amplifier at *2.5* range. The required gauge factors were *4.98±0.02* and *5.25±0.03* for the sliding and fixed motor respectively. The intelligent multi-meter (connected to amplifier) was adjusted to give a response of *100±3* digital units for *1 Nm* applied torque.

The intelligent multi-meter records the total torques $T_m$ and $T_g$ acting on the motor and generator casings respectively. The total torque on the casing has components

- $T$, from the belt. This is transmitted to the casing via the shaft and magnetic flux between the shaft and casing.
- $T_w$, from wind resistance to rotation of the rotor.
- $T_b$, from the shaft bearings.
- $T_t$, from the trunnion bearings.

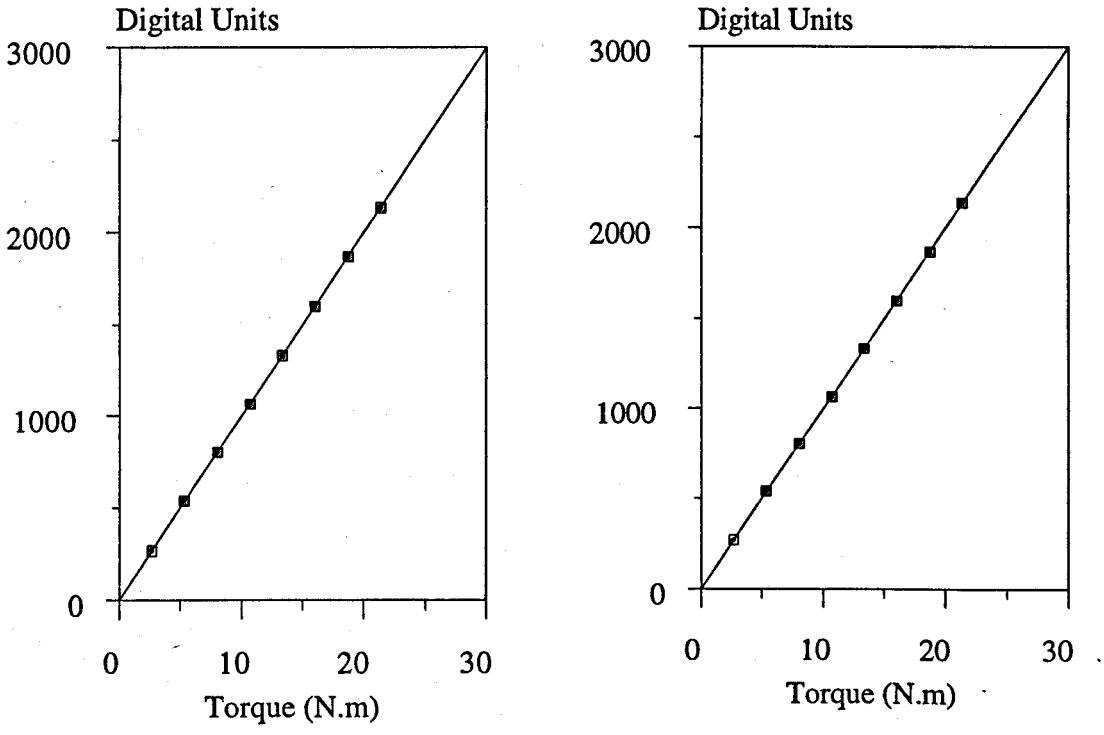


**(a) Sliding motor** **(b) Fixed motor**

**Fig. 4.5 Response between transducer and digital output**

Table 4.2 Experimental results for linearity between digital units and applied torque

| applied torque (N.m) | digital units (sliding motor) | digital units (fixed motor) |
|---|---|---|
| 2.67 | 267 | 266 |
| 5.34 | 536 | 535 |
| 8.01 | 800 | 801 |
| 10.67 | 1068 | 1067 |
| 13.35 | 1335 | 1336 |
| 16.02 | 1602 | 1601 |
| 18.69 | 1868 | 1869 |
| 21.35 | 2135 | 2136 |

Cowburn [1] showed that losses due to bearings are negligible. To determine the torque due to windage without the cooling fans on, the motors were run un-coupled. Torque was measured for speeds between *625* and *3000 RPM*. Results for the fixed and sliding motors rotating clockwise and anti-clockwise are shown in Fig. 4.6. The data is presented in table 4.3. The windage torque versus speed plot shows almost a linear relationship up to *3000 RPM*. Calibration equation for windage versus speed in *rpm*, approximately is

$$T_w = 0.01 + 30 \times 10^{-6} \omega \quad (Nm) \tag{4.4}$$

The motors were mounted with shaft facing shaft, when they were coupled with a belt their directions of rotation were opposite. The total torque loss is calculated by

$$T_L = (T_m - T_g) - (T_{wdg} + T_{wdn}) \tag{4.5}$$

For $\omega$=*2000RPM*

$$T_L = (T_m - T_g) - 0.14 \quad (Nm) \tag{4.6}$$

The accuracy of device was approximately $\pm$*0.03 Nm.* This gives a large uncertainty in the results at low values of torque loss.

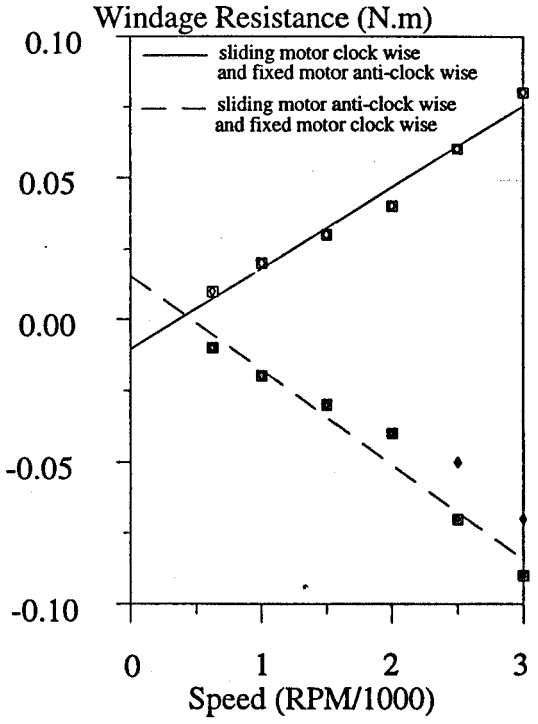


**F.g. 4.6 Windage resistance against speed**

Table 4.3 Experimental results for windage calibration

| speed (RPM) | sliding motor clock wise (Nm) | sliding motor anti-clock wise (Nm) | fixed motor clock wise (Nm) | fixed motor anti-clock wise (Nm) |
|---|---|---|---|---|
| 625 | .01 | -.01 | -.01 | .01 |
| 1000 | .02 | -.02 | -.02 | .02 |
| 1500 | .03 | -.03 | -.03 | .03 |
| 2000 | .04 | -.04 | -.04 | .04 |
| 2500 | .06 | -.07 | -.06 | .05 |
| 3000 | .08 | -.09 | -.08 | .07 |

### 4.4.4 Total Tension Calibration

Tension was applied to the belt by the dead weights hanging on a steel cable attached to the sliding motor and running over a v-notched pulley fitted with ball bearings. The sliding motor was mounted on rolling bearings. A coefficient of friction of *0.005* was quoted for these bearings, but during a static test this was found to be near *0.01*, requiring *50 N* to produce steady motion.

The friction under dynamic conditions was determined from the full skid limit torque. Thus, when the belt approaches full skidding, the traction coefficient, $\lambda = (F_t - F_r)/(F_t + F_r)$ has a limiting value.

Euler's equation (equation 2.11) is valid for the v-belt and the v-ribbed belt without rib bottom/ groove tip contact (see chapter 3). The limiting traction coefficient is then given by

$$\lambda_{max} = \frac{e^{\mu\alpha/\sin\beta} - 1}{e^{\mu\alpha/\sin\beta} + 1} \tag{4.7}$$

For the values of $\mu = 0.32$, $\alpha = \pi$ and $\beta = 20°$ (see section 5.3.3), $\lambda_{max} = 0.899$. Therefore a dynamic means of measuring total tension $(F_t + F_r)$is

$$(F_t + F_r) = \frac{T_m}{R_{dg} \cdot \lambda_{max}} \tag{4.8}$$

Full skid slip tests are presented in chapter 6. The additional friction correction load of *50 N* was considered in these tests. The reduction of contact angle$\alpha$, also, must be considered.

# CHAPTER FIVE

# V-RIBBED BELT MATERIAL PROPERTIES

## 5.1 Introduction

There are two basic types of v-ribbed belt construction. Both types use a single-unit tensile section (one row of tensile cords) which extends across the entire width of the belt. These two types differ in the method use to form the ribs on the bottom side of the belt.

- Fully molded ribs as shown in Fig. 5.1. These ribs are often covered with a rubber impregnated fabric to give better wear characteristics of the drive.
- Ribs formed by grinding (cutting) the rib profile in a cured slab as shown in Fig. 5.2.

There are a total of five individual cross sections available for use on v-ribbed type drives. These are the *H, J, K, L,* and *M* cross section designations when working with conventional English or USA units. The cross section designations for SI metric units remain the same except that a "P" is added before the cross section designation letter (*PH, PJ, PK, PL,* and *PM*).

Table 5.1 and Fig. 5.3 give the sheave or pulley groove dimensions for v-ribbed belts of these five cross sections. These sheave groove dimensions are standardised by The Rubber Manufacturers Association, The Mechanical Power Transmission and The Rubber Association of Canada in standard IP-26. The distinctive feature of each cross section is the spacing between the ribs [29].

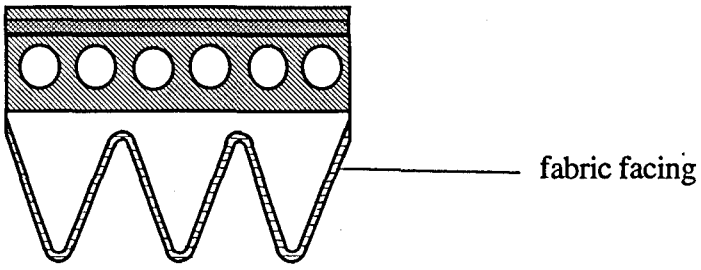


**Fig. 5.1 Fully molded v-ribbed belt construction [29]**

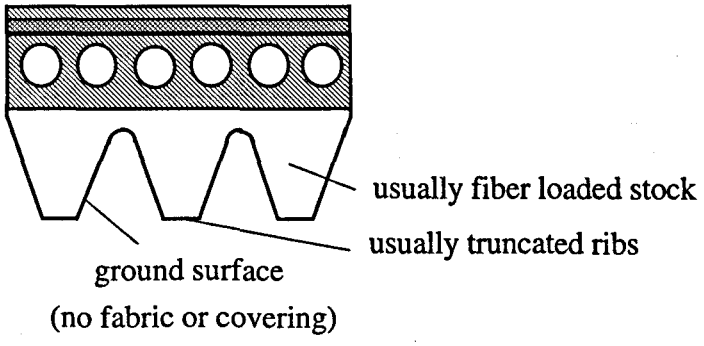


**Fig. 5.2 V-ribbed belt with ribs formed by grinding [29]**

Table 5.1 Sheave or pulley groove dimensions for v-ribbed belts

| Cross Section | H | J | K | L | M |
|---|---|---|---|---|---|
| Minimum Recommended Outside Diameter | 0.50 | 0.80 | 1.50 | 3.00 | 7.00 |
| Groove Angle $\pm 0.25°$ | 40 | 40 | 40 | 40 | 40 |
| $S_g^*$ | 0.063 $\pm 0.001$ | 0.092 $\pm 0.001$ | 0.140 $\pm 0.002$ | 0.185 $\pm 0.002$ | 0.370 $\pm 0.003$ |
| $r_t$ +0.005 -0.000 | 0.005 | 0.008 | 0.010 | 0.015 | 0.030 |
| 2a | 0.020 | 0.030 | 0.038 | 0.058 | 0.116 |
| $r_b$ | 0.013 +0.000 -0/005 | 0.015 +0.000 -0.005 | 0.020 +0.000 -0.005 | 0.015 +0.000 -0.005 | 0.030 +0.000 -.010 |
| $h_g$ (Minimum) | 0.041 | 0.071 | 0.122 | 0.183 | 0.377 |
| $d_B$ | 0.0469 | 0.0625 | 0.1093 | 0.1406 | 0.2612 |
| $S_e$ | 0.080 +0.020 -0/010 | 0.125 +0.030 -0.015 | 0.125 +0.050 -0.000 | 0.375 +0.075 -0.000 | 0.500 +0.100 -0.000 |

**Summation of the deviations from "$S_g$" for all grooves in any one sheave shall not exceed $\pm 0.010$"*

Source: Ref.[29]

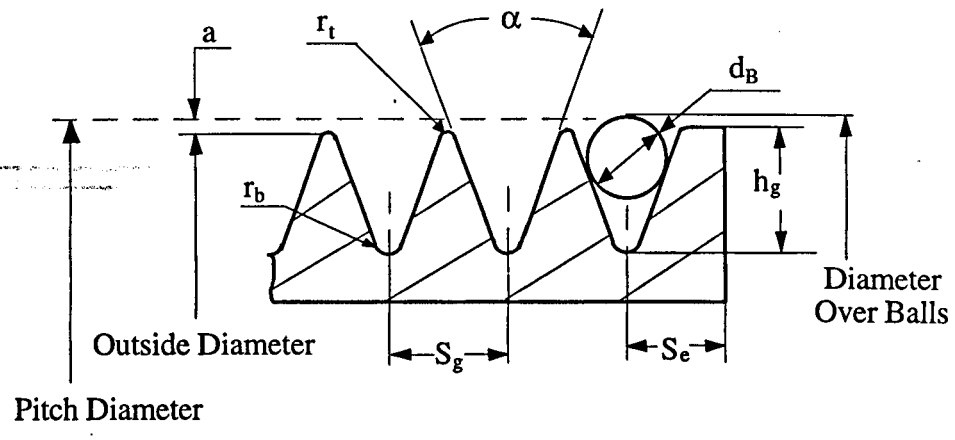


**Fig. 5.3 Standard groove dimensions [29]**

A v-ribbed pulley for the automotive industry is characterised by the number of grooves, the profile and the diameter. It is designated by a series of numbers and letters as follows:

- The first letter "P" indicates a pulley.
- The first set of numbers indicates the number of grooves.
- The second set of letters indicates the groove profile.
- The second set of numbers indicates the effective diameter (outside diameter), in millimetres.

**EXAMPLE**

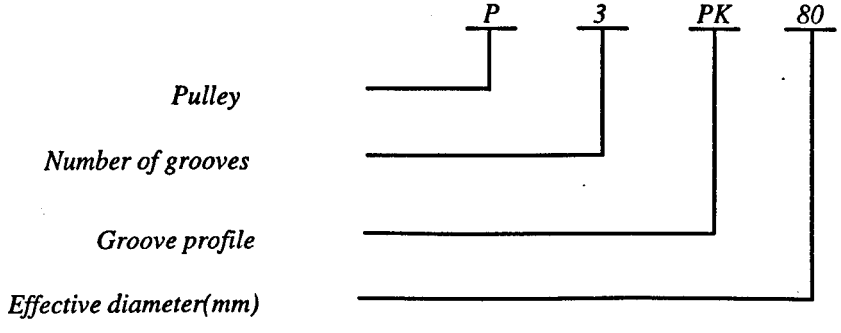

A v-ribbed belt for the automotive industry is characterised by the number of belt ribs, the profile (Fig. 2.14) and effective length. It is designated by a series of numbers and letters as follows:

- The first set of numbers indicates the number of belt ribs.
- The letters indicate the belt profile.
- The second set of numbers indicates the effective length, in millimetres [46].

**EXAMPLE**

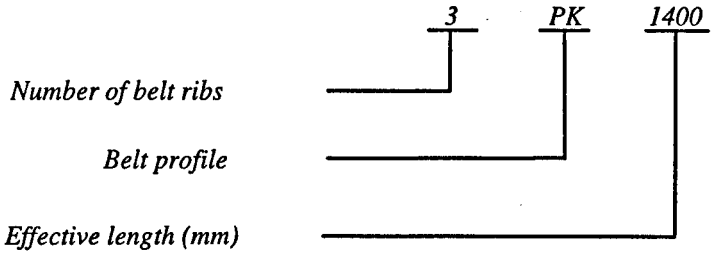


All of the main experiments in this work were carried out with a v-ribbed belt of type 3-PK-1400 (cut, manufactured by Pirelli, Italy). Two pairs of equal size of pulleys P-3-PK-80 and P-3-PK-45 were run with the belt. Subsidiary tests on torque and speed loss were also carried out with cut, molded and anti-wear v-ribbed belts of type 3-PK-900 (manufactured by Dayco, Italy). Both the molded and anti-wear belts differed from the cut belts in their mode of manufacture. They were molded, without a cover, but were made from different materials.

In the following the required material properties for the theoretical part of the v-ribbed belt calculations will be investigated.

## 5.2 Radial Spring Constants

V-ribbed belt radial movement is dependent upon the forces acting on the belt. The amount of settle is then determined by the elastic properties of the belt and the friction acting at the wedge interface.

At a preliminary test ( next section) the v-ribbed belt showed the same value of radial movement for flat belt part and v-belt part. The mathematical model developed for mechanical performance of v-ribbed belt (chapter 3), requires two spring constants $k_V$ and $k_F$. In this theory two different cases were discussed. Before rib bottom / groove tip contact, the radial movement $x_V$ is linearly related to the force $F$ acting in the immediate region by a constant $1/k_V$. In this case the v-ribbed acts as a v-belt. When rib bottom / groove tip contact occurs, the radial movement is related to the force by a constant $k_{VR} = k_V + k_F$ , where $k_F$ is the radial spring constant of flat belt part.

### 5.2.1 Preliminary Test

By the help of Non-Contact Laser Displacement Meter (NCLDM) the variation of the difference between the top of the belt cord and pulley shoulder $H_T$ (Fig. 3.4) across the belt width was measured, for different belts (new and used) and for two cases, with rib bottom/groove tip contact and without rib bottom/groove tip contact. It was tested for different transmitting torques (0-23 *Nmm*) at *13* steps [Appendix D].

It was found that the variation of $H_T = \pm 0.005mm$ across the belt width (table 5.2), for all of tested conditions. This could be related to the much higher stiffness of the cord compared with the rubber. Therefore we can assume v-ribbed belt is a combination of a flat belt and a v-belt, where they have the same amount of radial movement.

Then the theory developed (chapter 3) for mechanical performance of v-ribbed belt drives and the required values for theory were determined by the following arrangements.

Table 5.2 Tests for the variation of $H_T$ across the belt width at angular position 90°

| pulley sizes $d_e$, mm | total tension ($F_t + F_r$), N | applied torque (T), Nm | readings $H_T \pm 0.005$(mm) |
|---|---|---|---|
| 45 (new belt) | 200 | 0 | 3.422 |
| | | 4 | 3.508 |
| | 300 | 0 | 3.380 |
| | | 6 | 3.508 |
| 80 (used belt) | 200 | 0 | 2.997 |
| | | 8 | 3.047 |
| | 600 | 0 | 2.936 |
| | | 23 | 3.018 |

## 5.2.2 Tests for Determination of Radial Spring Constant $k_V$

A new v-ribbed belt was run on the two pairs of equal size of pulleys $d_e$=*45mm* and $d_e$=*80mm*, at a speed of *625 RPM* with different belt tensions. To alleviate the effect of miss-fitting, dead weights were hung on the drive to a total of *2F=588 N* and reduced to *2F=98.5 N* (unloading) in *11*steps. The rig ran at no load (*T=0*) and no slip (*s=0*) conditions. The sliding angle was $\gamma = 180°$ for this case. To avoid different uncertainties arising from moving the sensor head of NCLDM, the sensor head was fixed at the middle of the contact angle (angular position =90 degrees) and the pulley was moved on its shaft to measure $H_T$. The maximum drive radius $R_T$ (Fig. 4.4) can be calculated from

$$R_T = H_T + R_{ea} \tag{5.1}$$

The variation of $R_T$ versus the belt tension is shown in Figs. 5.4a and 5.4b for actual effective diameter $d_{ea}$=*45.160mm* and $d_{ea}$=*80.150mm*, respectively. The data is given at table 5.3. The following points must be considered:

**(i)** With respect to the K-section v-ribbed belt geometry (Fig. 2.14), rib bottom / groove tip contact will not occur if $H_T$>*3.1mm*. The results showed no rib bottom / groove tip contact for the applied tensions. This means v-ribbed belt acts as a v-belt and the only spring constant is $k_V$.

$$k_V = -\frac{\Delta F}{R \cdot \Delta R_T} \tag{5.2}$$

where

$$R \cong R_T - 1.6mm \tag{5.3}$$

**(ii)** As can be seen $\Delta F / \Delta R_T$ is almost constant at high belt tensions (more than *150 N*), but at low tensions the relationship becomes distinctly non-linear. This arises from the belt not quite fitting the groove. In practice this occurs in a drive transmitting high torque for the slack side at entry to the driven pulley. The developed v-ribbed theory also is not applicable for entry to pulley and exit from pulley regions.

**(iii)** The other reason for a non-linear relationship between $R_T$ and $F$ even at high belt tensions is due to variable belt contact depth in the case of v-ribbed belt. A v-belt has a constant contact depth, but the contact depth of a v-ribbed belt increases with radial movement (Fig. 3.4), or

$$H_V = \text{constant for v - belt}$$
$$H_V = H_{Vm} + x$$

In the case of v-ribbed belt (equation 3.7) the maximum variation of $k_1$, can be calculated from

$$k_1 = \frac{4 \tan\beta \, E \, H_V}{B_V} \tag{5.4}$$

where $H_V$ is

$$H_V = \frac{H_{VM} + H_{Vm}}{2} \tag{5.5}$$

$$\frac{\Delta k_1}{k_1} = \pm \frac{(H_M - H_m)}{(H_M + H_m)} \tag{5.6}$$

In the practical case, $H_M - H_m \cong 0.2$ *(mm)*. Considering the geometry of K-section v-ribbed belt $H_M \cong 2.4$. $\Delta k_1 / k_1 = \pm 0.04$. The effect of variable depth is negligible.

**(iv)** The variation of $k_V$ for $d_{ea}$=*80.150mm* is from *33.22* $N/mm^2$ to *76.1* $N/mm^2$ and for $d_{ea}$=*45.160mm* is from *38.12* $N/mm^2$ to *117.57* $N/mm^2$. The upper values are related to linear parts of the curves. For the pulleys of two sizes, difference in $k_V$ may arise from the fit of the belt in its pulley groove. The change in the wedge angle of a belt due to bending from its natural radius to the pulley radius has been considered by some authors [1,18,30]. In this work for each pulley size the high tension value of $k_V$ was chosen to represent belt radial stiffness in the theoretical modelling, e.g. for $d_e$=*45mm*, $k_V$=*117* $N/mm^2$ and for $d_e$=*80mm*, $k_V$=*76* $N/mm^2$.

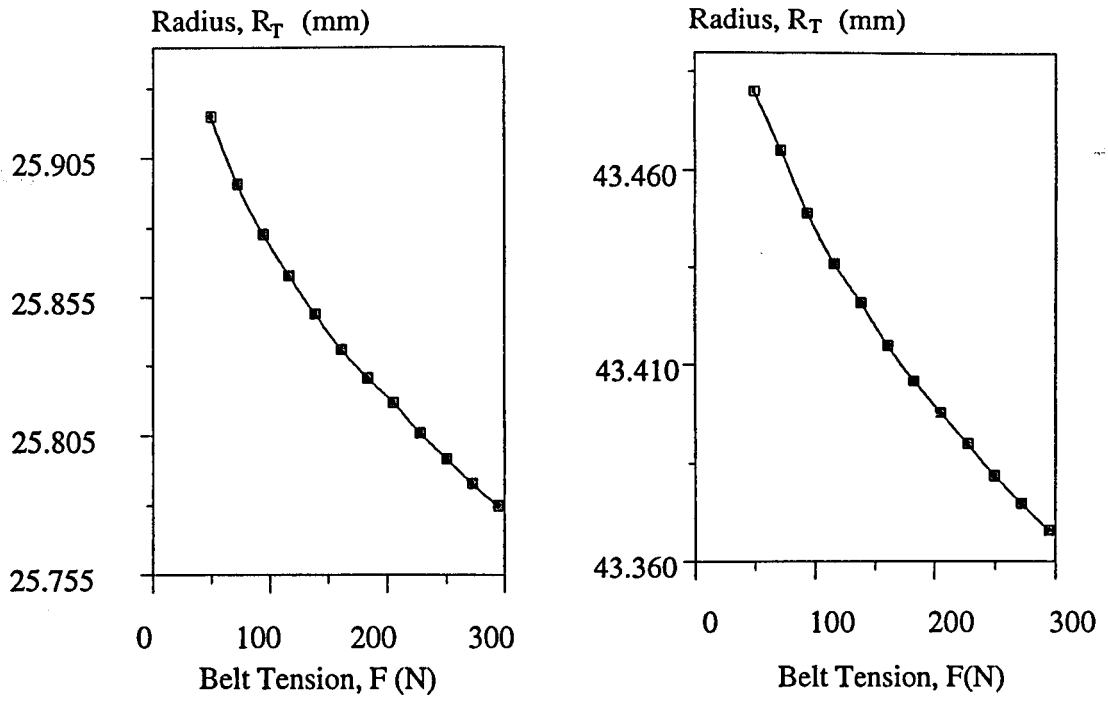


(a) $d_e$ =45mm (b) $d_e$ =80mm

**Fig. 5.4 The variation of radius $R_T$ against belt tension $F$, for a new v-ribbed belt**

Table 5.3 Tests for determination of $k_v$

| belt tension $F(N)$ | reading, $H_T(mm)$ ($d_{ea}$=45.160mm) | reading, $H_T(mm)$ ($d_{ea}$=80.150mm) | radius, $R_T(mm)$ ($d_{ea}$=45.160mm) | radius, $R_T(mm)$ ($d_{ea}$=80.150mm) |
|---|---|---|---|---|
| 49.25 | 3.340 | 3.405 | 25.920 | 43.480 |
| 71.50 | 3.316 | 3.390 | 25.896 | 43.465 |
| 93.75 | 3.298 | 3.374 | 25.878 | 43.449 |
| 116.00 | 3.283 | 3.361 | 25.863 | 43.436 |
| 138.25 | 3.269 | 3.351 | 25.849 | 43.426 |
| 160.50 | 3.256 | 3.340 | 25.836 | 43.415 |
| 182.75 | 3.246 | 3.331 | 25.826 | 43.406 |
| 205.00 | 3.237 | 3.323 | 25.817 | 43.398 |
| 227.25 | 3.226 | 3.315 | 25.806 | 43.390 |
| 249.50 | 3.217 | 3.307 | 25.797 | 43.382 |
| 271.75 | 3.208 | 3.300 | 25.788 | 43.375 |
| 294.00 | 3.200 | 3.293 | 25.780 | 43.368 |

### 5.2.3 Tests for Determination of Radial Spring Constant $k_F$

After rib bottom / groove tip contact, the force $F$, has two components $F_V$ and $F_F$. For this case a used v-ribbed belt was run in the same conditions as a new belt. The variation of $R_T$ versus the belt tension is shown in Figs. 5.5a and 5.5b for actual effective diameter $d_{ea}$=45.160mm and $d_{ea}$=80.150mm, respectively. The data is given in table 5.4. The results showed for the applied tensions there is rib bottom / groove tip contact at all steps of test ($H_T$<3.1mm). This means that the v-ribbed belt acts as a combined flat and v-belt and the spring constant is

$$k_{VR} = -\frac{\Delta F}{R_e \cdot \Delta R_T} \tag{5.7}$$

Where

$$k_{VR} = k_V + k_F$$

The variation of v-ribbed radial constant $k_{VR}$ for $d_{ea}$=80.150mm is from $53.74 N/mm^2$ to $97.77 N/mm^2$ and for $d_{ea}$=45.160mm is from $37.32 N/mm^2$ to $135.1 N/mm^2$. A value of $k_{VR}$=$140 N/mm^2$ was recorded by Gerbert [28] for a 4-PK-890 type v-ribbed belt. Considering the values for $k_V$, the variation of $k_F$ for $d_{ea}$=80.150mm is from $20.52 N/mm^2$ to $21.76 N/mm^2$ and for $d_{ea}$=45.160mm is from $-0.8 N/mm^2$ to $17.53 N/mm^2$.The upper values are related to linear parts of the curves. In this work the value of $k_F$=$20 N/mm^2$was chosen. According to our model (sections 3.3.1 and 3.3.2), and putting $f(\gamma = 90) = 1.291$ and $k_1 / k_2 = 0.67$ (equation 3.23), we have $k_V$=$1.61 k_1$. From section 3.3.2 and putting $k_1 / k_F = 2$, we can get $k_V$=$3.22 k_F$. But $k_F$ depends on $H_F$ (equation 3.27) and $H_F$ varies by running time of the belt and wear.

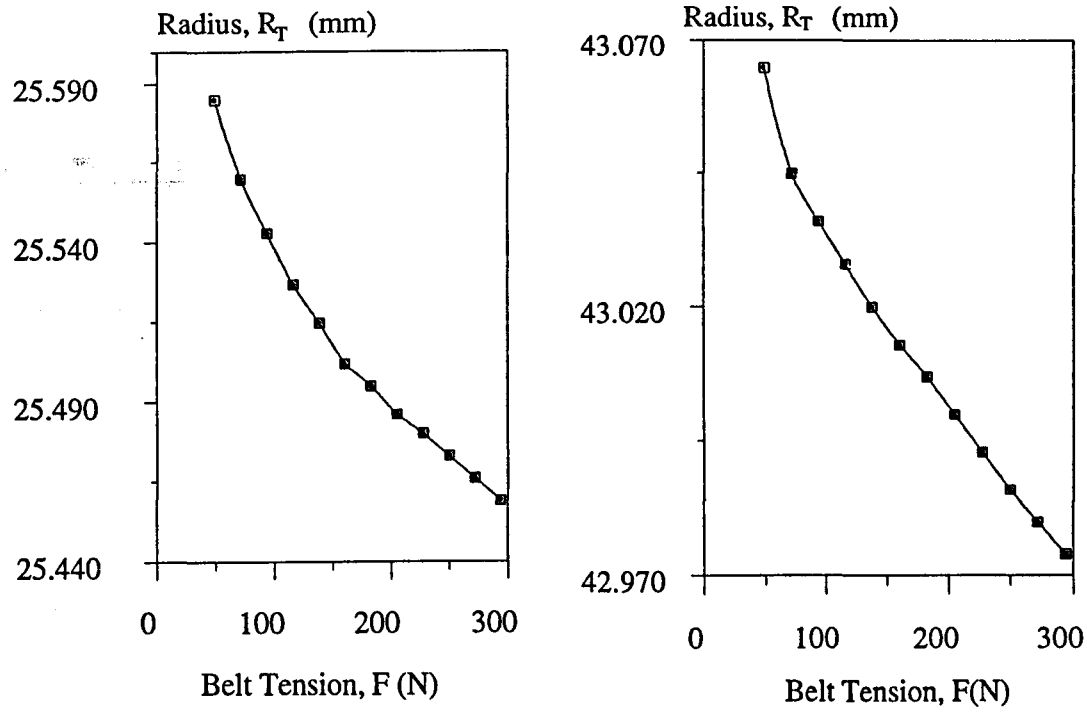


(a) $d_e$ =45mm (b) $d_e$ =80mm

**Fig. 5.5 The variation of radius $R_T$ against belt tension $F$, for a used v-ribbed belt**

Table 5.4 Tests for determination of $k_F$

| belt tension $F(N)$ | reading, $H_T(mm)$ ($d_{ea}$=45.160mm) | reading, $H_T(mm)$ ($d_{ea}$=80.150mm) | radius, $R_T(mm)$ ($d_{ea}$=45.160mm) | radius, $R_T(mm)$ ($d_{ea}$=80.150mm) |
|---|---|---|---|---|
| 49.25 | 3.005 | 2.990 | 25.585 | 43.065 |
| 71.50 | 2.980 | 2.970 | 25.560 | 43.045 |
| 93.75 | 2.963 | 2.961 | 25.543 | 43.036 |
| 116.00 | 2.947 | 2.953 | 25.527 | 43.028 |
| 138.25 | 2.935 | 2.945 | 25.515 | 43.020 |
| 160.50 | 2.922 | 2.938 | 25.502 | 43.013 |
| 182.75 | 2.915 | 2.932 | 25.495 | 43.007 |
| 205.00 | 2.906 | 2.925 | 25.486 | 43.000 |
| 227.25 | 2.900 | 2.918 | 25.480 | 42.993 |
| 249.50 | 2.893 | 2.911 | 25.473 | 42.986 |
| 271.75 | 2.886 | 2.905 | 25.466 | 42.980 |
| 294.00 | 2.879 | 2.899 | 25.459 | 42.974 |

## 5.3 Coefficient of Friction

The transmision capacity of a belt is considerably dominated by frictional characteristics of belt surface contacting with pulley [47]. In the following some relevant works will be reviewed. The results of an experimental work for determination of coefficient of friction of v-ribbed belt will be shown at the end of this section.

### 5.3.1 Introduction

A detailed account of the development of rubber friction theory and experimental discovery is reviewed by Roberts [48] and Barquins [49]. A brief account of the relevant works is given in the following.

Classical theory of friction states that the coefficient of friction is independent of load, sliding speed and the apparent area of contact and it is material dependent and its static value is higher than its sliding value. Experimentally it was discovered [50,51] that the friction coefficient of rubber increased with speed and decreased with load [1].

A new approach to the study of the tribological properties of rubber was opened in 1971 when Johnson et al.[52] showed that the area of contact between a rigid sphere and the flat, smooth surface of a rubber-like material is greater than that value which can be deduced from the classical theory of elasticity, because of the intervention of molecular attraction forces of the van der Waals type for elastomers. Schallamach [53] also observed that, in certain circumstances, when a blunt rigid asperity moves over a rubber surface, the true sliding friction does not occur. Indeed, waves of detachment propagate across the interface from the leading edge to the trailing edge of contact area, with a velocity greater than the imposed speed, and it is these provides relative motion between the two surfaces. When the viscous properties of rubbers are increased, the detachment wave phenomenon does not

occur, waves are replaced by ridges which remain engraved on the rubber surface and can lead rapidly to hard wear. Barquins [49] explained that when a blunt, rigid asperity is brought normally near a smooth surface of a highly elastic solid such as rubber, as soon as the distance becomes smaller than a few tenths of a micrometer, the two solids are subject to molecular attraction forces of the van der Waals type. These forces, which are predominant for distances greater than $20A^{\circ}$, are the prime cause of the adherence of solids. Indeed, stronger bonding forces are usually screened off by impurities absorbed on the surface. When the contact occurs under an applied load $P$, molecular attraction forces act into and around the contact area and are added to the load so that the contact is maintained by apparent load $P_1 > P$. The difference $P_1 - P$ represents an adherence force depending on the load $P$, on the contact geometry (shape and size) and on the mechanical and surface properties of the elastic solid. According to Barquins [49] some authors [51,54,55,56] showed that the frictional force of rubber is very sensitive to changes in the applied load, sliding speed and surface geometry.

Although much experimental work has been done studying friction, theoretical developments are not yet advanced to be able to predict friction coefficient for rubbers [1,57]. Experimental measurements is therefore needed.

### 5.3.2 Coefficient of Friction for V-ribbed belts

Determination of coefficient or friction for v- and v-ribbed belts is more complicated than flat belts due to their wedging action and laminate construction of several materials.

Wada, N. and Uchiyama, Y. [58] carried out an experimental work on friction and wear properties of short-fibre-reinforced chloroprence rubber composites. These composites have been used widely in hoses, v-belts, etc.[59,60]. The composites were examined in three sliding directions, corresponding to the longitudinal,

transverse and normal directions of the uniaxially oriented polyamid fibres under various loads at various sliding speeds, using both metal gauze and abrasive paper. They reported very high speed dependence of coefficient of friction for some experimental cases.

According to Gerbert [3] several empirical formulas are reported to estimate coefficient of friction for v-belts [61,62,63]. These empirical and semi-empirical formulas generally are given for classical construction wrapped belts. It is unclear how these can be applied to other belts with different constructions.

However, the above review gives an insight into the factors that might influence rubber belt friction.

### 5.3.3 Measurement Methods

A value for the coefficient of friction is required in belt theories. Gerbert [3] and Cowburn [1] determined the coefficient of friction for v-belts experimentally, in a testing rig at wholly slipping conditions. Then they followed Euler's equation

$$\frac{F_t}{F_r} = \exp\left(\frac{\mu\alpha}{\sin\beta}\right)$$

Dalgarno et al. [64] for synchronous belt carried out a test basically in the same way. In the case of v-ribbed belt Gerbert and Hansson [28] estimated the coefficient of friction from the gross slip limit in their experiments. The value of coefficient of friction was given as $\mu = 0.31$.

Recently Dalgarno et al. [65] using a test rig (Fig. 5.6) measured the tight side tension of a v-ribbed belt $F_t$ with a load cell and hanging a dead weight (*40N*) on the slack side, for four types of v-ribbed belts (moulded, anti-wear, new and used cut belts, the same as in this project), at pulley speeds between *0-30RPM*. The contact

angle between belt and pulley was 90° and the pulley effective diameter was *80mm*. The results of measurement showed the friction of moulded and anti-wear belts steadily increased with sliding speed. For the used cut belt the friction was constant over most of the speed range. The friction of the new cut belt decreased with sliding speed in low speed range, and afterwards kept constant [65]. The results, also, showed that the molded and anti-wear v-ribbed belts have the highest friction. The used belt showed higher friction than the new belt.

A v-ribbed belt without rib bottom / groove tip contact acts as a v-belt (see Chapter 3). At complete slip the sliding angle $\gamma = 90°$. Therefore it is reasonable to apply Euler's formula to estimate the coefficient of friction for v-ribbed belt without rib bottom / groove tip contact.

$$\mu = \frac{\sin\beta}{\alpha} \ln \frac{F_t}{F_r} \tag{5.8}$$

In this work the same rig (Fig. 5.8) was used hanging *30 N* dead weight to a half used cut belt (without rib bottom/groove tip contact) running with sliding speed of *15 RPM*. A typical drive will have a typical sliding speed greater than *10 mm/sec* [1] which gives the pulley speed of *15 RPM* for the pulley diameter of *80mm*. The contact angle between belt and pulley was 90°. The measured value for $F_t$ under these conditions was $F_t$=*130 N*. Applying Euler's formula for $\beta = 20°$, $\alpha = \pi/2$ and $F_r = 30N$ gives $\mu = 0.32$.

However this may not be the true value operating in a real drive, but it is very near to it. Further work in this area is recommended.

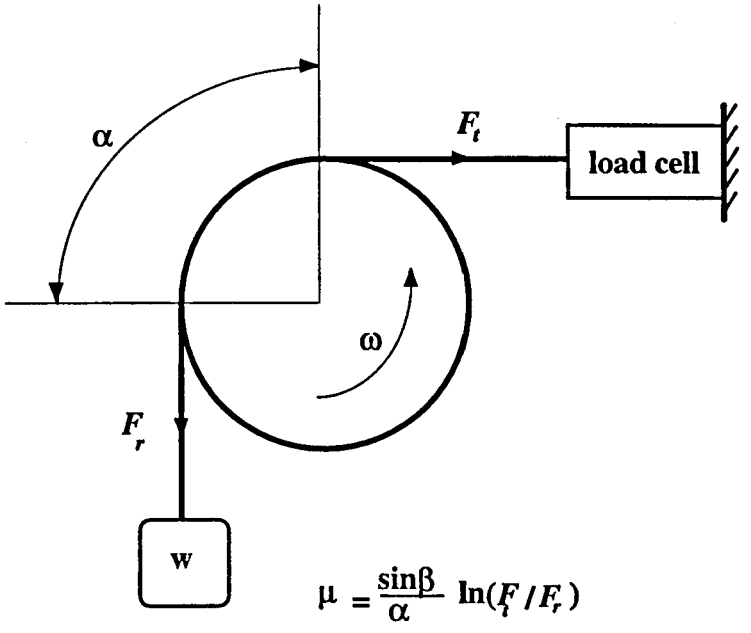


**Fig. 5.6 Test rig for coefficient of friction measurements**

## 5.4 Extension Modulus, c

In belt theories an extension modulus $c$ is defined by

$$c = \frac{F}{\varepsilon} \tag{5.9}$$

Where $F$ is belt force and $\varepsilon$ is longitudinal strain. The extension modulus is assumed constant in these theories. Cowburn [1] experimentally measured the value of $c$, for three types of un-cut AV10 v-belts (raw-edge, wrapped and cogged) and a cut piece of these v-belts. He reported up to a *25%* reduced $c$ value for cut belts. Also it is reported [1,6] that belts may have *5%* variation in extensional modulus due to repeated loading.

However, Moore [66] carried out some tensile tests which showed the variation of the belt tensile stiffness with temperature for six different types of belts. V-ribbed belt had lowest stiffness, because of the cord being polyester rather than glass fibre. The tests were carried out with a *9.525 mm* gauge length of a 3-PK v-ribbed belt

[67]. At the temperature of 80°C tensile stiffness of v-ribbed belt was *7.3 KN/mm-length*. The value of $c$ can be calculated by

$$c = 7.3 \times 9.525 = 69.5 KN$$

Moore [66] carried out the tests with the same type and same manufacturer's v-ribbed belt which have been used in the present work. Because of slightly low temperature at experimental investigations (section 6.2), due to long period of setting (normally 1 hour) and short running time (normally 20 minute), the value of $c$=*80 KN* was chosen for the extensional modulus. Gerbert and Hansson [28] reported a value of *93KN* for a 4-PK-1100 v-ribbed belt. The value of non-dimensional extensional modulus

$$c_o = \frac{c}{k_v R^2} \tag{5.10}$$

was calculated for two different pulley diameters $d_e = 80mm$ and $d_e = 45mm$. The pulley pitch radius $R$ was chosen *1.5mm* greater than effective radius [46].

# CHAPTER SIX

# EXPERIMENTAL INVESTIGATION OF V-RIBBED BELT PERFORMANCE

## 6.1 Introduction

Due to the shape of the v-ribbed belt (Fig. 2.14), it is not obvious if a v-ribbed drive functions as a v-belt or a flat belt. The design and shape of a v-ribbed belt affects its radial movement in the pulley grooves. When rib bottom / groove tip contact occurs the wedge action decreases. The beginning of the contact depends on belt tension, fit between rib and groove, wear and material properties [28].

In the following chapter tests have been carried out with three conditions of belts: with rib bottom / groove tip contact and without contact and mixed contact. The variation of v-ribbed belt radius (radial movement) at working conditions, slip (speed loss) and torque loss on a two pulley rig are experimentally determined. The rig is as described in chapter four.

Particular attention is paid to the radial movement and its dependence on other factors. For the first time a Non-Contact Laser Displacement Meter (NCLDM) has been used for measuring radial movement of the v-ribbed belt in this work. By the

help of this device the variation of radial movement could be measured at the actual working conditions and with very high precision.

## 6.2 Experimental Method

The beginning of the rib bottom / groove tip contact around the pulley depends on belt tension, fit between rib and groove, material properties and wear. Thus any particular belt has a unique value of radial movement $x$, related to the start of rib bottom / groove tip contact, and it is not possible theoretically to predict this value. But for all standard v-ribbed belts, considering their geometry (Fig. 2.14), a reference point could be chosen for $H_T$ (Fig. 4.4), which shows the start of contact. For a PK section v-ribbed belt we can write

$$H_{Tcontact} = 3.1(mm)$$

$$R_{Tcontact} = R_{ea} + H_{Tcontact}$$

By the help of NCLDM the values of $H_T$ were determined for all of the tested v-ribbed belts. Thus it is possible to determine starting point of rib bottom / groove tip contact.

The three type of contact: with rib bottom /groove tip contact, without rib bottom contact and mixed contact were obtained with new and used cut belts all of which had the same material properties. In the following, tests described as "new v-ribbed belt" refer to most tests in which the new v-ribbed belts were used : $H_T$ values greater than $3.1mm$ indicated no-rib bottom / groove tip contact. In few cases, at high tension ($F_t + F_r = 600\ N$) on a small radius pulley ($d_e = 45mm$), the new belt gave mixed contact: this will be referred to as the "extreme condition" test. Other tests were carried out on a cut belt that had been used long enough to create rib

bottom / groove tip contact in all conditions. These tests will be described as "used v-ribbed belt" tests.

New v-ribbed belt = Test without rib bottom / groove tip contact

Used v-ribbed belt = Test with rib bottom / groove tip contact

Extreme conditions test = Test with mixed contact

Eight sets of experiments were carried out for each driven and driving pulley. Two sizes of standard pulleys were used for mechanical testing. These were paired with nominal effective diameters, $d_e$=*45 mm* and $d_e$=*80 mm* (nominal angle of wrap on each pulley is 180°). The minimum recommended effective diameter, $d_e$ , for PK pulleys is *45 mm*. The tests were carried out at the speed of $\omega$ =*2000 RPM*, which was the smoothest running speed for the drive.

Table 6.1 lists the experimental tension and torque conditions. At each set of experimental work, torque applied to the drive at three, four or five stages from *0* to maximum (skidding condition).

Also some subsidiary tests were carried out with smaller intervals of applied torque *T*, and five different v-ribbed belts, new, half-used, used (cut), new molded and new anti-wear. During these tests slip and torque loss were determined experimentally at two different speeds of $\omega$=*1000RPM* and $\omega$=*2000RPM* to better compare variation of slip and torque loss between different belts at different speeds.

The variation of drive radius around the pulley was measured at *11* steps of angular position,$\alpha_p$= *0, 10, 20, 30, 60, 90, 120, 150, 160, 170, 180* degrees. At entry to the pulley and exit from the pulley regions, up to angular position of 30°, the intervals were chosen 10°. At the other positions the measurements were carried out at 30° intervals.

Table 6.1 Range of variables in mechanical tests

| Variables | pulley sizes $d_e$, mm | total tension ($F_t + F_r$), N | applied torque (T), Nm | figure numbers |
|---|---|---|---|---|
| driven pulley | 45 | 200 | 0, 2.5, 4 | 6.1a, 6.2a |
| | | 300 | 0, 2.5, 5, 6 | 6.3a, 6.4a |
| | | 600 * | 0, 5, 10, 13 | 6.9a |
| | 80 | 200 | 0, 5, 8 | 6.5a, 6.6a |
| | | 600 | 0, 5, 10, 15, 23 | 6.7a, 6.8a |
| driving pulley | 45 | 200 | 0, 2.5, 4 | 6.1b, 6.2b |
| | | 300 | 0, 2.5, 5, 6 | 6.3b, 6.4b |
| | | 600 * | 0, 5, 10, 13 | 6.9b |
| | 80 | 200 | 0, 5, 8 | 6.5b, 6.6b |
| | | 600 | 0, 5, 10, 15, 23 | 6.7b, 6.8b |

* Extreme conditions test

The extreme conditions test was carried out on a pair of pulley sizes of $d_e = 45\,mm$ for driven and driving pulleys. In this case, the variation of drive radius was measured at *19* steps from *0* to *195* degrees, to consider entry to the pulley and exit from the pulley regions, for maximum tight side belt tension and radial movement.

To avoid different uncertainties, the sensor head of NCLDM was fixed at each angular position, then the reference surface (pulley shoulder) and measuring surface (top surface of the belt) was brought under the laser beam by moving the pulley on its shaft. At each angular position the following steps carried out one by one;

1. Fixing the sensor head at the measuring angular position
2. Putting the reference surface under the laser beam
3. Hanging the required dead weight
4. Running the rig at no torque, *T=0*

5. Setting the laser meter to zero
6. Switching off the rig and removing the dead weight
7. Putting the measuring surface under the laser beam
8. Hanging the dead weight and running the rig
9. Applying the required torque and reading the meter

This method took a long time for each set, but it was completely convenient that the collected data was accurate [Appendix C]. The readings showed the value of $H_T$ (Fig. 4.4) for each running condition.

NCLDM was attached to the fixed motor and the measurements for driven and driving pulleys were carried out by changing the role of motors as a motor or generator.

As discussed earlier (section 4.4.1) at low belt tensions the actual radial movement $x$, was very unstable, therefore determination of exact value for pitch radius (origin for $x$ ) experimentally, is difficult. At no torque ($T=0$) and no slip ($s=0$) conditions for every value of total tension the readings showed a very good stability and repeatability, especially at angular position $\alpha_p = 90°$. Thus this point was chosen as a reference point for the experimental measurements of the variation of radial movement ($x_e$).

$$\Delta x_e = \Delta x = -\Delta H_T$$

It is possible to reconcile the theoretical results to this reference point.

Due to long running time of belts at each set of experiment (see section 6.2) a small value of wear occurred during the test. These values were measured and recorded (table 6.2) for each set by measuring $H_T$ at the beginning and end of each set.

Speed ratio and torque loss were measured during the tests, usually choosing the runs when radial movement measurements were taken at angular position 10° and 170°, i.e. near the first and last test of run.

Table 6.2 The amount of wear during each set of tests ($\mu m$)

| Fig. 6.1 | | Fig. 6.2 | | Fig. 6.3 | | Fig. 6.4 | | Fig. 6.5 | | Fig. 6.6 | | Fig. 6.7 | | Fig. 6.8 | | Fig. 6.9 | |
|---|---|---|---|---|---|---|---|---|---|---|---|---|---|---|---|---|---|
| a | b | a | b | a | b | a | b | a | b | a | b | a | b | a | b | a | b |
| 12 | 18 | 17 | 5 | 12 | 18 | 17 | 5 | 4 | 5 | 3 | 6 | 8 | 5 | 6 | 6 | 36 | 40 |

## 6.3 Fundamental Experiments

In the following section the radial movement, speed loss and torque loss occurring on a two pulley rig are experimentally determined.

### 6.3.1 Radial Movement

The variation of drive radius $R_T = R_{ea} + H_T$, versus the different angular position is the subject of Figs. 6.1 (a and b) to 6.8 (a and b) for driven and driving pulleys respectively. The variation of experimental radial movement $x_e$ is represented at the right side of each figure. In each figure there are three, four or five graphs relating to the values of applied torques. These figures, have been constructed from the data given in tables 6.3 to 6.6 and the experimental points have been omitted from figures 6.1 to 6.9 for clarity but can be deduced from the tables. The results for different values of applied torque are compared.

In all of the figures the starting point for rib bottom / groove tip contact is represented by a horizontal line. It can be seen that rib bottom contact does not occur at any angular position for new belts. In the case of used belts, rib bottom contact takes place at most tests, only for some few set of tests (Figs. 6.2 and 6.4) over some part of angular position (towards slack side) at maximum transmitting torque the belt comes out of rib bottom contact.

Considering the relationship between $R_T$ and radial movement $x$, ($\Delta R_T = -\Delta x$) it can be seen that for a driven pulley in the initial stages of entry to the pulley, radial movement increases slightly and a more rapid increase occurs at exit region. In the case of the driving pulley radial movement decreases slightly with increasing angular position for the applied torque values less than the skidding condition (increasing positive $x$, means movement towards the pulley centre).

For both pulleys (driven and driving) radial movement increases with increasing values of applied torque.

The trend of variation of radial movement for the new belt (without rib bottom / groove tip contact) is almost the same as for used belt (with rib bottom \ groove tip contact), but it will be discussed in the next chapter that the value of radial movement for used belt is less than new belt at all of the tested cases.

The bending stiffness of the belt reduces the arc of contact. The amount of reduction of contact angle can be estimated from these figures for each set of tests. It can be seen from figures 6.7, 6.8 6.9 that, due to low bending stiffness value of v-ribbed belt and high belt tension, at tight side for both driven and driving pulleys there is not any reduction of contact angle. At relaxed side the reduction of contact angle increases with increasing the value of applied torque.

Figs. 6.9 (a and b) show the result of an extreme condition test for driven and driving pulleys (data is given in table 6.7). The test were carried out with the smallest recommended size of pulley ($d_e = 45mm$) for PK section v-ribbed belts with total belt

tension $(F_t + F_r) = 600\,N$. The test covered 15° beyond the arc of contact (exit region). The results for driven pulley show more rapid increase of radial movement, and even after the geometric arc of contact. For the driving pulley there is a rapid decrease of radial movement at the middle of the arc of contact and an increase afterward.

Due to high value of total belt tension, $(F_t + F_r) = 600\,N$, mixed rib bottom / groove tip contact takes place almost at all transmitting torques.

The amount of wear during this set is very much higher than the earlier sets and it can be seen from the slope of the zero torque (*Torque=0*) radial movement. For driven pulley $\Delta H_{T)T=0} = 36\mu\,mm$ and for driving $\Delta H_{T)T=0} = 40\mu\,m$.

During the extreme condition tests the ribs of the two new v-ribbed belts collapsed. This can be attributed to the internal shear force (at the rubber) between flat belt part and v-belt part of v-ribbed belt. In section 7.6 we will discuss more about this phenomena.

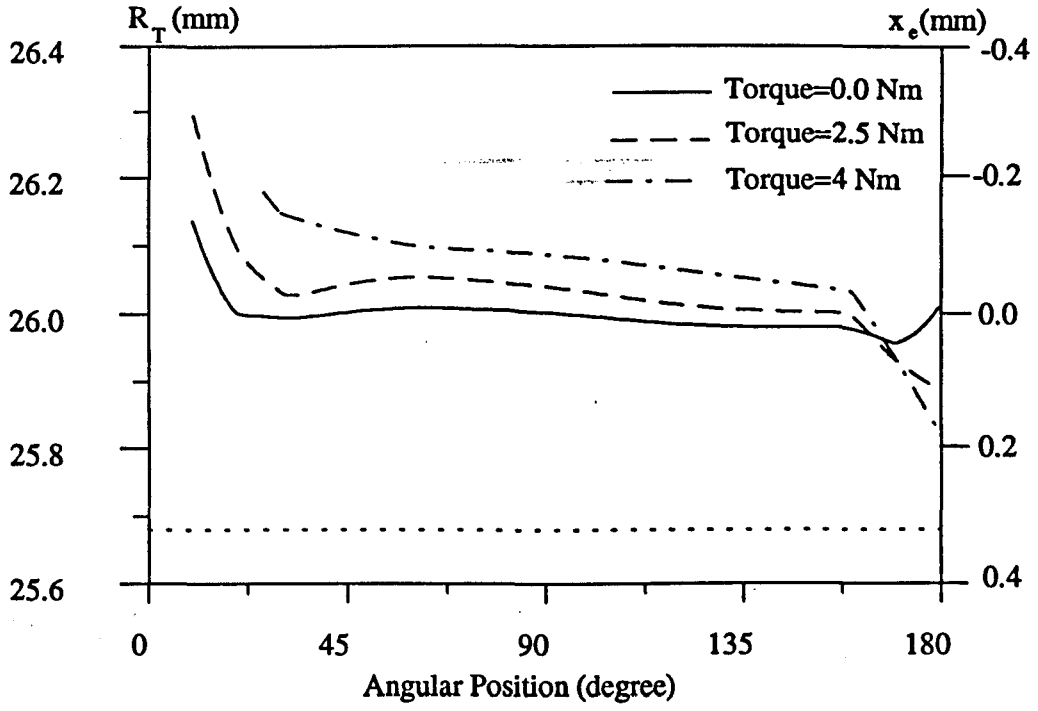


**(a) Driven pulley**

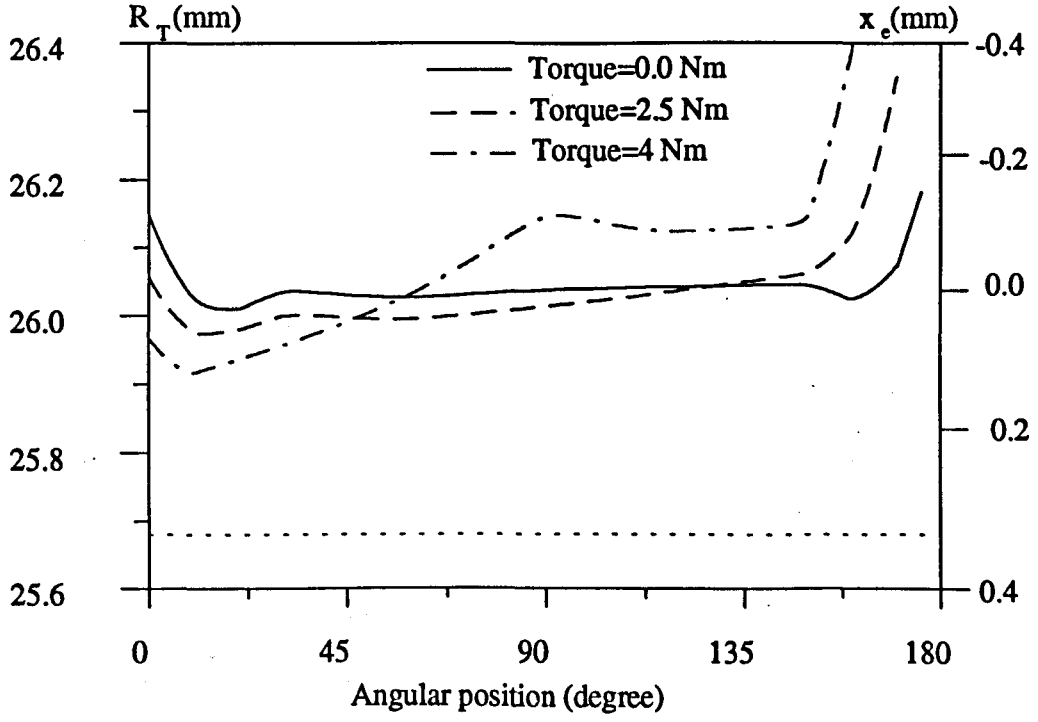


**(b) Driving pulley**

**Fig. 6.1 Variation of drive radius and radial movement against angular position for a new v-ribbed belt (without rib bottom contact)** ($F_t + F_r = 200\ N$, $d_e = 45\ mm$)

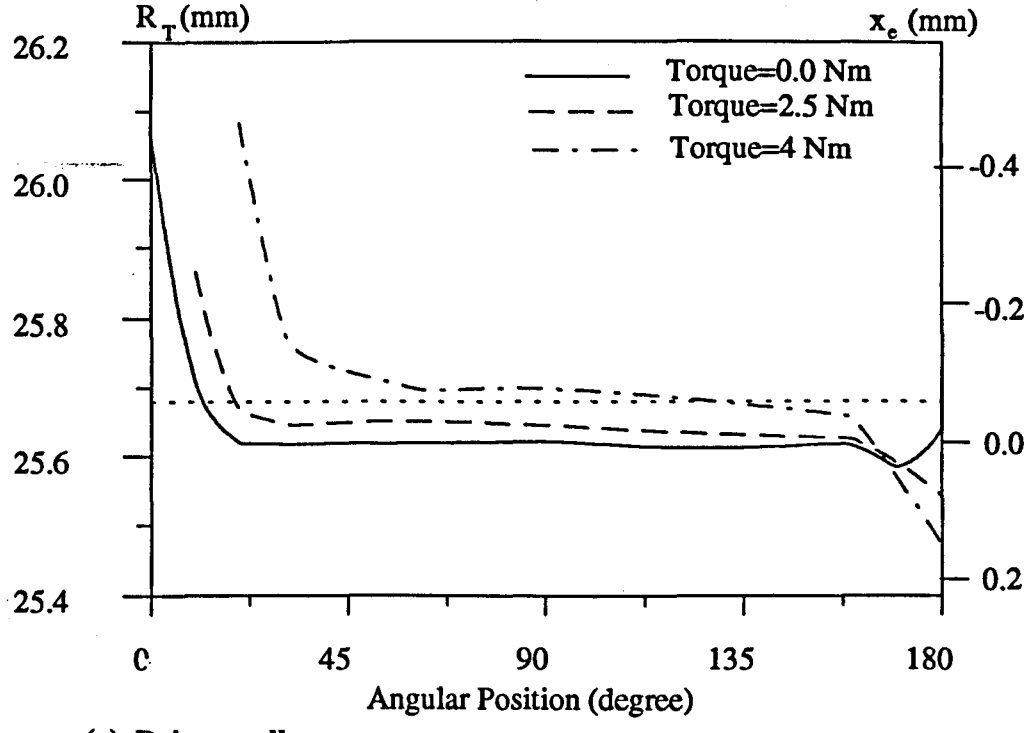


**(a) Driven pulley**

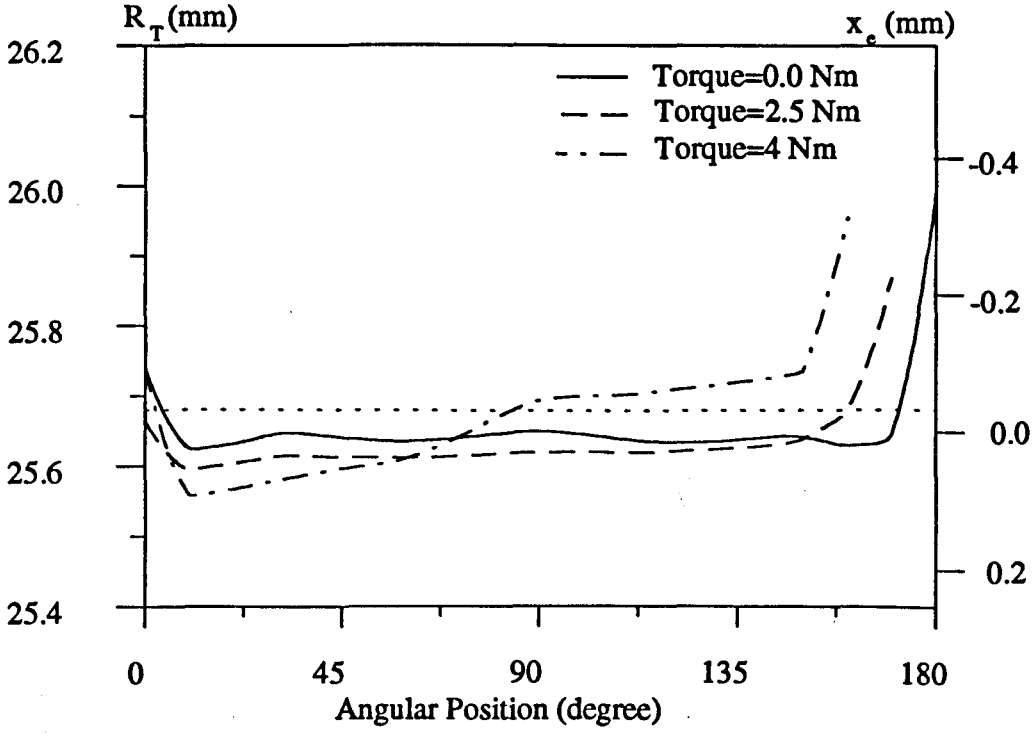


**(b) Driving pulley**

**Fig. 6.2 Variation of drive radius and radial movement against angular position for a used v-ribbed belt (with rib bottom contact) ($F_t + F_r$=200 N, $d_e$=45 mm)**

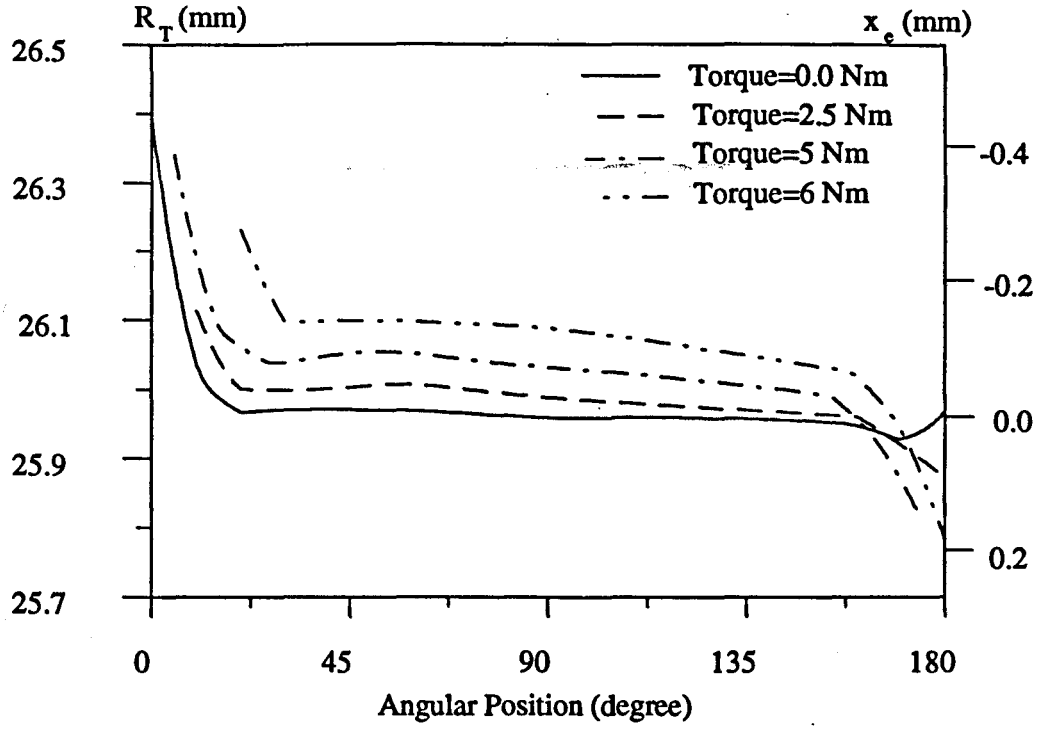


**(a) Driven pulley**

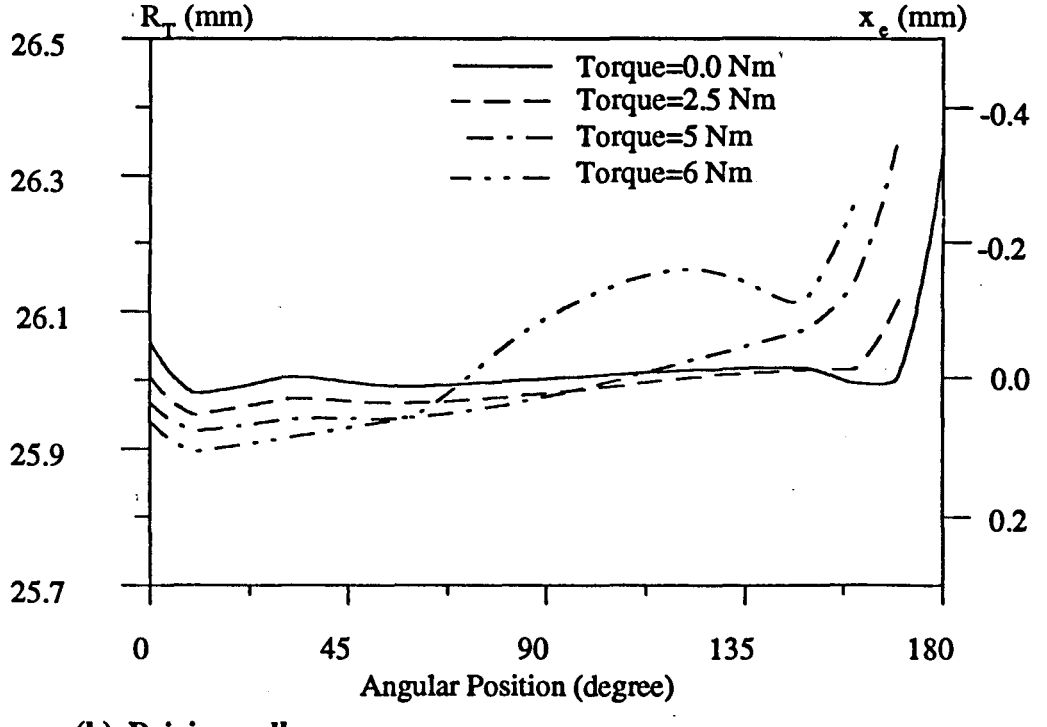


**(b) Driving pulley**

**Fig. 6.3 Variation of drive radius and radial movement against angular position for a new v-ribbed belt (without rib bottom contact) ($F_t + F_r = 300\ N$, $d_e = 45\ mm$)**

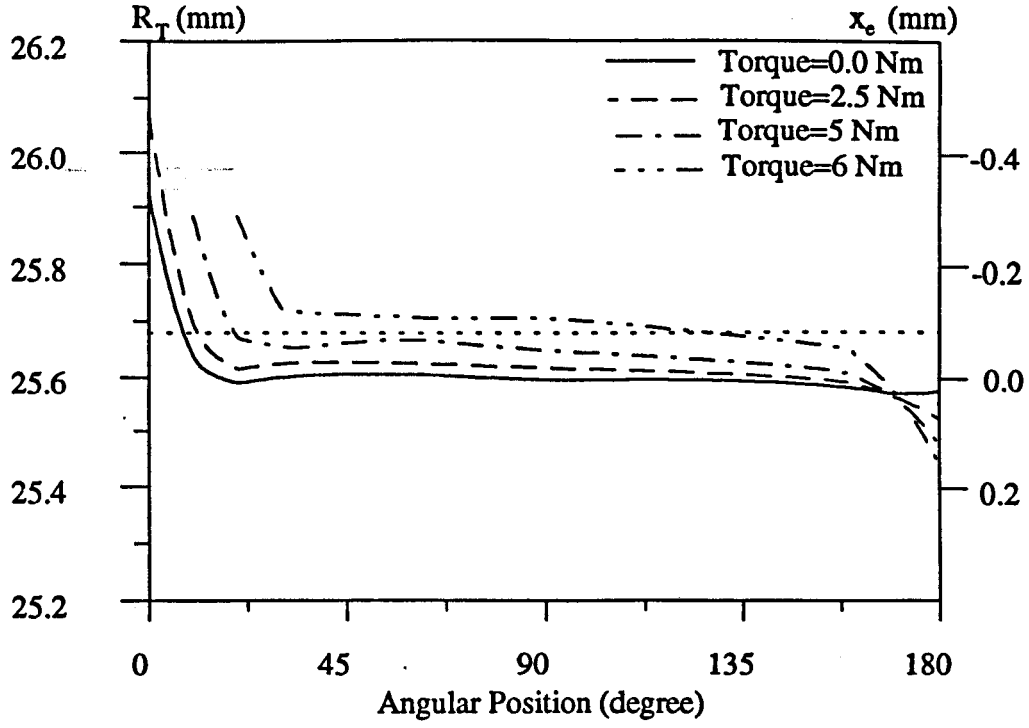


**(a) Driven pulley**

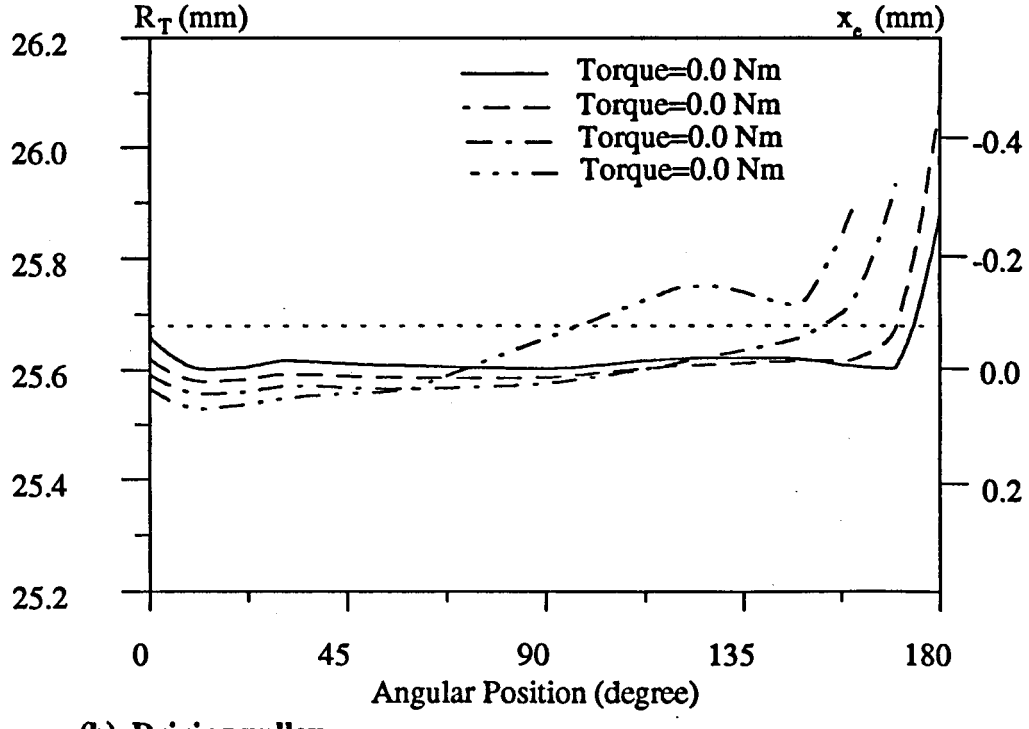


**(b) Driving pulley**

**Fig. 6.4 Variation of drive radius and radial movement against angular position for a used v-ribbed belt (with rib bottom contact) ($F_t + F_r$=300 N, $d_e$=45 mm)**

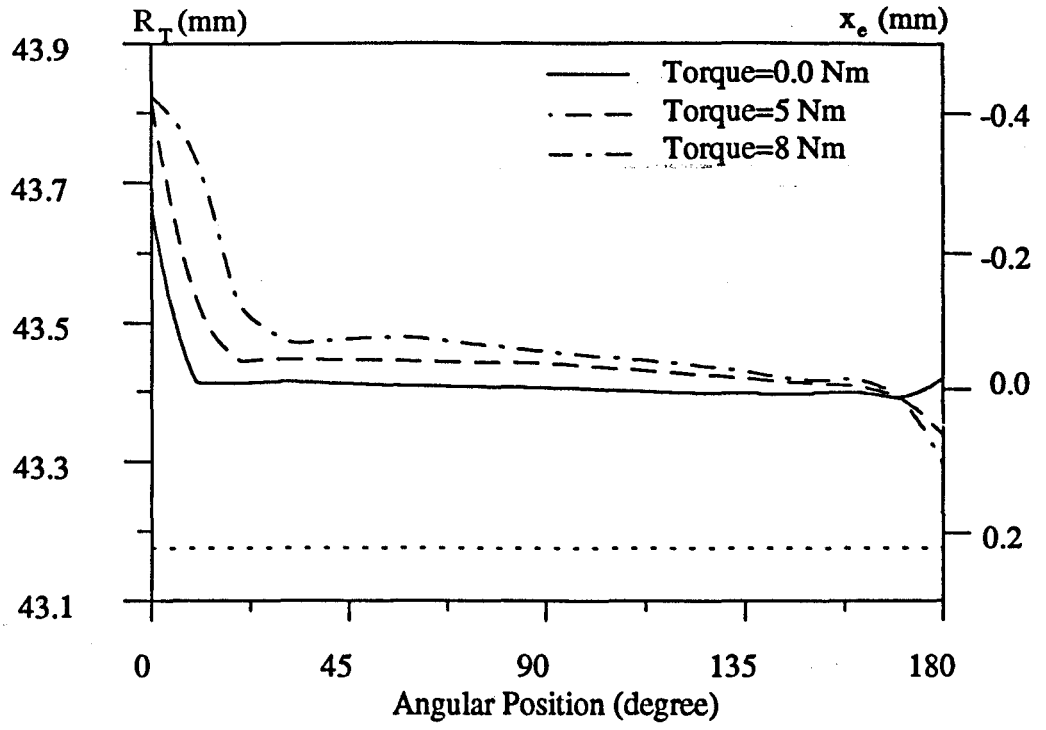


**(a) Driven pulley**

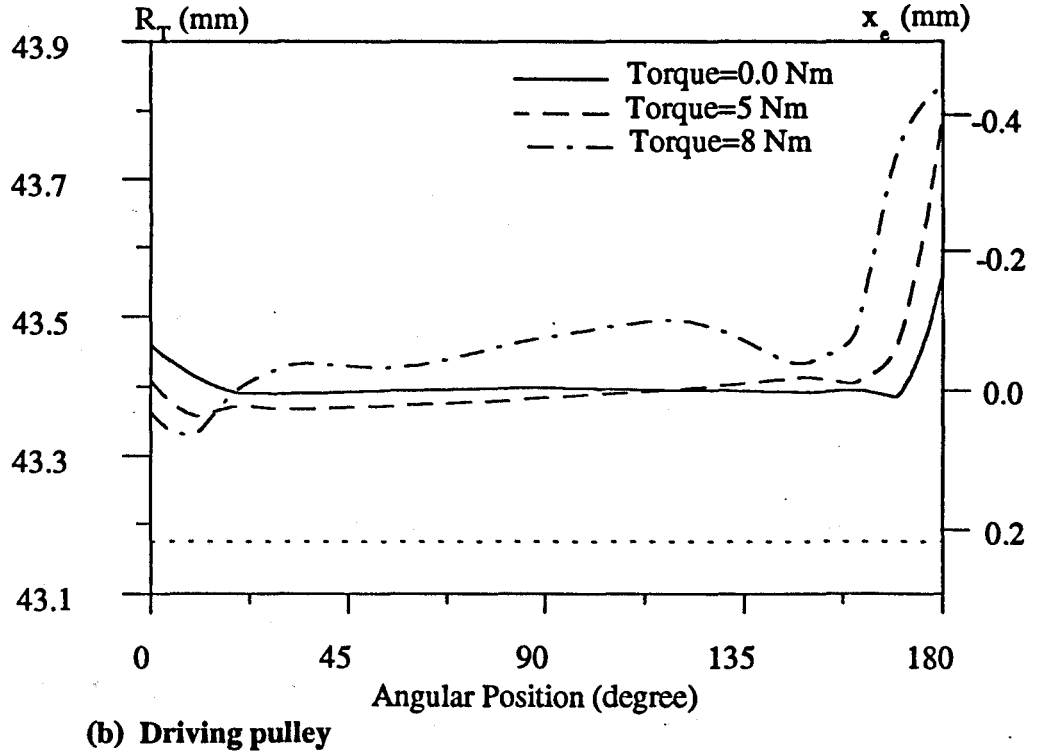


**(b) Driving pulley**

**Fig. 6.5 Variation of drive radius and radial movement against angular position for a new v-ribbed belt (without rib bottom contact) ($F_t + F_r$=200 N, $d_e$=80 mm)**

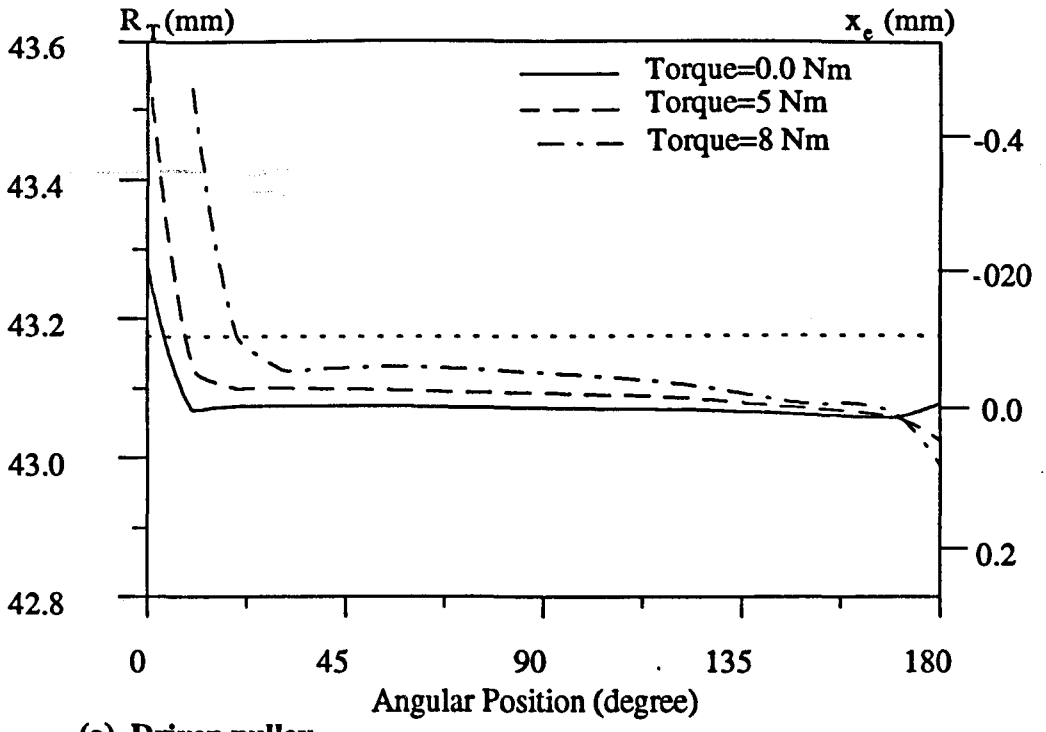


**(a) Driven pulley**

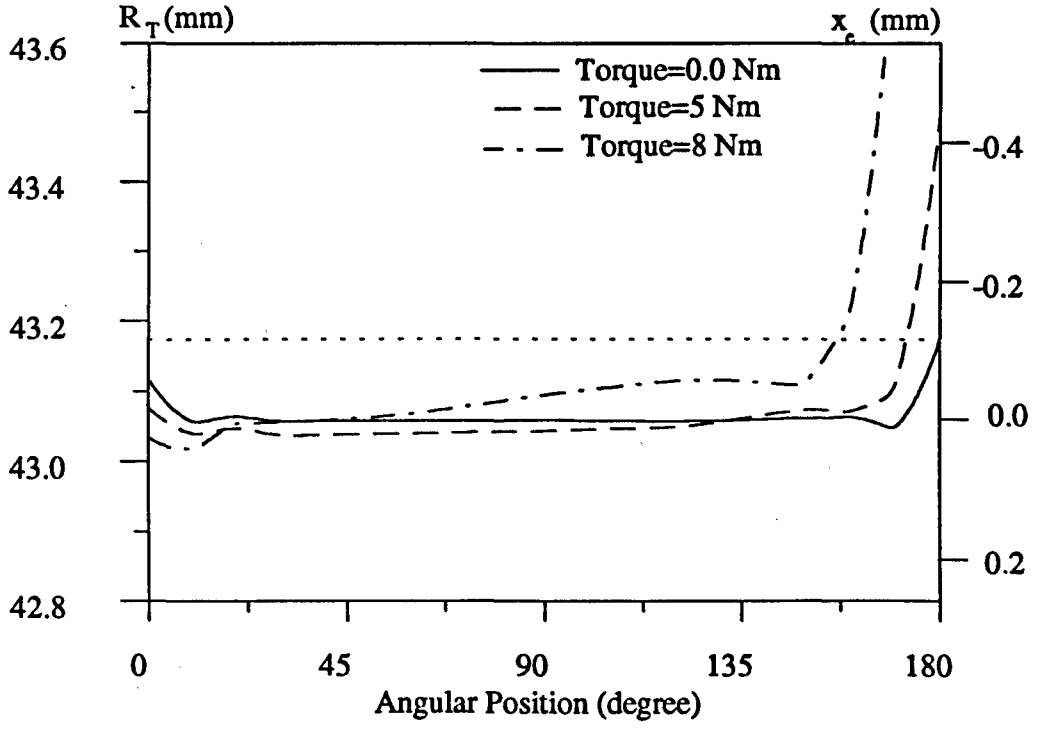


**(b) Driving pulley**

**Fig. 6.6 Variation of drive radius and radial movement against angular position for a used v-ribbed belt (with rib bottom contact) ($F_t + F_r$=200 N, $d_e$=80 mm)**

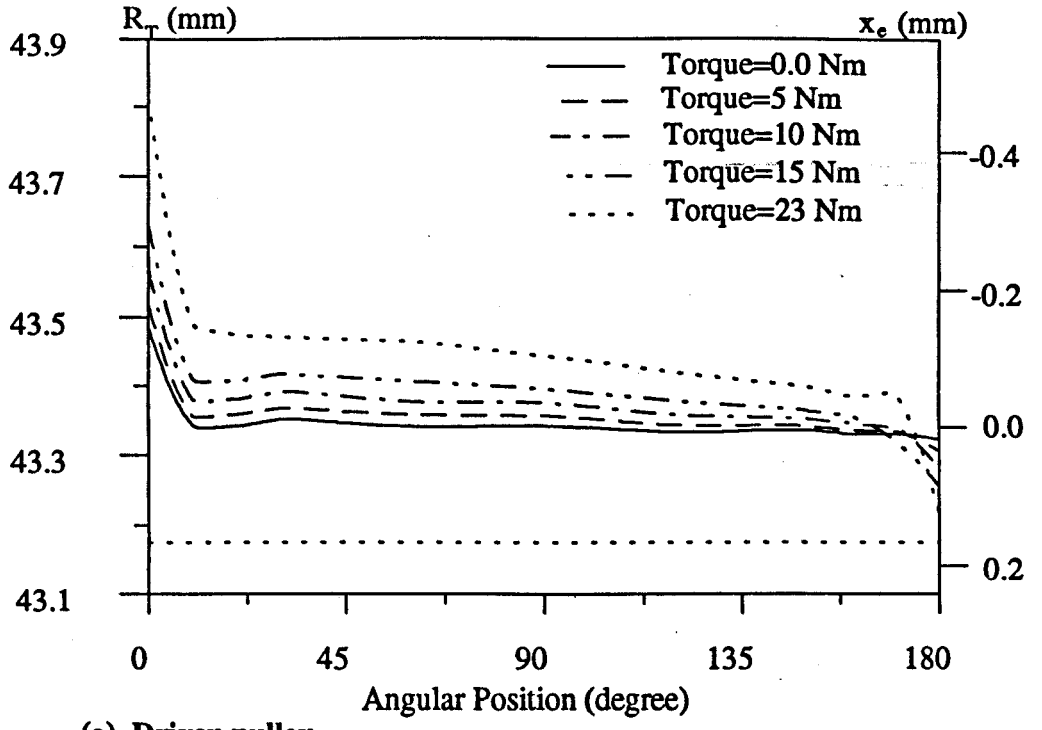


**(a) Driven pulley**

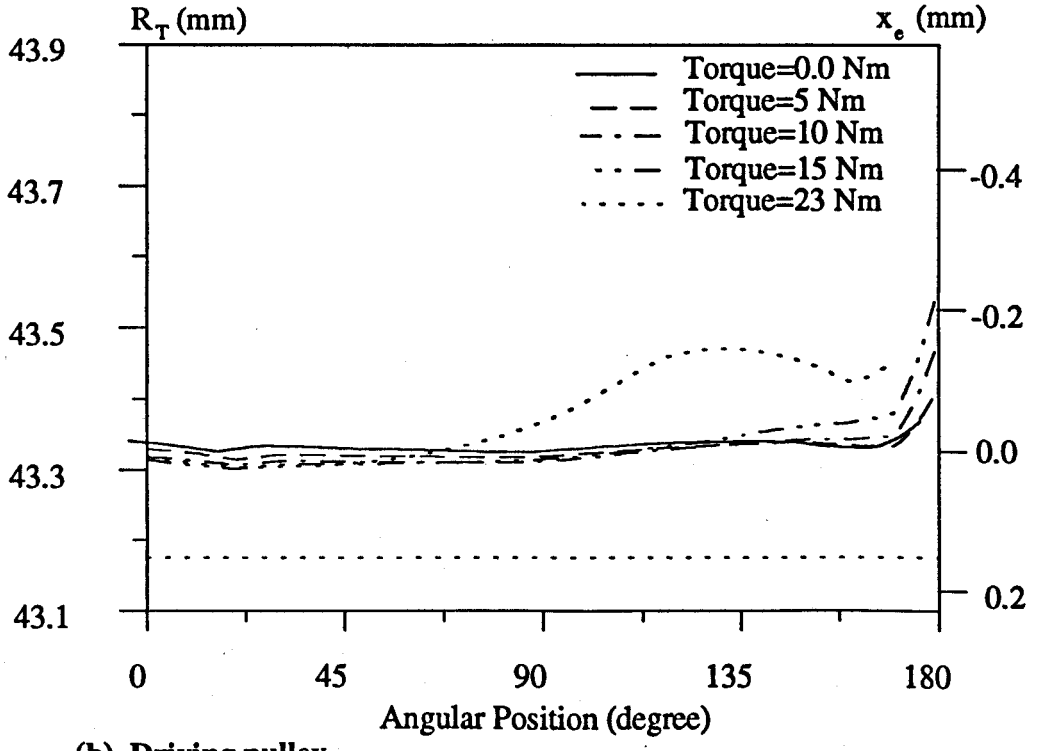


**(b) Driving pulley**

**Fig. 6.7 Variation of drive radius and radial movement against angular position for a new v-ribbed belt (without rib bottom contact) ($F_t + F_r$=600 N, $d_e$=80 mm)**

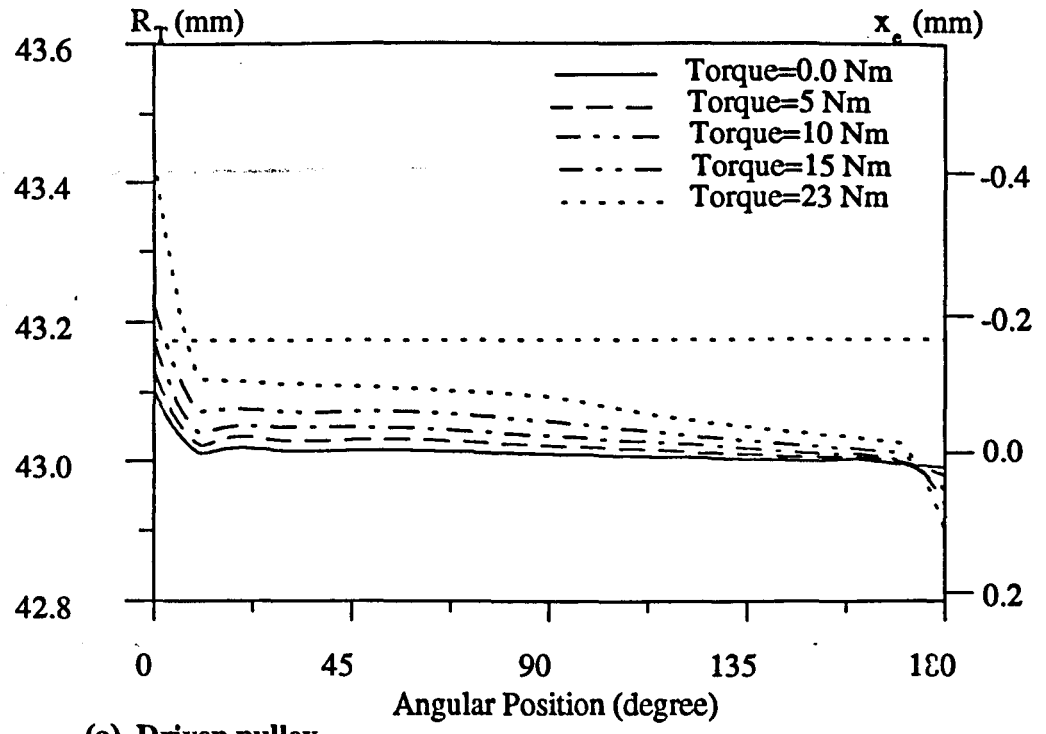


**(a) Driven pulley**

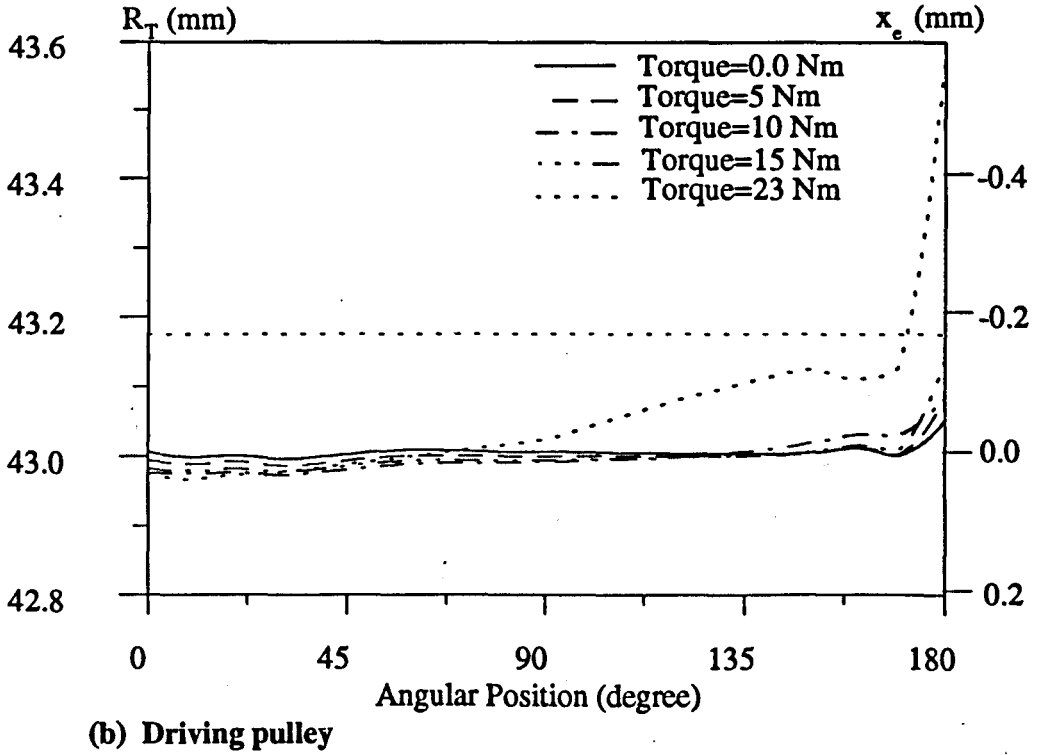


**(b) Driving pulley**

**Fig. 6.8 Variation of drive radius and radial movement against angular position for a used v-ribbed belt (with rib bottom contact) ($F_t + F_r$=600 N, $d_e$=80 mm)**

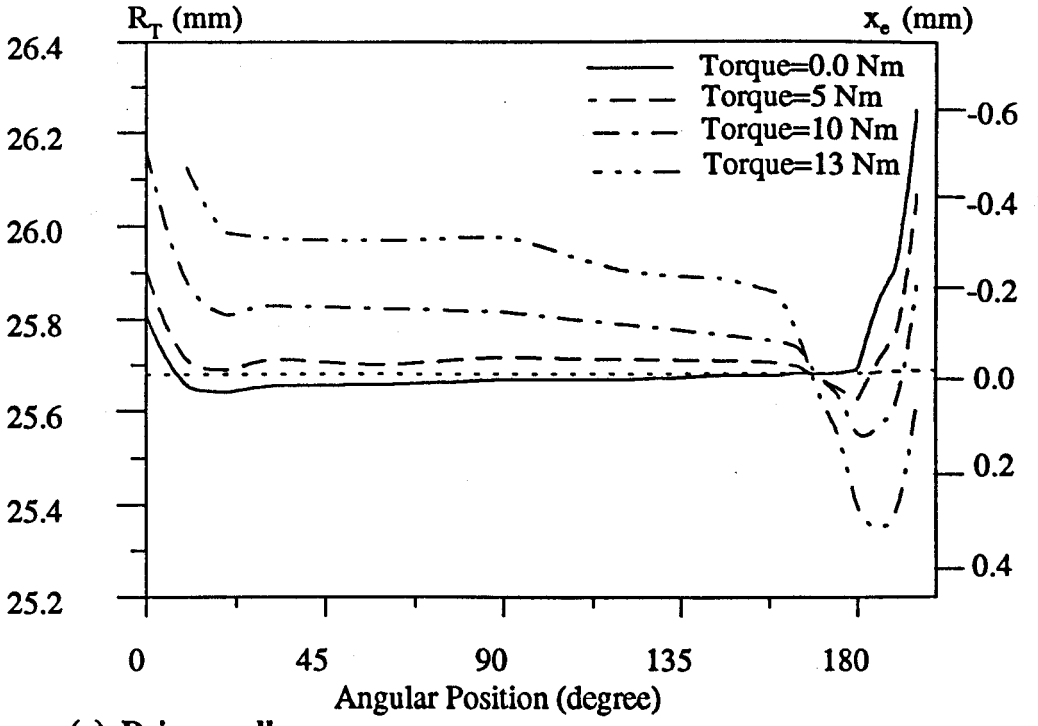


**(a) Driven pulley**

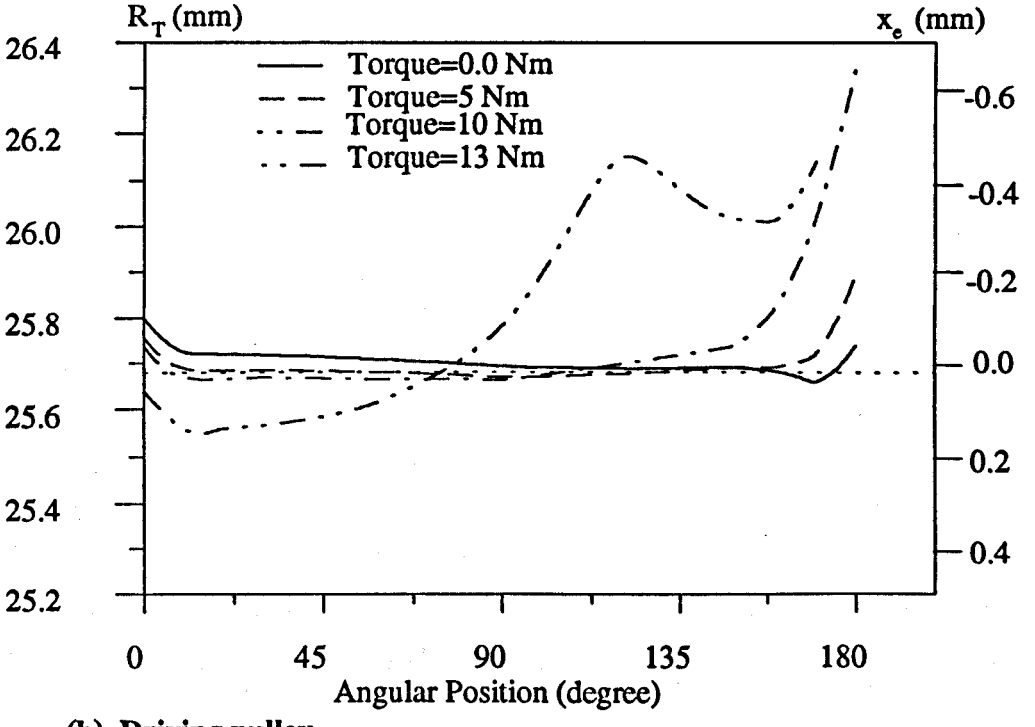


**(b) Driving pulley**

**Fig. 6.9 Variation of drive radius and radial movement against angular position for a new v-ribbed belt (extreme coditions test with mixed rib bottom contact)** ($F_t + F_r$=600 N, $d_e$=45 mm)

### 6.3.2 Slip and Torque Loss

During each set of tests the value of speed ratio $\omega_{dn}/\omega_{dg}$, the acting torque on motor $T_m$ and torque difference between motor and generator $T_m - T_g$ was collected at least four times. The average of these readings are represented in tables 6.8 and 6.9 for $d_e$=*45mm* and $d_e$=*80mm* respectively.

Slip in the drive was calculated according to equation (4.2), taking account of manufacturing errors of pulley diameter by including actual values of radii rather than the nominal equal values.

$$s = 1 - \frac{(\omega R)_{dn}}{(\omega R)_{dg}} = 1 - \frac{\omega_{dn}}{\omega_{dg}} \cdot \frac{R_{dn}}{R_{dg}}$$

Torque loss $T_L$ was determined by equation (4.6), taking account of the effect of windage of *0.14 Nm*.

$$T_L = (T_m - T_g) - 0.14\,Nm$$

The difference between tight and relaxed side tension $(F_t - F_r)$ was calculated by

$$F_t - F_r = \frac{T_m}{(R_e + 1.5)/1000}$$

Here $d_e$ is in millimetres and it was assumed that $T_m \approx T_{dg}$.

Figs. 6.10 and 6.11 show the variation of slip versus the difference between tight and relaxed side tensions $(F_t - F_r)$. In Fig. 6.10 the graphs are related to the new and used belts and two values of $(F_t + F_r)$=*200N*, $F_t + F_r$=*300N* and $F_t + F_r$=*600N* for $d_e$=*45mm*.

In Fig. 6.11 the graphs are related to the new and used belts and two values of $(F_t + F_r)$=*200N* and $F_t + F_r$=*600N* for $d_e$=*80mm*.

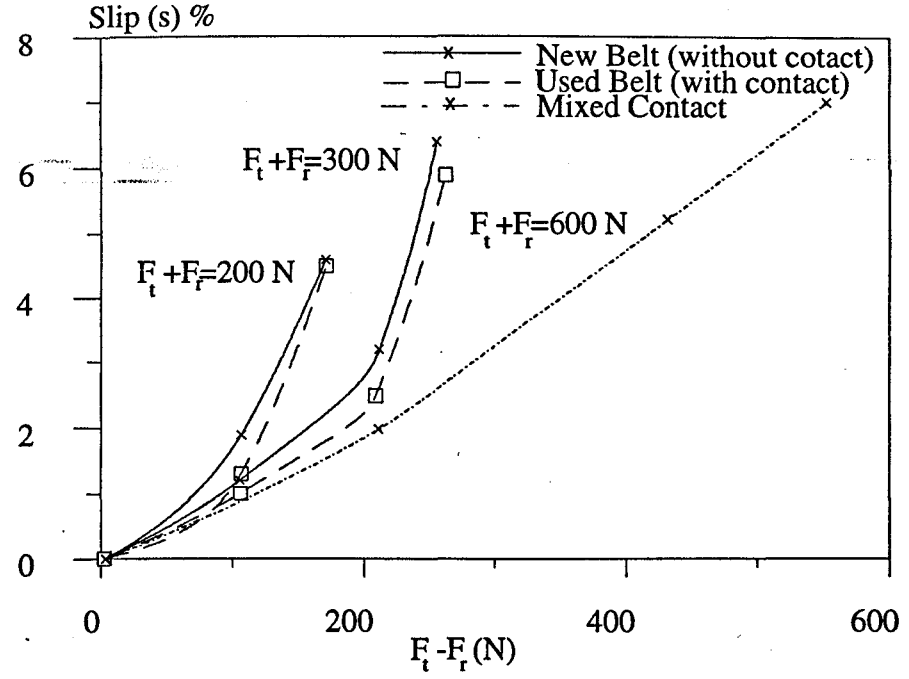


**Fig. 6.10 Slip (s) verses ($F_t - F_r$) for new (without rib bottom contact) and used (with rib bottom contact) v-ribbed belts and extreme conditions test (mixed contact) ($d_e$=45mm)**

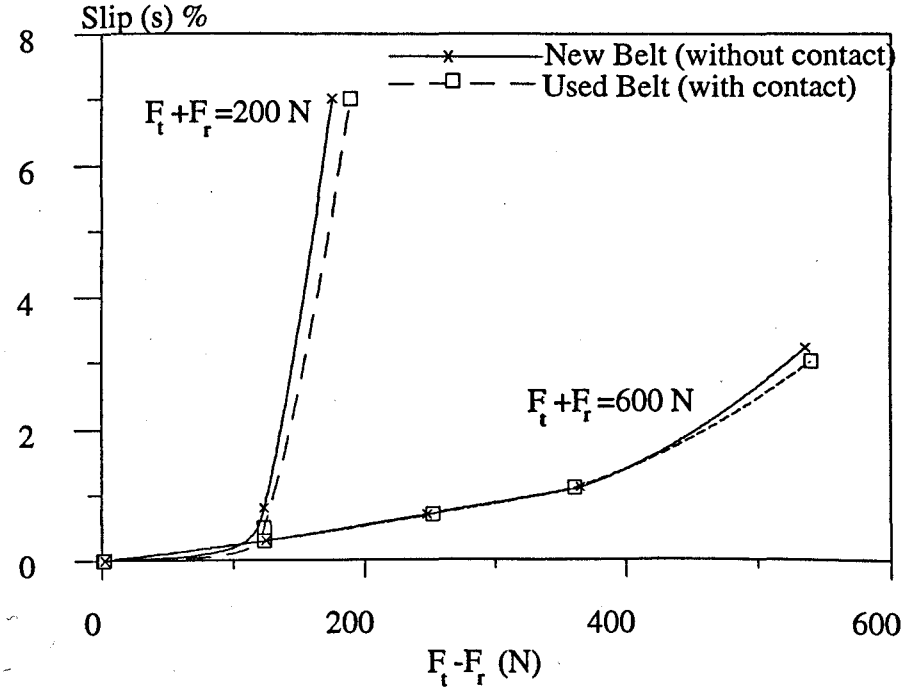


**Fig. 6.11 Slip (s) verses ($F_t - F_r$) for new (without rib bottom contact) and used (with rib bottom contact) v-ribbed belts ($d_e$=80mm)**

It can be seen that in the initial stages slip increase slightly and a more rapid increase occurs at higher values of $(F_t - F_r)$ when the belt begins slipping over the whole of the arc of contact and approaches the full skidding condition. The results showed a very small difference between new and used belts. Slip for the used belts is up to 0.3% lower than new belts, while the maximum $(F_t - F_r)$ is slightly higher than new belts.

Figs. 6.12 (a, b and c) and 6.13 show the variation of torque loss $T_L$ versus the difference between tight and relaxed side tensions $(F_t - F_r)$. Figs. 6.12 (a, b) are related to the new and used belts and two values of $(F_t + F_r)$=*200N*, $F_t + F_r$=*300N* for $d_e$=*45mm* respectively. Fig. 612c is related to $F_t + F_r$=*600N* for $d_e$=*45mm*. Figs. 6.13 (a and b) are related to the new and used belts and two values of $(F_t + F_r)$=*200N* and $F_t + F_r$=*600N* for $d_e$=*80mm* respectively.

The results show no significant difference between new and used belts, but a very small lower value of torque loss for new belts. The maximum difference between new and used belt torque loss during the carried out tests was a value of *0.028 Nm.* Increasing the transmitted power $(F_t - F_r)$ increases torque loss in all of the cases. In spite of large uncertainty of torque loss at low values, the no-load value of torque loss at $(F_t - F_r)$=0 can be attributed to belt bending hysteresis and wedge action and it is increasing with the total belt tension $(F_t + F_r)$.

Some subsidiary tests carried out with smaller intervals of $(F_t - F_r)$ are reported in the next section, to have better comparisons.

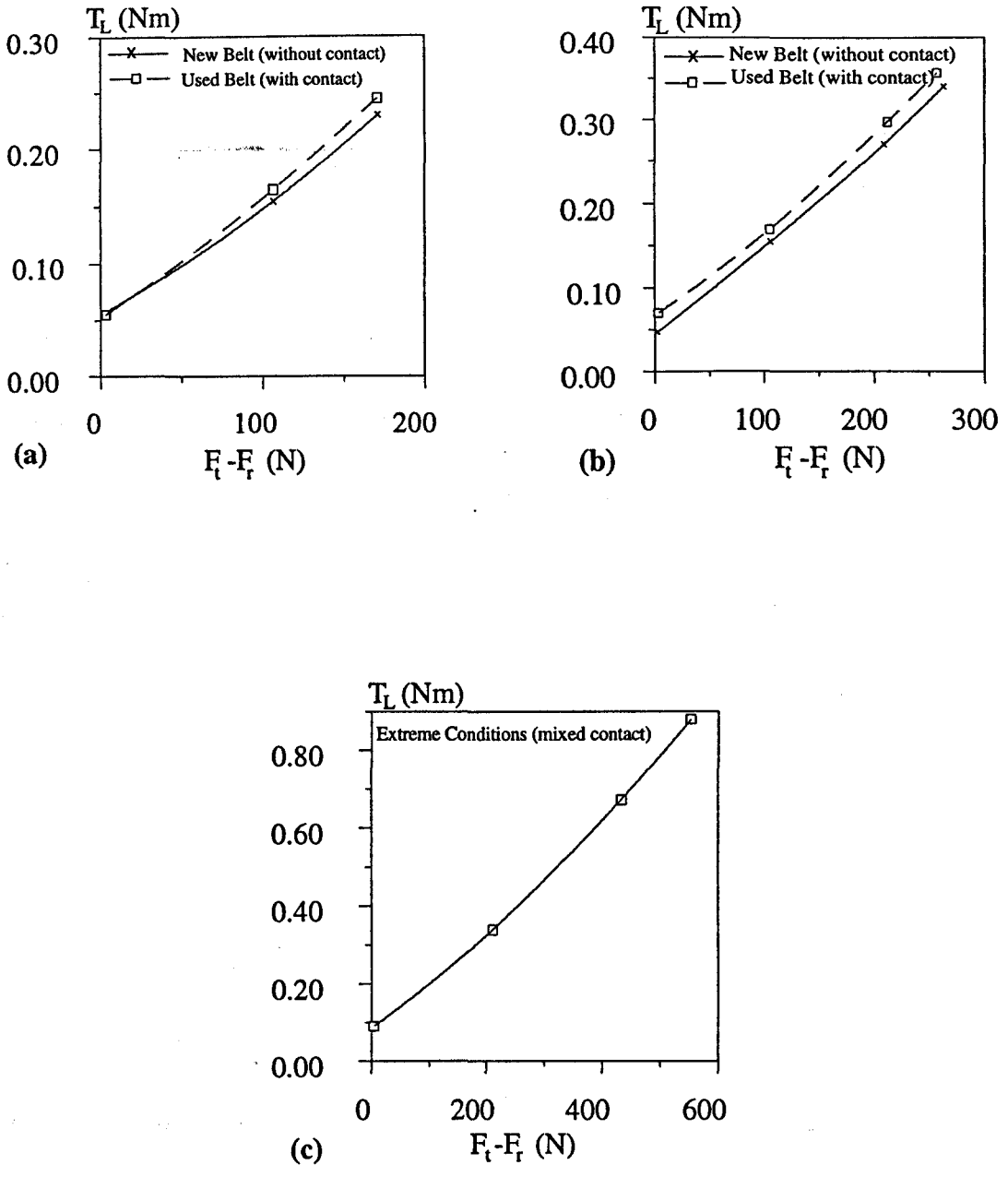


**Fig. 6.12 Torque loss($T_L$) verses ($F_t - F_r$) for new (without rib bottom contact) and used (with rib bottom contact) v-ribbed belts ($d_e$=45mm), (a) $F_t + F_r$ =200 N, (b) $F_t + F_r$ =300 N, (c) extreme conditions test (mixed contact), $F_t + F_r$ =600 N**

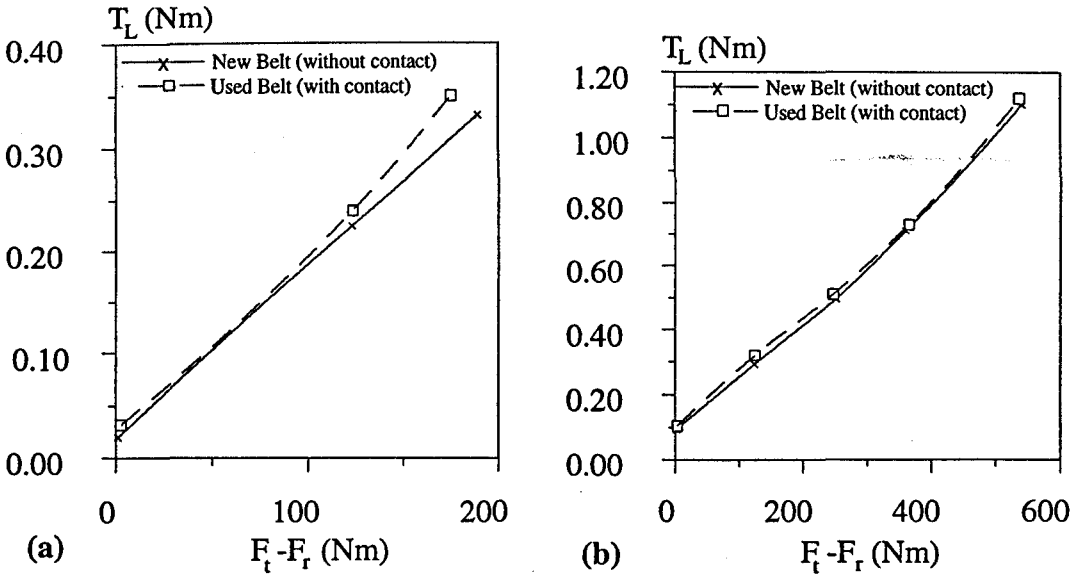


**Fig. 6.13 Torque loss($T_L$) verses ($F_t - F_r$) for new (without rib bottom contact) and used (with rib bottom contact) v-ribbed belts ($d_e$=80mm), (a) $F_t + F_r$ =200 N, (b) $F_t + F_r$ =600 N**

## 6.3.3 Subsidiary Tests for Slip and Torque Loss

To have a more detailed investigation on performance of v-ribbed belts additional torque loss and slip measurements were carried out with five different v-ribbed belts running on a pair of equal size pulleys, $d_e$=45mm. Used (cut), half-used (cut), new (cut), new molded and new anti-wear v-ribbed belts were examined at *470 N* total tension and running at two speeds of $\omega$=*1000RPM* and $\omega$=*2000RPM*. These measurements were carried out at eight stages of applied torque, $T_m$. The values of $H_T$ for the tested belts at no-load (zero torque) condition are

| | |
|---|---|
| cut used belt 3-PK-900 | *2.977 mm* |
| cut half-used belt 3-PK-900 | *3.021 mm* |

| | |
|---|---|
| cut new belt 3-PK-900 | *3.098 mm* |
| molded new belt 3-PK-900 | *2.337 mm* |
| anti-wear new belt 3-PK-900 | *3.068 mm* |

Figs. 6.14 (a, b and c) and 6.15 (a, b and c) show the variation of slip and torque loss versus the difference between tight and relaxed side tensions $(F_t - F_r)$ respectively. In the Figs. 6.14a and 6.15a the graphs are related to the new, used and half-used cut belts at $\omega = 1000RPM$. Figs. 6.14b and 6.15b show the variation of slip and torque loss for cut, molded and anti-wear belts at $\omega = 1000RPM$. The effect of speed on slip and torque loss is shown on Figs. 6.14c and 6.15c for a new cut belt at $\omega = 1000RPM$ and $\omega = 2000RPM$. In aid of clarification only the data for new cut belt have been plotted. These figures have been constructed from data given in table 6.10.

It can be seen that the new molded belt had lower slip and higher torque capacity. Also the half-used belt had lower slip comparing new and used belt. The running speed had negligible effect on slip. Torque loss for all the cases showed a similar trend and an approximately linear relationship with $(F_t - F_r)$. Cowburn [1] in his experimental measurements for v-belt has reported that the torque loss remained constant with $(F_t - F_r)$, and developed a theoretical model on this base. The same rig has been used in this work for v-ribbed belt experimental investigations (see chapter 4). It has been found a faulty device for measuring the difference between torques of driving and driven pulleys. Probably, his results have been affected by this device.

The next chapter will deal with the comparison of the theoretical and experimental results.

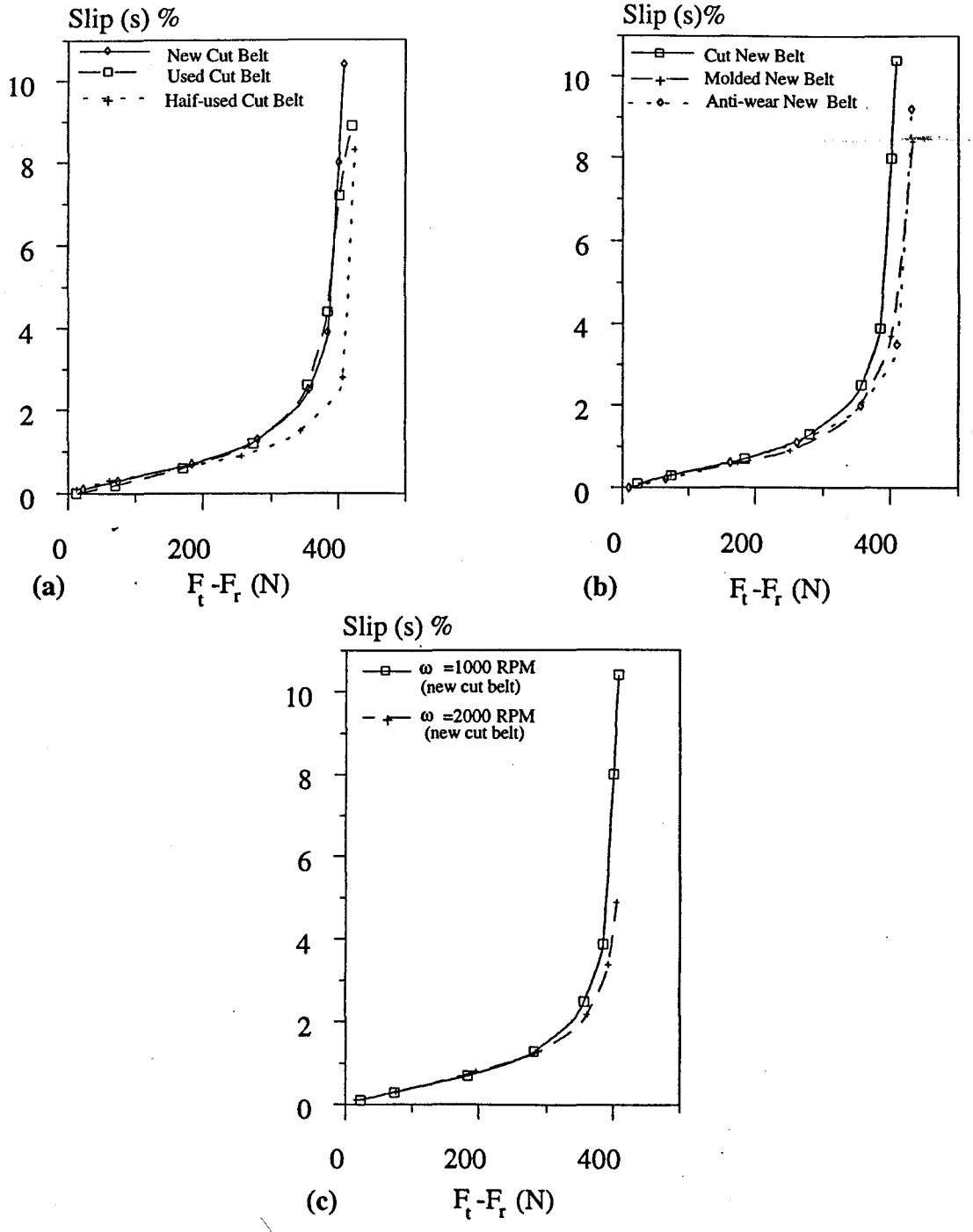


**Fig. 6.14 Slip (s) verses $(F_t - F_r)$ for (a) new, half-used and used cut belts (b) new cut, new molded and new anti-wear belts (c) new cut, ω=*1000 RPM* and ω=*2000 RPM* ($d_e$=*80mm*, $F_t + F_r$ =*470 N*)**

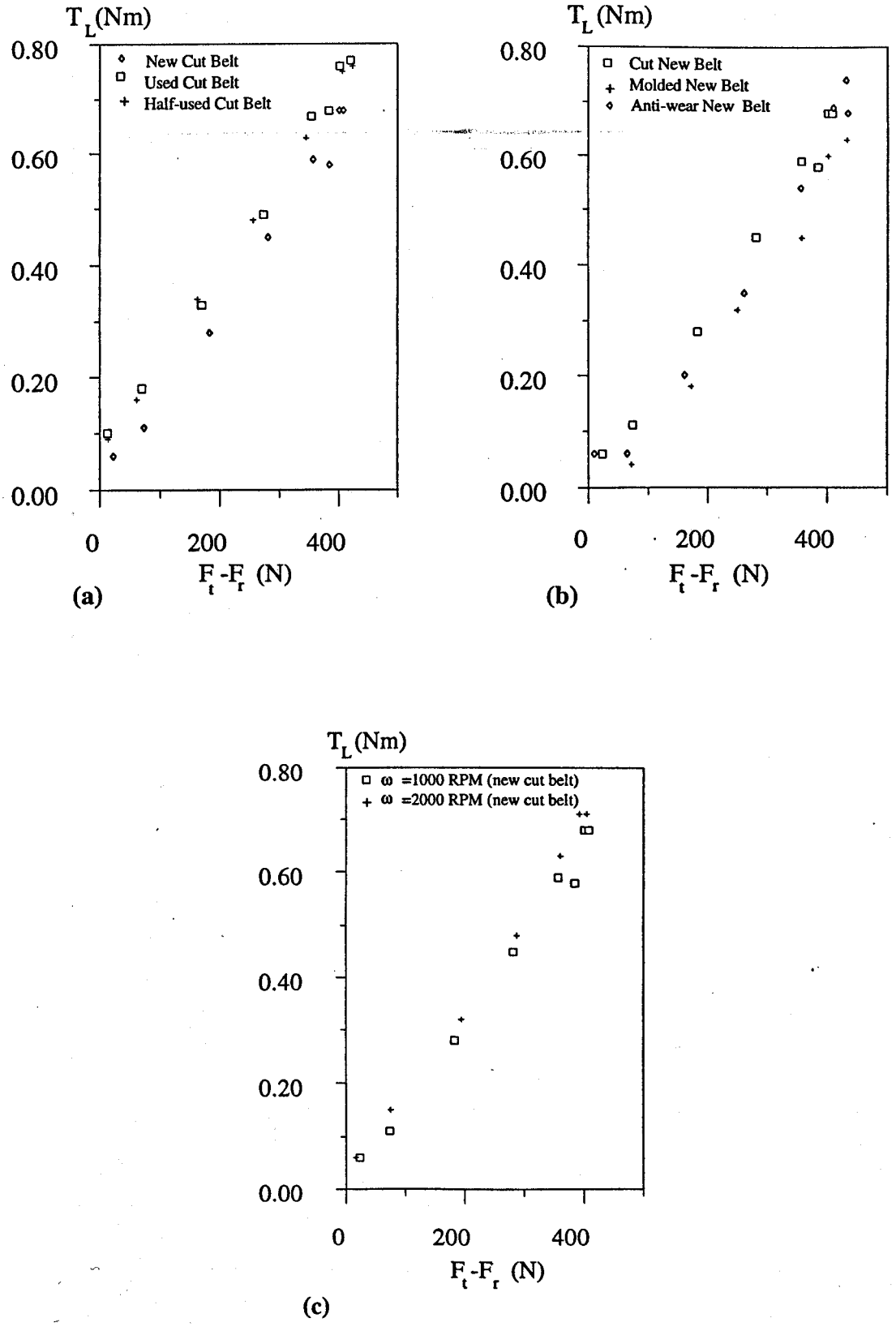


**Fig. 6.15 Torque loss verses $(F_t - F_r)$ for (a) new, half-used and used belts (b) cut, molded and anti-wear belts (c) ω=*1000 RPM*, ω=*2000 RPM* ($d_e$=*80mm*, $F_t + F_r$ =*470 N*)**

Table 6.3 Experimental readings of $H_T$ (mm), for ($F_t + F_r$=200 N, $d_e$=45 mm)

(a) new v-ribbed belt

| NEW BELT | driven pulley ($F_t + F_r$=200 N, $d_e$=45 mm) | | | driving pulley ($F_t + F_r$=200 N, $d_e$=45 mm) | | |
|---|---|---|---|---|---|---|
| Angular position (degree) | *T=0 Nm* | *T=2.5 Nm* | *T=4 Nm* | *T=0 Nm* | *T=2.5 Nm* | *T=4 Nm* |
| 0 | 4.005 | 4.087 | 4.953 | 3.569 | 3.476 | 3.388 |
| 10 | 3.560 | 3.719 | 4.046 | 3.448 | 3.398 | 3.336 |
| 20 | 3.423 | 3.520 | 3.799 | 3.429 | 3.399 | 3.355 |
| 30 | 3.416 | 3.453 | 3.568 | 3.453 | 3.418 | 3.375 |
| 60 | 3.430 | 3.475 | 3.521 | 3.447 | 3.415 | 3.453 |
| 90 | 3.422 | 3.460 | 3.508 | 3.458 | 3.434 | 3.565 |
| 120 | 3.405 | 3.434 | 3.485 | 3.464 | 3.458 | 3.545 |
| 150 | | | | 3.465 | 3.483 | 3.575 |
| 160 | 3.397 | 3.415 | 3.450 | 3.446 | 3.546 | 3.820 |
| 170 | 3.377 | 3.350 | 3.351 | 3.493 | 3.772 | 4.101 |
| 180 | 3.433 | 3.307 | 3.239 | 3.946 | 4.099 | |

(b) used v-ribbed belt

| USED BELT | driven pulley ($F_t + F_r$=200 N, $d_e$=45 mm) | | | driving pulley ($F_t + F_r$=200 N, $d_e$=45 mm) | | |
|---|---|---|---|---|---|---|
| Angular position (degree) | *T=0 Nm* | *T=2.5 Nm* | *T=4 Nm* | *T=0 Nm* | *T=2.5 Nm* | *T=4 Nm* |
| 0 | 3.485 | 3.860 | 4.087 | 3.160 | 3.085 | 3.036 |
| 10 | 3.131 | 3.290 | 3.917 | 3.046 | 3.015 | 2.980 |
| 20 | 3.040 | 3.090 | 3.509 | 3.052 | 3.024 | 2.987 |
| 30 | 3.039 | 3.068 | 3.209 | 3.066 | 3.034 | 3.000 |
| 60 | 3.040 | 3.071 | 3.119 | 3.057 | 3.033 | 3.033 |
| 90 | 3.042 | 3.066 | 3.119 | 3.071 | 3.041 | 3.115 |
| 120 | 3.033 | 3.055 | 3.105 | 3.055 | 3.042 | 3.129 |
| 150 | | | | 3.062 | 3.060 | 3.159 |
| 160 | 3.035 | 3.044 | 3.072 | 3.050 | 3.102 | 3.375 |
| 170 | 3.005 | | 2.987 | 3.067 | 3.289 | 3.873 |
| 180 | 3.059 | 2.963 | 2.892 | 3.416 | 3.915 | 4.090 |

Table 6.4 Experimental readings of $H_T$ (mm), for ($F_t + F_r$=300 N, $d_e$=45 mm)

(a) new v-ribbed belt

| NEW BELT | driven pulley ($F_t + F_r$=300 N, $d_e$=45 mm) | | | | driving pulley ($F_t + F_r$=300 N, $d_e$=45 mm) | | | |
|---|---|---|---|---|---|---|---|---|
| angular position degree | T=0 Nm | T=2.5 Nm | T=5 Nm | T=6 Nm | T=0 Nm | T=2.5 Nm | T=5 Nm | T=6 Nm |
| 0 | 3.814 | 3.960 | 4.071 | 4.073 | 3.476 | 3.426 | 3.388 | 3.360 |
| 10 | 3.460 | 3.536 | 3.765 | 3.999 | 3.402 | 3.370 | 3.346 | 3.316 |
| 20 | 3.388 | 3.422 | 3.512 | 3.655 | 3.410 | 3.380 | 3.353 | 3.325 |
| 30 | 3.391 | 3.420 | 3.963 | 3.520 | 3.424 | 3.392 | 3.362 | 3.335 |
| 60 | 3.390 | 3.418 | 3.475 | 3.518 | 3.411 | 3.387 | 3.366 | 3.369 |
| 90 | 3.380 | 3.409 | 3.455 | 3.508 | 3.422 | 3.401 | 3.396 | 3.510 |
| 120 | 3.380 | 3.396 | 3.439 | 3.483 | 3.434 | 3.422 | 3.444 | 3.581 |
| 150 | | | | | 3.437 | 3.435 | 3.497 | 3.545 |
| 160 | 3.367 | 3.380 | 3.405 | 3.438 | 3.416 | 3.436 | 3.562 | 3.680 |
| 170 | 3.348 | 3.339 | 3.339 | 3.361 | 3.427 | 3.538 | 3.780 | 4.026 |
| 180 | 3.387 | 3.292 | 3.228 | 3.199 | 3.760 | 4.029 | 4.099 | |

(b) used v-ribbed belt

| USED BELT | driven pulley ($F_t + F_r$=300 N, $d_e$=45 mm) | | | | driving pulley ($F_t + F_r$=300 N, $d_e$=45 mm) | | | |
|---|---|---|---|---|---|---|---|---|
| angular position degree | T=0 Nm | T=2.5 Nm | T=5 Nm | T=6 Nm | T=0 Nm | T=2.5 Nm | T=5 Nm | T=6 Nm |
| 0 | 3.345 | 3.488 | 3.920 | 4.071 | 3.080 | 3.040 | 3.012 | 2.987 |
| 10 | 3.060 | 3.119 | 3.309 | 3.830 | 3.025 | 3.001 | 2.978 | 2.950 |
| 20 | 3.010 | 3.036 | 3.094 | 3.308 | 3.024 | 3.002 | 2.979 | 2.955 |
| 30 | 3.020 | 3.045 | 3.076 | 3.146 | 3.036 | 3.012 | 2.990 | 2.967 |
| 60 | 3.025 | 3.046 | 3.088 | 3.128 | 3.028 | 3.006 | 2.987 | 2.987 |
| 90 | 3.016 | 3.037 | 3.069 | 3.126 | 3.023 | 3.007 | 2.996 | 3.078 |
| 120 | 3.016 | 3.030 | 3.056 | 3.106 | 3.040 | 3.028 | 3.033 | 3.168 |
| 150 | | | | | 3.038 | 3.036 | 3.085 | 3.153 |
| 160 | 2.999 | 3.007 | 3.022 | 3.064 | 3.028 | 3.038 | 3.142 | 3.306 |
| 170 | 2.988 | 2.982 | 2.980 | 2.987 | 3.026 | 3.099 | 3.353 | 3.649 |
| 180 | 2.992 | 2.940 | 2.892 | 2.857 | 3.299 | 3.500 | 3.999 | 4.099 |

Table 6.5 Experimental readings of $H_T$ (mm), for ($F_t + F_r$=200 N, $d_e$=80 mm)

(a) new v-ribbed belt

| NEW BELT | driven pulley ($F_t + F_r$=200 N, $d_e$=80 mm) | | | driving pulley ($F_t + F_r$=200 N, $d_e$=80 mm) | | |
|---|---|---|---|---|---|---|
| Angular position (degree) | *T=0 Nm* | *T=5 Nm* | *T=8 Nm* | *T=0 Nm* | *T=5 Nm* | *T=8 Nm* |
| 0 | 3.586 | 3.740 | 3.747 | 3.384 | 3.334 | 3.288 |
| 10 | 3.340 | 3.460 | 3.660 | 3.340 | 3.283 | 3.257 |
| 20 | 3.338 | 3.370 | 3.451 | 3.316 | 3.297 | 3.322 |
| 30 | 3.340 | 3.373 | 3.401 | 3.315 | 3.293 | 3.353 |
| 60 | 3.334 | 3.370 | 3.404 | 3.320 | 3.299 | 3.355 |
| 90 | 3.331 | 3.366 | 3.383 | 3.323 | 3.309 | 3.395 |
| 120 | 3.324 | 3.352 | 3.366 | 3.320 | 3.321 | 3.420 |
| 150 | 3.322 | 3.336 | 3.341 | 3.317 | 3.338 | 3.360 |
| 160 | 3.323 | 3.332 | 3.342 | 3.320 | 3.330 | 3.400 |
| 170 | 3.316 | 3.315 | 3.314 | 3.312 | 3.390 | 3.670 |
| 180 | 3.343 | 3.260 | 3.218 | 3.483 | 3.720 | 3.760 |

(b) used v-ribbed belt

| USED BELT | driven pulley ($F_t + F_r$=200 N, $d_e$=80 mm) | | | driving pulley ($F_t + F_r$=200 N, $d_e$=80 mm) | | |
|---|---|---|---|---|---|---|
| Angular position (degree) | *T=0 Nm* | *T=5 Nm* | *T=8 Nm* | *T=0 Nm* | *T=5 Nm* | *T=8 Nm* |
| 0 | 3.200 | 3.500 | 3.750 | 3.042 | 3.002 | 2.960 |
| 10 | 2.995 | 3.060 | 3.464 | 2.983 | 2.966 | 2.945 |
| 20 | 3.000 | 3.025 | 3.104 | 2.990 | 2.973 | 2.980 |
| 30 | 3.000 | 3.026 | 3.053 | 2.983 | 2.963 | 2.982 |
| 60 | 3.000 | 3.022 | 3.056 | 2.984 | 2.966 | 2.994 |
| 90 | 2.997 | 3.018 | 3.047 | 2.985 | 2.970 | 3.020 |
| 120 | 2.995 | 3.012 | 3.032 | 2.983 | 2.975 | 3.040 |
| 150 | 2.987 | 2.996 | 3.003 | 2.988 | 2.999 | 3.040 |
| 160 | 2.984 | 2.991 | 3.003 | 2.990 | 2.998 | 3.150 |
| 170 | 2.983 | 2.983 | 2.987 | 2.976 | 3.037 | 3.700 |
| 180 | 3.003 | 2.949 | 2.913 | 3.100 | 3.422 | |

Table 6.6 Experimental readings of $H_T$ (mm), for ($F_t + F_r$=200 N, $d_e$=80mm

(a) new v-ribbed belt

| NEW BELT | driven pulley ($F_t + F_r$=600 N, $d_e$=80 mm) | | | | |
|---|---|---|---|---|---|
| Angular position (degree) | *T=0 Nm* | *T=5 Nm* | *T=10 Nm* | *T=15 Nm* | *T=23 Nm* |
| 0 | 3.409 | 3.442 | 3.493 | 3.557 | 3.737 |
| 10 | 3.268 | 3.281 | 3.305 | 3.335 | 3.416 |
| 20 | 3.267 | 3.284 | 3.306 | 3.333 | 3.399 |
| 30 | 3.276 | 3.292 | 3.316 | 3.342 | 3.396 |
| 60 | 3.266 | 3.283 | 3.302 | 3.331 | 3.388 |
| 90 | 3.266 | 3.280 | 3.299 | 3.319 | 3.367 |
| 120 | 3.257 | 3.267 | 3.282 | 3.302 | 3.343 |
| 150 | 3.260 | 3.266 | 3.276 | 3.288 | 3.322 |
| 160 | 3.255 | 3.260 | 3.270 | 3.280 | 3.309 |
| 170 | 3.255 | 3.258 | 3.264 | 3.305 | 3.312 |
| 180 | 3.247 | 3.230 | 3.203 | 3.180 | 3.138 |

| NEW BELT | driving pulley ($F_t + F_r$=600 N, $d_e$=80 mm) | | | | |
|---|---|---|---|---|---|
| Angular position (degree) | *T=0 Nm* | *T=5 Nm* | *T=10 Nm* | *T=15 Nm* | *T=23 Nm* |
| 0 | 3.266 | 3.255 | 3.244 | 3.240 | 3.245 |
| 10 | 3.260 | 3.250 | 3.240 | 3.233 | 3.236 |
| 20 | 3.252 | 3.241 | 3.233 | 3.228 | 3.230 |
| 30 | 3.259 | 3.247 | 3.238 | 3.233 | 3.230 |
| 60 | 3.254 | 3.245 | 3.237 | 3.235 | 3.245 |
| 90 | 3.251 | 3.245 | 3.238 | 3.241 | 3.293 |
| 120 | 3.262 | 3.257 | 3.255 | 3.260 | 3.386 |
| 150 | 3.264 | 3.264 | 3.268 | 3.287 | 3.375 |
| 160 | 3.258 | 3.260 | 3.269 | 3.292 | 3.350 |
| 170 | 3.258 | 3.260 | 3.276 | 3.307 | 3.380 |
| 180 | 3.294 | 3.342 | 3.410 | 3.485 | 4.00 |

Continued Over...

(b) used v-ribbed belt

| USED BELT | driven pulley ($F_t + F_r$=600 N, $d_e$=80 mm) | | | | |
|---|---|---|---|---|---|
| Angular position (degree) | *T=0 Nm* | *T=5 Nm* | *T=10 Nm* | *T=15 Nm* | *T=23 Nm* |
| 0 | 3.026 | 3.053 | 3.095 | 3.148 | 3.361 |
| 10 | 2.938 | 2.950 | 2.968 | 2.999 | 3.046 |
| 20 | 2.945 | 2.961 | 2.977 | 3.001 | 3.040 |
| 30 | 2.940 | 2.955 | 2.975 | 2.997 | 3.037 |
| 60 | 2.941 | 2.957 | 2.973 | 2.997 | 3.030 |
| 90 | 2.936 | 2.948 | 2.962 | 2.983 | 3.018 |
| 120 | 2.931 | 2.940 | 2.951 | 2.964 | 2.987 |
| 150 | 2.925 | 2.930 | 2.936 | 2.946 | 2.964 |
| 160 | 2.927 | 2.930 | 2.935 | 2.942 | 2.958 |
| 170 | 2.920 | 2.923 | 2.924 | 2.935 | 2.950 |
| 180 | 2.916 | 2.903 | 2.882 | 2.863 | 2.826 |

| USED BELT | driving pulley ($F_t + F_r$=600 N, $d_e$=80 mm) | | | | |
|---|---|---|---|---|---|
| 0 | 2.932 | 2.920 | 2.908 | 2.902 | 2.902 |
| 10 | 2.924 | 2.914 | 2.905 | 2.901 | 2.892 |
| 20 | 2.927 | 2.918 | 2.908 | 2.903 | 2.899 |
| 30 | 2.922 | 2.912 | 2.904 | 2.899 | 2.903 |
| 60 | 2.935 | 2.927 | 2.920 | 2.915 | 2.926 |
| 90 | 2.932 | 2.926 | 2.920 | 2.918 | 2.950 |
| 120 | 2.930 | 2.925 | 2.924 | 2.924 | 3.005 |
| 150 | 2.931 | 2.930 | 2.932 | 2.945 | 3.049 |
| 160 | 2.938 | 2.939 | 2.942 | 2.957 | 3.035 |
| 170 | 2.927 | 2.929 | 2.936 | 2.957 | 3.06 |
| 180 | 2.977 | 3.009 | 3.062 | 3.0123 | 3.499 |

Table 6.7 Experimental readings of $H_T$ (mm), for ($F_t + F_r$=600 N, $d_e$=45 mm)

| | driven pulley ($F_t + F_r$=600 N, $d_e$=45 mm) | | | | driving pulley ($F_t + F_r$=600 N, $d_e$=45 mm) | | | |
|---|---|---|---|---|---|---|---|---|
| angular position degree | *T=0 Nm* | *T=5 Nm* | *T=10 Nm* | *T=13 Nm* | *T=0 Nm* | *T=5 Nm* | *T=10 Nm* | *T=13 Nm* |
| -5 | | | | | 3.351 | 3.300 | 3.253 | 3.144 |
| 0 | 3.231 | 3.325 | 3.585 | 4.005 | 3.220 | 3.178 | 3.158 | 3.060 |
| 5 | | | | | 3.172 | 3.130 | 3.110 | 3.015 |
| 10 | 3.078 | 3.134 | 3.305 | 3.550 | 3.145 | 3.110 | 3.090 | 2.980 |
| 15 | | | | | 3.141 | 3.104 | 3.085 | 2.970 |
| 20 | 3.061 | 3.110 | 3.230 | 3.406 | 3.140 | 3.104 | 3.086 | 2.980 |
| 30 | 3.073 | 3.130 | 3.250 | 3.395 | 3.138 | 3.104 | 3.088 | 2.987 |
| 60 | 3.077 | 3.121 | 3.243 | 3.390 | 3.128 | 3.100 | 3.085 | 3.040 |
| 90 | 3.087 | 3.136 | 3.235 | 3.395 | 3.114 | 3.090 | 3.083 | 3.198 |
| 120 | 3.087 | 3.131 | 3.208 | 3.324 | 3.109 | 3.096 | 3.118 | 3.567 |
| 150 | 3.096 | 3.127 | 3.180 | 3.297 | 3.111 | 3.110 | 3.160 | 3.435 |
| 160 | 3.096 | 3.122 | 3.170 | 3.270 | 3.102 | 3.112 | 3.245 | 3.435 |
| 165 | 3.100 | 3.115 | 3.155 | 3.185 | | | | |
| 170 | 3.098 | 3.090 | 3.095 | 3.061 | 3.080 | 3.140 | 3.440 | 3.560 |
| 175 | 3.100 | 3.067 | 3.052 | 2.968 | | | | |
| 180 | 3.110 | 3.042 | 2.970 | 2.815 | 3.158 | 3.314 | 3.770 | 4.100 |
| 185 | 3.245 | 3.120 | 2.980 | 2.770 | | | | |
| 190 | 3.340 | 3.190 | 3.040 | 2.810 | | | | |
| 195 | 3.670 | 3.485 | 3.290 | 3.035 | | | | |

Table 6.8 Experimental data for slip and torque loss, $d_e$=45mm

| new v-ribbed belt $F_t+F_r$=200N, $d_e$=45mm | | | | used v-ribbed belt $F_t+F_r$=200N, $d_e$=45mm | | | |
|---|---|---|---|---|---|---|---|
| $T_m$ (Nm) | $\frac{\omega_{dn}}{\omega_{dg}}$ | $F_t-F_r$ (N) | $T_m-T_g$ (Nm) | $T_m$ (Nm) | $\frac{\omega_{dn}}{\omega_{dg}}$ | $F_t-F_r$ (N) | $T_m-T_g$ (Nm) |
| .07 | 1 | 3 | .197 | 0.06 | 1 | 2 | .195 |
| 2.55 | .981 | 106 | .295 | 2.55 | .987 | 106 | .305 |
| 4.09 | .954 | 170 | .370 | 4.10 | .955 | 171 | .385 |

| new v-ribbed belt $F_t+F_r$=300N, $d_e$=45mm | | | | used v-ribbed belt $F_t+F_r$=300N, $d_e$=45mm | | | |
|---|---|---|---|---|---|---|---|
| $T_m$ (Nm) | $\frac{\omega_{dn}}{\omega_{dg}}$ | $F_t-F_r$ (N) | $T_m-T_g$ (Nm) | $T_m$ (Nm) | $\frac{\omega_{dn}}{\omega_{dg}}$ | $F_t-F_r$ (N) | $T_m-T_g$ (Nm) |
| .07 | 1 | 3 | .187 | .05 | 1 | 2 | .210 |
| 2.53 | .988 | 105 | .295 | 2.54 | .990 | 106 | .310 |
| 5.08 | .968 | 212 | .410 | 5.01 | .975 | 209 | .437 |
| 6.15 | .936 | 256 | .480 | 6.30 | .941 | 262 | .497 |

| v-ribbed belt $F_t+F_r$=600N, $d_e$=45mm | | | |
|---|---|---|---|
| $T_m$ (Nm) | $\omega_{dn}/\omega_{dg}$ | $F_t-F_r$ (N) | $T_m-T_g$ (Nm) |
| .09 | 1 | 4 | .230 |
| 5.07 | .980 | 211 | .480 |
| 10.38 | .948 | 432 | .812 |
| 13.26 | .900 | 552 | 1.020 |

Table 6.9 Experimental data for slip and torque loss, $d_e$=80mm

| new v-ribbed belt $F_t+F_r$=200N, $d_e$=80mm | | | | used v-ribbed belt $F_t+F_r$=200N, $d_e$=80mm | | | |
|---|---|---|---|---|---|---|---|
| $T_m$ (Nm) | $\frac{\omega_{dn}}{\omega_{dg}}$ | $F_t-F_r$ (N) | $T_m-T_g$ (Nm) | $T_m$ (Nm) | $\frac{\omega_{dn}}{\omega_{dg}}$ | $F_t-F_r$ (N) | $T_m-T_g$ (Nm) |
| .1 | 1 | 2 | .160 | 0.04 | 1 | 1 | .172 |
| 5.12 | .992 | 123 | .365 | 5.11 | .995 | 123 | .380 |
| 7.27 | .922 | 175 | .472 | 7.85 | .922 | 189 | .490 |

| new v-ribbed belt $F_t+F_r$=600N, $d_e$=80mm | | | | used v-ribbed belt $F_t+F_r$=600N, $d_e$=80mm | | | |
|---|---|---|---|---|---|---|---|
| $T_m$ (Nm) | $\frac{\omega_{dn}}{\omega_{dg}}$ | $F_t-F_r$ (N) | $T_m-T_g$ (Nm) | $T_m$ (Nm) | $\frac{\omega_{dn}}{\omega_{dg}}$ | $F_t-F_r$ (N) | $T_m-T_g$ (Nm) |
| .09 | 1 | 2 | .235 | .06 | 1 | 1 | .245 |
| 5.17 | .997 | 125 | .432 | 5.12 | .997 | 123 | .460 |
| 10.28 | .992 | 248 | .635 | 10.47 | .993 | 252 | .650 |
| 15.15 | .989 | 365 | .851 | 14.97 | .989 | 361 | .870 |
| 22.25 | .968 | 536 | 1.242 | 22.43 | .970 | 540 | 1.260 |

Table 6.10 Experimental data for slip and torque loss, subsidiary tests, $d_e$=80mm

| new v-ribbed belt $F_t+F_r$=470N, $d_e$=80mm, ω=1000RPM | | | | new v-ribbed belt $F_t+F_r$=470N, $d_e$=80mm, ω=2000RPM | | | |
|---|---|---|---|---|---|---|---|
| $T_m$ (Nm) | $\frac{\omega_{dn}}{\omega_{dg}}$ | $F_t-F_r$ (N) | $T_m-T_g$ (Nm) | $T_m$ (Nm) | $\frac{\omega_{dn}}{\omega_{dg}}$ | $F_t-F_r$ (N) | $T_m-T_g$ (Nm) |
| 0.93 | .999 | 22 | .20 | .67 | .999 | 16 | .20 |
| 3.04 | .997 | 73 | .25 | 3.14 | .997 | 76 | .29 |
| 7.60 | .993 | 183 | .42 | 8.01 | .992 | 195 | .46 |
| 11.67 | .987 | 281 | .59 | 11.96 | .987 | 288 | .62 |
| 14.80 | .975 | 357 | .73 | 14.96 | .978 | 361 | .77 |
| 15.95 | .961 | 384 | .72 | 16.27 | .966 | 392 | .85 |
| 16.62 | .920 | 400 | .82 | 16.78 | .951 | 404 | .85 |
| 16.93 | .896 | 408 | .82 | | | | |

| half used v-ribbed belt $F_t+F_r$=470N, $d_e$=80mm, ω=1000RPM | | | | half used v-ribbed belt $F_t+F_r$=470N, $d_e$=80mm, ω=2000RPM | | | |
|---|---|---|---|---|---|---|---|
| $T_m$ (Nm) | $\frac{\omega_{dn}}{\omega_{dg}}$ | $F_t-F_r$ (N) | $T_m-T_g$ (Nm) | $T_m$ (Nm) | $\frac{\omega_{dn}}{\omega_{dg}}$ | $F_t-F_r$ (N) | $T_m-T_g$ (Nm) |
| 0.53 | .999 | 13 | .23 | 0.50 | 1 | 12 | .3 |
| 2.54 | .997 | 61 | .30 | 3.41 | .997 | 82 | .4 |
| 6.75 | .994 | 163 | .48 | 6.51 | .995 | 157 | .56 |
| 10.64 | .991 | 256 | .62 | 10.37 | .991 | 250 | .72 |
| 14.30 | .985 | 345 | .77 | 14.13 | .984 | 341 | .83 |
| 16.86 | .972 | 406 | .89 | 16.57 | .966 | 400 | .97 |
| 17.60 | .917 | 424 | .90 | 17.35 | .930 | 418 | 1.02 |

Continued Over...

| used v-ribbed belt $F_t + F_r = 470N$, $d_e = 80mm$, $\omega = 1000RPM$ | | | | used v-ribbed belt $F_t + F_r = 470N$, $d_e = 80mm$, $\omega = 2000RPM$ | | | |
|---|---|---|---|---|---|---|---|
| $T_m$ (Nm) | $\frac{\omega_{dn}}{\omega_{dg}}$ | $F_t - F_r$ (N) | $T_m - T_g$ (Nm) | $T_m$ (Nm) | $\frac{\omega_{dn}}{\omega_{dg}}$ | $F_t - F_r$ (N) | $T_m - T_g$ (Nm) |
| 0.50 | 1 | 12 | .24 | 0.17 | 1 | 4 | .3 |
| 2.89 | .998 | 70 | .32 | 3.15 | .997 | 76 | .4 |
| 7.04 | .994 | 170 | .47 | 6.75 | .994 | 163 | .52 |
| 11.33 | .988 | 273 | .63 | 10.86 | .988 | 262 | .70 |
| 14.70 | .974 | 354 | .81 | 15.07 | .975 | 363 | .89 |
| 15.91 | .956 | 383 | .82 | 16.91 | .952 | 407 | .97 |
| 16.67 | .928 | 402 | .90 | 17.48 | .931 | 421 | 1.01 |
| 17.43 | .911 | 420 | .91 | | | | |

| molded v-ribbed belt $F_t + F_r = 470N$, $d_e = 80mm$, $\omega = 1000RPM$ | | | | molded v-ribbed belt $F_t + F_r = 470N$, $d_e = 80mm$, $\omega = 2000RPM$ | | | |
|---|---|---|---|---|---|---|---|
| $T_m$ (Nm) | $\frac{\omega_{dn}}{\omega_{dg}}$ | $F_t - F_r$ (N) | $T_m - T_g$ (Nm) | $T_m$ (Nm) | $\frac{\omega_{dn}}{\omega_{dg}}$ | $F_t - F_r$ (N) | $T_m - T_g$ (Nm) |
| 0.51 | 1 | 12 | .2 | 0.60 | 1 | 15 | .2 |
| 3.00 | .997 | 72 | .18 | 3.22 | .997 | 78 | .26 |
| 7.18 | .994 | 173 | .32 | 8.02 | .994 | 194 | .46 |
| 10.43 | .991 | 251 | .46 | 10.68 | .990 | 257 | .53 |
| 14.85 | .979 | 358 | .59 | 15.11 | .979 | 364 | .71 |
| 16.63 | .963 | 401 | .74 | 17.93 | .945 | 432 | .85 |
| 17.91 | .916 | 432 | .77 | 19.98 | .916 | 481 | .90 |

Continued Over...

| anti-wear v-ribbed belt $F_t + F_r = 470N$, $d_e = 80mm$, $\omega = 1000RPM$ | | | | anti-wear v-ribbed belt $F_t + F_r = 470N$, $d_e = 80mm$, $\omega = 2000RPM$ | | | |
|---|---|---|---|---|---|---|---|
| $T_m$ (Nm) | $\frac{\omega_{dn}}{\omega_{dg}}$ | $F_t - F_r$ (N) | $T_m - T_g$ (Nm) | $T_m$ (Nm) | $\frac{\omega_{dn}}{\omega_{dg}}$ | $F_t - F_r$ (N) | $T_m - T_g$ (Nm) |
| 0.40 | 1 | 10 | .2 | 0.55 | 1 | 13 | .2 |
| 2.70 | .998 | 65 | .20 | 3.11 | .997 | 75 | .32 |
| 6.71 | .994 | 162 | .34 | 6.68 | .993 | 161 | .43 |
| 10.86 | .989 | 262 | .49 | 11.03 | .988 | 266 | .60 |
| 14.77 | .980 | 356 | .68 | 15.08 | .977 | 363 | .77 |
| 16.98 | .965 | 409 | .83 | 17.51 | .958 | 422 | .88 |
| 18.01 | .937 | 434 | .82 | 17.82 | .910 | 430 | .93 |
| 17.88 | .908 | 431 | .88 | 18.55 | .900 | 447 | .95 |

# CHAPTER SEVEN

# DISCUSSION OF THE THEORETICAL AND EXPERIMENTAL RESULTS

## 7.1 Introduction

Experiments have been carried out with a two pulley, constant tension drive. With this type of drive the radial movement, torque and speed losses have been measured for 3-PK-1400 type v-ribbed belts, as presented in the last chapter. The design and constraints of a v-ribbed belt affect its radial movement in the pulley groove. A v-ribbed belt without rib bottom / groove tip contact may be considered as a v-belt, when dealing with speed loss and radial movement. In the case of a v-ribbed belt with rib bottom / groove tip contact, a new theoretical model has been developed and presented in chapter three. Torque loss contribution to the power loss has been measured only experimentally.

In the following, theoretical and experimental results of radial movement, slip and maximum traction will be compared and discussed. Finally, mechanical performance of v-ribbed belts and v-belts and their experimental efficiencies will be compared.

## 7.2 Radial Movement

Wedge action and radial movement of a v-ribbed belt are the fundamental differences in action between an ordinary v-belt and a v-ribbed belt. A v-ribbed belt without rib bottom groove tip contact acts as a v-belt. In the experiments carried out it has been attempted to measure the value of radial movement for three different identical cases:

- Without rib bottom / groove tip contact (new cut v-ribbed belt)
- With rib bottom / groove tip contact (used cut v-ribbed belt)
- With mixed contact (extreme conditions tests, new cut v-ribbed belt)

Theoretical results for a v-belt or a v-ribbed belt without rib bottom / groove tip contact (section 2.3.3.2) and v-ribbed belt with contact (section 3.4.1) are in non-dimensional forms, while experimental radial movement variation has been measured (section 6.2) from a reference surface (pulley shoulder). In the following, it will be shown how to reconcile these two results. The belt property and geometric values are taken from chapter five.

### 7.2.1 Experimental Results

Generally belt theories relate the radial movement $x_s$ to belt tension $F_s$ by the linear relationship $x_s / F_s = 1/k$ (equations 2.34 and 3.31). In figures 5.4 and 5.5 it was shown that the real relation is not linear. A large initial radial movement occurred for $F<150N$. At very low belt tensions ($F<50N$), it was also unstable and as a consequence it was difficult to establish a true origin for radial movement $x$ at $F=0$. For this reason, experimental measurements of radial moment ( $x_e$ ) were carried out from an arbitrary datum (the pulley shoulder) as represented in the last chapter. These

tests were carried out in dynamic conditions. It has been attempted to determine the maximum value of $H_T$ in static conditions by hanging the belt over the pulley and measuring the value of $H_T$, but this was also unstable. A non-linear relationship between radial movement and belt tension at low belt tensions has been mentioned by some authors, and they have introduced different methods to overcome this problem. Gerbert [3] placed the beginning of the theoretical curves on the experimental curves to compare the radial movement results. Cowburn [1] assumed a non- linear relationship between radial movement and belt tension at low belt tension regions.

Finally, an approximate value of $H_{T\max} = (3.550 \pm 0.050)mm$ was determined by putting a small piece of new v-ribbed belt ($30mm$) on the pulley groove and measuring $H_T$. However, by taking into account that for slip studies the value of $(x_{sdg} - x_{sdn})$ is required and in a practical belt drive the belt tension never is $F=0$, here the maximum measured value of $H_T$ during the static test was chosen as an approximate origin for experimental radial movement curves. As is mentioned earlier (4.5 and 6.2), the value of $H_T$ is dependant on belt tension and wear. Considering the measured values of $H_T$ from tables 6.3 to 6.7 at $T=0$ for new and used tested v-ribbed belts and comparing these with measured values of $H_T$ in tables 5.3 and 5.4 for the same total belt tensions $(F_t + F_r)$, the approximate amount of wear and then the value of $H_{T\max}$ $(x=0)$ can be determined for each belt. Table 7.1 lists the results. Then the radial movement will be

$$x = H_{T\max} - H_T$$

Measured values of $x$, will be compared with theory in figures 7.1 to 7.9.

Table 7.1 Determination of $H_{T\max}$ $(mm)$

(a) v-ribbed belt without rib bottom / groove tip contact (new cut belt)

| Variables | pulley sizes $d_e$, mm | total tension $(F_t + F_r)$, N | $H_{Tmax}$ (mm) | figure numbers |
|---|---|---|---|---|
| driven pulley | 45 | 200 | 3.672 | 7.1a, 7.2a |
| | | 300 | 3.662 | 7.3a, 7.4a |
| | | 600 * | 3.437 | 7.9a |
| | 80 | 200 | 3.512 | 7.5a, 7.6a |
| | | 600 | 3.526 | 7.7a, 7.8a |
| driving pulley | 45 | 200 | 3.708 | 7.1b, 7.2b |
| | | 300 | 3.704 | 7.3b, 7.4b |
| | | 600 * | 3.464 | 7.9b |
| | 80 | 200 | 3.506 | 7.5b, 7.6b |
| | | 600 | 3.511 | 7.7b, 7.8b |

* Extreme conditions test (mixed contact)

(b) v-ribbed belt with rib bottom / groove tip contact (used cut belt)

| Variables | pulley sizes $d_e$, mm | total tension $(F_t + F_r)$, N | $H_{Tmax}$ (mm) | figure numbers |
|---|---|---|---|---|
| driven pulley | 45 | 200 | 3.292 | 7.1a, 7.2a |
| | | 300 | 3.298 | 7.3a, 7.4a |
| | | 600 * | 3.437 | 7.9a |
| | 80 | 200 | 3.180 | 7.5a, 7.6a |
| | | 600 | 3.196 | 7.7a, 7.8a |
| driving pulley | 45 | 200 | 3.321 | 7.1b, 7.2b |
| | | 300 | 3.305 | 7.3b, 7.4b |
| | | 600 * | 3.464 | 7.9b |
| | 80 | 200 | 3.168 | 7.5b, 7.6b |
| | | 600 | 3.192 | 7.7b, 7.8b |

* Extreme conditions test (mixed contact)

### 7.2.2 Theoretical Non-Skidding Condition Results

Generally the relative motion (slip) does not occur over the whole arc of contact and there exists an active arc in which the belt slips and an arc of adhesion (idle arc) where the forces are not overcome and there is no relative motion between belt and pulley (see section 2.3.2). When the whole angle of wrap becomes active the speed loss (slip) is not related to belt tension linearly. In practice, the driving pulley always has an idle arc when contact arcs are equal, because torque is limited by slip on the driven pulley. In the case of non-skidding condition, for a certain value of $F_t / F_r$ we can use the theoretical results for v-belt or a new v-ribbed belt without rib bottom / groove tip contact (section 3.4.1) and used v-ribbed belt with rib bottom contact (sections 2.3.3.2) to determine the values of $F_s$ and $x_s$. Then the value of radial movement $x$, can be determined.

The actual values of $x$, for non-skidding condition will be compared with experimental results in figures 7.1, 7.3, 7.5 and 7.7.

### 7.2.3 Theoretical Skidding Condition Results

When the belt approaches the whole skidding condition (maximum traction), the sliding angle $\gamma \cong 90°$. Then for a driven pulley and a v-belt or a new v-ribbed belt without rib bottom / groove tip contact the ratio of belt and relaxed side tensions is (from equation 2.23)

$$\frac{F}{F_r} = \exp\left(\frac{\mu}{\sin\beta} \cdot \alpha_p\right) \tag{7.1}$$

Where $\alpha_p$ is the angular position and it varies from $0°$ to $180°$ for a drive with two pulleys of equal size, and $F$ is the belt tension at related angular position. For the driving pulley we can write

$$\frac{F}{F_t} = \exp\left(-\frac{\mu}{\sin\beta} \cdot \alpha_p\right) \tag{7.2}$$

The values of $F_t$ and $F_r$ for a certain total belt tension $F_t + F_r$ can be calculated from

$$\frac{F_t}{F_r} = \exp\left(\frac{\mu}{\sin\beta} \cdot \alpha\right) \tag{7.3}$$

where $\alpha$ is the arc of wrap and for a drive with two pulleys of equal size $\alpha = 180°$. After determination of $F$, the radial movement is given by

$$x = \frac{F}{R} \cdot \frac{1}{k_{V(\gamma=90°)}} \tag{7.4}$$

where $k_{V(\gamma=90°)}$ can be calculated from equation (3.23).

In the case of a v-ribbed belt with rib bottom / groove tip contact at skidding condition ($\gamma = 90°$) for driven pulley we can write (from equation 3.38)

$$\frac{F}{F_r} = \exp\left(\mu \cdot \frac{\frac{1}{\sin\beta} + \frac{k_F}{k_{V(\gamma=90°)}}}{1 + \frac{k_F}{k_V}} \cdot \alpha_p\right) \tag{7.5}$$

For a driving pulley the variation of belt tension around the pulley is given by

$$\frac{F}{F_t} = \exp\left(-\mu \cdot \frac{\frac{1}{\sin\beta} + \frac{k_F}{k_{V(\gamma=90°)}}}{1 + \frac{k_F}{k_V}} \cdot \alpha_p\right) \tag{7.6}$$

The values of $F_t$ and $F_r$ for a certain total belt tension $F_t + F_r$ can be calculated from

$$\frac{F_t}{F_r} = \exp\left(\mu \cdot \frac{\frac{1}{\sin\beta} + \frac{k_F}{k_{V(\gamma=90°)}}}{1 + \frac{k_F}{k_V}} \cdot \alpha\right) \tag{7.7}$$

Similar to v-belt, after determination of $F$, the radial movement will be

$$x = \frac{F}{R} \cdot \frac{1}{k_{VR(\gamma=90°)}} \tag{7.8}$$

and $k_{VR(\gamma=90°)}$ can be calculated from equations (3.23 and 3.31a)

Calculated values of $x$, for skidding condition will be compared with experimental results in figures 7.2, 7.4, 7.6 and 7.8.

### 7.2.4 Mixed Contact

In practice rib bottom /groove tip contact in a v-ribbed belt occurs over some part of the wrap angle. Due to wear and running time of the belt and its fitting on the pulley groove every particular belt has a unique value of radial movement $x$, related to the start of contact. By the help of NCLDM (non-contact laser displacement meter) the start of rib bottom / groove tip contact can be determined for each belt. Now for that part of wrap angle without contact, the v-belt theory can be applied (equations 7.1 and 7.2 for driven and driving pulleys respectively). For the remaining part of wrap angle the v-ribbed belt theory (equations 7.5 and 7.6 for driven and driving pulleys respectively) is applicable. The values of $F_t$ and $F_r$ for a certain total belt tension $F_t + F_r$ can be calculated from equation (3.50 a and b) and putting $\gamma = 90°$ for skidding condition.

$$\frac{F_t}{F_r} = \exp[(\mu\varphi_F \cdot \frac{\frac{1}{\sin\beta} + \frac{K_F}{k_V}}{1 + \frac{k_F}{K_V}}) + (\frac{\mu\varphi_V}{\sin\beta})] \qquad (7.9)$$

After determination of $F$, the radial movement for each part can be calculated from equations (7.4) and (7.8) for v-ribbed belt without contact and with contact parts of a v-ribbed belt respectively.

Calculated values of $x$, for skidding condition and mixed contact will be compared with experimental results in figures 7.9 (a and b).

Figures 7.1 to 7.4 and 7.5 to 7.8 are related to pulley effective diameters $d_e$=*45mm* ($F_t + F_r$=*200N* and $F_t + F_r$=*300N*) and $d_e$=*80mm* ($F_t + F_r$=*200N* and $F_t + F_r$=*600N*) respectively. Figures 7.1, 7.3, 7.5 and 7.7 show the experimental and theoretical results for non-skidding condition and figures 7.2, 7.4, 7.6 and 7.8 for skidding condition. In aid of clarification only one of the non-skidding conditions for each set of experiments has been plotted. The extreme condition test ($d_e$=*45mm*, $F_t + F_r$=*600N*) at skidding condition had a mixed contact. Mixed contact theoretical and experimental results are presented in figures 7.9 (a and b) for driven and driving pulleys receptively.

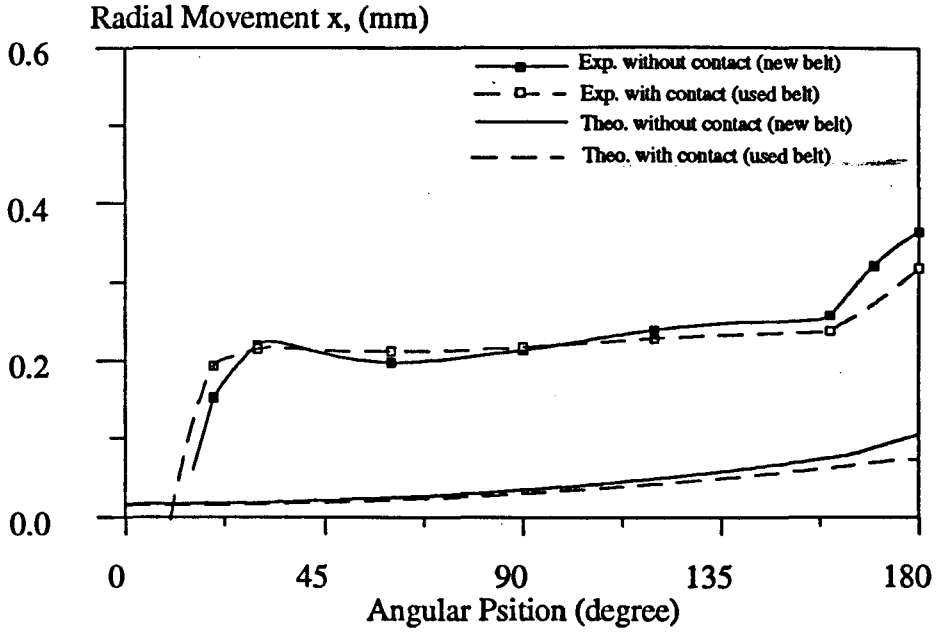


**(a) Driven Pulley**

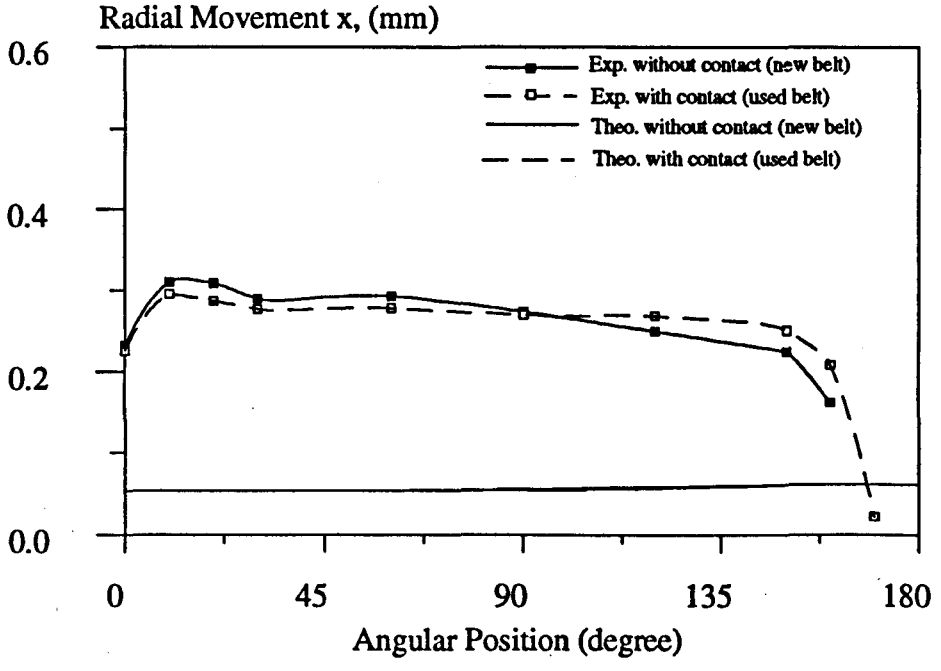


**(b) Driving Pulley**

**Fig. 7.1 Experimental and theoretical results of radial movement against angular position for v-ribbed belt with rib bottom / groove tip contact (used belt) and without contact (new belt), ($d_e$=45mm, $F_t + F_r$=200N.m, non-skidding condition, Torque =2.5N.m)**

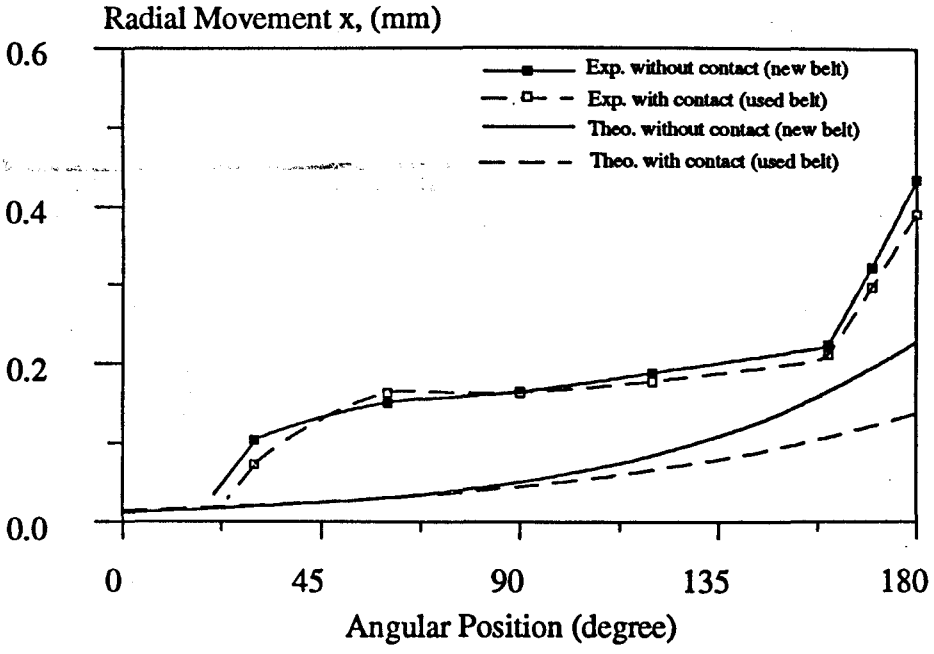


**(a) Driven Pulley**

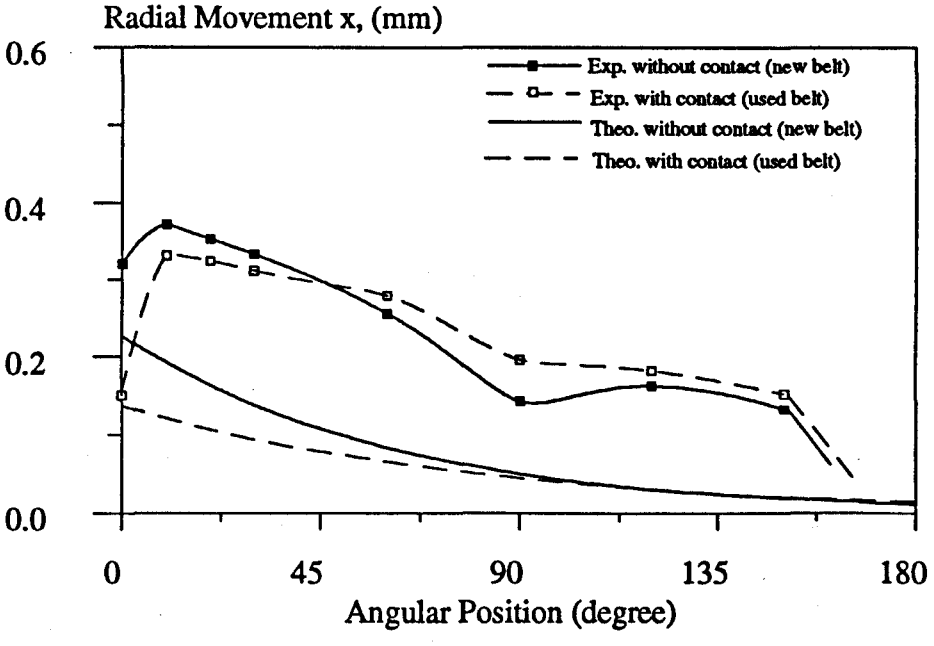


**(b) Driving Pulley**

**Fig. 7.2 Experimental and theoretical results of radial movement against angular position for v-ribbed belt with rib bottom / groove tip contact (used belt) and without contact (new belt), ($d_e$=45mm, $F_t+F_r$=200N.m, skidding condition, Torque=4N.m)**

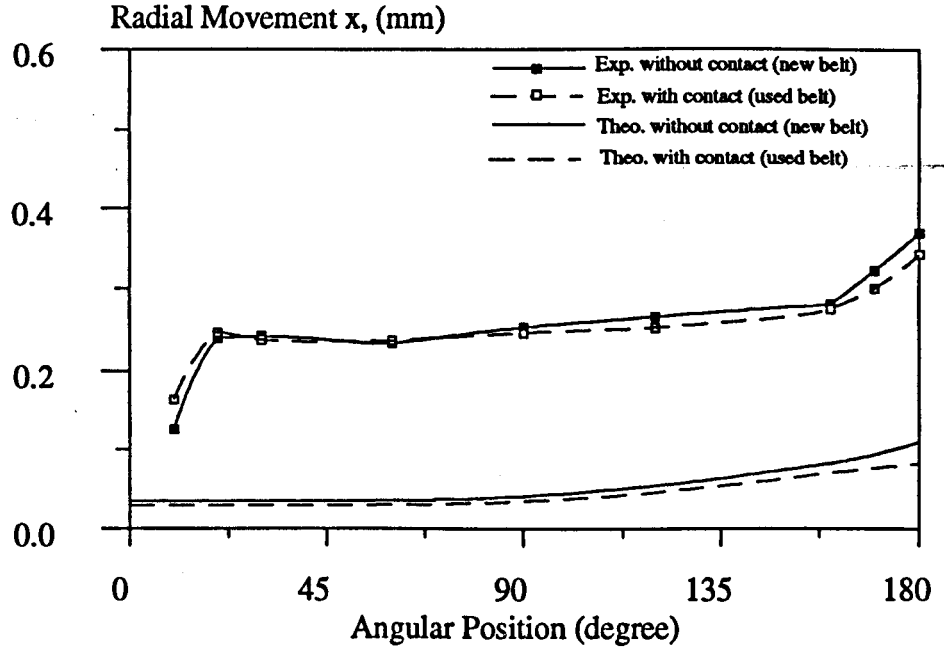


**(a) Driven Pulley**

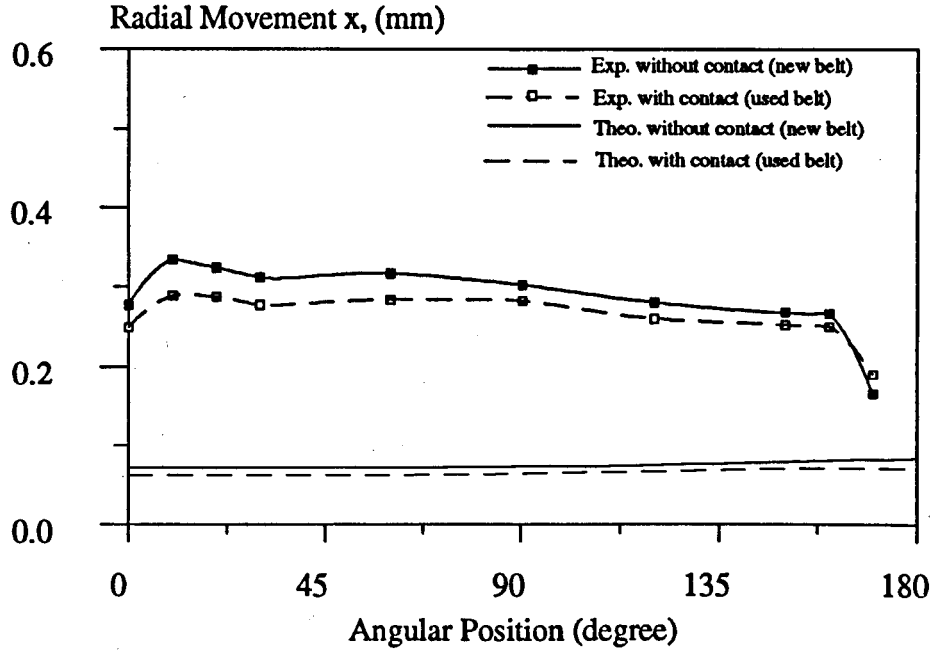


**(b) Driving Pulley**

**Fig. 7.3 Experimental and theoretical results of radial movement against angular position for v-ribbed belt with rib bottom / groove tip contact (used belt) and without contact (new belt), ($d_e$=45mm, $F_t + F_r$=300N.m, non-skidding condition, Torque=2.5N.m)**

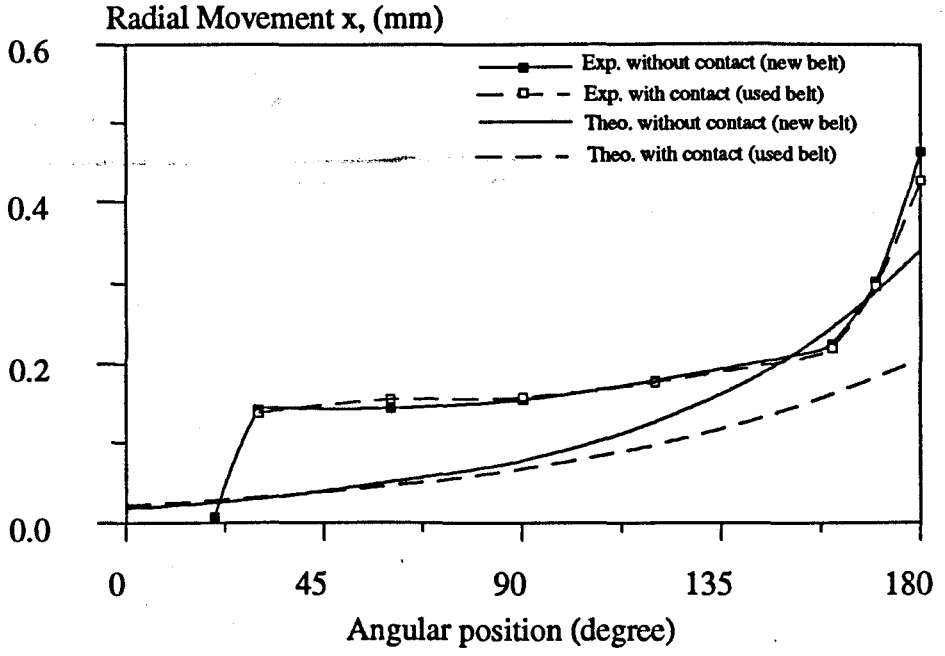


**(a) Driven Pulley**

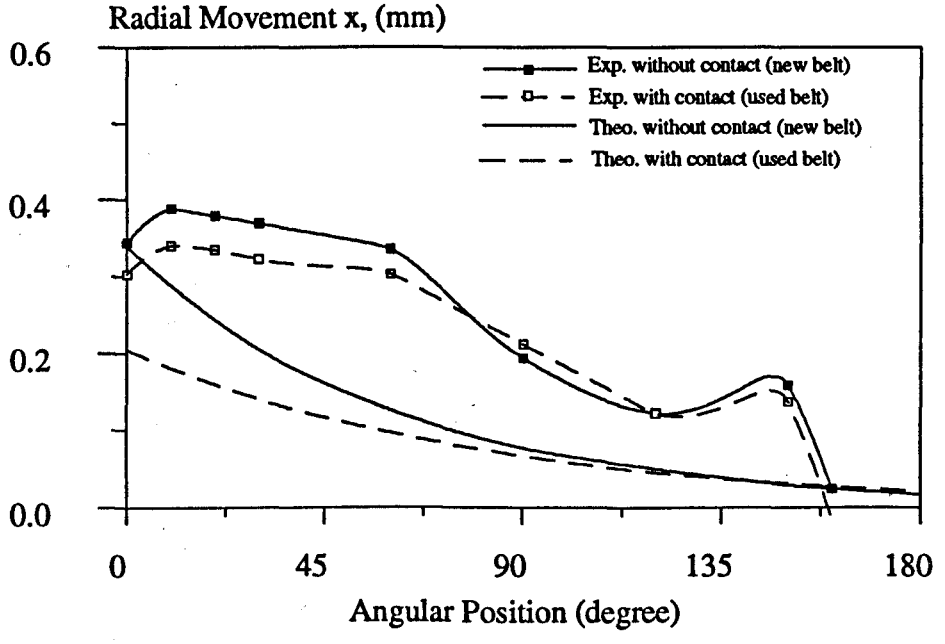


**(b) Driving Pulley**

**Fig. 7.4 Experimental and theoretical results of radial movement against angular position for v-ribbed belt with rib bottom / groove tip contact (used belt) and without contact (new belt), (*$d_e$=45mm, $F_t+F_r$=300N.m, skidding condition, Torque=6N.m*)**

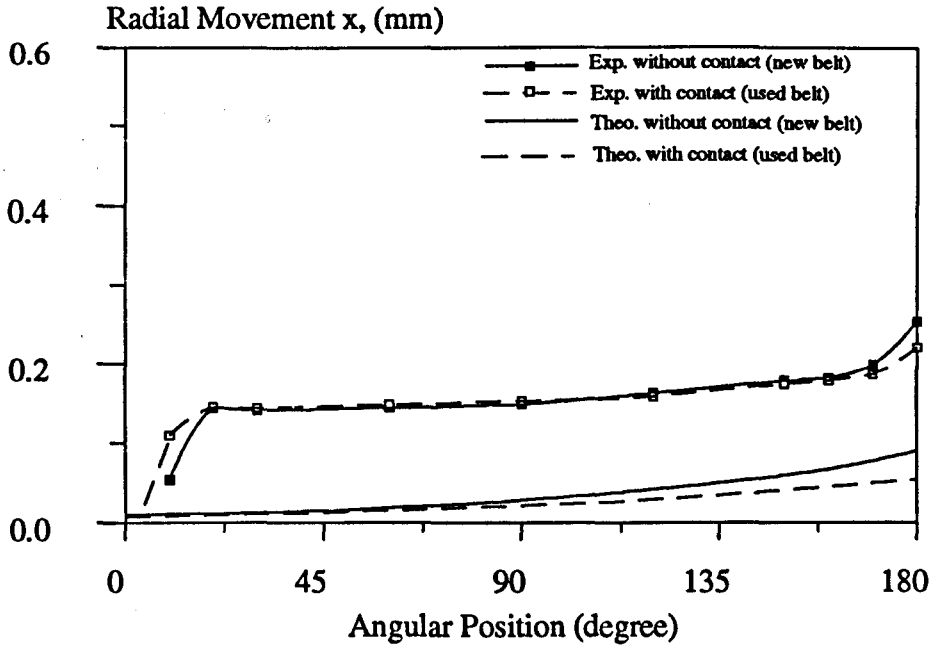


**(a) Driven Pulley**

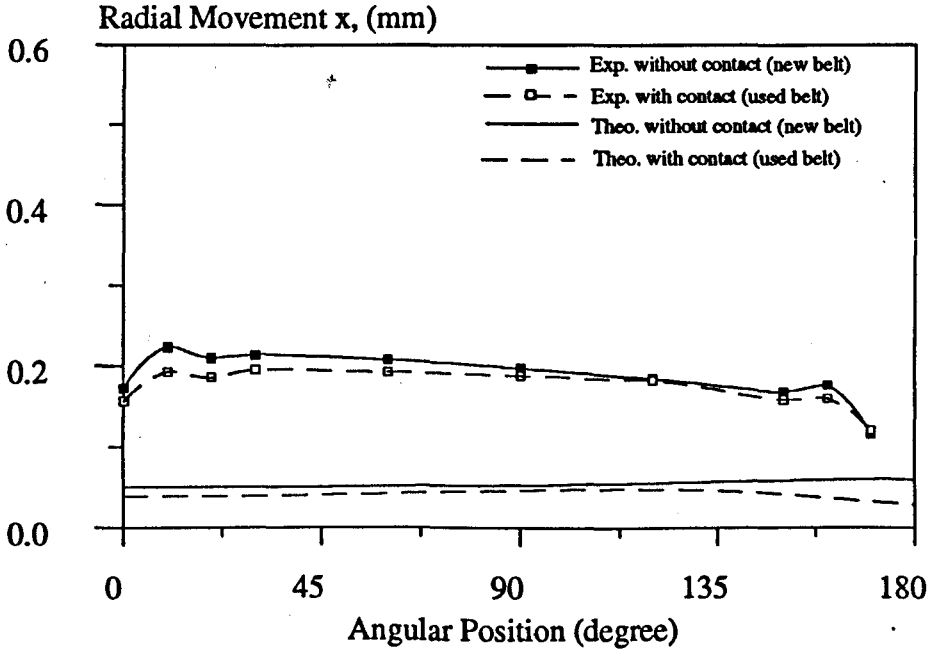


**(b) Driving Pulley**

**Fig. 7.5 Experimental and theoretical results of radial movement against angular position for v-ribbed belt with rib bottom / groove tip contact (used belt) and without contact (new belt), ($d_e$=80mm, $F_t + F_r$=200N.m, non-skidding condition, Torque=5N.m)**

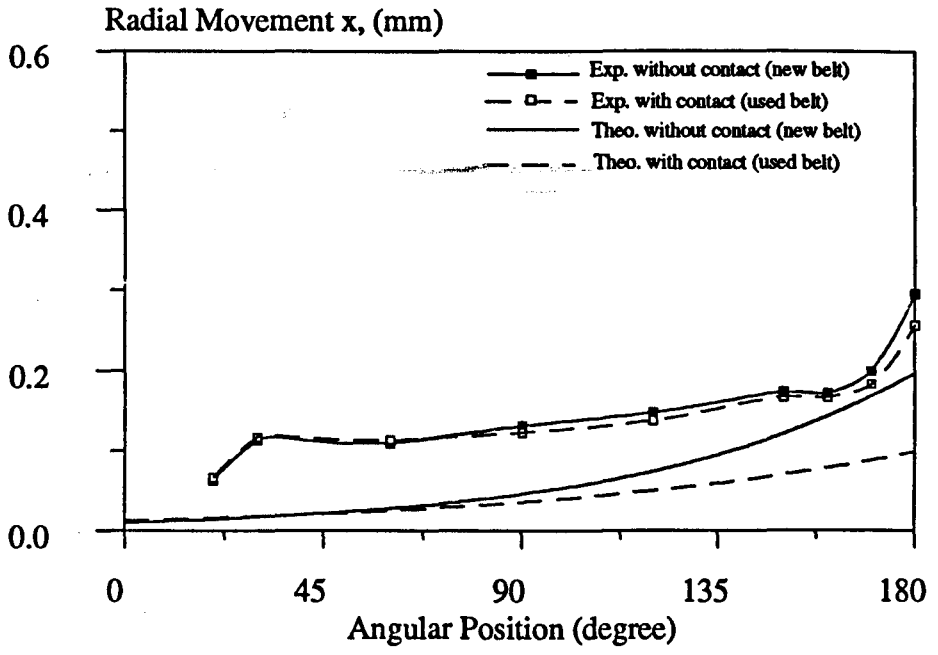


**(a) Driven Pulley**

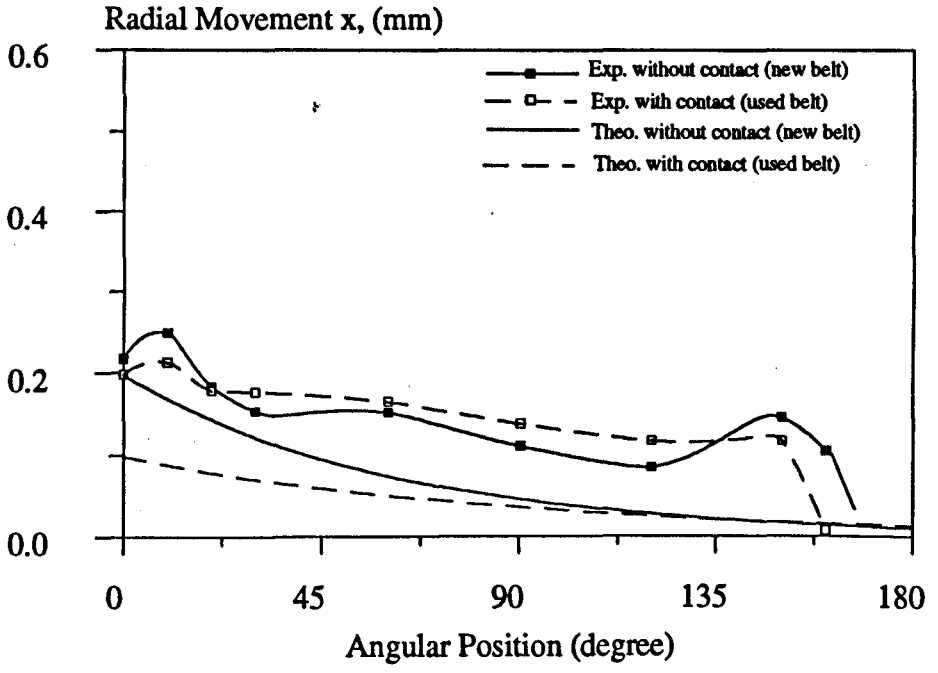


**(b) Driving Pulley**

**Fig. 7.6 Experimental and theoretical results of radial movement against angular position for v-ribbed belt with rib bottom / groove tip contact (used belt) and without contact (new belt), ($d_e$=80mm, $F_t + F_r$=200N.m, skidding condition, Torque=8N.m)**

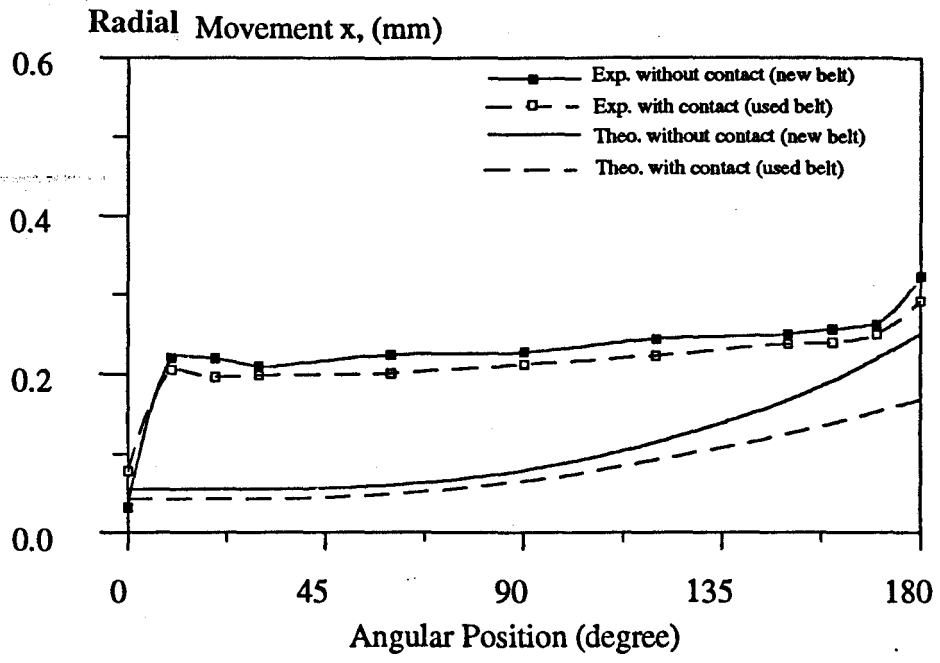


**(a) Driven Pulley**

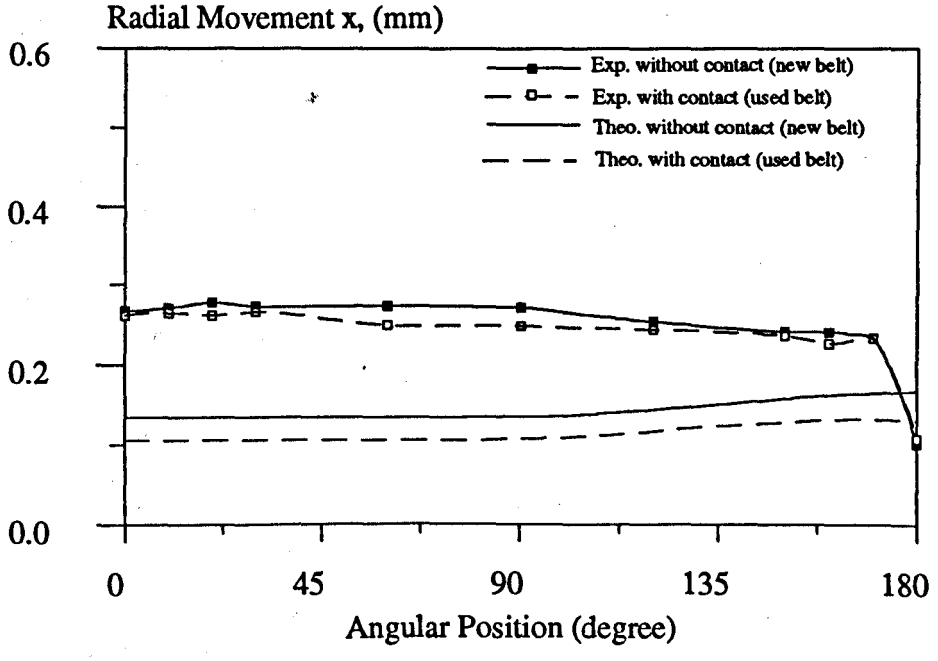


**(b) Driving Pulley**

**Fig. 7.7 Experimental and theoretical results of radial movement against angular position for v-ribbed belt with rib bottom / groove tip contact (used belt) and without contact (new belt), ($d_e$=80mm, $F_t + F_r$=600N.m, non-skidding condition, Torque=10N.m)**

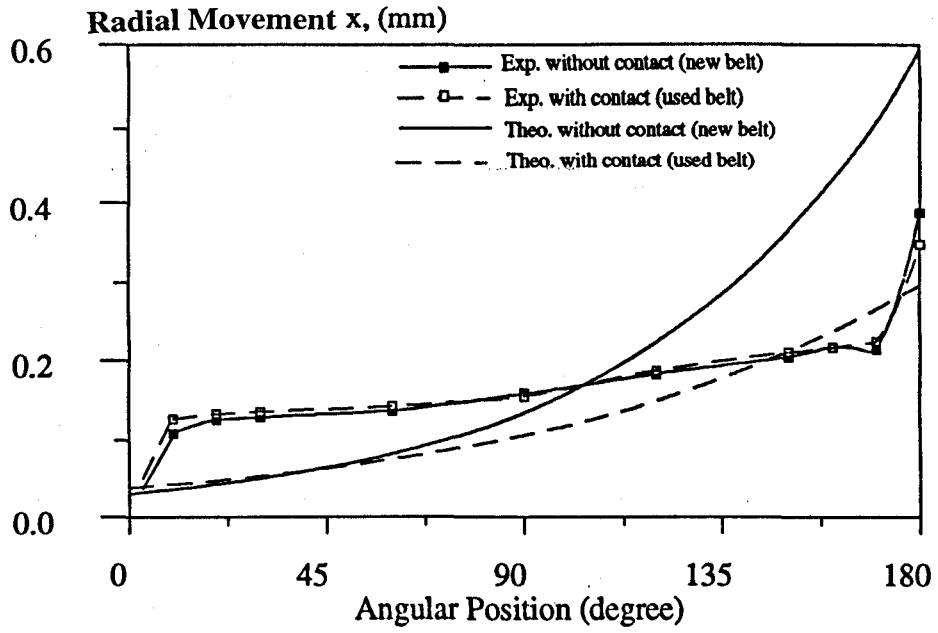


**(a) Driven Pulley**

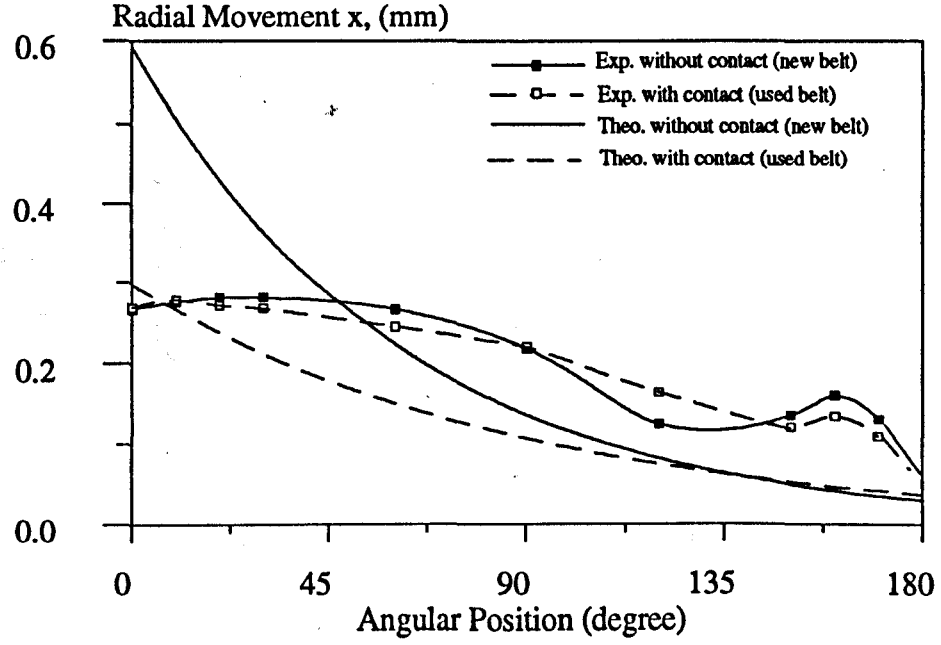


**(b) Driving Pulley**

**Fig. 7.8 Experimental and theoretical results of radial movement against angular position for v-ribbed belt with rib bottom / groove tip contact (used belt) and without contact (new belt), ($d_e$=80mm, $F_t + F_r$=600N.m, skidding condition, Torque=23N.m)**

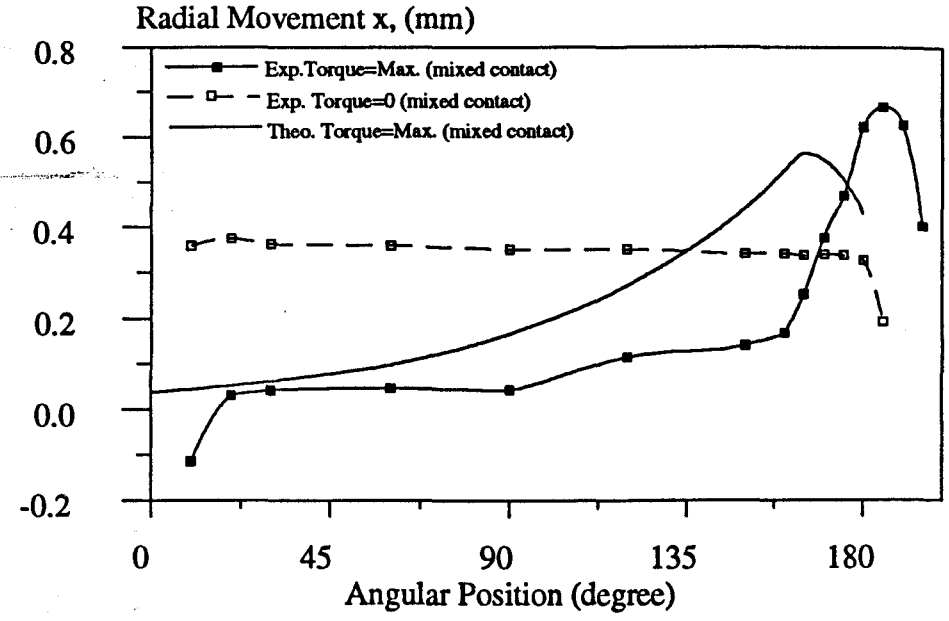


**(a) Driven Pulley**

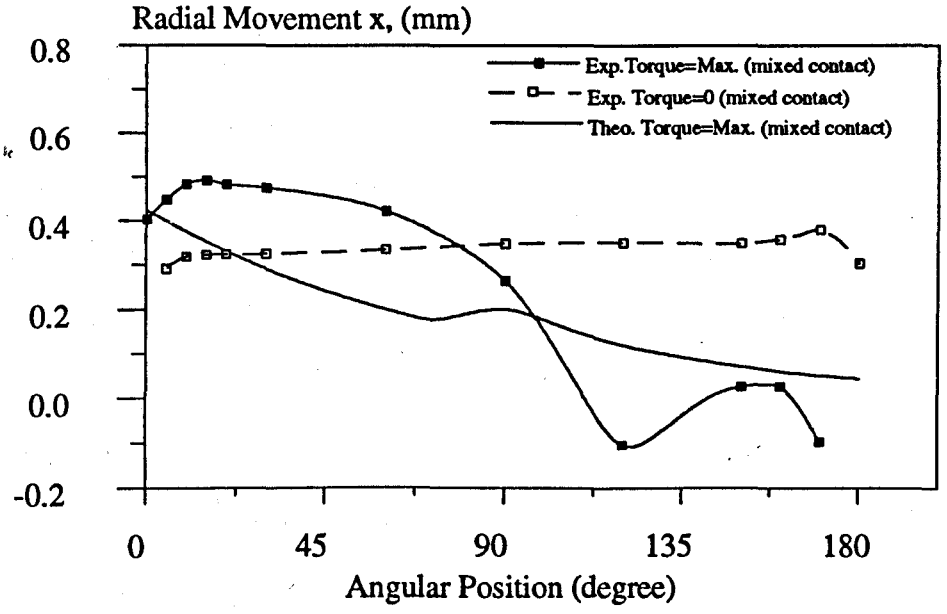


**(b) Driving Pulley**

**Fig. 7.9 Experimental and theoretical results of radial movement against angular position for new v-ribbed belt (extreme condition test) with mixed rib bottm / groove tip contact (*$d_e$=45mm, $F_t + F_r$=600N.m, skidding condition, Torque=13N.m*)**

### 7.2.5 Discussion of Results

Comparison of the experimental and theoretical results (figures 7.1 to 7.9) show that the theoretical values of radial movement are fundamentally lower than experimental results at low belt tensions and the amount of radial movement is lower than that predicted theoretically, at very high belt tensions. The value of belt tension around the pulley $F$, mainly depends on initial total tension $F_t + F_r$ and angular position. This deviation between the theoretical and experimental results can be attributed to the following points.

Radial movement in v- and v-ribbed theories is related linearly to belt tension. In sections 5.2.2 and 5.2.3 it was shown that radial movement is not linear, and large initial radial movement occurred for $F<150N$. The amount of radial movement depends highly on the pressure distribution between belt and pulley interface. Hansson [33] showed that the pressure distribution in a well-designed drive are independent of pulley diameter and to achieve uniform pressure along the rib flank suggested the wedge angle of the pulley should be varied with pulley diameter. In this thesis to reduce the effect of mis-matching of wedge angle between a pulley and belt two different values of $k_v$ were determined experimentally for two pulley diameters of $d_e=45mm$ and $d_e=80mm$, but still the problem of non-linear relationship between $x$, and $F$ at low and even high belt tensions exists.

In sections 5.2.2 and 5.2.3 the variation of $H_T$, was measured experimentally against belt tension $F$, for a v-ribbed belt without rib bottom / groove tip contact (new belt) and with rib bottom / groove tip contact (used belt) respectively. These data from tables 5.3 and 5.4 again has been plotted in figures 7.10 and 7.11 (a and b) showing the variation of $F/R$ against $H_T$ for v-ribbed belt without and with rib bottom / groove tip contact respectively. Figures 7.10a and 7.11a are related to $d_e=45mm$ and figures 7.10b and 7.11b to $d_e=80mm$. It has been found that a second order curve, fits with nearly good accuracy for each case, for belt tensions $F>50N$. The equations of these curves are given by

(without contact, $d_e$=*45mm*) $$\frac{F}{R} = 3400 - 2003.2(H_T) + 295.2(H_T)^2 \quad (7.10)$$

(without contact, $d_e$=*80mm*) $$\frac{F}{R} = 2833.5 - 1637.8(H_T) + 236.7(H_T)^2 \quad (711)$$

(with contact, $d_e$=*45mm*) $$\frac{F}{R} = 4711.5 - 3119.7(H_T) + 516.7(H_T)^2 \quad (7.12)$$

(with contact, $d_e$=*80mm*) $$\frac{F}{R} = 3241.4 - 2132.2(H_T) + 350.6(H_T)^2 \quad (7.13)$$

It can be seen that even at high values of *F/R* there is a non-linear relationship between radial movement and belt tension, and therefore, $k_V$ and $k_{VR}$ (radial spring constants of v-ribbed belt without and with rib bottom / groove tip contact) are not constant. However, it seems the major error between experimental and theoretical results is due to assuming this linear relationship in v- and v-ribbed belts theories.

The second reason of deviation between theory and experiment is due to not considering the effect of the seating and unseating regions in applied theories (see sections 2.2.2 and 2.4.2). At the exit region of driven pulley there is a high rate of increase in measured values of radial movement, and changing of direction of radial movement at the entry region of driving pulley, due to changing of direction of frictional force.

The experimental and theoretical results (figures 7,1 to 7.8) showed that the value of radial movement for v-ribbed belt with rib bottom / groove tip contact is less than its values for the case of without contact and same running conditions. At low belt tensions the experimental differences are very small, but theoretical results shows more differences at high belt tensions due to assuming constant values for $k_V$ and $k_{VR}$.

In the case of mixed contact, it can be seen from Fig. 6.9 that for the driven pulley rib bottom / groove tip contact starts at angular position of $\alpha_p = 165°$ and for the driving pulley it comes out of contact at $\alpha_p = 70°$.

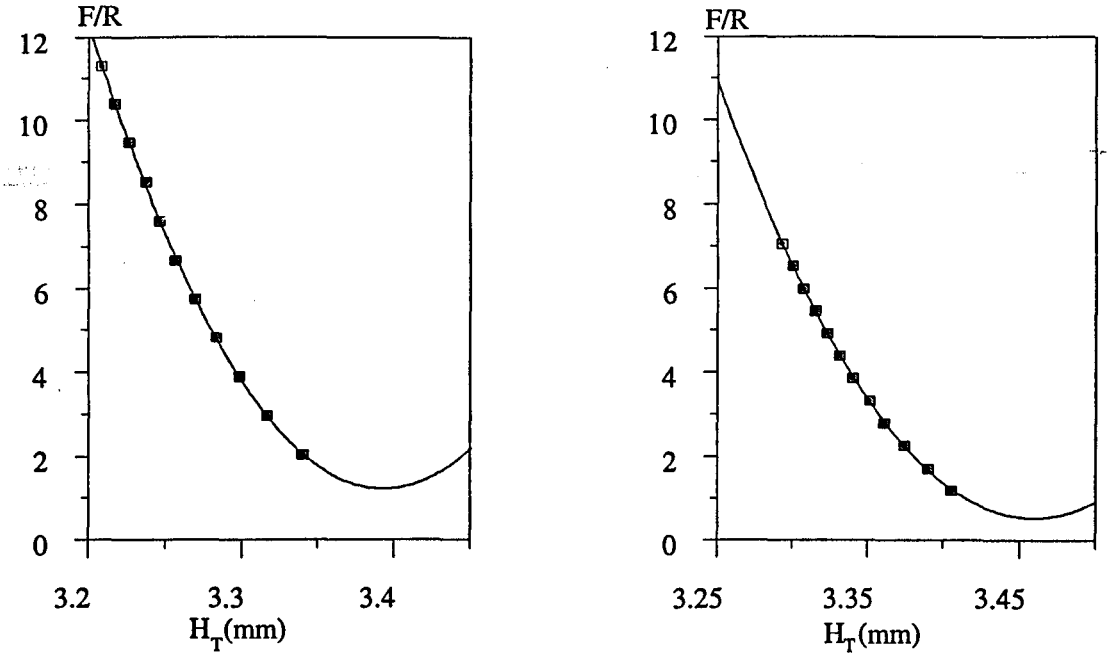


(a) $d_e$=45mm (b) $d_e$=80mm

**Fig. 7.10 Variation of *F/R* against $H_T$, for a new v-ribbed belt or without rib bottom / groove tip contact (data from table 5.3)**

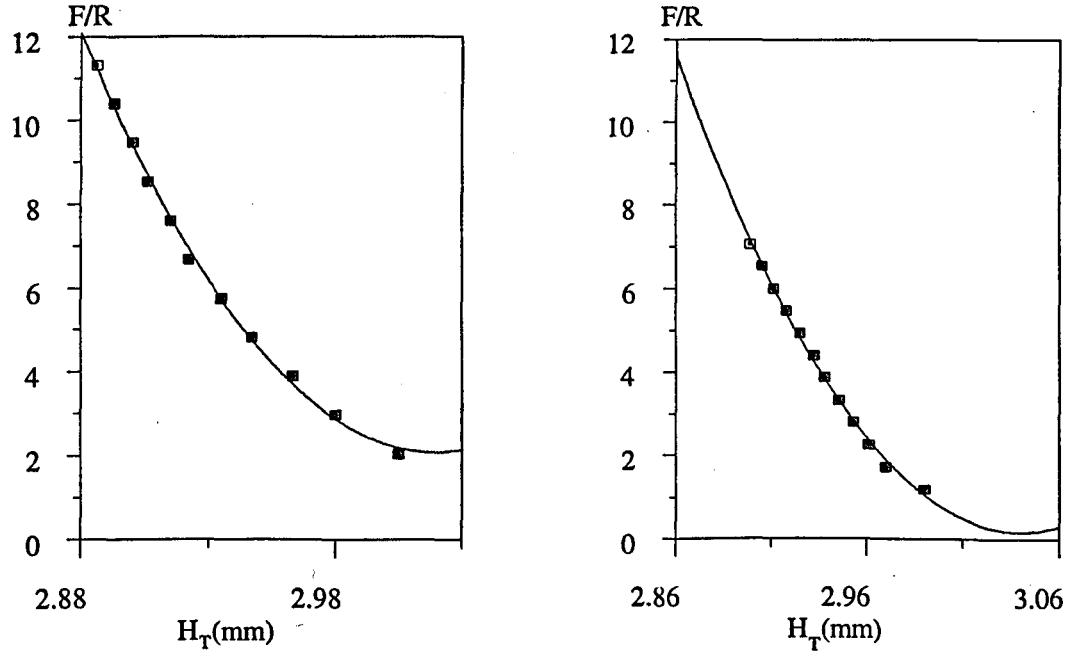


(a) $d_e$=45mm (b) $d_e$=80mm

**Fig. 7.11 Variation of *F/R* against $H_T$, for a used v-ribbed belt or with rib bottom / groove tip contact (data from table 5.4)**

The measurement of radial movement carried out only on fixed motor and the role of this motor was changed as a generator to enable to measure the value of radial movement for driven pulley. Therefore, the measurement radial movement for driven and driving pulleys were not simultaneous. Due to wear during each set of the tests (see section 6.2) and different type of variation of belt tension on driven and driving pulleys the beginning of contact on driven and driving pulleys is not in the same angular position. At the driven pulley the contact occurs at around the exit region, but at the driving pulley it is at angular position of $\alpha_p = 70°$. Radial movement up to $\alpha_p = 70°$ was calculated according to v-ribbed belt theory and for the remaining part, it was obtained from v-belt theory.

When the belt passes the rib bottom contact point (coming out of contact), $p_F = 0$ (Fig. 3.3 and equations 3.3 and 3.4 and equations 3.54 and 3.55), total normal load per unit length $p_N = p_{VN}$. This causes an increase on v-belt part normal load per unit length and thus an increase on radial movement and again rib bottom contact. This would be repeated again and again. This means at this point some sort of vibration occurs due to sudden change of constants from $k_{VR}$ to $k_V$ .This phenomena was not detected in experimental measurements. More experiments and theoretical studies for this point are recommended.

## 7.3 Slip

Slip and speed loss of v-ribbed belt in different running conditions have been measured experimentally (chapter 6) and have been calculated theoretically (sections 2.3.3.3 and 3.4.2). In this section the results will be compared and discussed.

The variation of slip quantity $(s \cdot c)/(F_t + F_r)$, against the coefficient of traction $\lambda = (F_t - F_r)/(F_t + F_r)$ has been plotted in figures 7.12 (a and b) for $d_e$=*45mm* without and with rib bottom / groove tip contact, and figures 7.13 (a and b) for $d_e$=*80mm* respectively (data from tables 2.1, 2.2, 3.1 and 3.2). In each figure there

are one graph related to the theoretical results and two sets of points. One set is from the directly measured values of slip and the other is as modified by actual radial movement measurements. In the following, the arrangement will be explained.

During the experimental measurements of radial movement, the values of speed ratio $\omega_{dn}/\omega_{dg}$ , and the acting torque on the motor $T_m$, were collected (tables 6.8 and 6.9) at certain transmitted torques. The values of $(s\cdot c)/(F_t+F_r)$ have been calculated by considering $c=80000\ N$ (section 5.4) and related total belt tensions $(F_t+F_r)$. The difference between tight and relaxed side tension $(F_t-F_r)$ was calculated by

$$F_t-F_r=\frac{T_m}{(R_e+1.5)/1000}$$

Then the coefficient of traction $\lambda=(F_t-F_r)/(F_t+F_r)$, have been determined by putting the related values of $(F_t+F_r)$. The results are shown in figures 7.12 (a and b) and 7.13 (a and b) to compare with theoretical results (from Fig. 3.11). It can be seen that the measured values of $(s\cdot c)/(F_t+F_r)$ are higher than the theoretical values.

As discussed earlier (section 7.2.5) this can be attributed to the lower theoretical results of radial movement. This can be studied using the more fundamental form of the slip equation given in section 2.3.2.

$$s=\frac{F_t-F_r}{c}+\frac{x_{sdg}-x_{sdn}}{R}$$

The value of $x_{sdg}$ is related to the radial movement of the driving pulley at the origin when $\gamma=180°$, and it is equal to the radial movement at entry region for the driving pulley, because the driving pulley always has an idle arc (see section 2.3.3.3). The value of $x_{sdn}$ is related to the radial movement of the driven pulley at the origin and it also can be assumed equal to the radial movement of the driven pulley at exit

region because from figures 6.1 to 6.8 it can be seen that the variation of radial movement at this exit region is very low specially for non-skidding condition. Then the values of $(x_{sdg} - x_{sdn})$ can be obtained from figures 6.1 to 6.8 because $\Delta x = \Delta x_e$. The results of this calculation are presented in figures 7.12 (a and b) and 7.13 (a and b) as the semi-theoretical results (data from tables 6.4, 6.5 and 6.6). These results show higher values of $(s \cdot c)/(F_t + F_r)$, than theoretical slip, but still the experimental slip is higher. This can be attributed to the following points:

**(i)** In the applied v- and v-ribbed belt theories in this thesis the effect of shear deflection was neglected (see sections 2.2.2 and 2.4.2).

**(ii)** The applied v-belt and developed theory for v-ribbed belt mechanical performance is not valid in entry and exit regions. At the driven pulley, direction of the frictional forces in seating and unseating regions are coincident with those in the adhesion (idle) and sliding (active) zones. However, at the driving pulley the direction of frictional forces are counter directed. Gerbert [18] schematically showed the variation of belt tension at driving pulley is according to Fig. 2.3. Also, bending stiffness in the belt reduces the contact arc and thereby the non-sliding arc (idle arc) which contributes the belt slip [18].

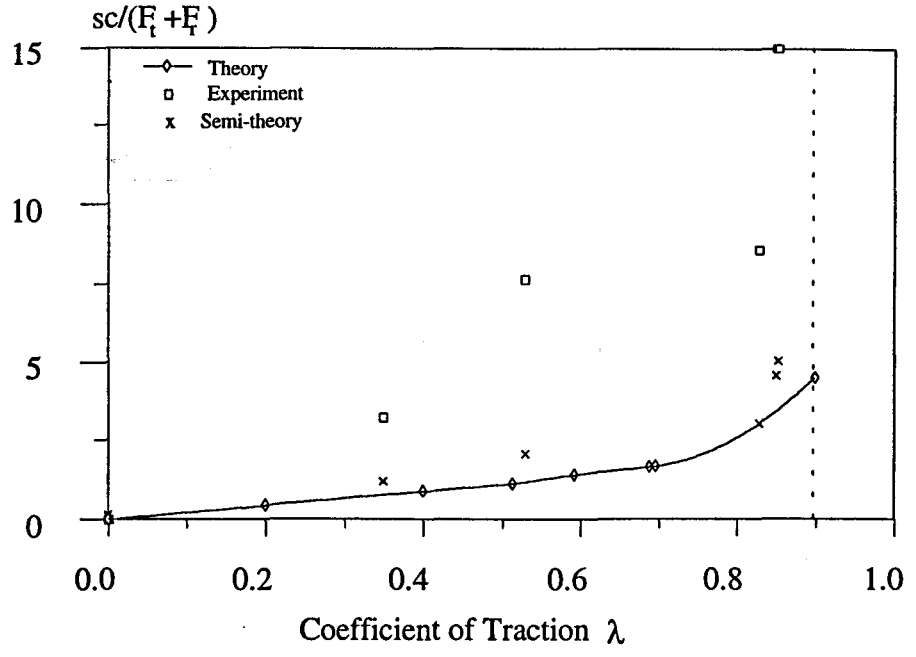


**(a) V-ribbed belt without rib bottom / groove tip contact (new belt)**

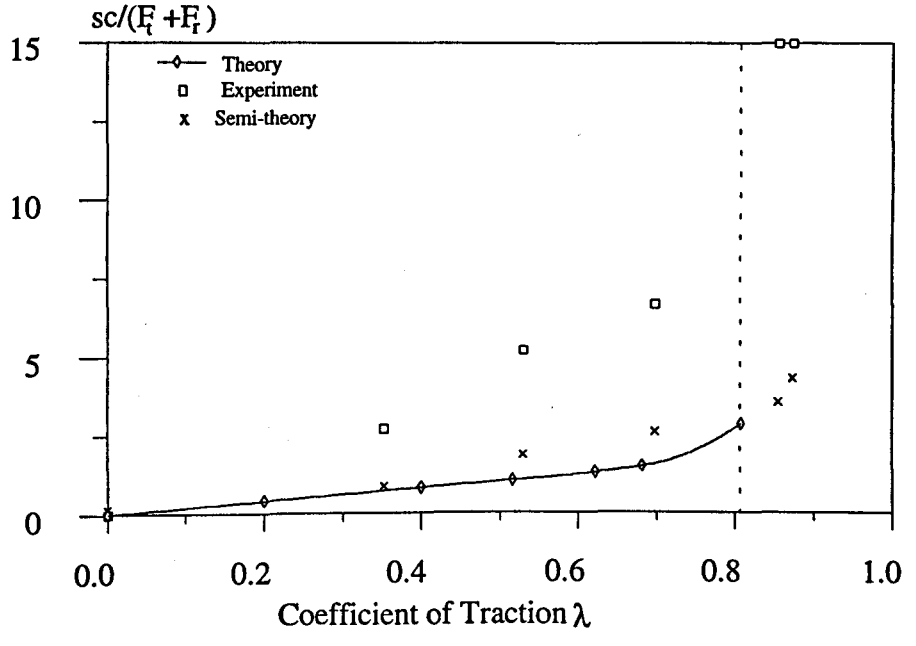


**(b) V-ribbed belt with rib bottom / groove tip contact (used belt)**

**Fig. 7.12 Experimental, theoretical and semi-theoretical slip $(s \cdot c)/(F_t + F_r)$ as a function of traction coefficient ($d_e$=45mm)**

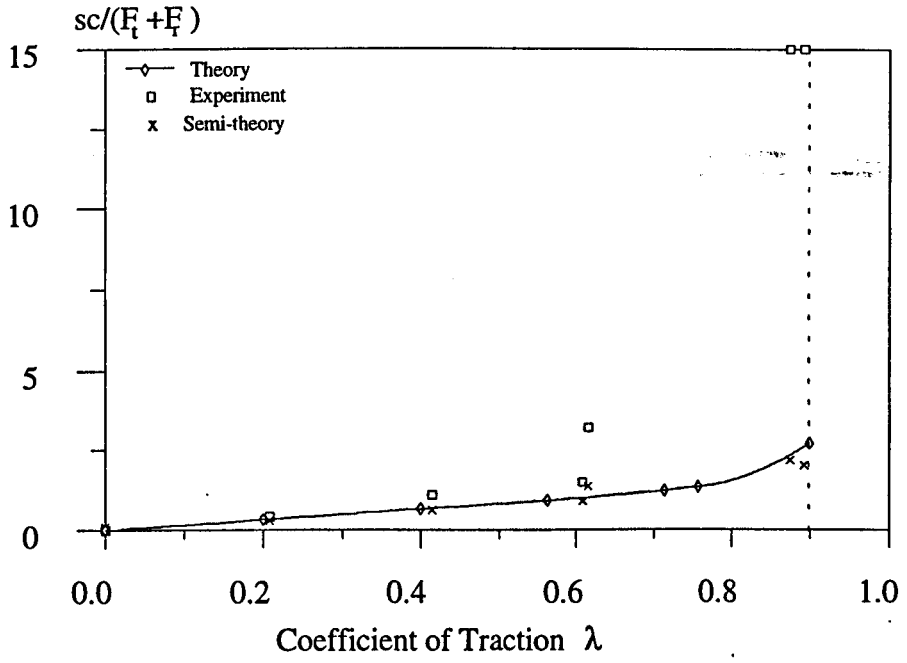


**(a) V-ribbed belt without rib bottom / groove tip contact (new belt)**

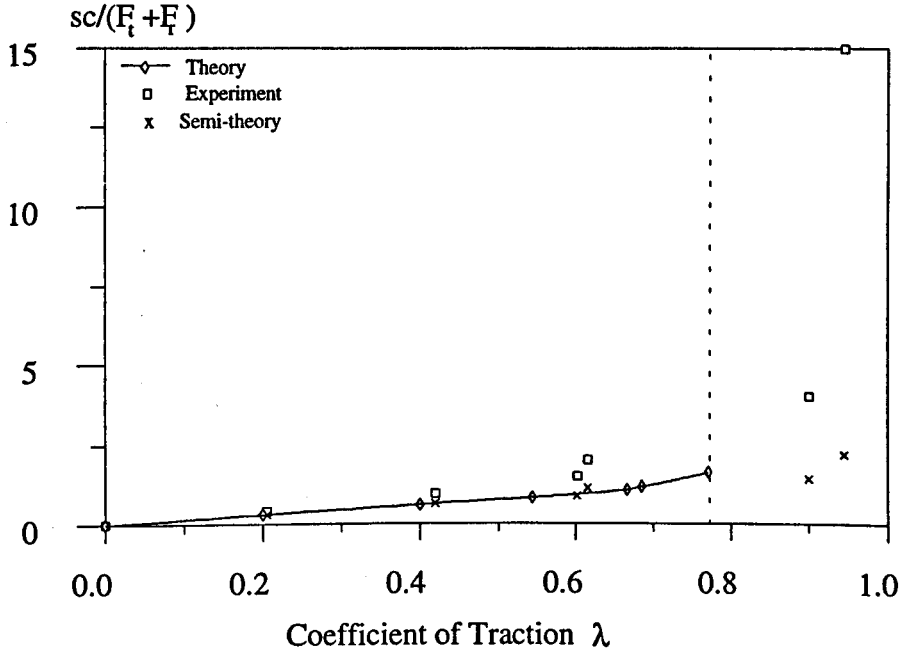


**(b) V-ribbed belt with rib bottom / groove tip contact (used belt)**

**Fig. 7.13 Experimental, theoretical and semi-theoretical slip $(s \cdot c)/(F_t + F_r)$ as a function of traction coefficient ($d_e$=80mm)**

**(iii)** As was expected (because $k_{VR} > k_V$), theoretical and experimental values of slip for v-ribbed belt without rib bottom / groove tip contact are slightly higher than values for v-ribbed belt with rib bottom / groove tip contact. Due to large intervals in radial movement measurements, some subsidiary tests were carried out (section 6.33) to compare the slip behaviour for v-ribbed belt without and with rib bottom / groove tip contact, and the same results obtained. This means that a v-ribbed belt with rib bottom contact acts as a belt between a flat belt and a v-belt. But, experimental results of maximum traction capacity and gross slip limit for a v-ribbed belt with rib bottom contact is higher than its values for the case without rib bottom contact (contrary the theoretical results). The maximum traction capacity will be discussed in next section.

## 7.4 Maximum Traction

Figures 7.12 and 7.13 (a and b) show the variation of slip quantity $(s \cdot c)/(F_t + F_r)$, with the coefficient of traction $\lambda = (F_t - F_r)/(F_t + F_r)$. Theoretical maximum traction is shown by the vertical line in each figure. Theoretical maximum belt tension ratio $F_t / F_r$, can be determined by

$$\left(\frac{F_t}{F_r}\right)_{max} = \exp\left(\frac{\mu\alpha}{\sin\beta}\right) \qquad \text{(for v-ribbed belt without rib bottom contact)}$$

$$\left(\frac{F_t}{F_r}\right)_{max} = \exp\left[\frac{\left(\frac{1}{\sin\beta} + \frac{k_F}{k_V}\right)\mu\alpha}{1 + \frac{k_F}{k_V}}\right] \qquad \text{(for v-ribbed belt with rib bottom contact)}$$

Then the maximum coefficient of traction is

$$\lambda_{max} = \frac{\left(\frac{F_t}{F_r}\right)_{max} - 1}{\left(\frac{F_t}{F_r}\right)_{max} + 1} \qquad (7.14)$$

$\lambda_{max}$ for v-ribbed belt without contact (v-belt theory) is independent of spring constant $k_V$, but maximum traction of v-ribbed belt with contact is related to $k_F / k_V$. The calculated values of $\lambda_{max}$ for $\beta = 20°$ and $\mu = 0.32$ are

$\lambda_{max}$=*0.899* (for v-ribbed belt without contact)

$\lambda_{max}$=*0.807* (for v-ribbed belt with contact, $d_e$ =*45mm* and $k_F / k_V$=*20/117=0.171*)

$\lambda_{max}$=*0.770* (for v-ribbed belt with contact, $d_e$ =*80mm* and $k_F / k_V$=*20/76=0.263*)

However, the experimental measured values for a new v-ribbed belt without rib bottom contact are slightly lower than the theoretical values, and for a v-ribbed belt with rib bottom contact are higher (table 7.2).

Table 7.2 Experimental values of $\lambda_{max}$ for new belt (without rib bottom contact) and used belt (with rib bottom contact) and extreme condition test (mixed contact)

| | pulley sizes $d_e$, mm | total tension ($F_t$ +$F_r$ ), N | $\lambda_{max}$ |
|---|---|---|---|
| new belt (without contact) | 45 | 200 | 0.850 |
| | | 300 | 0.853 |
| | 80 | 200 | 0.875 |
| | | 600 | 0.893 |
| used belt (with contact) | 45 | 200 | 0.855 |
| | | 300 | 0.873 |
| | 80 | 200 | 0.945 |
| | | 600 | 0.900 |
| extrem conditions (mixed contact) | 45 | 600 | 0.920 |

Bending stiffness in the belt reduces the arc of contact and thereby the maximum coefficient of traction. Table 7.3 shows the approximate values of lack of contact angle, obtained from figures 6.1 to 6.9 for different cases of carried out tests (only for *Torque =max*).

Table 7.3 Experimental values of lack of contact angle

(a) v-ribbed belt without rib bottom / groove tip contact

| | pulley sizes $d_e$, mm | total tension ($F_t + F_r$), N | lack of contact angle (degree) | figure numbers |
|---|---|---|---|---|
| driven pulley | 45 | 200 | 22 | 6.1a |
| | | 300 | 20 | 6.3a |
| | | 600 * | 5 | 6.9a |
| | 80 | 200 | 12 | 6.5a |
| | | 600 | 5 | 6.7a |
| driving pulley | 45 | 200 | 28 | 6.1b |
| | | 300 | 18 | 6.3b |
| | | 600 * | 20 | 6.9b |
| | 80 | 200 | 12 | 6.5b |
| | | 600 | 5 | 6.7b |

* Extreme conditions test (mixed contact)

(b) v-ribbed belt with rib bottom / groove tip contact

| | pulley sizes $d_e$, mm | total tension ($F_t + F_r$), N | lack of contact angle (degree) | figure numbers |
|---|---|---|---|---|
| driven pulley | 45 | 200 | 26 | 6.2a |
| | | 300 | 20 | 6.4a |
| | | 600 * | 5 | 6.9a |
| | 80 | 200 | 12 | 6.6a |
| | | 600 | 5 | 6.8a |
| driving pulley | 45 | 200 | 26 | 6.2b |
| | | 300 | 18 | 6.4b |
| | | 600 * | 20 | 6.9b |
| | 80 | 200 | 12 | 6.6b |
| | | 600 | 5 | 6.8b |

* Extreme conditions test (mixed contact)

In the case of the v-ribbed belt with rib bottom / groove tip contact, the higher value of experimental $\lambda_{max}$ is probably due to the increasing friction coefficient of the used belt. Hansson [31] in his experimental work found that the maximum traction of new v-ribbed belts (without contact) and used v-ribbed belts (with contact) are almost same, and reported the visual change of the surface of the used belt. Dalgarno et al. [65] reported a higher friction force for a used v-ribbed belt. In this thesis during subsidiary tests (section 6.3.3) the half-used v-ribbed belt (with mixed contact) had the highest traction compared with a used and new belt. Therefore it can be concluded that the friction coefficient increases with running time up to a steady value and then the half-used belt has the higher friction coefficient and higher traction. After increasing the running time, due to wear or high belt tension, rib bottom / groove tip contact occurs and the maximum traction reduces. Also the higher traction of the anti-wear and molded v-ribbed belts can be attributed to their greater friction coefficient.

## 7.5 Torque Loss and Efficiency

Torque loss studies were out side the aim of this thesis, but during the subsidiary tests torque loss and slip have been measured for five different types of v-belts running on a pair of equal size pulleys, $d_e = 45mm$, $F_t + F_r = 470N$ and two running speeds of $\omega = 1000RPM$ and $\omega = 2000RPM$. In section 2.1 fractional power loss is defined as $P_L / P = T_L / T + s$. Then, efficiency $\eta$ is

$$\eta = 1 - \frac{P_L}{P} \tag{7.15}$$

In figures 7.14 (a, b, c and d ) the experimental results of efficiency for different v-ribbed belts are compared (data from table 6.10).

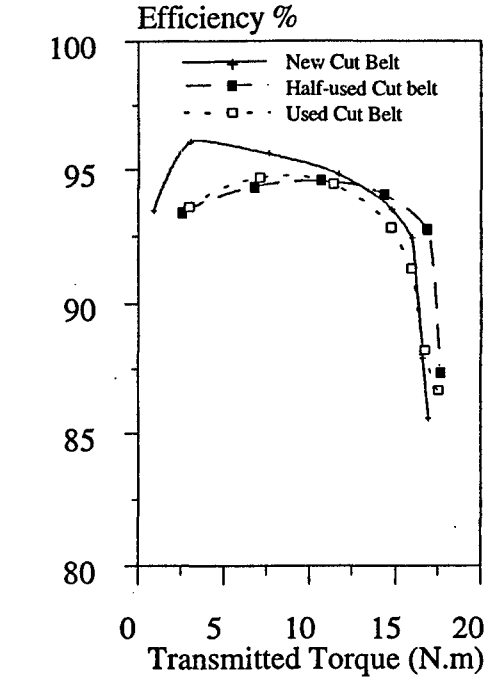


(a) ω=*1000RPM*

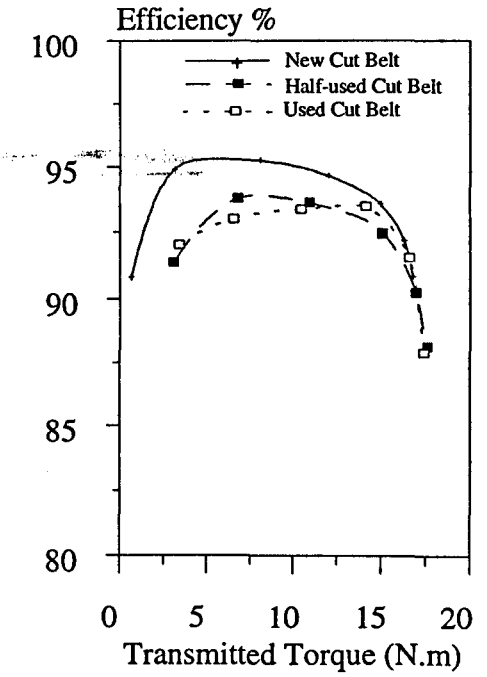


(b) ω=*2000RPM*

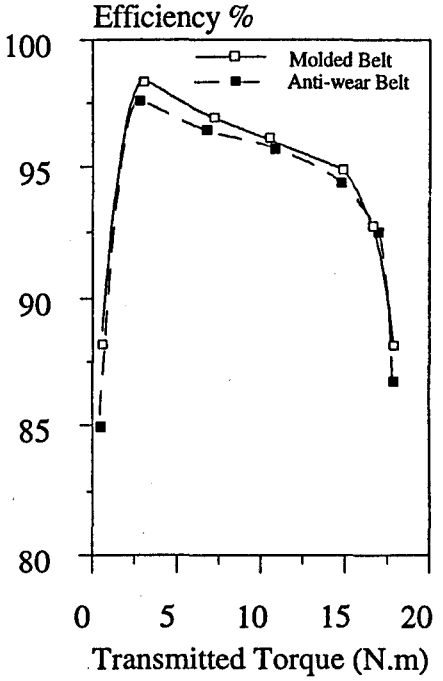


(c) ω=*1000RPM*

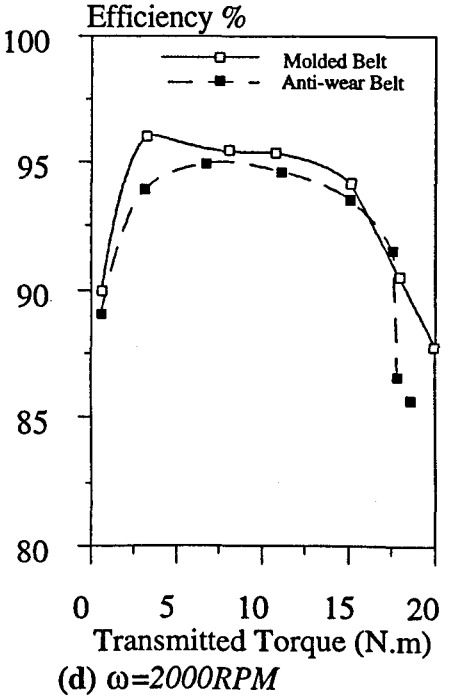


(d) ω=*2000RPM*

**Fig. 7.14 Efficiency versus transmitted torque for new, half-used, used, molded, anti-wear v-ribbed belt (ω=*1000RPM* and ω=*2000RPM*)**

Figures 714 (a and b) show the results of $\omega=1000RPM$ and $\omega=2000RPM$ respectively, for v-ribbed belt without rib bottom / groove tip contact (new belt), with contact (used belt) and mixed contact (half used belt) and figures 7.17 (c and d) the results of $\omega=1000RPM$ and $\omega=2000RPM$ respectively, for molded and anti-wear new v-ribbed belt (without contact). Used and half-used v-ribbed belt, in spite of lower speed loss, have lower efficiency than new v-ribbed belt, due to higher value of torque loss. At higher speed, $\omega=2000RPM$ the efficiency is slightly lower than $\omega=1000RPM$. However, more torque loss studies are recommended.

## 7.6 Is the V-ribbed Belt a V-belt or Flat Belt?

Gerbert [34] replied a v-belt has wedge action when it runs in the pulley grooves. This implies that the apparent friction is considerably higher than if the belt was running on a flat pulley. A properly designed v-ribbed belt also exhibits wedge action. Due to the shape of the belt the ribs can not penetrate the pulley grooves individually. Maximum penetration and maximum radial movement (due to high belt tension or rib wear) is limited by the outer radius of the pulley. When rib bottom / groove tip contact occurs the wedge action decreases. The extent of the reduction in wedge action depends on belt tension, fit between rib and groove, wear and material properties. When rib bottom contact occurs the wedge action decreases and thereby the gross slip limit (torque capacity) and maximum traction decreases. Gerbert then assumed that the additional normal load, after contact, increases to the same extent between the flat belt part and v-belt part of a v-ribbed belt and developed a theory, which has been discussed in section 2.4.3.

A v-ribbed belt without rib bottom / groove tip contact considered as a v-belt and in this thesis for the case of rib bottom contact a new theory has been developed and compared with experimental results. The developed theory considered the v-ribbed belt as a combination of a flat belt and a v-belt with the same value of radial

movement and two different radial spring constants $k_F$ and $k_V$. The total v-ribbed belt radial spring constant determined by

$$k_{VR} = k_V + k_F$$

Theoretical assumptions were supported by experimental measurements. The main difference between a v-ribbed belt without contact and with contact is the appearance of the spring constant of a flat belt part $k_F$ in the equations after contact occurs. In section 3.3.2 the value of $k_F$ has been related to the material properties and geometry of v-ribbed belt by

$$k_F = \frac{B_F\ E}{H_F} \tag{7.16}$$

Here $B_F$ is the flat belt part width, $E$ is modulus of elasticity and $H_F$ is the flat belt part thickness (see Fig. 3.4). Considering the geometry of K-section v-ribbed belt, it can be seen that $H_F$ is very smaller than the v-belt part height $H_V$ (Fig. 3.4) and therefore, a very small amount of wear can increase the value of $k_F$. However, in section 5.2.3 experimental and theoretical values of $k_F$ and $k_V$ were compared. The appearance of $k_F$ in the equations causes lower radial movement for v-ribbed belt with rib bottom / groove tip contact and therefore lower maximum torque capacity. In spite of a small reduction of radial movement measurements and theoretical results and same trends, in a v-ribbed belt with rib bottom / groove tip contact, the theoretical results showed fundamentally lower radial movement at low belt tensions and higher values of radial movement at high belt tensions. This attributed to assuming linear relationship between radial movement and belt tension (section 7.2.5).

It has been observed experimentally that the slip of a v-ribbed belt with rib bottom / groove tip contact is slightly less than in the case of no bottom contact. These measurements showed that the slip of the v-ribbed belt running on small pulleys ($d_e$=45mm) is much higher than the slip of the belt running on big pulleys ($d_e$=80mm). The theoretical results showed the same trend, but with lower values of slip relative to each experimental tests due to not considering the effect of shear deflection and seating and unseating zones in the applied v-ribbed belt theory (section 7.3).

Maximum torque capacity measurements showed more or less the same values for the cases of v-ribbed belts without bottom contact, with bottom contact and mixed contact. Half used v-ribbed belt (mixed contact) had highest maximum torque capacity, but theory predicts lower maximum traction for v-ribbed belt with contact. This deviation can be attributed to the increase of the coefficient of friction with running time. (section 7.4).

Experimental measurements of torque loss for all of the cases (with contact, without contact and mixed contact) showed approximately linear relationship with $(F_t - F_r)$, and v-ribbed belt without contact had slightly lower torque loss compared to the v-ribbed belt with contact. The v-ribbed belt without rib bottom / groove tip contact is more efficient compared to the case of without contact due to lower torque loss (section 7.5).

In spite of, more or less, apparent similar experimental performance and slip of the v-ribbed belt with rib bottom / groove tip contact and without contact, the appearance of $k_F$ in the equations causes that the belt total traction $T$ to be divided into two components of $T_F$ and $T_V$, tractions of flat and v-belt parts of a v-ribbed belt (Figs. 3.9 and 3.10), and total normal load $p_N$, to be divided into two components of $p_{NF}$ and $p_{NV}$, flat and v-belt parts of a v-ribbed belt (Figs. 3.11 and 3.12). In figuers 3.11 and 3.12 theoretical results showed very sharp variation for normal load ratio

$p_{NF} / p_N$ and $p_{NV} / p_N$. On driving pulley $p_{NF} = 0.14(p_N)$ to $0.62(p_N)$. The variation of $T_F / T$ and $T_V / T$ and $p_{NF} / p_N$ and $p_{NV} / p_N$ across the active arc of contact $\varphi$ depends on the value of $k_F / k_V$ and sliding angle $\gamma$ (equations 3.57, 3.58, 3.59 and 3.60). $k_F / k_V$ has an important role on variation of $(T_V - T_F)$ and $(p_{VN} - p_{FN})$. Gerbert's assumption about the increasing vertical load to the **same extent** leads to $k_{V(\gamma=90)} = k_F$. But $k_V$ and $k_F$ depend on fit between rib and groove, wear and material properties (section 5.2.3). Therefore, it not obvious if these are equal. Now two different cases regarding the tip bottom / groove tip contact can be studied.

### (i) Contact due to running time of the belt and wear

From geometry of a v-ribbed belt it can be seen that (Fig. 3.4) $p_F$ causes very high pressure on flat belt part of a v-ribbed belt (due to small $B_F$). Therefore, there is higher rate of wear compared to v-belt part, and wedge action even at a worn v-ribbed belt. In this case even a worn v-ribbed belt will have approximately same slip behaviour compared to the new v-ribbed belt. It seems there is a balance between the normal load of flat belt and v-belt parts of a v-ribbed belt and $p_V - p_F \cong constant.$

### (ii) Contact due to sudden increase of total belt tension $(F_t + F_r)$ or transmitted torque

In this case the variation of $T_F$ and $T_V$ will be according to equations (3.57 and 3.58) and $(T_V - T_F)$ will cause an internal shear tension between the two parts.

It may be that this internal shear is responsible for the collapse of ribs of the belt. Hansson [30] attributed the collapse of ribs to the variation of pressure distribution due to different wedge angle of the v-ribbed belt at different pulley diameters.

During the extreme condition tests (section 6.3) the ribs of the two new v-ribbed belts collapsed. However, more experimental work with the help of NCLDM (non-contact laser displacement meter) to investigate the variation of the ribs with running time is recommended.

# CHAPTER EIGHT

# CONCLUSION AND RECOMMENDATIONS FOR FUTURE WORK

## 8.1 Conclusions

The experimental and theoretical conclusions that may be drawn from this thesis can be summarised as follows:

- A v-ribbed belt without rib bottom / groove tip contact considered as a v-belt and in this thesis for the case of rib bottom contact a new theory has been developed and compared with experimental results. The developed theory considered the v-ribbed belt as a combination of a flat belt and a v-belt with the same value of radial movement and two different radial spring constants. Theoretical assumptions were supported by experimental measurements.

- The experimental and theoretical results show that the values of radial movement for v-ribbed belt with rib bottom / groove tip contact is less than its values for the

case of no bottom contact in the same running conditions. Comparison of the experimental and theoretical results showed that the theoretical values of radial movement are fundamentally lower than the experimental results at low belt tensions and the amount of radial movement is higher than that predicted theoretically at very high belt tensions. This deviation between the theoretical and experimental results can be attributed to assuming linear relationship between belt tension and radial movement in belt theories. Dynamic measurements of v-ribbed belt radial movement with and without rib bottom / groove tip contact at no-load ($T=0$) and no-slip ($s=0$) conditions showed non-linear relationship between belt tension and radial movement. At low belt tensions variation of radial movement is very high and it is non-linear even at higher belt tensions.

- It has been observed experimentally that the slip of a v-ribbed belt with rib bottom / groove tip contact is slightly less than in the case of no bottom contact. These measurements showed that the slip of the v-ribbed belt running on small pulleys ($d_e=45mm$) is much higher than the slip of the belt running on big pulleys ($d_e=80mm$). The theoretical results showed the same trend, but with lower values of slip relative to each experimental tests due to not considering the effect of shear deflection and seating and unseating zones in the applied v-ribbed belt theory.

- Maximum torque capacity measurements showed more or less the same values for the cases of v-ribbed belts without bottom contact, with bottom contact and mixed contact. Half used v-ribbed belt (mixed contact) had highest maximum torque capacity, but theory predicts lower maximum traction for v-ribbed belt with contact. This deviation can be attributed to the increase of the coefficient of friction with running time.

- Experimental measurements of torque loss for all of the cases (with contact, without contact and mixed contact) showed approximately linear relationship with $(F_t - F_r)$, and v-ribbed belt without contact had slightly lower torque loss compared to the v-ribbed belt with contact.

- The v-ribbed belt without rib bottom / groove tip contact is more efficient compared to the case of without contact due to lower torque loss.

- In spite of more or less apparent similar performance of v-ribbed belt with and without contact, it is found experimentally and theoretically that the compressed rubber of the belt (between cord and pulley) is subjected to a variable internal shear force around the pulley after contact.

## 8.2 Recommendations for Future Work

The following recommendations are made for future experimental and theoretical work:

- To minimise uncertainties during the tests of radial movement measurements, the experimental method took a long time for each set of tests. It is suggested to design a more stable stand for the sensor head of the non-contact laser displacement meter, to reduce the time of measurements. This will allow the variation of radial movement around the arc of wrap to be studied in more detail.

- Belt theories assume a linear relationship between belt tension and radial movement. It has been found that this is not the case. Theoretical and experimental studies, especially on the effect of wear and running time on the fit between belt and pulley groove are recommended.

- The developed theory for v-ribbed belt slip is not valid for exit and entry regions and also does not consider the effect of shear deflection on the belt slip. Considering these factors in theoretical modelling is recommended.

- Coefficient of friction has been assumed to be constant under different running conditions. Experimental measurements of maximum torque capacity for v-ribbed belt showed an increase of the coefficient of friction for a used v-ribbed belt. Future work in this area is recommended.

- In this work torque loss has been measured only experimentally. Theoretical modelling for v-ribbed belt torque loss is recommended.

# REFERENCES

[1] Cowburn, D. "The Mechanical Performance of Automotive V-belts", PhD thesis, University of Bradford, UK, 1984.

[2] Euler, L, " Remarques sur l' effect du frottement dans l' equilibre' ", Me m, Acad. Sci. Berlin, No. 18, pp. 265-278, 1762, cited in Ref. 10.

[3] Gerbert, B. G. "Force and Slip Behaviour in V-belt Drives", Acta Polytechnica Scandinavica, Mech. Eng. Series, No. 67, Helsinki, 1972.

[4] Eytelwein, J. A. "Handbuch der Statik fester korper", Bd. 1, 311, Reimer, Berlin, 1832.

[5] Norman, C.A. "Experiments on Belt-drive Fundamentals", The Ohio State University Engineering Experiment Station Bulletin, No. 13, Vol. 18, n. 1, pp. 1-36, 1949.

[6] Hornung, K. G. "Factors Influencing the Fatigue Characteristics of Rubber-Textile Machine Elements", PhD Dissertation, The Ohio State Univ. , 1959.

[7] Swift, H. W. "Power Transmission of Belts:an investigation of Fundamentals", Proc. I. Mech. E. Vol. 2, pp. 659-699, 1928, cited in Ref. 3.

[8] Dittrich, O. "Theorie des Umschlingungrgetriebes mit Keilformigen Reibscheibenflanlen", Dissertation, Technische Horchschule Karlsruhe, 1953, cited in Ref. 1.

[9] Reynolds, O. "On the Efficiency of Belts or Straps as Communicators of Work", The Engineer, Vol. 38, 1874, pp. 396, cited in Ref. 1.

[10] Childs, T. H. C. and Cowburn, D. "Power Transmission Losses in V-belt Drives", Part II, Proc Institution of Mechanical Engineers, 201, No. DI, pp. 33-53, 1987.

[11] Childs,T.H.C. and Parker, J.K. "Power Transmission by Flat, V and Timing Belts",15$^{th}$ Leeds-Lyon Symposium in Leeds, Sep. 1988.

[12] Gerbert, B. G. "On Flat Belt Slip", Internal Report, Machine and Vehicle Design, Chalmers University of Technology, Goteborg, Sweden, 1989.

[13] Grashof, F. "Theoretische Maschinenlehre", Bd2. Leopold Voss, Hamburg, 1883.

[14] Firbank, T. C. "Mechanics of the Belt Drive", Int. J. Mech. ,Sci. , Vol.12, pp. 1053-1063, 1970.

[15] Viabov, RV. "The Traction Properties of Belt Drives", Russian Engineering Journal, 49, No.7, pp. 40-44, 1969.

[16] Amijima, S. "Some Basic Problems about the Belts", The Science and Engineering Review of Doshisha Univ., 2, No. 3-4, pp. 151-163, 1962.

[17] Sonntag, G. "Kraftubertragung Zwischen Rolle und Band", Forsch. Ing. Wes, 41, No 1, pp. 29-31, 1975.

[18] Gerbert, B. G. "Belt Slip -a Unified Approach", DE-Vol, 43-1, International Power Transmission and Gearing Conference, Vol. 1, ASME, pp. 335-342, 1992.

[19] Gerbert, B. G. "Power Loss and Optimum Tensioning of V-belt Drives", J. Eng. Ind. Trans. ASME, Vol. 96, Ser. B, No. 3, pp. 877-885, Aug. 1974.

[20] Childs, T. H. C. and Cowburn, D. "Power Transmission Losses in V-belt Drives", Part I, Proc Institution of Mechanical Engineers, 201, No. DI, pp. 33-53, 1987.

[21] Gerbert, B. G. "Contribution to the Knowledge of Flat Belt Mechanics and Torque Losses", Internal Report, MF 890630, Machine and Vehicle Design, Chalmers University of Technology, Goteborg, Sweden, 1989.

[22] Morgan, M. E. "Investigation of Variable Speed Ratio V-belt Drives", Master's thesis, University of California, Los Angelos, Sep. 1953, cited in Ref. 1.

[23] Worley, W. S. "Designing Adjustable-speed V-belt Drives for Farm Implements", SAE Trans. Vol. 63, pp. 321-333, 1955, cited in Ref. 1.

[24] Gervas, K. I. and Pronin, B. A. "Calculation of Power Losses in Belt Drives", Russ. , Eng. , J. , Vol. 47, No. 3, pp. 26-29, 1970.

[25] Gervas, K. I. "Determining the Power Losses in V-belt Drives During Flexure", Sov. , Rubber Technol, Vol. 28, No. 2, pp. 42-43, 1969.

[26] Gerbert, B. G. "Tensile Stress Distribution in the Cord of V-belts" J. Eng. Ind. Trans. ASME, Vol. 97, Ser. B, No.1, pp. 14-22, Feb. 1975.

[27] Gerbert, B. G. "Some Notes on V-belt Drives", J. Mech. Design, Trans. ASME, Vol.103, No.1, pp. 8-18, 1981.

[28] Gerbert, B. G. and Hansson, H. "Slip in V-ribbed Belt Drives", Machine and Vehicle Design, Chalmers University of Technology, Goteborg, Sweden, 1990.

[29] Wallace, D.E. "Belt Selection and Application for Engineers", Gates Rubber Company, Denver, Colorado, 1987.

[30] Hansson, H. "Geometry Conditions for Good Power Capacity in a V-ribbed Belt Drive", ASME, Proceedings of the 1989, International Power Transmission and Gearing Conference, Vol.1, Book No. 10288 A, pp. 59-64.

[31] Hansson, H. "Mechanics of V-ribbed Belt Drives", Thesis for the DEgreeof LICENIATE of Engineering, Chalmers University of Technology, Sweden, 1989.

[32] Connell, J. E. and Rorre, R. A. L. "Friction Induced Vibration in V-ribbed Belt Applications", DE-Vol. 49, Book No. Goo735, 1992.

[33] Amijima , S. , Fujii , T. , Tani , K. and Inukai, M. " Study on V - ribbed Belt ( The Relation Between Rib Deformation and Transmitted Force of the V-ribbed Belt )", Bulletin JSME, 29, No. 253, pp. 2317-2322, 1986.

[34] Gerbert, B. G. "Gross Slip Limit of V-ribbed Belts", European Belt Drive Seminar, 22 Feb. 1994, IMechE, London.

[35] Gerbert, B. G. "Private Communication", IMech E, London. 22 Feb. 1994.

[36] Gerbert, B. G. "Pressure Distribution and Belt Deformation in V-belt Drives", J. Eng. Ind. Trans. ASME, Vol. 97, Ser B, No.3, pp. 476-982, Aug. 1976.

[37] British Standard, BS AU150 "Specification for Automotive V-belt drives", BSI, pp. 1-19, !973, cited in Ref. 1.

[38] The Gates Rubber Company, "Micro-V-Drive Design Manual, For Vribbed Belt Applications", 1990.

[39] Hyunsoo, K. and Jaeshin, L. "Analysis of Belt Behavior and Slip Characteristics for a Metal V-belt CVT", Mech. Mach. Theory Vol. 29, No. 6, pp. 865-876, 1994.

[40] Byung-Dae, C. and Hyun-Soo, K. "Analysis of Belt Behavior for an Automotive V-belt CVT", Proc. 6th Int. Pacific Con, Automotive Engineering, pp. 263-269, 1991.

[41] Serge, A. "Vibration of Belts and Belt Drives", Mech. Mach. Theory Vol. 27, No. 6. pp. 645-659,1992.

[42] Fawcett, J. N. Burdess, J. S. and Hewit, J. R., Proc. 1989 Int. Power Transmission and Gearing Conf., Chicago, IL, pp. 25-29, 25-28 Apr. 1989, cited in Ref. 41.

[43] Koyoma, T., Watanabe, K., Nagai, K. and Kagotani, M. "A Study on Timing Belt Noise (How to Reduce Resonant Noise)", Journal of Mech. Design Vol. 112, pp. 419-423, Sep. 1990.

[44] Koyoma, T., Watanabe, K., Nagai, K. and Kagotani, M. "A Study on Timing Belt Noise (Theoretical Analysis for Forced Transverse Vibration of Timing Belt With Parametric Excitation)", Journal of Mech. Design Vol. 112, pp. 424-429, Sep. 1990.

[45] Anritsu Corporation "KL130 Series Displacement Meter Instruction Manual" 1989.

[46] British Standard Automobile Series, "Specification for Automotive V-ribbed belt drives- Dimensions of pulleys and belts of PK profile" BS, AU, 248, 1993.

[47] Nakajima, T., Ohashi, K. and Yamamoto, S. "Grinding Process of Aramid Fiber Reinforced Rubber (2nd Report) Projection Fiber Left Unremoved on Ground Surface and Frictional Characteristics",Journal of the Japan Society for Precision Engineering, Vol. 60, No. 9, pp. 1299-1303, 1994.

[48] Roberts, A. D. "Theories of Dry Rubber Friction", Tribology Int., Vol. 9, No.2, pp 75-81, 1976.

[49] Barquins, M. "Friction and Wear of Rubber-like Materials", Wear, Vol. 160, No. pp 1-11, 1993.

[50] Ariano, R., Politecnico, Vol.2, No.10 & 11, 1929, cited in Ref. 1.

[51] Roth, F. L., Driscoll, R. L. and Holt, W. L. "Friction Properties of Rubber", J. Res. Natl. Bur. Standards, Vol.28, pp. 439, 1942, cited in Ref.1.

[52] Johnson, K. L., Kendal, K. and Roberts, A. D. "Surface Energy and the Contact of Elastic Solids", Proc. R. Soc. London, Ser. A, 324, pp. 301-313, 1971, cited in Ref. 49.

[53] Schallamach, A. "How does Rubber Silde?", Wear, 17, pp. 301-312, 1971, cited in Ref. 49.

[54] Schallamach, A. "The Velocity and Temperature Dependence of Rubber Friction", Proc. Phys. Soc. B, 66, pp. 386-392, 1953, cited in Ref. 49.

[55] Bartenev, G. M. and El' kin, A. I. "Friction Properties of Highly Ellastic Materials", Wear, 8, pp. 8-21, 1965, cited in Ref. 49.

[56] Thirion, P. "Les Coefficient d'adherence du Caoutchouce", Rev. Gene. Caout., 23, pp. 101-106, 1946, cited in Ref. 49.

[57] Roberts, A. D. "Guide to Estimate the Friction of Rubber", JN, Rubber Chemistry and Technology, Vol. 62, No. 3 pp. 637-686, Jul. 1992.

[58] Wada, N. and Uchiyama, Y. "Friction and Wear of Short-fiber-reinforced Rubber Composits under Various Sliding Speeds and Loads", Wear, 162-164, pp. 930-938, 1993.

[59] Goettler, L. A., Leib, R. I. and Lambright, A. J. "Short Fiber Reinforced Hose - a New Concept in Production and Performance", Prop. Meet. Rubber Div. Am. Chem. Soc., 115 (20), pp.67, 1979, cited in Ref. 58.

[60] Rogers, J. Y. "Reinforced Elastomers. The use of Fibers in V-belt Compounds", Rubber World, 183(6), pp. 27-31, 1981.

[61] Schlums, K. D. "Untersuchugen an Umschlingungsgetriebe", Dissertation, Technische Hochschule Braunschweig, 1959, cited in Ref. 3.

[62] Amijima, S. "Some Problems Associated with the Friction Between Belt and Pulley", Doshisha Univ. Sci. Engng Rev. 3, pp.9, 1962, cited in Ref. 3.

[63] Lutz, O. and Schlums, K. D. "Scheibenspreizkrafte und Scheibenanpressvorrichtung in verstellbaren Keilscheiben-Umschlingungsgetrieben", VDIZ.108, 23, pp.1128, 1966, cited in Ref.3.

[64] Dalgarno, K. W. "Synchronous Belt Materials; Durability and Performance", PhD Thesis, University of Bradford UK, 1991.

[65] Dalgarno, K. W., Moore, R. B., Childs, T. H. C. and Yu, D. "Performance and Design of Automotive Belt Drives and Materials", Fifteenth Progress Report, University of Leeds, Leeds, UK, 1995.

[66] Moore, R. B. "Characterisation and Modelling of Power Transmission Belts", PhD Transfer Report, Univ. Bradford, UK, Ref.AJD/10/1994.

[67] Dalgarno, K. W. "Private Communication About Specification of Test Data", University of Leeds, Leeds, UK, Oct. 1995.

## Appendix A (Solving v- and v-ribbed belt equations)

## (using Maple V sotware)

Maple V is used through Windows software. Information is given in three stages:

1- Giving values to constants

2- Definition of functions

3- definition of differential equations

In the following one example can be seen.

**> b:=Pi/9;**

$$\beta = \pi / 9$$

**> kv:=76;**

$$k_V = 76 \qquad (k_V = 117 \text{ for } r = 24)$$

**> kf:=20;**

$$k_F = 20 \qquad \text{(in the case of v-belt } k_F = 0)$$

**> mu:=0.32;**

**> c:=80000:**

$$c = 80000$$

**> r:=41.5;**

$$r = 41.5 \qquad (r = 24 \text{for } k_V = 117)$$

---

> co:=c/(kv*r**2);

$$c_o = \frac{c}{k_V r^2}$$

> bs:=evalf(arctan(tan(b)*cos(j(phi))));

$$\beta_s = \arctan(\tan\beta \cdot \cos\gamma)$$

> f(j):=evalf((cos(b)+mu*sin(bs))/(sin(b)-mu*cos(bs)*cos(j(phi))));

$$f(\gamma) = \frac{\cos\beta + \mu \sin\beta_s}{\sin\beta - \mu \cos\beta_s \cos\gamma}$$

> f(js):=evalf(subs(j(phi)=Pi,f(j)));

$$f(\gamma = 180°) = \text{substitution of } \gamma = \pi \text{ in } f(\gamma)$$

> kvj:=evalf(kv*((f(js)-0.67)/(f(j)-0.67)));

$$k_{V(\gamma)} = \frac{k_V[f(\gamma = 180°) - 0.67]}{k_V[f(\gamma) - 0.67]}$$

> g(j):=evalf((mu*cos(bs)*sin(j(phi)))/(sin(b)-mu*cos(bs)*cos(j(phi))));

$$g(\gamma) = \frac{\mu \cos\beta_s \sin\gamma}{\sin\beta - \mu \cos\beta_s \cos\gamma}$$

> h(j):=evalf((g(j)+(mu*kf)/(kvj))/(1+(kf)/(kvj)));

$$h(\gamma) = \frac{g(\gamma) \pm \mu \dfrac{k_F}{k_{V(\gamma)}}}{1 + \dfrac{k_F}{k_{V(\gamma)}}}$$

(positive for driven pulley and negative for driving pulley)

> Tvo:=evalf((g(j))/((mu*kf/kvj)+g(j)));

$$\frac{T_V}{T} = \frac{g(\gamma)}{\mu \cdot \dfrac{k_F}{k_{V(\gamma)}} + g(\gamma)}$$

> Tfo:=evalf((mu*kf/kvj)/((mu*kf/kvj)+g(j)));

$$\frac{T_F}{T} = \frac{\mu \cdot \dfrac{k_F}{k_{V(\gamma)}}}{\mu \cdot \dfrac{k_F}{k_{V(\gamma)}} + g(\gamma)}$$

**> xo(phi):=FO(phi)*(kv+kf)/(kvj+kf):**

$$x_o = F_o(\frac{k_V + k_F}{k_{V(\gamma)} + k_F})$$

**> Fvo(phi):=FO(phi)*(kvj)/(kf+kvj);**

$$F_{Vo} = F_o \cdot \frac{k_{V(\gamma)}}{k_{V(\gamma)} + k_F}$$

**> Fvso(phi):=FO(phi)*(kvj)/(kf+kvj)*(kv+kf)/(kv);**

$$\frac{F_V}{F_{Vs}} = F_o \cdot \frac{k_{V(\gamma)}}{k_F + k_{V(\gamma)}} \cdot \frac{k_F + k_V}{k_V}$$

**> Ffo(phi):=FO(phi)*(kf)/(kf+kvj);**

$$F_{Fo} = F_o \cdot \frac{k_F}{k_{V(\gamma)} + k_F}$$

---

**> FO1:=diff(FO(phi),phi)=FO(phi)*h(j),diff(xo(phi),phi)=((1-xo(phi))+**

**(1-Fvso(phi))/(co))*cot(j(phi)):fcns:={FO(phi),j(phi)}:**

$$\frac{dF_o}{d\varphi} = F_o h(\gamma)$$

$$\frac{d(\frac{x}{x_s})}{d\varphi} \tan\gamma = 1 - (\frac{x}{x_s}) + \frac{1 - (\frac{F}{F_s})}{c_o}$$

**> FO2:=dsolve({FO1,FO(0)=1,j(0)=Pi)},fcns,numeric,value=array([0,.5,1,1.5,2,**

**2.5, 3,3.5,4,4.5]));**

Solve above differential equations numerically by puttin

$F_o(0) = 1$ and $\gamma(0) = \pi$ and

$\varphi = (0, .5, 1, 1.5, 2, 2.5, 3, 3.5, 4, 4.5)$

---

| φ | γ | $F_o$ |
|---|---|---|
| 0 | 3.142 | 1 |
| .5 | 2.694 | 1.084 |
| 1 | 2.41 | 1.257 |
| 1.5 | 2.222 | 1.528 |
| 2 | 2.102 | 1.914 |
| 2.5 | 2.027 | 2.441 |
| 3 | 1.980 | 3.148 |
| 3.5 | 1.950 | 4.089 |
| 4 | 1.930 | 5.335 |
| 4.5 | 1.916 | 6.982 |

**> jj:=col(Fo2[2,1],2);**

select column 2 or γ

γ=3.142, 2.694, 2.411, 2.222, 2.102, 2.027, 1.980, 1.950, 1.930, 1.916

**> jx:=evalf(map(->subs(j(phi)=x,x0(phi)),jj));**

substitute γ in $x_o$

$x_o$=$F_o$[1, 1.088, 1.243, 1.395, 1.513, 1.595, 1.650, 1.687, 1.713, 1.730]

**> jtvo:=evalf(map(x->subs(j(phi)=x,Tvo),jj));**

substitute γ in $T_V$ / $T$

$T_V / T$=[0, .694, .762, .780, .785, .787, .787, .786, .786, 786]

**> jtfo:=evalf(map(x->subs(j(phi)=x,Tfo),jj));**

substitute $\gamma$ in $T_F / T$

$T_F / T$=[1, .305, .237, .219, .214, .212, .212, .213, .213, .213]

**> jf1:=evalf(map(x->subs(j(phi)=x,Fvo(phi)),jj));**

substitute $\gamma$ in $F_{Vo} = p_{VN} / p_N$

$F_{Vo} = p_{VN} / p_N = F_o$[.791, .773, .740, .709, .684, .667, .656, .648, .643, .639]

**> jf2:=evalf(map(x->subs(j(phi)=x,Ffo(phi)),jj));**

substitute $\gamma$ in $F_{Fo} = p_{FN} / p_N$

$F_{Fo} = p_{FN} / p_N = F_o$[.208, .226, .259, .290, .315, .332, .343, .351, .356, .360]

# Appendix B (Specifications of Non-Contact Laser Displacement Metre)

| Item | | | Sensor head | KL130B | KL131B | KL132B | KL133B | KL135B | KL137B |
|---|---|---|---|---|---|---|---|---|---|
| Performance | Measuring rabge (MR) | | | 160 μm | 400 μm | 1600 μm | 5 mm | 20 mm | 80 mm |
| | Precision | Repeatability *1 | One averaging. | ±0.03% MR | | | | | |
| | | | | ±0.05 μm | ±0.12 μm | ±0.48 μm | ±1.5 μm | ±6 μm | ±24 μm |
| | | Linearity *1 | | ±0.05% MR | | | | | |
| | | | | ±0.08 μm | ±0.2 μm | ±0.8 μm | ±2.5 μm | ±10 μm | ±40 μm |
| | | Stability (±5°C) | | ±0.2% MR | | ±0.1% MR | | ±0.05% MR | |
| | | | | ±0.32 μm | ±0.8 μm | ±1.6 μm | ±2.5 μm | ±10 μm | ±40 μm |
| | Working distance | | | 7 mm | 10 mm | 15 mm | 25 m | 56 mm | 105 mm |
| | Minimum light spot diamter, maximum light spot diamter *2 | | | 10-20 μm | 12-35 μm | 25-50 μm | 80-90 μm | 110-150 μm | 180-280 μm |
| | Light source | | | Semiconductor laser, 670 nm wavelength, 1 mW max output. (Class Ⅱ) | | | | | |
| | | | | 62 dB (12 dB + 50 dB) | | | | | |
| | Responsivity | Sampling times | | 16 kHz (Sempling period : 62.5 μs) | | | | | |
| | | Frequency response | | 4 kHz (−3 dB) | | | | | |
| | | Response time | | 0.3 ms. (90% response) | | | | | |
| | Averaging times | | | 16-step switching of 1, 2, 4, 8 to 32768 ; $2^n$ (n=0 to 15) | | | | | |
| | Output period | | | Averaging times×62.5 μs. | | | | | |
| | Warm up time | | | 15 minutes | | | | | |
| Input/output | Digital output | Displacement output | | 16-bit parallel binary, negative logic, TTL level | | | | | |
| | | | | 0.005 μm/bit | 0.0125 μm/bit | 0.05 μm/bit | 0.15625 μm/bit | 0.625 μm/bit | 2.5 μm/bit |
| | | Alarm output | | FAR, NEAR, light alarm, light saturation, higher and lower limit alarm, TTL level | | | | | |
| | | Intensity output | | 8-bit binary, output of −1 to −120 dB in 1-dB steps, negative logic, TTL level | | | | | |
| | Analog displacement output *3 | | | 50-ohm max output impedance, 5 mA max current capacity, ±0.05% Precision | | | | | |
| | | | | 16 μm/V | 40 μm/V | 160 μm/V | 0.5 mm/V | 2 mm/V | 8 mm/V |
| | Interface | | | RS232C serial interface (baud rate 600, 1200, 2400, 4800, 9600, 19200 bps). | | | | | |
| | External control | | | Laser emission, measurement instruction, setting of various measuring conditions (zero-set, averaging times, higher and lower limit value, gain, alarm activation light level, sense), and TTL level | | | | | |
| Display | Displacement display *4 | | | ±160.00 μm | ±400.00 μm | ±1600.0 μm | ±5.0000 mm | ±20.000 mm | ±80.000 mm |
| | Displacement resolution | | | 0.01 μm | 0.02 μm | 0.1 μm | 0.0002 mm | 0.001 mm | 0.004 mm |
| | Display period | | | Approximately 0.25 sec. | | | | | |
| | Intensity display | | | 12-division LED display | | | | | |
| Set function | | | | Zero-set, averaging times, higher and lower limit value, gain, alarm activation light intensity level, and sense. | | | | | |
| Power supply | | | | 90-25 VAC or 200-250 VAC (Factory preset) 80VA MAX 50/60 Hz | | | | | |
| Dimensions and weight | Sensor head | | KL13X | W53×H25.5×D110 mm, 0.5 kg | | | W 69 x H 26 x D 79.5 mm, 0.3 kg | W73×H26×D76 mm, 0.3 kg | |
| | Display unit | | KL330B | W284×H120×D283 mm, 5.6 kg (Including KL230B sensor processing unit) | | | | | |
| | Sensor processing unit | | KL230B | W197×H55×D235 mm, 1.2 kg | | | | | |
| Working temperature and humidity | | | | 0-40°C, 30%-85% RH (non-condesing) | | | | | |
| | | | | Voltage +10 ~ −15 %, frequency +2 ~ −2 % | | | | | |
| | | | | 100 %, 1/2 cycle, 50 %, 1 cycle | | | | | |
| | Power supply noise | | | 1 kV, 1 μsec | | | | | |
| | | | | 8 kV | | | | | |
| | | | | AC1 kV, 1min | | | | | |

*1. Depends on object. This value is obtained when measuring the standard test piece in Anritsu. The KL130B/131B/132B uses a mirror with a reflection factor of 80%, the KL133B/135B/137B uses a standard white object test piece.

*2. The spot diameter is the minimum value at the center of the measuring range.

*3. If a precision close to the precision limit is required, use the digital output.

*4 The zero-point can be set to any point in the measuring range.

## Appendix C

## More detailed description of experimental method and non-contact laser displacement meter

The KL133 type displacement meter is a non-contact displacement gauge which uses laser-beam triangulation. The equipment can:

1-Measure the dimensions of an object, including the height, step difference, width and thickness,

2-Measure shapes including wrap and waviness,

3-Measure the vibration of rotating shafts or vibrating objects,

4-Measure the dynamic response of mechanical elements.

The equipment has high speed and high precision. The repeatability is $\pm 0.03\%$ of the measuring range. For the example, the equipment can measure a mirror surface with a response frequency of *4 kHz* and a repeatability of $\pm 1.5 \mu m$ (when using one averaging). When the number of averaging is *16*, the repeatability is $\pm 0.01 \mu m$.

The equipment samples *16 kHz* (a sampling period of $62.5 \mu \sec$) and the outputs the measured data at the same period (maximum). Averaging the measured data reduces fluctuation. The following number of averaging times can be set: *1, 2, 4, 8, 16, 32, 64, 128, 256, 512, 1024, 2048, 4096, 8192, 16384* and *32768*.

In the following cases, averaging is effective for improving the measurement precision.

1-When the response frequency is low at though the received laser intensity is small. When the averaging times are to $N$, the fluctuation is reduced by approximately $1/\sqrt{N}$. However, the measured data output period becomes $N \times 62.5 \mu \sec$.

2-When the measured surface is rough or the output fluctuation is large due to a difference in scattering characteristics [45].

In this thesis the experimental investigations carried out at maximum averaging time, due to rough and black surface of belt and vibration. This gives

$$output\ period = 32768(62.5/10^6) = 2.05\,\text{sec}$$

Considering the speed of drive ($\omega = 2000 RPM$) and length of tested v-ribbed belts (*1400mm*), at every *2.05 sec*, for the tests with $R_e$ =*45mm, 6.9* times and for the tests with $R_e$=*80mm, 12.27* times whole belt variation will be averaged. This means that for a *45mm* radius pulley the belt makes *6.9* rotations and for *80mm* radius it makes *12.27* rotations while *1* measurement is being taken.

However, to examine the accuracy and repeatability of tests a v-ribbed belt was run on the one pairs of equal size of pulleys $R_e$=*80mm,* at a speed of *2000RPM* with total belt tension of $F_t + F_r = 600N$.

The direction of rotation the rig was changed and the values of $H_T$ were measured for driven pulley at *11* steps of angular position (see section 6.2 for experimental method) and *4* different steps of applied torque to the drive: *0, 10, 15* and *20* (Fig. C1, data from table C1). The direction of rotation has not any effect on radial movement. The results showed maximum error of $\pm 7\mu m$, although away from entry and exit regions maximum error is $\pm 5\mu m$. The higher uncertainties at entry and exit regions are probably due to weight of belt.

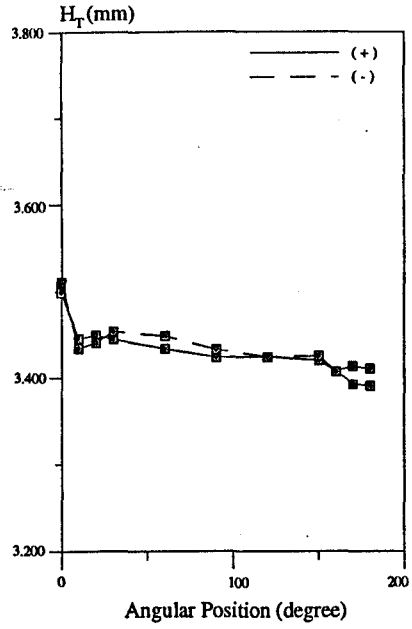


(a) Torque=0 Nm

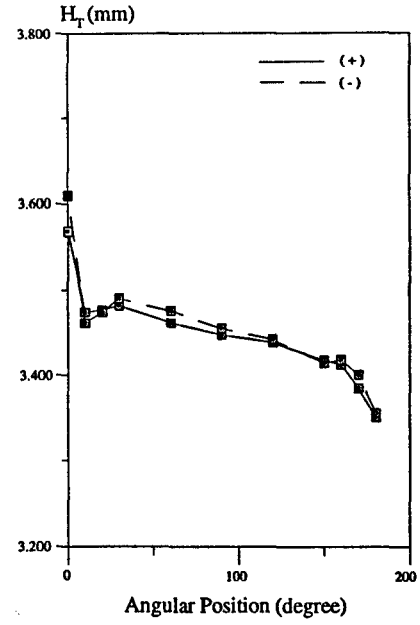


(b) Torque=10 Nm

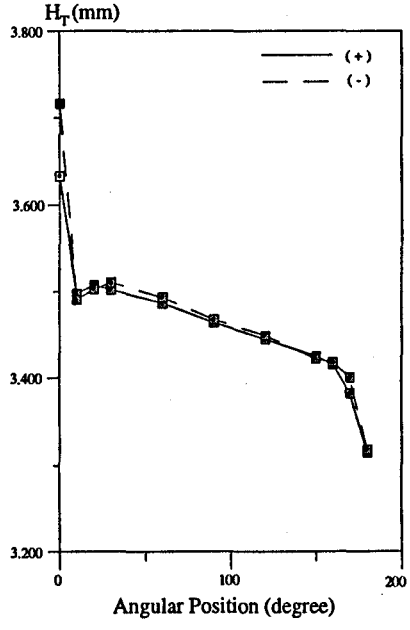


(c) Torque=15 Nm

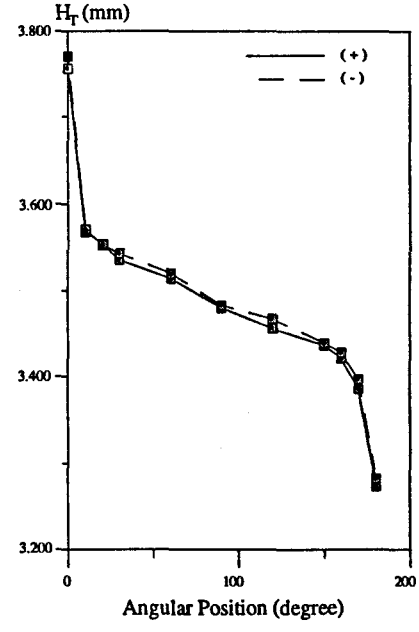


(d) Torque=20 Nm

**Fig. C1 Comparison of $H_T$ , for two different directions of rotation (driven pulley, $d_e$=80mm, $F_t + F_r$=600N)**

Table C1 Readings of $H_T$ (mm), for two different directions

| Angular position (degree) | T=0 Nm | | T=10 Nm | | T=15 Nm | | T=20 Nm | |
|---|---|---|---|---|---|---|---|---|
| direction | + | - | + | - | + | - | + | - |
| 0 | 3.500 | 3.512 | 3.568 | 3.609 | 3.633 | 3.716 | 3.756 | 3.770 |
| 10 | 3.445 | 3.434 | 3.474 | 3.461 | 3.498 | 3.491 | 3.568 | 3.571 |
| 20 | 3.450 | 3.441 | 3.476 | 3.474 | 3.507 | 3.503 | 3.554 | 3.553 |
| 30 | 3.445 | 3.454 | 3.482 | 3.490 | 3.502 | 3.510 | 3.536 | 3.543 |
| 60 | 3.434 | 3.449 | 3.461 | 3.475 | 3.486 | 3.493 | 3.514 | 3.520 |
| 90 | 3.424 | 3.433 | 3.447 | 3.455 | 3.463 | 3.467 | 3.480 | 3.483 |
| 120 | 3.424 | 3.424 | 3.438 | 3.442 | 3.444 | 3.448 | 3.456 | 3.467 |
| 150 | 3.420 | 3.425 | 3.417 | 3.414 | 3.424 | 3.421 | 3.436 | 3.439 |
| 160 | 3.407 | 3.407 | 3.412 | 3.418 | 3.415 | 3.417 | 3.421 | 3.428 |
| 170 | 3.392 | 3.413 | 3.384 | 3.400 | 3.382 | 3.400 | 3.386 | 3.397 |
| 180 | 3.390 | 3.410 | 3.350 | 3.355 | 3.314 | 3.317 | 3.274 | 3.283 |

# Appendix D

## Details of tests for variation of $H_T$ across the belt width at angular position 90°

| pulley sizes | 45 mm (new belt) | | | | 80 mm (used belt) | | | |
|---|---|---|---|---|---|---|---|---|
| total tension | 200 N | | 300 N | | 200 N | | 600 N | |
| torque (Nm) | 0 | 4 | 0 | 6 | 0 | 8 | 0 | 23 |
| 1 | 3.423 | 3.510 | 3.384 | 3.511 | 2.999 | 3.044 | 2.939 | 3.019 |
| 2 | 3.419 | 3.504 | 3.380 | 3.505 | 3.001 | 3.050 | 2.935 | 3.017 |
| 3 | 3.424 | 3.512 | 3.379 | 3.513 | 3.000 | 3.049 | 2.938 | 3.020 |
| 4 | 3.417 | 3.511 | 3.376 | 3.511 | 2.997 | 3.043 | 2.942 | 3.022 |
| 5 | 3.424 | 3.513 | 3.377 | 3.511 | 2.994 | 3.051 | 2.933 | 3.014 |
| 6 | 3.424 | 3.505 | 3.382 | 3.506 | 2.997 | 3.045 | 2.939 | 3.018 |
| 7 | 3.426 | 3.506 | 3.379 | 3.506 | 3.002 | 3.048 | 2.935 | 3.023 |
| 8 | 3.423 | 3.509 | 3.384 | 3.508 | 2.993 | 3.049 | 2.941 | 3.014 |
| 9 | 3.422 | 3.508 | 3.381 | 3.508 | 2.999 | 3.047 | 2.940 | 3.019 |
| 10 | 3.420 | 3.503 | 3.380 | 3.504 | 2.998 | 3.046 | 2.938 | 3.020 |
| 11 | 3.418 | 3.504 | 3.376 | 3.504 | 2.997 | 3.051 | 2.933 | 3.021 |
| 12 | 3.425 | 3.504 | 3.384 | 3.505 | 3.001 | 3.047 | 2.940 | 3.016 |
| 13 | 3.422 | 3.509 | 3.383 | 3.508 | 3.000 | 3.050 | 2.937 | 3.020 |